Objective Measurements of Patient Agitation in Critical Care Using Physiological Signals and Fuzzy Systems

Franck Agogué

A thesis presented for the degree of
Doctor of Philosophy
in
Electrical and Computer Engineering
at the
University of Canterbury,
Christchurch, New Zealand.

9 March 2005

Acknowledgements

This research would have been impossible without the continuous support of many people, and I would like to begin this thesis by acknowledging them. The list of people that helped me directly and indirectly during the last twenty six years, and more specifically the last three years, unfortunately does not fit on this page and only a few contributors can be personally acknowledged here.

My family has always helped me to access the best education available. They understood and supported my decision to go overseas for long periods of time, with the necessary psychological and financial support.

My supervisors Associate Professors J. Geoffrey Chase and Harsha Sirisena from the University of Canterbury, along with Dr Geoffrey M. Shaw from the Canterbury District Health Board, provided the scientific and medical expertise, believed in me, and supported me in the best and worst moods.

The Christchurch ICU staff contributed very positively and enthusiastically to this research with their co-operation and precious feedback on possible improvements.

The Canterbury Medical Research Foundation and the ICU trust have contributed some very helpful funds to this research.

Fellow researchers Christina Starfinger, Andrew Rudge, Zhuhui Lam, and Amol Malla have contributed to the progress of this research with their different, complimentary skills as computer scientists, mechanical and electrical engineers, to overcome the challenges encountered in this research.

The Centre for Bioengineering provides arguably the best working environment, and unarguably the best coffee on campus.

New Zealand and New Zealanders offer a unique wilderness paradise for adventurers of all kinds. The "New Zealand Lifestyle" helps to balance a computer-based work with world class outdoor terrain. I would also like to express a special thought to the University of Canterbury Canoe Club for the people it gathers and the structure it provides to overseas kayakers, which made my dreams come true.

Again, this is a very limited list, and I'd like to thank all the people that contributed directly and indirectly to the success of this research with their scientific, financial and social inputs.

Contents

List of Figures

List of Tables

Nomenclature

ABP	arterial blood pressure
AF	atrial fibrillation
ANN	artificial neural networks
ANS	autonomic nervous system
AR	auto regressive
avi	audio-video interleaved
BIS	bispectral index
BP	blood pressure, (mmHg)
BPD	blood pressure derivative, (mmHg/min)
BPV	blood pressure variability
bpm	beats per minute, heart rate
BR	breathing rate
BRD	breathing rate derivative
CCD	charge couple device
CDHB	Canterbury district health board
cov	covariance
CPT	cold pressor test
CPU	central processing unit
DBP	diastolic blood pressure
ECG	electrocardiogram
EEG	electroencephalogram
ETT	endotracheal tube
FIS	fuzzy inference system
FRLS	fast recursive least squares
FSM	finite state machine
h	hours
HF	high frequency
HR	heart rate, (beats/min)
HRD	heart rate derivative, (beats/min^2)
HRV	heart rate variability
ICU	intensive care unit
IQR	inter quartile range
ISU	international system unit
L	litres
LB	lower boundary

LF	low frequencies
Lpm	litres per minute, flow unit
MAAS	motor activity assessment scale
MF	membership function
mmHg	millimeters of Mercury, pressure unit: 1mmHg = 1Torr = 133.322 Pa
OAA/S	observer's assessment of alertness/sedation
p	order of AR filter
Pa	Pascal, ISU pressure unit
PSD	power spectral density
RASS	Richmond agitation sedation scale
rd	radians, angle unit
rd/s	radians per seconds, pulsation unit
RLS	recursive least squares
RMS	root mean square
RR	time interval between two R peaks in the ECG signal
s	seconds
SaO_2	arterial oxygen saturation
SAS	sedation / agitation scale
SBP	systolic blood pressure, (mmHg)
SD	standard deviation
SDdRR	standard deviation of the difference between consecutive RR intervals
SDdSYS	standard deviation of the difference between consecutive SBP values
SDRR	standard deviation of RR intervals
SDSYS	standard deviation of systolic blood pressure values
SE	standard error
STFT	short time Fourier transform
SpO_2	pulse oximetry
UB	upper boundary
USB	universal serial bus
VAR	variance
VAS	visual analogue scale
VICS	Vancouver interaction and calmness scale
VLF	very low frequencies
WT	wavelet transform
WCST	word color Stroop test
μ	degree of membership
σ	standard deviation
ω	AR forgetting factor

Abstract

Agitation-sedation cycling in ICU patients is characterised by oscillations between states of agitation and over-sedation. This cycling damages health and increases both length of stay and health care cost. A mathematical model that quantifies agitation is developed to achieve an agitation-feedback sedation controller with a long term goal of being used to improve their sedation management.

To quantify agitation, physiological signals readily available from common patient monitoring devices are filtered and processed. Motion sensing is performed using frame-to-frame correlation of regions of interest. The resulting physiological markers are combined with motion sensing information by fuzzy inference systems to produce an agitation index.

The initial goal of this objective agitation sensor is to assist the nursing staff by providing more information on agitation than currently available, in an objective and preferably preemptive manner, before it can be directly fed back to the semi-automated sedation controller. The signal-processing algorithms are first developed and validated off-line from the trials on 12 ICU patients as well as 10 healthy individuals. The agitation sensor is then statistically assessed in real-time during a second set of clinical trials. Clinical trials combined with observation increase the knowledge of agitation and permit to improve the structure of the sensor toward a reliable clinical tool.

Chapter 1

Introduction

Effective sedation is fundamental for ensuring comfort and pain relief of critically ill patients. However, current sedation methods often lead to over-sedation, which damages patients health and increases their length of stay and health care cost. The daily interruption of sedative infusion is a simplistic but efficient way to reduce over-sedation, consequently decreasing the length of stay of mechanically ventilated ICU patients by up to 35% [Kress et al., 2000].

However, a daily interruption of sedative drug infusion can lead to under-sedation, which results in sudden changes in the level of consciousness due to mental and physical stress. These changes provoke inadequate ventilation, hypertension, tachycardia and discomfort [Carrasco, 2000], all of which have adverse consequences for the outcome of ICU patients and can lead to agitation.

In the hospitalised adult, agitation is defined as an excessive motor or verbal behavior that interferes with patient care, patient or staff safety, and medical therapies. It can be a manifestation of an organic disturbance, emotional or physical discomfort, or psychiatric illness such as delirium and dementia [Haskell et al., 1997].

Agitation affects as many as 74% of ICU patients [Fraser and Riker, 2001] and is associated with potentially dangerous complications such as self-extubation, removal of arterial and venous catheters, and failure to participate in therapeutic endeavors [Riker et al., 1999]. Along with pain and anxiety, a primary underlying cause of agitation is delirium, a reversible, global impairment of cognitive processes, associated with disorientation, impaired short-term memory, short attention span, altered perceptions, abnormal thought processes and inappropriate

behaviour [Crippen, 1990].

Agitation and sedation management is a frequent clinical problem that adds significant morbidity and mortality to the ICU course. Current research explores how a semi-automated sedation controller has the potential to improve agitation management. A combination of agitation/sedation interaction and sedative pharmacokinetic models is used to develop new sedation infusion protocols. A bolus-driven approach shows the potential to reduce both patient agitation and drug consumption, as well as minimising agitation-sedation cycling. The model focuses on patient agitation feedback, and is based on an objective scale to improve agitation control [Rudge et al., 2004].

However, an objective quantified agitation index for use in feedback control is an essential element of such a system. Hence, the development of an objective agitation sensor is required to enable several new, and potentially significantly improved, avenues of sedation management. It could also provide insight into agitation in critical care and patient condition that is not currently available.

1.1 Agitation assessment on subjective scales

This research is an attempt to objectively quantify agitation in ICU patients, and no objective agitation assessment method has yet been validated and recommended for clinical use to the author's knowledge. Agitation is currently assessed on subjective scales. The concept of subjectivity, and more particularly subjective assessment, is introduced in this chapter. The most current subjective agitation scales are presented and discussed to delineate the current state of the art in agitation assessment.

1.1.1 Subjective assessment

A scale is deemed subjective if the resulting grade may fluctuate between two clinicians assessing the same patients on this scale (inter-rater subjectivity). Basically, the same patient can be assigned two different scores when assessed on the modified Riker sedation/agitation scale (SAS), the existing gold standard

in subjective agitation/sedation assessment in Christchurch ICU. Moreover, the grade of a same clinician may fluctuate between two similar patients, or the same patient in the same condition at different times (intra-rater subjectivity). To the clinicians' credit, the subjectivity of the agitation assessment is partly due to the evaluation parameters of the different grades that often allow confusion. It is also due to the varying experience of the clinicians.

The "Cohen's kappa (κ) inter-rater agreement" [Fleiss, 1973] is a means to estimate the inter rater subjectivity of a scale [Carrasco, 2000]. The following example illustrates how to determine the Cohen's kappa score. Let raters A and B assess the level of agitation of 100 ICU patients on a subjective scale that ranges from 0 (calm) to 3 (very agitated). The inter-rater analysis can be summarized in a table that lists how many patients are assessed similarly by both raters, as well as patients classified differently. Table 1.1 shows a matrix of assessment where the diagonal elements represent cases where raters A and B made the same assessment.

Table 1.1 An example of 100 subjects assessed by two raters A and B

	Rater A				
Rater B	0	1	2	3	Total
0	25	3	2	0	30
1	4	27	4	0	35
2	2	7	10	1	20
3	0	1	4	10	15
Total	31	38	20	11	100

From Table 1.1 the proportion of inter-rater agreement can be evaluated, and is defined:

$$p_o = \frac{n_{00} + n_{11} + n_{22} + n_{33}}{n_{\bullet\bullet}} \tag{1.1}$$

where $n_{i\bullet}$ is the entire population graded "i" by rater A, $n_{\bullet j}$ is the entire population graded "j" by rater B, and $n_{\bullet\bullet}$ is the overall population enrolled in the given test. Hence, n_{12} is the population of patients with grade "1" agitation as assessed by rater A, and a grade "2" agitation as assessed by rater B. For this particular set of data the proportion of agreement is $p_o = 0.72$.

However, some degree of agreement is expected purely by chance and therefore the proportion of agreement p_0 is not an adequate measure of reliability. The overall proportion of agreement expected by chance alone is defined:

$$p_c = \frac{n_{0\bullet}n_{\bullet 0} + n_{1\bullet}n_{\bullet 1} + n_{2\bullet}n_{\bullet 2} + n_{3\bullet}n_{\bullet 3}}{n_{\bullet\bullet}^2} \tag{1.2}$$

For the data in Table 1.1 the proportion of agreement expected by chance is $p_c = 0.28$. However, a better measure of agreement than p_o alone is the difference $p_o - p_c$. This value represents how much agreement exists beyond the amount expected by chance. This metric is normalised for convenience, so that a maximum proportion of agreement equals 1, producing the kappa score.

$$\kappa = \frac{p_o - p_c}{1 - p_c} \tag{1.3}$$

where if $p_o < p_c$ then $\kappa < 0$ and the proportion of agreement is less than the chance agreement. If $p_o = p_c$, then $\kappa = 0$ and this condition relies on chance only. Finally if $p_0 = 1$ then $\kappa = 1$ and that means perfect agreement between raters using a given assessment method, and thus a 100% consistent method. More generally, if κ tends towards 1, the scale is less subjective and more objective, consistent, and hence potentially more reliable.

The example set of data given in Table 1.1 gives an inter-rater agreement of $\kappa = 0.61$, which is smaller than the biased proportion of agreement first established in Equation (1.1). To assess the statistical significance of κ its standard deviation is required. The standard deviation (SD) is defined as the square root of the variance [Fleiss, 1973].

$$Var(\kappa) = \frac{1}{N(1-p_c)^2}\left(p_c + p_c^2 - \sum_{i=0}^{3} p_{i\bullet}p_{\bullet i}(p_{i\bullet} + p_{\bullet i})\right) \tag{1.4}$$

where N is equal to $n_{\bullet\bullet}$, the size of the whole population. $p_{i\bullet}$ is equal to the ratio $\frac{n_{i\bullet}}{n_{\bullet\bullet}}$. In this particular example the variance is equal to 3.6×10^{-3} and the corresponding standard error SE(κ) equals 6.0×10^{-2}. In this context SE

equals SD, because the deviation is the error between the true result and the approximation.

The statistical significance of κ, and the data set on which it is determined, may also be assessed by referring to the quantity z defined in Equation (1.5). If z is significantly large ($z >> 1$), the observed inter-rater agreement of the particular data set reflects the reliability. If it is small ($z << 1$) the observed inter-rater agreement may only reflect random results.

$$z = \frac{\kappa}{SE(\kappa)} \tag{1.5}$$

For instance, the data in Table 1.1 yields $z = \frac{0.61}{6.0 \times 10^{-2}} = 10.17$ so the kappa score does reflect the reliability of the scale and not only random results based on a fortunate set of data. Overall, the inter-rater reliability of a subjective scale is said to be reasonable for $0.70 < \kappa < 0.80$, good for $0.80 < \kappa < 0.90$ and excellent for $0.90 < \kappa < 1.00$ [Fraser and Riker, 2001].

1.1.2 The Ramsay scale

The first scale developed to assess the level of agitation and sedation of critically ill patients was the Ramsay scale developed in 1974 [Ramsay et al., 1974]. It consists of a 6-grade scale ranging from 1 (agitated) to 6 (unarousable, over-sedated). These different grades are detailed in Table 1.2.

Table 1.2 Ramsay scale [Carrasco, 2000]

Level	Characteristics
1	Patient awake, anxious, agitated or restless
2	Patient awake, cooperative, orientated and tranquil
3	Patient drowsy, with response to commands
4	Patient asleep, brisk response to glabella tap or loud auditory stimulus
5	Patient asleep, sluggish response to stimulus
6	Patient has no response to firm nail-bed pressure or other noxious stimuli

The subjectivity of this scale was first estimated in 1999 [Riker et al., 1999], with an excellent inter-rater agreement ($\kappa = 0.88$). Unfortunately, the Ramsay scale classifies all different levels of agitation into one single level including be-

haviours from mild anxiety to dangerous agitation [Ramsay et al., 1974]. In spite of this limitation, the Ramsay scale remains one of the most widely used scales for monitoring sedation in daily practice as well as clinical research [Carrasco, 2000].

1.1.3 The Riker sedation/agitation scale

The Riker Sedation/Agitation Scale (SAS) was first developed in 1994, and subsequently improved in 1999 [Riker et al., 1999]. It provides a symmetric approach of 3 grades each to assess the patient's levels of agitation and sedation, and a middle grade for calm and co-operative patients — a total of 7 possible levels.

The Riker SAS has an excellent inter-rater of $\kappa = 0.92$. The intra-rater agreement has not been evaluated. The validity of this scale has also been assessed through agreement with other subjective scales [Riker et al., 1999], and the bispectral index (BIS) derived from the EEG, an objective metric that specifically evaluate sedation [Fraser and Riker, 2001; Nasraway Jr et al., 2002]. However, there is a key limitation in the Riker SAS, since the patient is classified as either agitated, or sedated, but not both.

Recent research by Shaw et al. [Shaw et al., 2004] has proven that a patient can be simultaneously agitated and sedated. Therefore, it is more consistent to assign the patient with both an agitation index and a sedation index. A modified version of the original Riker SAS, referred to as the modified SAS, is shown in Table 1.3. This scale has been developed and used in the Christchurch Hospital ICU, to assess agitation and sedation levels separately, creating two concurrent indices, around the "0" score.

Some guidelines for the Riker and modified SAS assessment [Riker et al., 1999] help differentiate different levels of sedation. First, agitated patients are scored by their most severe degree of agitation in the 0–3 range. Then, sedated patients are scored similarly for level of sedation on the -3–0 range. Finally, both scores are reported as concurrent indices. In the context of this research, the focus is on the agitation assessment, which is similar in both the Riker and modified SAS scales if considered independently from the sedation side of the scale. Therefore, this thesis refers to both scales as the SAS scale and its grades of agitation.

Table 1.3 Modified version of the SAS scale

Score	Term	Description
Agitation score		
3	Dangerous Agitation	Pulling at Endotracheal Tube (ETT), trying to remove catheters, climbing over bed rail, striking at staff, thrashing side-to-side
2	Very Agitated	Requiring restraint and frequent verbal reminding of limits, biting ETT
1	Agitated	Anxious or physically agitated, calms to verbal instructions
0	Calm	Calm
Sedation score		
0	Cooperative	Easily arousable, follows commands
-1	Sedated	Difficult to arouse but awakens to verbal stimuli or gentle shaking, follows simple commands but drifts off again
-2	Very Sedated	Arouses to physical stimuli but does not communicate or follow commands, may move spontaneously
-3	Unarousable	Minimal or no response to noxious stimuli, does not communicate or follow commands

1.1.4 The motor activity assessment scale

The Motor Activity Assessment Scale (MAAS) has been developed from the SAS and is also a 7-level scale with three categories for both agitation and sedation, as well as a middle level for calm patients [Fraser and Riker, 2001]. Behavioural descriptors are provided to assist medical experts in patient assessment, as defined in Table 1.4). The MAAS has shown an inter-rater agreement of $\kappa = 0.83$, and the validity of this scale has been confirmed through comparisons with other subjective scales and clinical parameters such as changes in vital signs [Fraser and Riker, 2001]. However, the validity of the MAAS has only been assessed in surgical ICU patients, and further study should be carried out on critically ill patients [Carrasco, 2000].

Table 1.4 The motor activity assessment scale

Score	Term	Description
6	Dangerously agitated, uncooperative	No external stimulus is required to elicit movement, and patient pulls at tubes or catheters or thrashes side-to-side or strikes at staff or tries to climb out of bed and does not calm down when asked
5	Agitated	No external stimulus is required to elicit movement, and attempts to sit up or moves limbs out of bed and does not consistently follow commands (e.g., will lie down when asked but soon reverts to attempts to sit up or move limbs out of bed)
4	Restless and cooperative	No external stimulus is required to elicit movement and patient picks at sheets or tubes or uncovers self and follow commands
3	Calm and cooperative	No external stimulus is required to elicit movement and patient adjusts sheets or clothes purposefully and follow commands
2	Responsive to touch or name	Opens eyes or raises eyebrows or turns head toward stimulus OR moves limbs when touched or name is loudly spoken
1	Responsive only to noxious stimuli	Opens eyes or raises eyebrows or turns head toward stimulus or moves limbs with noxious stimulus
0	Unresponsive	Does not move with noxious stimulus

1.1.5 The Harris scale

First developed in 1991, the Harris scale was not tested for reliability until 1999 [Fraser and Riker, 2001]. This scale assesses the patient condition from three different aspects: general condition, compliance with mechanical ventilation, and response to endotracheal suctioning. It reveals an excellent inter-rater agreement of $\kappa = 0.90$ and good agreement with other subjective scales confirmed its validity [Fraser and Riker, 2001]. The Harris scale focuses additional attention on patient acceptance of mechanical ventilation. Hence, it shows great potential to compare different ventilation systems.

1.1.6 The Sheffield scale

The Sheffield scale is an 8-level scale with extra categories "asleep" and "paralyzed" [Fraser and Riker, 2001]. The score depends on the patient's extreme level

over an hour. It demonstrated a fair inter-rater reliability of $\kappa = 0.73$. However, it has the same limitation as the Ramsay scale. It classifies mildly agitated and extremely agitated patients with the same grade. Therefore, the Sheffield scale does not offer a great resolution for agitation assessment. However, it remains a proven reliable sedation scale.

1.1.7 The Vancouver interaction and calmness scale

The Vancouver interaction and calmness scale (VICS) consists of two five-grade sub-scales for calmness and interaction, each with a possible score between 6 and 30 points [Fraser and Riker, 2001]. The inter-rater agreement is excellent ($\kappa = 0.90$) with additional complicated statistical support for the validity and responsiveness of the scale. Because there are 10 sub-scales assessment may take longer than simpler scores. However, this scale has been developed with epidemiologic and statistical techniques and may contribute to sedation assessment in a unique way [Fraser and Riker, 2001].

1.1.8 The visual analogue scale

Often used for pain assessment the visual analogue scale (VAS) uses a 100mm line bounded by descriptive terms such as "very sedated" and "wide awake" [Fraser and Riker, 2001]. Observers draw a perpendicular mark through this baseline at a relevant point. Then the distance from the left of the line to the mark is measured. It is considered a standard tool although few studies have tested its reliability, and it does not match the performance of the Riker SAS or MAAS scales [Fraser and Riker, 2001].

1.1.9 Other subjective scales

There are more assessment tools available to evaluate the level of sedation and agitation of a patient. Among those are the Observer's Assessment of Alertnes/Sedation (OAA/S), the COMFORT scale [Jaarsma et al., 2001], and the Richmond Agitation Sedation Scale (RASS)[Sessler et al., 2002]. They all provide a reliable

assessment tool with advantages and disadvantages, and they may focus more or less on different aspects. However, these scales are more subjective and they are not presented in more detail in this thesis. Literature can easily provide a detailed description of any agitation and sedation scale.

1.1.10 Summary of subjective scales

Among the literature concerning agitation and sedation assessment methods, Fraser et al. [Fraser and Riker, 2001] recommend that each intensive care units select one scale proven to be valid and reliable, and includes that scale in their agitation and sedation protocols. Because of the ease of use, proven reliability and validity, behavioural descriptors to guide patient classification, and the capability of monitoring both agitation and sedation, Christchurch Hospital ICU uses the modified Riker SAS [Shaw et al., 2004]. However, no data confirms that this scale is superior to others. More importantly, all the scales described share the requirement of subjective assessment with relatively limited (3-5) levels of resolution for agitation. They all also bundle both agitation and sedation as a single issue, rather than separate states, which is a fundamental part of the approach in this thesis. Note that the results of different scales subjectivity given by the κ inter-rater agreement from other research groups presented in this section were not provided with the quantity z, which leaves room for argument on the reliability of the different studies.

1.1.11 Issues related to subjective diagnosis

The subjective assessment of the levels of sedation and agitation of a patient provides a variable diagnosis, which may lead to inconsistent sedation management and over-sedation, particularly for scales with little resolution. Such scales can be prone to significant inter-rater variations between clinicians, as well as intra-rater variations [Chase et al., 2004b]. Inter-rater variability has been assessed by Riker et al. [Riker et al., 1999] for several subjective scales, and most give a good κ index of low subjectivity, but the intra-rater subjectivity has not been assessed and it considerably impairs the overall reliability of these scales.

The resulting over-sedation, partly due to the subjectivity of the agitation assessment, extends the duration of mechanical ventilation and the overall length of stay of the patient in the ICU. It can also impede daily neurological examinations. Furthermore, over-sedation increases the need to assess alterations in mental status for delirium or dementia [Kress et al., 2000]. Therefore, the development of a more reliable, objective agitation scale is the first step towards the improvement of agitation control and sedation management based on agitation feedback control.

1.2 Objective quantification of agitation

1.2.1 Physiological signals

To be objective, the agitation assessment has to based on quantifiable physiological variables (measurement system approach) [Carrasco, 2000]. This methodology avoids the limitations of subjective human assessments based on the scoring systems presented in the previous section. Physiological signals are not subjective to clinicians, and can used to objectively assess the level of agitation of a patient.

A broad range of physiological signals can be readily measured on the human body. A basic hospital ICU bed is surrounded by the appropriate hardware to continuously monitor electrocardiogram (ECG), arterial blood pressure (ABP), breathing rate (BR) and pulse oximetry (SpO_2), the latter of which is an estimation of the percentage of haemoglobin saturated in oxygen SaO_2.

In essence, this research attempts to develop an agitation sensor that does not require additional monitoring devices to those available in a standard ICU environment. Specific patients require the monitoring of other signals such as the electroencephalogram (EEG). Some indices derived from the EEG such as the bispectral index (BIS) may be used to track the patient condition during the ICU stay [Nasraway Jr et al., 2002], but it is not yet validated as a clinical method to continuously assess agitation and sedation [Fraser and Riker, 2001]. Power spectral variables used to compute the BIS have been shown a correlation with the depth of sedation, responsiveness and consciousness. However, no correlation between EEG, or BIS, and agitation has yet been observed by previous research.

Moreover, many sedatives alter the EEG response, making interpretation very difficult. Finally continuous EEG monitoring cannot be recommended for routine monitoring in the ICU [Carrasco, 2000].

The breathing rate is a commonly monitored signal that may correlate well with agitation episodes under conditions where the patient is breathing spontaneously [Lam et al., 2003]. More specifically, symptoms such as pain and anxiety may influence the breathing rate and consequent arterial oxygen saturation (SAO_2) of a patient. However, most sedated ICU patients are mechanically ventilated during most of their stay and therefore do not breath spontaneously. This aspect considerably reduces the period of time during which the breathing rate provides a meaningful information, different from the ventilator setup. Hence, the use of the breathing rate as an input of the agitation sensor is initially left aside but might be added. Pulse oximetry may also be added if it provides significant information on agitation.

1.2.2 Objective agitation sensing concept

Agitation is mainly triggered by anxiety and pain, as well as delirium or dementia. These symptoms are well known to stress the patient and affect physiological signals, which are thus expected to be key factors in agitation sensing. There is limited space for experimental research on patients suffering pain or psychological stress such as anxiety, for ethical reasons. However, similar research has been carried out on comparable species of mammals such as rats. Such experiments yield relevant findings on the effect of stress on physiological signals. Inagaki et al. [Inagaki et al., 2004] examined rats under psychological stress to reveal, among several findings, that the rats under stress show a significant heart rate increase. Therefore HR and its dynamics may aid to track events of agitation triggered by anxiety and fear.

Psychologists can also stimulate mental stress and anxiety on normal subjects using procedures such as colour word test or cold pressor test [Lam et al., 2003; Starfinger et al., 2003], which are assumed to provoke an agitation-like response on physiological signals. These common techniques provide useful information and first guidelines on possible physiological responses, without threatening patient safety. Shinn et al. [Shinn et al., 2001] investigated the possible correlation

between hypertension and anxiety in normotensive adults. In their study both depression and anxiety were not significantly related to fluctuations in blood pressure values. However, the possibility that anxiety and depression are risk factors for hypertension is not excluded.

Given that the literature only provides ambiguous clues on how a physiological signal will react to anxiety and agitation, an alternative approach is to record signals and correlate them graphically with occurrences of agitation. The agitation measurement is made difficult by the many different conditions of ICU patients. Therefore, information about the next occurrence of agitation may be patient-specific. This variation is due to the different therapies and clinical background of the broad population of ICU patients. For these reasons, several physiological signals are selected in an attempt to objectively quantify agitation. Ethics approval is obtained to include the addition of patient video records along with physiological signal acquisition. The addition of video recording and processing adds consistency in the agitation sensing technique, because the agitation assessment done by the clinicians is mainly defined by the patient motion.

The physiological and video signals are first recorded along with the feedback of the nursing staff in care of the patient, based on the SAS, and are then processed and combined into an agitation index. The signal-processing is performed concurrently using several methods, including spectral, temporal and non-linear analysis, to obtain signal patterns specific to episodes of agitation. Two categories of information are usually added by a signal. Firstly concurrent information can help understanding different patterns between different signals when agitation takes place. Secondly, recurrent information can improve the detection of agitation, and lack of recurrent information can identify an artifact. In essence, there are no obsolete signals in this approach where several methods focus on the same trend of the signals to develop the optimal signal-processing techniques.

1.2.3 From physiological signals to agitation index

This thesis outlines the progressive steps from the original work by Starfinger et al. [Starfinger et al., 2003; Starfinger, 2003], Lam et al. [Lam et al., 2003; Lam, 2003] and Chase et al. [Chase et al., 2003, 2004c], to the current implementation of a real-time objective agitation sensor. Each selected signal is processed to

produce potential physiological markers of agitation.

The signal-processing methods are described in Part I. Chapter 2 describes the signal-processing methods applied on the electrocardiogram (ECG). Chapter 4 presents the signal-processing algorithms applied on the arterial blood pressure signal (ABP). Chapter 5 introduces the potential additional information contained in markers derived from the airway pressure, air flow and pulse oximetry signals. Chapter 6 outlines the video-processing techniques that perform motion sensing. These physiological and video signals are pre-processed by both crisp and fuzzy algorithms to produce a set of intermediate metrics. Hence, a description of the so-called "Fuzzy Inference Systems (FIS)" and their use to combine the intermediate metrics into the agitation index, are provided in Part II.

The concept of physiological agitation sensing is then verified with clinical trials presented in Part III. The methodology of each set of trials is first described in Chapter 10. The first development and calibration of the algorithms is based on clinical trial of normal individuals. These results allow the first proof-of-concept of objective agitation sensing, and the methodology and results obtained during this first clinical study are described in Chapter 11. The algorithms and subsequent system are calibrated and tested on 12 ICU patients. These patients differ from normal individuals by providing real agitation data. A lot of improvements result from these trials. The patients' data is first acquired, and then processed off-line. The final signal-processing stage is fine-tuned on these clinical trials data. The trials performed on ICU patients are then described in Chapter 12.

All of stages of signal- and video-processing are finally combined in a standalone application to perform real-time agitation sensing and nurse feedback acquisition. These final clinical trials are gathered in a database to allow off-line statistical validation of the sensor. The results of these final ICU trials are given in Chapter 13. The statistical analysis of the set of ICU trials is described in Chapter 14. Finally, the conclusions on the current state of the agitation sensor and the potential future work are presented in part IV.

Part I

Signal-processing

Chapter 2

Electrocardiograms and agitation

The electrocardiogram (ECG) is a record of the electrical activity of the heart, and is one of the most commonly used physiological signals in patient assessment. The ECG signal is measured by placing a series of electrodes on specific parts of the upper body to sense changes in electrical potential at the surface of the body as a result of heart muscle contraction and relaxation through the cardiac cycle. The shape of one period of the ECG signal, with the several local extrema from a normal subject, is shown in Figure 2.1.

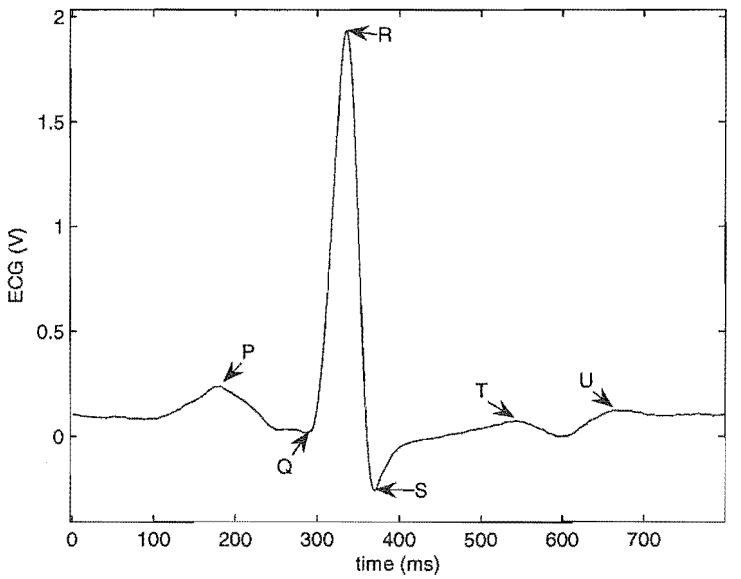

Figure 2.1 ECG period with detailed local extrema.

The ECG is regularly used by medical staff to assess general patient condition as well as special cardiac conditions [Guyton and Hall, 1996]. Hence, it is used to monitor most critically ill patients. In this context, patients suffer primarily

from pain and anxiety, possibly combined with delirium, which involve stress potentially reflected in the ECG. The ECG signal is therefore a fundamental component of this research. A wide range of studies have observed a correlation between pain management and heart rate, as well as heart rate fluctuations, associated with different situations of physical and mental stress [Inagaki et al., 2004; Bianchi et al., 1993; Chase et al., 2004c; Bartels et al., 2004; De Jong et al., 2004].

There is an established relationship between each of the P, Q, R, S and T waves of an ECG period and the cardiac cycle. These waves, shown in Figure 2.1, are electrical potentials produced by the heart and recorded by the ECG on the surface of the upper body. The P wave is due to the spread of depolarization through the two atria, shown in Figure 2.2. This action is followed by atrial contraction to squeeze more blood into the ventricles.

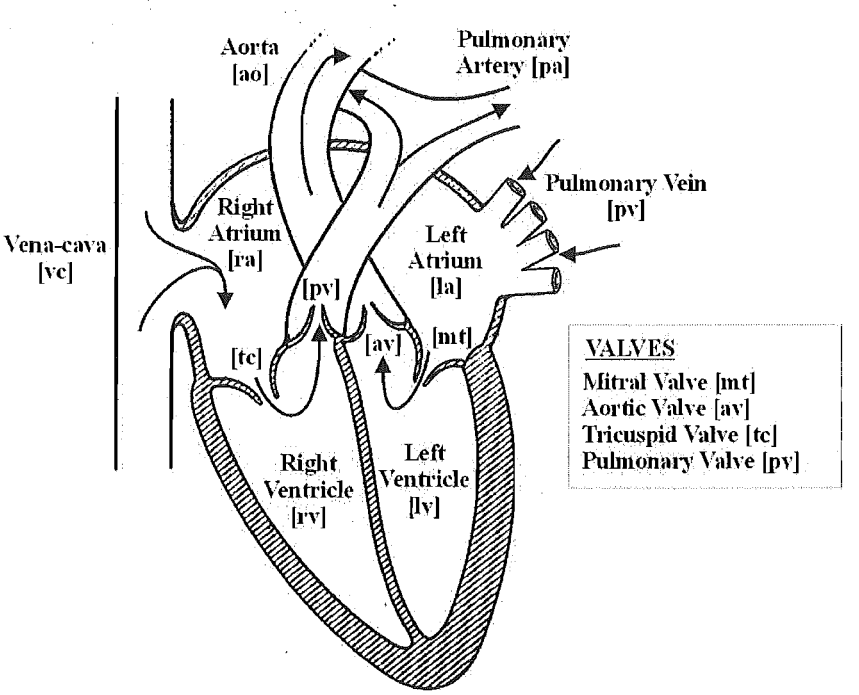

Figure 2.2 Cross-section of the heart [Fung, 1997].

The QRS complex of waves is the result of the depolarization of the two ventricles, initiating ventricular contraction and the corresponding rise in ventricular pressure. Finally the T wave represents the repolarization of the ventricles, in which fibers begin to relax [Guyton and Hall, 1996]. Occasionally, a further small, shallow wave immediately follows the T wave, with the same polarity as the T wave, and this is referred to as the U wave. Its origin is unclear, but it may be

either late repolarization of the ventricles or septal repolarization [Guyton and Hall, 1996], the septum being the wall between the two ventricles.

These waves, particularly their latency, their shape and their magnitude, can provide precious information on the heart and the autonomic nervous system (ANS), which in turn can provide information on patient condition. The ECG signal can be processed in time, frequency and time-frequency domains using common methods such as statistical analysis, Fourier transform and time-frequency distribution [Bianchi et al., 1993; Pfeiffer and Netzer, 1997; Seong et al., 2004]. There are also some emerging non-linear methods that provide additional information, or recurrent information in a different form [Paskeviciute et al., 2001; Niskanen et al., 2004; Thong et al., 2004].

Time domain analysis represents a simple and easy-to-compute method for studying the ECG. The heart rate, cycle period, variance or standard deviation of an ECG signal may be determined using time domain analysis, such as peak detection. Frequency or time-frequency distribution, such as Auto-Regressive (AR) Power Spectral Density (PSD) estimation or wavelet transform, can be used to track the dynamics of the heart.

This chapter presents the theoretical background of the different signal-processing methods implemented on the ECG signal. The aim is to provide the foundation for using ECG signals in patient agitation quantification. Hence, this chapter presents the ECG signal in that context.

2.1 Effect of agitation symptoms on the ECG

Clinicians knowledge indicates that agitation episodes are triggered mainly by pain and discomfort, often referred to as physical stress, and anxiety, also called mental stress. These symptoms have been studied and their effects on the ECG have been considered. These studies offer a first proof of concept for measuring agitation in critical care with the ECG signal as an input.

Previous work [Lam et al., 2003; Starfinger et al., 2003; Shaw et al., 2003; Chase et al., 2004c] associates events of agitation with a reaction of the heart rate (HR) and heart rate variability (HRV). Inagaki et al. [Inagaki et al., 2004]

associate psychological stress, such as the fear witnessed in ICU patients, with a significant increase in HR as well as HRV. In contrast, De Jong et al. [De Jong et al., 2004] did not observe significant correlation between anxiety and elevated HR. The investigation of pain predictors during invasive medical procedures by Logan et al. [Logan et al., 2002] reported a lower pain report from patients whose heart rate increased during surgery. Moreover, Lindh et al have also observed increased HR and HRV on patients affected by physical stress, such as infants during invasive neonatal procedures [Lindh et al., 1997, 1999].

The ANS responds to surgical or ICU pain, partly due to inappropriate sedation and analgesia of patients, by changing different physiological factors, such as increased blood flow. This increased blood flow is potentially due to increased heart rate and will be associated with such changes. More specifically, a response of the sympathetic part of the ANS is triggered by mental and/or physical stress [Guyton and Hall, 1996]. It is called the sympathetic stress response and its consequences include increased heart rate and hypertension. The activity of the ANS is estimated by the heart rate variability (HRV) method, and the development of patient mental and physical stress can potentially be detected through the HRV metrics. However, the lack of consistency among the literature in this subject requires further investigation to determine a reliable relationship between heart rate dynamics and patient agitation.

2.2 Heart rate

The heart rate (HR), measured in beats per minute (bpm), is the first metric derived from the ECG signal in a clinical assessment. The HR is computed from the time between the peaks of two consecutive R waves of the ECG signal, measured in seconds (s). This time intervals are also called RR interval, and form the tachogram signal. The detection of R waves in the ECG signal can be performed using several techniques. In this section, the baseline removal by high-pass filtering is compared with the wavelet transform (WT) method to detect R waves. The output of this first signal-processing step is then processed by peak detection to compute the tachogram, the heart rate and derived metrics.

2.2.1 Baseline removal

To evaluate the heart rate and related metrics, the first step is to locate the R peak in each period of the ECG. This task is complicated by the fluctuating baseline of the ECG signal, which needs to be removed for efficient peak detection.

The ECG records over time the difference between electrical potentials recorded from electrodes precisely located on the upper body of the patient. The conductivity of the electrodes may vary depending on whether the patient is calm and has dry skin, or exhibits excess motor activity combined with sweaty skin. This phenomenon translates to a floating baseline on the ECG signal.

The floating baseline of the signal does not permit direct peak detection, because this method is based on a level threshold that is determined from the extreme values of the signal. However, a relatively strong shift of the baseline of the ECG makes the current threshold level too low or too high, and peaks cannot be detected anymore, or artifacts are processed as R peaks, and the resulting information is false. A typical baseline shift is illustrated in Figure 2.3 for an ICU patient. The ECG baseline is currently removed by the high-pass filtering and wavelet transform methods presented in this section.

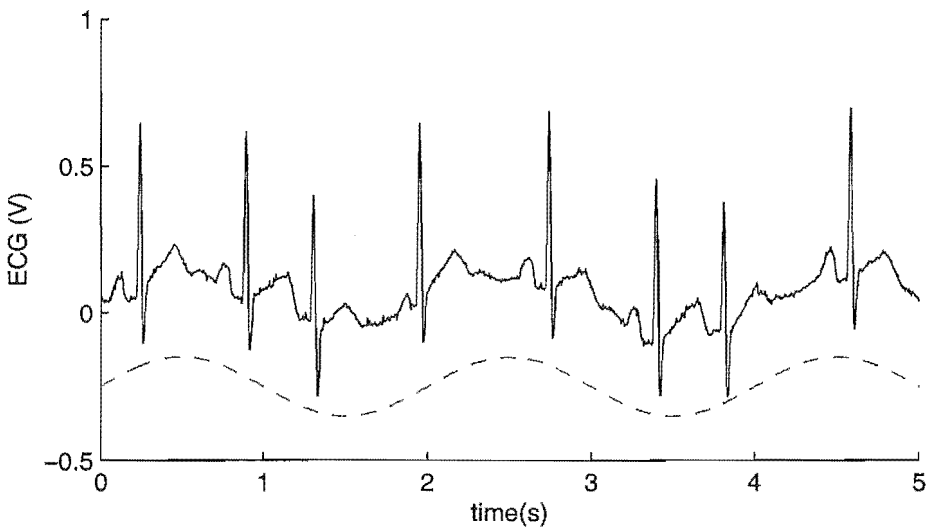

Figure 2.3 ECG signal in solid line, with the floating baseline that oscillates over time in dashed line.

Using the high-pass filtering method, the baseline of the ECG signal is smoothed, thus removing the low frequency fluctuations, partly due to the variable conduc-

tivity of the ECG electrodes, as well as other mechanisms that can potentially increase baseline shift. This filtering allows the detection of the location of R wave peaks among other extrema, namely P, Q, R, S, T and U waves. The low frequency baseline estimated by a moving average over a time window is subtracted from the ECG signal to keep only the high frequency component of the ECG signal.

The length of the moving average (MA) filter is crucial for effectiveness. Too short a time window tends to smooth the whole signal and make the peak detection nearly impossible, because of the lack of contrast between the baseline and the different extrema, including the R peak of interest. This effect is worsened by the presence of high frequency noise and patient motion that can produce artifacts in the signal. In contrast a long time window does not remove the entire slow trend and leaves some undesirable low-frequency fluctuations, as well as being computationally intense due to the larger shift register of the MA filter. This tradeoff is illustrated when processing the signal through MA filter of different time window length. The ECG signal is processed by removing the baseline estimated by a 20ms, 100ms and 500ms MA filters.

The relatively short 20ms time window MA filter eliminates all but the R wave peaks of the ECG signal, but the signal to noise ratio of the filtered signal is not optimal. The signal processed by the longer 500ms time window MA filter still contains low frequency noise, because the smoothing is not effective. The 100ms time window offers the best compromise and the filtered signal does not contain low frequency noise. It maintains a good signal-to-noise ratio between the R waves and the rest of the signal. The processing of the ECG signal through different MA filters is illustrated in Figure 2.4.

The 100ms-long MA filter is therefore used in this research, because it offers the best compromise between extrema-baseline contrast and baseline removal. The method used to remove the average value of a signal over a N-sample-wide time window (high-pass filtering) is defined:

$$FilteredECG[T] = ECG[T] - \frac{\sum_{i=T-N}^{T} ECG(T)}{N} \tag{2.1}$$

where T is the current discrete time value in samples, and N is the size of the

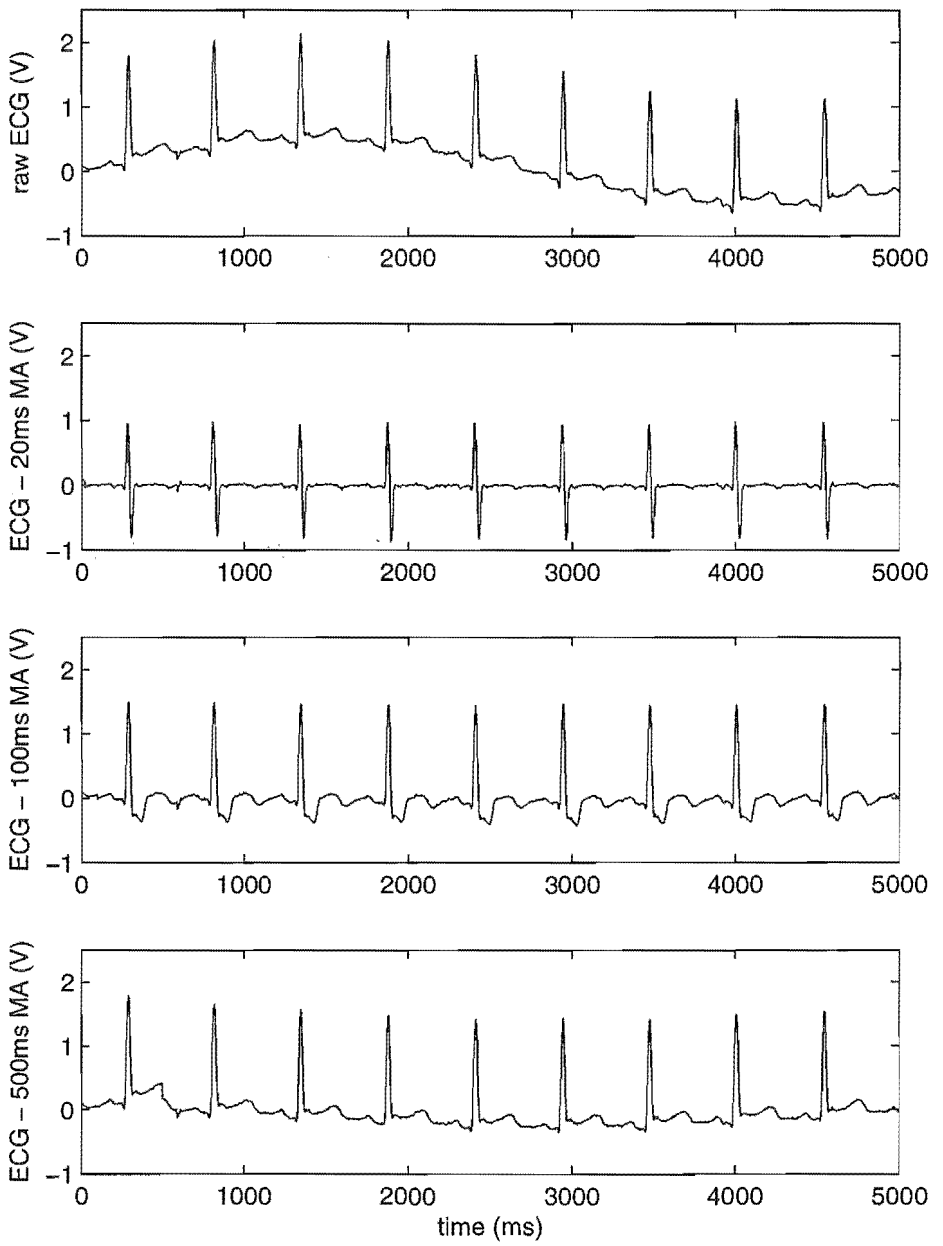

Figure 2.4 comparison between different Moving Average lengths.

moving average window, also measured in samples. This filter requires N samples to initialize in a real-time application. The ECG signal is sampled at a frequency of 250Hz, and the MA filter is 100ms long therefore $N = 25$ samples.

This high-pass filter distorts the shape of the waves in the ECG signal. However, it does not modify the latency of these waves and the goal of this signal-

processing stage is to facilitate the detection of R wave peaks time locations, to compute the tachogram. Therefore, this distortion is not significant and high-pass filtering offers an effective method of R peak detection.

The second method of ECG pre-processing uses wavelet transform. The wavelet transform is a time-frequency decomposition very suitable for non-stationary signals, including most real world signals composed of varied structures with different periods. It is used in many signal-processing areas, such as feature detection, denoising and compression of signals such as audio or video records. It is particularly suitable for frequency domain analysis when the Fourier transform can be limited by the non-stationarity of the signal to be processed [Mallat, 1999].

A wavelet transform associates a given signal with a sum of translated and dilated wavelets forming a *wavelet family* or *wavelet basis*. A wavelet is a function ψ that belongs to $L^2(\mathbb{R})$, which means the wavelet follows the finite energy condition, with an average value of zero.

$$\int_{-\infty}^{+\infty} |\psi(t)|^2 dt < +\infty \tag{2.2}$$

$$\int_{-\infty}^{+\infty} \psi(t) dt = 0 \tag{2.3}$$

Wavelet functions are normalized $||\psi|| = 1$, and centered around $t = 0$. A family of wavelets, or time-frequency elements, is obtained from a mother (initial) wavelet scaled by s in width, and translated by τ over time, to cover the entire time-frequency plane. The complete definition is therefore given as:

$$\psi_{\tau,s}(t) = \frac{1}{\sqrt{s}} \psi\left(\frac{t-\tau}{s}\right) \tag{2.4}$$

The wavelet transform (WT) of a signal $f(t)$, at time τ and scale s is denoted $Wf(\tau, s)$ and is defined as an integral or a convolution product.

$$Wf(\tau, s) = \int_{-\infty}^{+\infty} f(t) \frac{1}{\sqrt{s}} \psi^*\left(\frac{t-\tau}{s}\right) = f \star \overline{\psi}_s(\tau). \tag{2.5}$$

where ψ^* is the complex conjugate of ψ. The convolution product $\star$ of two functions is defined.

$$f(t) \star g(t) = \int_0^t f(t-\tau)g(\tau)d\tau = \int_0^t f(\tau)g(t-\tau)d\tau \tag{2.6}$$

$\overline{\psi}_s(t)$ is defined:

$$\overline{\psi}_s(t) = \frac{1}{\sqrt{s}}\psi^*\left(\frac{-t}{s}\right) \tag{2.7}$$

Defining $\hat{\psi}(\omega)$ as the Fourier transform of ψ at frequency ω, the Fourier transform of $\overline{\psi}_s(t)$ is defined:

$$\hat{\overline{\psi}}_s(\omega) = \sqrt{s}\hat{\psi}^*(s\omega) \tag{2.8}$$

Using Equation (2.3), the Fourier transform at frequency $\omega = 0$ is defined:

$$\hat{\psi}(0) = \int_{-\infty}^{+\infty} \psi(t)dt = 0 \tag{2.9}$$

Therefore the Fourier transform of a wavelet is the transfer function of a band-pass filter whose band is shifted along the frequency range by the scale s. The Meyer wavelet and its Fourier transform are illustrated in Figure 2.5, where the frequency band is clearly seen in the right panel. The wavelet transform is therefore a band-pass filter, whose frequency band is defined by the scale of the wavelet.

In this thesis, as well as a part of the literature available on wavelet transform, the scale s is defined so that the smaller the scale, the narrower the wavelet in the time domain, the higher and wider the corresponding frequency band, and vice-versa [Couderc et al., 2000]. However, it is possible to encounter the opposite definition of the scale factor $s' = 1/s$ where the higher the scale s', the higher and wider the frequency band, and the narrower the time domain wavelet. Therefore, it is critical to ensure that the same definition of the scale is consistent along the

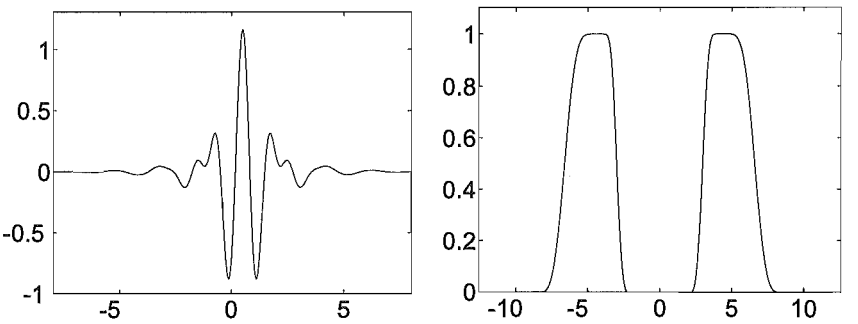

Figure 2.5 Meyer wavelet $\psi(t)$ and its Fourier transform modulus $|\hat{\psi}(\omega)|$.

whole wavelet transform.

The uncertainty principle [Mallat, 1999] states that the only way to increase the resolution in time, when using a time-frequency transform is to decrease the resolution in frequency, and vice-versa. The coverage of the time-frequency plane by two wavelets of different translation and scale is illustrated in Figure 2.6, where the mother wavelet $\psi_{u,1}$ (translation u, scale 1) covers a time-frequency area that is σ_ω radians per second (rd/s) wide along the frequency axis and σ_t seconds wide along the time axis. The resulting daughter wavelet of scale s covers an area that is σ_ω/s rd/s wide along the frequency axis and $\sigma_t \times s$ second wide along the time axis. This figure illustrates the uncertainty principle, as the wavelets all cover the same time-frequency area of $\sigma_\omega \times \sigma_t$ radians. The coverage of the time-frequency plane by an entire wavelet family is illustrated in Figure 2.7.

This uncertainty principle therefore limits most time-frequency distributions, including the short-time Fourier transform STFT, because different frequency bands may require different resolutions in time and frequency. However, unlike most other time-frequency transforms, the wavelet transform allows for the allocation of different time and frequency resolutions across the time-frequency plane. This behaviour is determined by the family of time-frequency atoms, another name for the wavelets, and provides a better time-frequency plane partitioning (see Figure 2.7) for most real world signals, which typically contain long periods of low frequency components and short periods of high frequency components [Mallat, 1999]. As a result, the transform needs good time resolution for high frequency components , and a lower time resolution is suitable for low frequency components, which can in turn benefit of a higher frequency resolution. This versatile definition of time frequency resolutions is a key feature of wavelet transforms that overcomes a strong limitation of the Short Time Fourier Transform

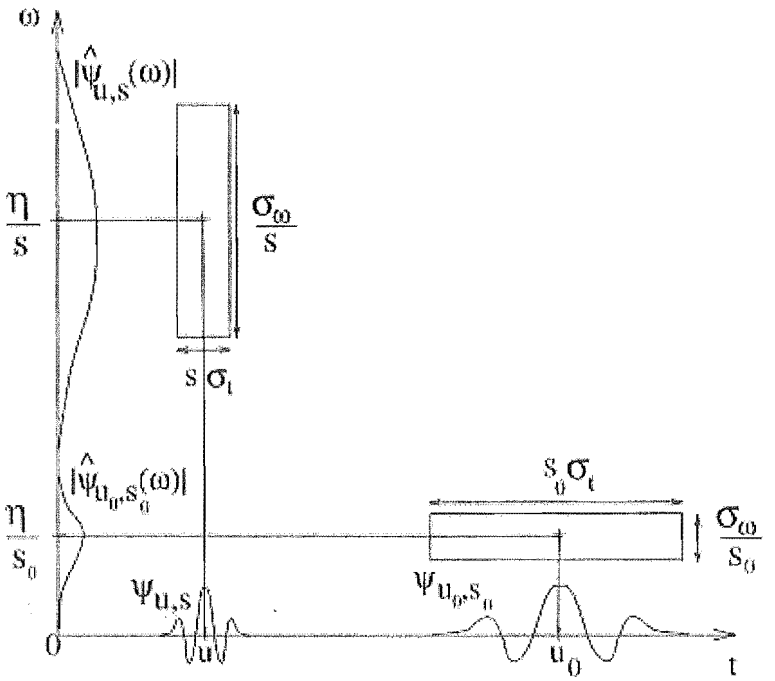

Figure 2.6 Time-frequency boxes of two wavelets $\psi_{u,s}$ and ψ_{u_0,s_0} [Mallat, 1999]

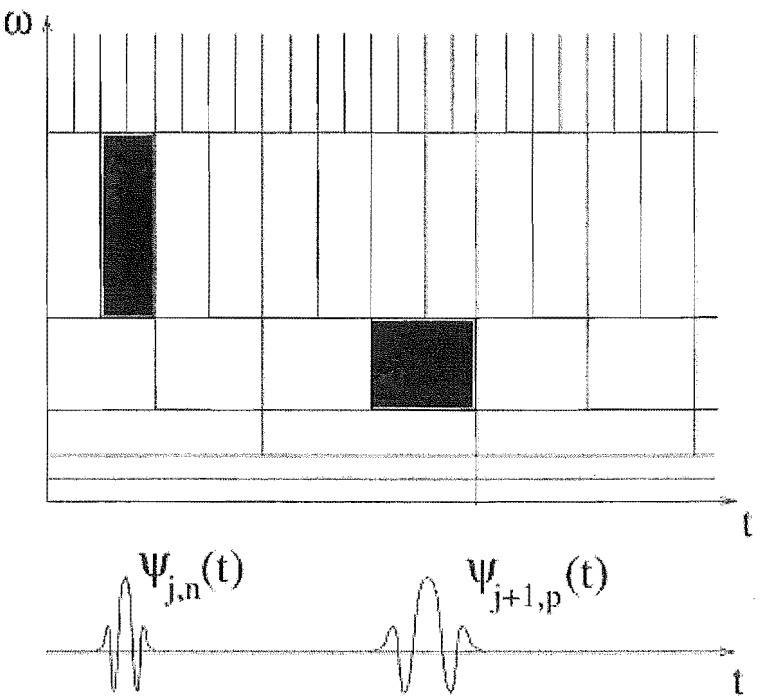

Figure 2.7 The time-frequency boxes of a wavelet family define a tiling of the time-frequency plane [Mallat, 1999]

(STFT) [Wiklund et al., 1997].

In this case, the ECG signal is non-stationary because different waves occur at different times in the ECG period, and each wave contains a different frequency spectrum. However, the aim of this signal processing step is not to obtain the frequency spectrum of the ECG signal over time, but to detect a particular wave. Therefore, the ECG signal does not need to be decomposed by an entire family of wavelets with different scales, but rather the wavelet whose frequency band best matches the spectrum of the R wave. This simplification significantly reduces the computational intensity, compared with other methods that use a whole wavelet family to cover the entire time-frequency plane and enhance the detection process [Bahoura et al., 1997].

The shape of the ECG signal allows the use of wavelets with different shapes and properties. For instance, Bahoura et al. [Bahoura et al., 1997] perform ECG waveform detection with a quadratic spline wavelet family. Another method is developed by Couderc et al. [Couderc et al., 2000] to analyze the ECG signal with a Meyer wavelet family, the mother wavelet of which is shown in Figure 2.5.

The Haar mother wavelet is used in this research and is shown in Figure 2.8. This wavelet is the simplest shape available and therefore the least computationally intense. It has also been successfully used for R wave detection by Chase et al. [Chase et al., 2004c].

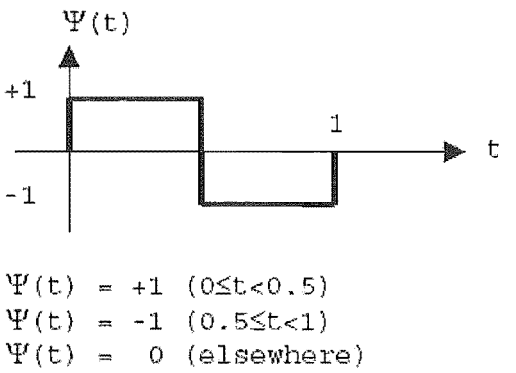

Figure 2.8 Haar mother wavelet.

The best scale for the wavelet is obtained by first decomposing the ECG signal with a whole family of wavelets. This approach is illustrated in Figure 2.9 by the time-frequency distribution of a noisy ECG signal given by the Haar WT for scale s in the range 1–1000, at a sampling rate of 1kHz.

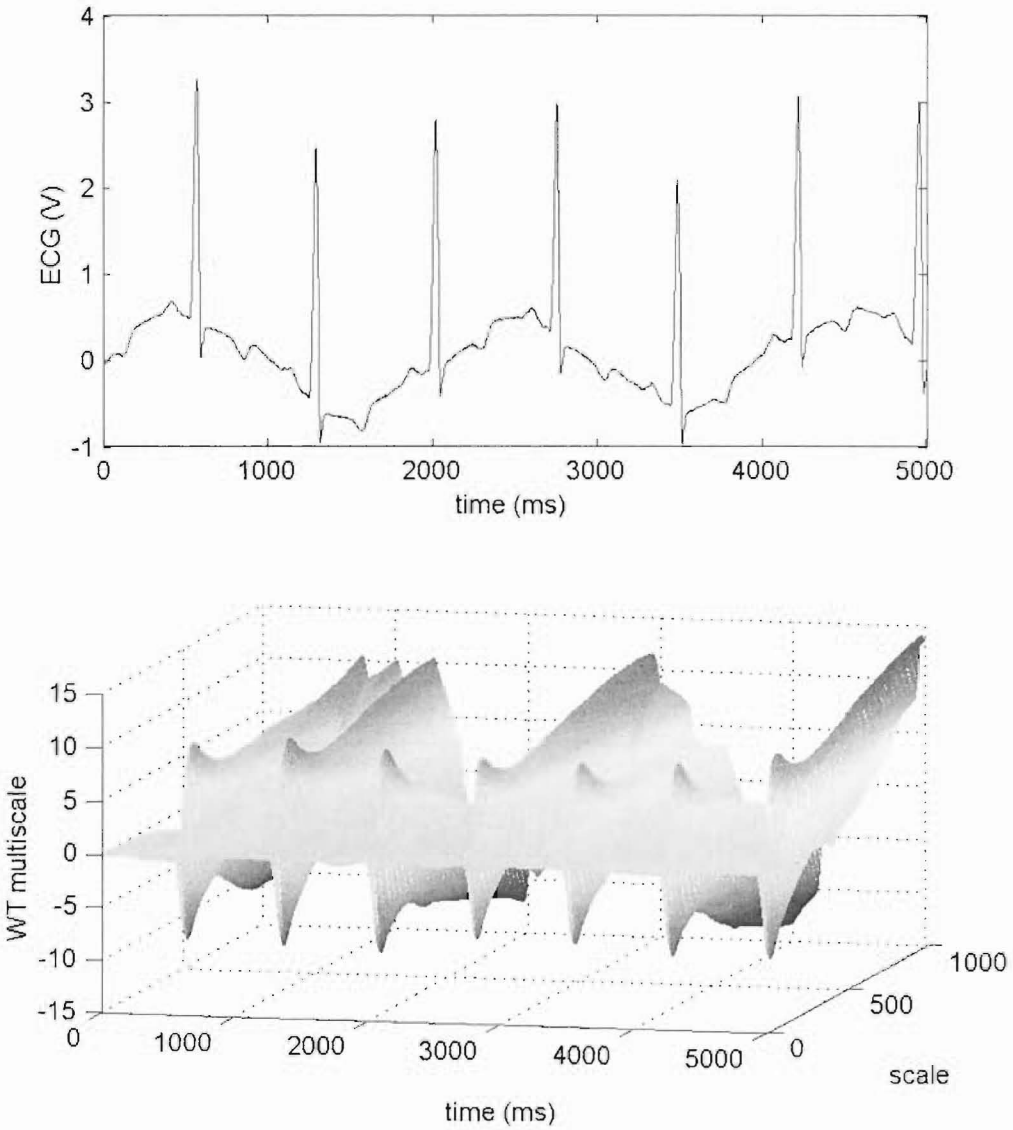

Figure 2.9 ECG signal with floating baseline and its Haar family wavelet transform.

The frequency spectrum of the analyzing wavelet is shifted towards lower frequencies as its scale s is increased. It is simpler to find the optimal scale from the wavelet family by sectioning the 3D time-frequency distribution and observe the contrast offered by the wavelet transform of different scales. Figure 2.10 displays the WT of the ECG signal by Haar wavelets of scale 1, 8, and 500.

The scale 1 wavelet transform does not produce large coefficients for any waves, because this wavelet contains frequencies higher than the entire spectrum

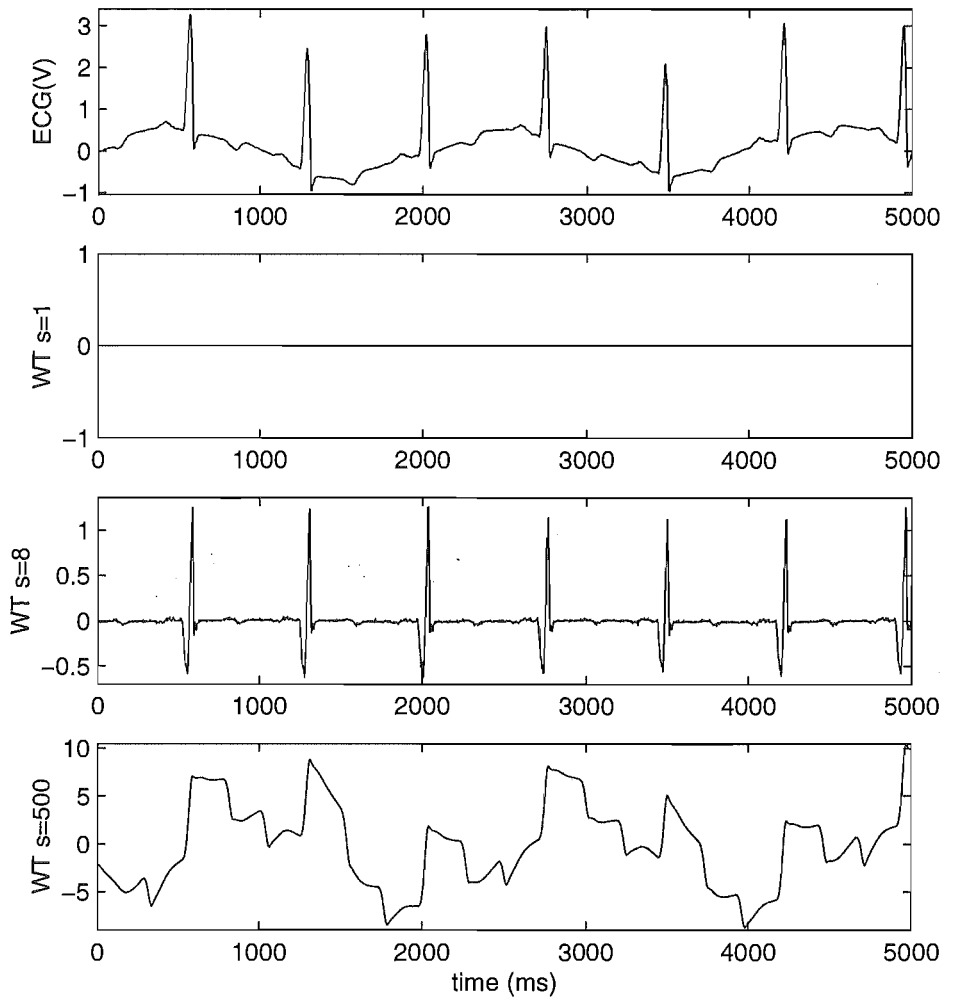

Figure 2.10 Wavelet transform of the ECG signal with different scales.

the ECG signal. As the scale increases, the frequency spectrum of the wavelet shifts towards lower frequencies. These lower frequencies progressively match some waves of the ECG signal, and the baseline of the ECG, as the scale increases. The output coefficients of a wavelet transform of scale 500 are plotted in the fourth frame of Figure 2.10. The wavelet transform at this scale emphasises the low-frequency baseline of the ECG signal. Therefore this scale is too high for the detection of R waves.

Starting at scale 1, the R wave is expected to be the first detected as the scale increases, because it is the sharpest and shortest wave of the ECG period,

so it contains the highest frequencies of the ECG signal. As the scale is increased, the wavelet and the R wave frequency spectra better match and the contrast of the wavelet transform between the R waves and the rest of the ECG signal is optimal with a scale $s = 8$, as shown in Figure 2.9. In other words, the daughter wavelet of scale 8 produces large coefficients when a R wave occurs, while the coefficients are small for the other components of the ECG signal, which are considered as noise in this context. If the scale is bigger than 8, the contrast is not enhanced because other waves also result in large wavelet coefficients and the contrast between different waves is therefore reduced. Figure 2.9 illustrates that higher scales wavelet transform detects other waves first, and then the baseline of the ECG, which correspond to lower frequency bands that the sharp R wave. Finally, the wavelet transform performed with a daughter wavelet of scale 8 is implemented in this research, as shown in the third frame of Figure 2.10.

The wavelet transform of the ECG signal allows the R wave peak detection, since there is no baseline shift or unwanted artifacts. The wavelet transform method also isolates the R peaks from other components of the ECG signal. In this context the difference of performance between high-pass and band-pass (wavelet transform) filtering is not obvious, because there is no high-frequency noise. However, in a different environment surrounded by many devices and sources of high frequency noise, the advantage of band-pass filtering over high-pass filtering would be more significant. The wavelet transform may be more complex theoretically and computationally, but the higher-level processing is simplified, which is critical in real-time environment. The R waves are now emphasized from the rest of the ECG signal, and peak detection can be applied to obtaining the tachogram, HR and subsequent metrics for the quantification of patient agitation.

2.2.2 R peak detection

To begin R peak detection, an initialisation routine first determines the maximal and minimal values of either the smoothed ECG signal, or the wavelet transform coefficients, as well as its variance and corresponding standard deviation. The variance (σ^2) and corresponding standard deviation (σ) are common measures of the fluctuations of a signal x around its mean value $\bar{x}$. The standard deviation

of the signal x over a N-sample-long time window is defined:

$$\sigma = \left[\frac{\sum_{i=1}^{N} (x(i) - \bar{x})^2}{N} \right]^{1/2} \tag{2.10}$$

Once the extrema and the standard deviation of the signal are evaluated, it becomes possible to determine a peak detection threshold, above which an R peak is expected. This threshold has to be determined carefully, or the system detects a local extremum, which may not correspond to a relevant R peak, and provide false results. Thresholds have been determined using the following two methods.

Method 1: Utilising the values of both extrema.

$$threshold1 = min(ECG) + \alpha \times (max(ECG) - min(ECG)) \tag{2.11}$$

where α is a scalar determined empirically from clinical trials and is set between 0.5 and 0.6 depending on the condition of the patient.

Method 2: Using the minimal value of the filtered ECG signal and its standard deviation (Equation 2.12).

$$threshold2 = min(ECG) + \alpha \times \sigma \tag{2.12}$$

σ is defined in Equation 2.10 and α is a constant scalar determined empirically and set between 2 and 2.5 depending on the patient physiology. Once the peak detection threshold is determined using Equation (2.11) or (2.12), the processing starts. The R peaks are detected, and their amplitudes and location in time are stored. Every new R peak triggers the computation of HR and corresponding derived metrics. Every new R peak is used to update the tachogram, HR, and other derived metrics, along with the detection threshold. This is known as the adaptive threshold method, and it is very important since the spectral content of the ECG varies with the heart rate, and the corresponding wavelet transform amplitude may fluctuate. Hence, an adaptive threshold is required to process the

ECG signal during an event of agitation when HR may fluctuate.

Figure 2.11 illustrates the peak detection algorithm. The value of sample 1 is below the threshold and its magnitude and position are not recorded in the temporary buffers. The system does not record anything as long as the amplitude of the signal remains below the threshold. The amplitude of sample 2 is greater than the threshold and therefore its value and position are recorded for further analysis. The temporary buffers are overwritten with the amplitude and time position every time a new sample with a greater amplitude is acquired. Therefore, these buffers are overwritten after the acquisition of every new sample until the acquisition of sample 3, which corresponds to the local maximum and desired R peak.

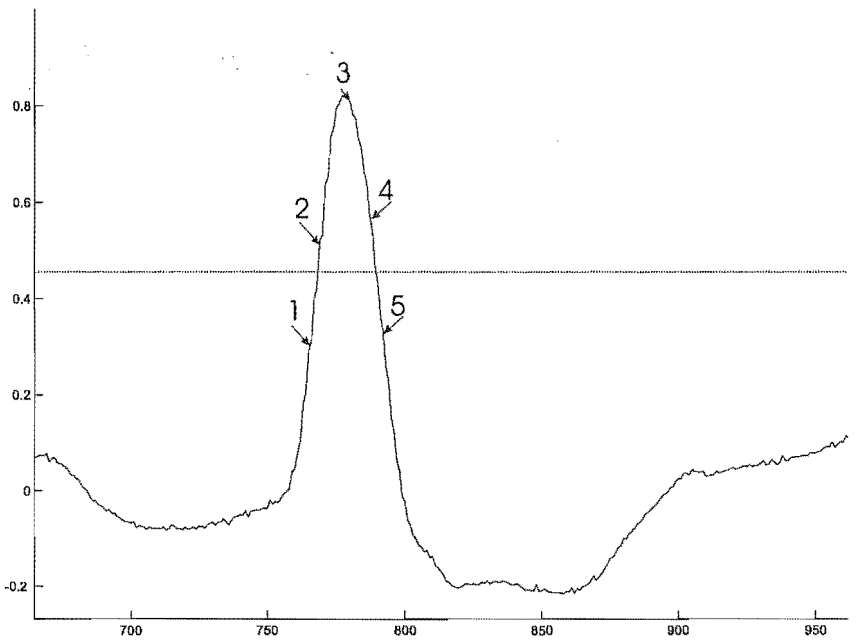

Figure 2.11 The different steps of the R peak detection in the ECG signal.

However, it is crucial not to validate the potential R peak at this stage because the system may encounter a false maximum. In fact, the signal can potentially decrease during a few samples after a false maximum, before rising to the relevant R peak. This behaviour can be due to several high frequency noise sources, including some patient motor activities that distort the ECG signal through the electrodes and skin conductivity, producing unwanted artifacts. This last point is critical for monitoring patient agitation which is often accompanied by significant patient motion.

Therefore, the amplitude and time position of sample 3 are recorded in the temporary buffer, and the process continues. The acquisition of sample 4 does not overwrite the temporary buffer because its amplitude is not greater than sample 3. Finally, the signal falls below the R peak detection threshold, and the system validates sample 3 as an R peak.

It is important to record both the amplitude and time position of each R peak. The amplitude is required to detect maxima, whereas the time position is required to compute the tachogram signal. The addition of hysteresis on the threshold (the signal needs to exceed 105% and drop below 95% of the threshold level) removes more artifacts than the use of a simple threshold to detect R peaks. Once the signal falls below half the threshold, this threshold is updated with the latest R peak as a maximum for the next R peak detection, also referred to as dynamic or adaptive threshold method.

There are two possible outcomes when a new R peak is validated. If it is the first R peak detected in the processing cycle, the system waits for the R peak. However, if previous R peaks have already been detected, the new R peak is used to update the tachogram. The result of the entire R-peak detection process is illustrated in Figure 2.12. The top frame displays the ECG signal and its fluctuating baseline. The second frame shows the wavelet transform performed by an Haar wavelet of scale 8, and the detection adaptive threshold based on signal statistics. The bottom frame displays the resulting tachogram, which consists of consecutive RR time intervals. Note that the tachogram starts after the detection of the second R-peak, which allows the first RR time interval computation.

Finally, a discrimination rule is implemented when validating a new RR interval. Two consecutive RR intervals shall not differ by more than 30%, in an attempt to filter artifacts due to premature beats. However, this rule can exclude some important data, particularly on patients with special heart dynamics such as atrial fibrillation [Huikuri et al., 1999], where two consecutive RR intervals may differ by more than 30%. Therefore, this research includes all RR intervals within physiological range, whether differing by more than 30%, and patients with atrial fibrillation are possibly assessed by this agitation sensor without the removal of this important data.

The combination of high-pass filtering or wavelet transform, with peak de-

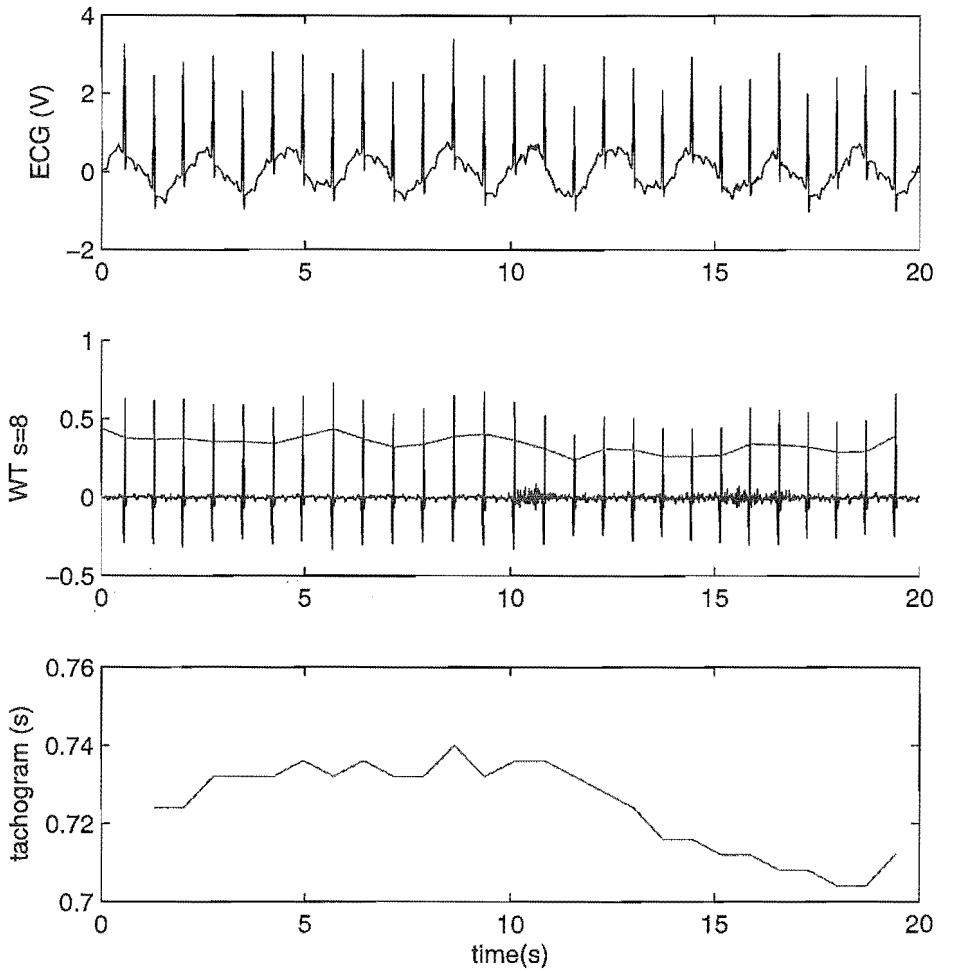

Figure 2.12 Tachogram derived from WT threshold method applied on ECG signal with baseline shift.

tection provides an efficient method to compute the tachogram from the ECG signal. This method minimises error and computational burden. Once the RR intervals are obtained, it becomes possible to compute the heart rate and other metrics derived from the ECG.

2.2.3 Heart rate

The instantaneous heart rate, HR, is the first metric of interest computed from the tachogram. It measures the pace at which the heart is beating, in beats per minutes (bpm). An instance of the tachogram and related HR is shown in Figure

2.13. The conversion from the RR interval to instantaneous HR is defined.

$$HR(bpm) = \frac{60}{RR(s)} \tag{2.13}$$

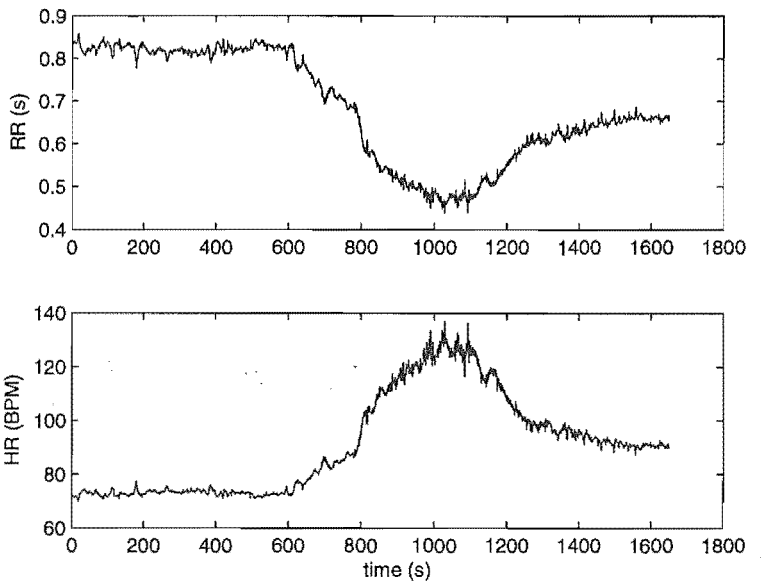

Figure 2.13 tachogram and instantaneous HR.

The expected range of the instantaneous HR is calibrated based on reported physiological data for critical care patients. The possible physiological range is defined:

$$50 < \text{HR (BPM)} < (220 - \text{patient's age (years)}) \tag{2.14}$$

While this value may restrict some individuals with very slow HR, no significant data should be lost with respect to critical care patient agitation.

The instantaneous HR can also be averaged over a few seconds depending on interest. The global agitation sensor is implemented on a patient on a long term basis, typically up to several days. The sedation infusion rate that is based on agitation feedback is typically updated from every minute to every hour [Rudge et al., 2004]. Therefore, there is little direct interest in the rapid beat-to-beat trend of the instantaneous HR in this context of agitation measurement for sedation management.

To smooth these fast fluctuations, the instantaneous heart rate can be processed through a moving average (MA) window, in which the HR values are summed up along a shift register and then divided by its time length. This process yields a smoothed HR metric. The size of the moving average window is defined to give a good compromise between smoothness and delay. If the moving average is computed using a short time window, then the resulting average HR signal will not be smoothed enough, and fast oscillations propagate to the final agitation index. Similarly, an unwanted delay will propagate between the time a physiological signal starts to respond to a symptom and the averaged signal shows that evolution. This delay could involve that the final system forecasts an event of agitation after its occurrence.

Patient specific cardiac conditions, such as atrial fibrillation or other dysrhythmias, also create complex HR dynamics. Their discrimination can improve the accuracy of the final diagnostic tool [Guyton and Hall, 1996]. Therefore, the instantaneous HR values may be potentially useful to characterize patients with specific symptoms. Because the instantaneous HR may improve the diagnosis, it is possible to employ another technique to smooth the output signal. The HR metrics is directly obtained from the instantaneous HR, that is the inverse of every RR interval. Then the fast fluctuations will propagate towards the output agitation index, and this output signal can be averaged. This enables a simpler control of the delay propagation than using a moving average filter on each metric. Further improvement of the agitation sensor may confirm the need to use either the instantaneous or averaged HR values. Currently the instantaneous HR value is used exclusively.

2.2.4 Summary on ECG and agitation

There is a wide variety of methods available in the literature to perform heart rate detection and computation with advantages in complexity and performance, but drawbacks in noise sensitivity and computational burden. This initial processing stage aims to perform real-time detection of heart rate in a noisy environment, with the best possible tradeoff between simplicity and noise sensitivity. The bandpass filtering of the ECG signal by a wavelet transform combined with adaptive thresholding is the most reliable method implemented in this research.

The computational burden is decreased by using a single scale wavelet transform with adaptive threshold, as opposed to a complete time-frequency distribution performed by a whole wavelet family. The threshold level is determined from extreme values rather than statistics, which require the update of a large time window shift register possibly heavy in real-time.

This tradeoff allow the signal-processing to run in real time, and strongly rejects low and high frequency noise encountered with ICU agitated patients. The information extracted from the ECG is combined with the information derived from the dynamics of the heart, and other inputs of the agitation sensor.

Chapter 3

Heart rate derived measures

The instantaneous and averaged HR values, presented in Chapter 2, are combined in this research with signal dynamic metrics derived from the heart rate variability (HRV) and heart rate derivative (HRD) methods. HRV is a means to associate the dynamics of the heart with the autonomic nervous system (ANS), which regulates the cardiovascular functions on a beat-to-beat basis. The ANS is composed of the sympathetic and para-sympathetic nerves, also known as the vagi, shown in Figure 3.1. HRV examines the beat-to-beat variations of RR intervals using spectral decomposition, statistical time domain analysis, or non-linear methods. The HRV method has been used by other research groups to quantify the level of anxiety [Inagaki et al., 2004] and pain [Lindh et al., 1997] of patients in various conditions. Therefore, anxiety and pain in the context of ICU agitation may also be evident in HRV metrics, and thus measured by examining HRV.

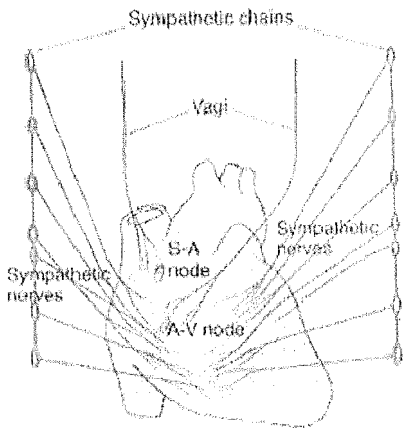

Figure 3.1 Autonomic nervous system [Guyton and Hall, 1996].

The different trends of the heart are observed using temporal, spectral or non-linear HRV decomposition. Spectral analysis can be performed using parametric or non-parametric algorithms. The long-term trend of the heart is emphasised

by the HRD method. The benefits and drawbacks of these different methods are discussed in this chapter. Results obtained from other research using the HRV method are reviewed, and the findings of HRV and HRD methods implemented in this research on ICU patients are presented and discussed.

3.1 Time domain HRV

Time domain HRV parameters are calculated directly from the tachogram. Initially, the mean and the standard deviation of the RR intervals are evaluated. The standard deviation of the RR intervals (SDRR) focuses on the overall evolution of the tachogram [Rajendra Acharya et al., 2004], whereas the standard deviation of the differences between consecutive RR intervals (SDdRR or SDSD) tracks the short-term fast variations [Niskanen et al., 2004].

RR50 and pRR50 are other common time domain HRV metrics [Gold et al., 2000]. RR50 is the number of consecutive RR intervals differing by over 50ms over a fixed time window. pRR50 is the percentage value, which is RR50 divided by the total number of RR intervals in the segment of tachogram analysed. The 50ms deviation represents a 5% variation at 60bpm and a 10% variation at 120bpm. It is worth noting that the RR interval can also be referred to as the Normal-to-Normal (NN) interval [Huikuri et al., 1999], and this notation gives the following temporal HRV notation and indices: SDNN, SDdNN, NN50 and pNN50. In practice, RR and NN time intervals are similar.

Additional information is available from geometric measures such as the RR triangular index and the TIRR, derived from the statistical histogram [Niskanen et al., 2004]. The RR triangular index is the integral of the RR interval histogram divided by the maximum value of the histogram. The TIRR, or TINN, is the baseline width of the RR interval histogram, in ms. The HRV-related information obtained from the statistical analysis of the tachogram is summarized in Table 3.1. Such a table is the common output of HRV temporal analysis software, such as the package designed by Niskanen et al. [Niskanen et al., 2004].

The time domain HRV metrics all contain important clinical information, and they can be compared to spectral HRV metrics for consistency. In particular, the short-term high frequency (HF) component of spectral HRV analysis is directly

Table 3.1 Variables derived from temporal HRV analysis

Variable	Units
Statistical Measures	
Mean RR	(s)
SDRR	(s)
Mean HR	(min^{-1})
SDHR	(min^{-1})
SDdRR	(s)
RR50	(count)
pRR50 (%)	
Geometrical Measures	
RR triangular index	
TIRR	(s)

proportional to SDdRR [Baynard et al., 2004], and the long-term low frequency (LF) component of the spectral method corresponds to the SDRR metric of the temporal method [Terathongkum and Pickler, 2004].

Time domain HRV metrics are especially robust to noisy conditions and do not require data pseudo-stationarity. Therefore it offers interesting characteristics in the agitation sensing context of this research where it is practically impossible to study pseudo-stationary data due to the constantly varying condition of the patients in critical care. Both time and frequency HRV methods provide metrics that focus on short-term and long-term variations, and both methods can therefore be applied and compared in the same context to increase the consistency and repeatability of the HRV analysis.

3.2 Frequency domain HRV

HRV analysis can be performed in the frequency domain after spectral decomposition. This task requires the tachogram to be processed by a frequency transform. In this approach, clinical information is obtained from the power contained in the different frequency bands of the power spectral density (PSD) that correspond to activity from different parts of the ANS. However, the tachogram is irregularly sampled, because the time between two heart beats is variable. Consequently, the PSD of the tachogram has a frequency scale in cycles per beat rather than cycles

per second (Hz). This phenomenon has to be taken into account or misleading results can be obtained from the PSD.

This irregular sampling issue may be overcome by interpolating the signal to produce a regularly sampled time series, before the frequency transform is applied to the series. Otherwise, the PSD may be biased and thus the HRV parameters extracted from it [Niskanen et al., 2004]. Other researchers do not interpolate the tachogram and compute a PSD in cycles per beat instead of Hertz [Bianchi et al., 1993; Pagani et al., 1986; Pfeiffer and Netzer, 1997]. This method is preferred for this research, according to a simple philosophy that the heart beat is the fundamental rhythm of all cardiovascular functions. Cammann et al. [Cammann and Michel, 2002] also suggest that rigid frequency band definitions are unsuitable for correct spectral analysis of HRV because these rigid bands do not reflect physiological realities of cardiovascular regulations. Therefore, it makes sense to base the frequency transform on the heart beat that gives a frequency unit of cycles per beats. It is also verified empirically when computing the frequency transform at different heart rates and therefore different sampling frequency. For example, Bianchi et al. [Bianchi et al., 1993] do not interpolate the tachogram, but they still produce the tachogram PSD with a frequency scale in Hertz, although it is accurately cycles per beat and not Hertz.

Having dealt with the issue of irregular sampling by interpolating the tachogram or not, the PSD is then calculated using parametric (Auto-Regressive models) or non-parametric (Fourier Transform based) methods. The success of parametric methods strongly depends on the choice of the parameters [Kuusela et al., 2003]. Ultimately, validation of the tachogram HRV analysis should be done concurrently using the results from different HRV methods.

3.2.1 Non-parametric method

The non-parametric approach computes the PSD of the tachogram from its Digital Fourier Transform (DFT) or Short Time Fourier Transform (STFT). The

digital Fourier transform is defined.

$$X(k) = \sum_{n=0}^{N-1} x(n) \times e^{-\frac{j2\pi kn}{N}} \qquad for \;\; k = 0, 1, \ldots, N-1 \tag{3.1}$$

where $x(n)$ is the n^{th} sample of the digital tachogram sampled at frequency f_s, N is the size of the time window, in samples, on which the Fourier transform is performed, k is the digital frequency index and the corresponding discrete frequency $f(k)$ is defined:

$$f(k) = k \times \frac{f_s}{N} \tag{3.2}$$

where f_s is the sampling frequency of the tachogram, $X(k)$ is the component of the Fourier transform of the tachogram $x(n)$, at frequency $f(k)$ defined in Equation (3.2). The Fourier transform is described by its complex magnitude with phase in the spectral domain, and the PSD is a conversion into power dimension that consequently ignores the phase information of the signal. The computation of the PSD from the magnitude of the frequency transform is defined.

$$PSD(k) = \frac{(X(k))^2}{N} \tag{3.3}$$

Note that the PSD components are normalised by N so the PSD does not vary with the sample size.

The Fourier transform applied on the entire time series loses the time location of the spectral components so it may detect an event, but cannot localise it in time. Hence, long term Fourier transform can be problematic for continuous monitoring. This is overcome using the STFT, which corresponds to a Fourier transform applied over a short time window, and translated along the entire tachogram. However, the time and frequency resolution of the short window is a drawback. More details on the limitations of non-parametric spectral HRV methods are described in detail by Starfinger et al. [Starfinger et al., 2003]. The limitations of the non-parametric methods encourage the use of parametric spectral HRV methods in this research. Finally, some researchers [Niskanen et al.,

2004; Kuusela et al., 2003] compute both parametric and non-parametric spectral methods concurrently to increase the consistency of their results, as well as to determine the optimal order of the parametric method. This research focuses on the AR parametric method based on the findings and recommendations of previous work on agitation sensing using HRV [Chase et al., 2004c; Lam, 2003; Kuusela et al., 2003].

3.2.2 Parametric method

The Auto-Regressive parametric method is chosen among others. The popularity of AR PSD estimation is due to the high-resolution and easy-to-compute linear equations used to update the model coefficients [Starfinger, 2003]. The AR method illustrated in Figure 3.2 consists of estimating the next sample of the tachogram signal from a weighted sum of previous samples. The difference between the sample and its estimation by the AR filter is the estimation error, assumed to be a white noise. The error variance is used to update the AR coefficients. The AR PSD estimation is performed using a Kalman filter with infinite impulse response (IIR) [Aboy et al., 2004; Kuo et al., 2002; Piovoso and Laplante, 2003; Simon, 2003].

$$\hat{x}(n) = \sum_{k=1}^{p} a_k \times x(n-k) \tag{3.4}$$

Where $x(n)$ is the n^{th} sample acquired, p is the order of the Kalman filter, and it corresponds to the number of previous samples used to estimate the new sample. Further, $x(n-k)$ is the k^{th} previous sample, a_k is the weight of sample $(n-k)$ in the estimation, also called the AR coefficients and $e_f(n)$ is the forward prediction error at time step n. It corresponds to the difference between the a-priori estimate $\hat{x}(n)$ and the actual value of sample $x(n)$.

$$x(n) = \hat{x}(n) + e_f(n) = \sum_{k=1}^{p} a_k \times x(n-k) + e_f(n) \tag{3.5}$$

The error variance is used along with the AR coefficients to determine the

PSD of the tachogram. Figure 3.2 is a diagram of the calculations involved to estimate $\hat{x}(n)$ from the p previous samples. The PSD is therefore estimated on a sample-to-sample basis, making it very suitable for real-time continuous processing of non-stationary signals.

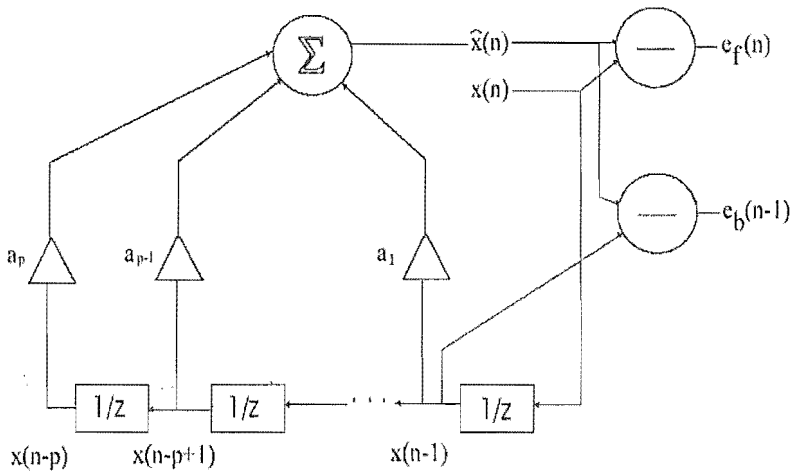

Figure 3.2 Diagram of AR filter. The filter estimates the sample $Y(n)$ a-priori from the p previous samples, and compares the estimation with the acquired sample a-posteriori to update the AR coefficients a_k.

The forward prediction error e_f is defined as the difference between a new sample $x(n)$ and its a-priori estimation $\widehat{x}(n)$:

$$e_f(n) = x(n) - \widehat{x}(n) = x(n) - \sum_{k=1}^{p} a_k \times x(n-k) \tag{3.6}$$

The new sample $x(n)$ is used to a-priori estimate the next sample $\widehat{x}(n+1)$. The backward prediction error e_b is defined as the difference between the new sample $x(n)$ and the estimation of the next sample $\widehat{x}(n+1)$.

$$e_b(n) = \widehat{x}(n+1) - x(n) = \sum_{k=1}^{p} a_k \times x(n-k+1) - x(n) \tag{3.7}$$

Both forward and backward errors along with a forgetting factor ω are used to update the coefficients a_k of the AR filter. The forgetting factor is weighting the

error vectors exponentially to attach more importance to the latest error values when updating the AR filter.

Note that some references in the literature use a different sign convention to define the AR estimation method of Equation (3.4), which consequently changes the sign of the AR coefficients. This doesn't change the final PSD as long as the same sign convention is kept throughout the whole algorithm.

A model of order p relies on $(p+1)$ coefficients. The model updates the coefficients a_1 to a_p whereas the coefficient a_0 is set to 1 before the whole vector a_f of size $(p+1)$ is Fourier-transformed to produce the PSD. However, the sign of the vector a_f components differs depending on which sign convention is used. Therefore, the PSD estimation will be computed from the following vector if the sign convention defined in Equation (3.4) is used [Marple, 1987; Starfinger, 2003]:

$$a_f = [1 \quad -a_1 \quad \ldots \quad -a_p] \tag{3.8}$$

The following vector is employed if the opposite sign convention is used [Bianchi et al., 1993].

$$a_f = [1 \quad a_1 \quad \ldots \quad a_p] \tag{3.9}$$

This confusion leads to a erroneous PSD if the sign conventions are mixed.

A PSD is then evaluated for every new sample.

$$PSD_n(k) = \left\| \frac{\sigma^2(n)}{A_n(k) \times f_s} \right\| \tag{3.10}$$

where $PSD_n(k)$ is the k^{th} component of the PSD at frequency $f(k)$ defined in Equation (3.2), after the update from the n^{th} sample, $\sigma(n)$ is the standard deviation of the estimation error $e(n)$ after the update from sample n, f_s is the sampling frequency, and $A_n(k)$ is the Fourier transform of the AR coefficients vector a_f, after update by sample n. The PSD estimation defined in Equation

(3.10) is a simplified version of the algorithm developed by Ljung [Ljung et al., 1978] because the signals analysed in this research are real valued, as opposed to complex.

The AR coefficients are also updated by a new sample, using the vector-based Fast Recursive Least Squares (FRLS) method. Generally, the RLS methods minimise the forward and backward estimation errors [Ljung et al., 1978]. The original version of the RLS method does not enable real-time implementation to update the AR coefficients, because it is based on matrix calculation. The original RLS method requires heavier computing, which can be heavy in real-time for a regular computer. For an AR estimation of order p, each update requires a computing time proportional to p^2 CPU (Central Processing Unit) cycles. Alternatively, the FRLS method developed by Marple [Marple, 1987] performs simple vector updates with less computation time required, proportional to p CPU cycles, and delivers comparable results.

Finally, this spectral parametric approach can deliver significant bias if the AR filter becomes unstable due to the oscillations of a signal that does not reasonably meet the assumption of pseudo-stationarity over the period analysed, which is the main limitation for long-term continuous agitation sensing.

3.2.3 Biomedical meaning of the PSD

The resulting PSD of the tachogram is then split into different frequency bands, and the power and peak frequency of each band is measured. There are three common frequency bands in the PSD. The very low frequencies (VLF) range from 0 to 0.04Hz, the low frequencies (LF) range from 0.04 to 0.15Hz and the High Frequencies (HF) range from the 0.15 to 0.4Hz [Bianchi et al., 1993]. These frequency bands are associated with different parts of the ANS, and hence, different cardiovascular functions [Wiklund et al., 1997].

The LF component is centered around 0.1Hz (10s period) and it has been related to the sympathetic activity, on the basis of pharmacological and clinical experiments [Pagani et al., 1986]. The HF component is found to be synchronized with the respiration rate. Precisely, it is considered to express the respiration disturbances mediated by the vagal activity of the ANS [Bianchi et al., 1993]. The

evaluation of the VLF component requires a long-term study to be meaningful. The scientific community is still divided on whether or not it is due to thermoregulatory factors [Bianchi et al., 1993; Pfeiffer and Netzer, 1997; Kuusela et al., 2003; Seong et al., 2004]. During short-term studies (<24h) the tachogram is detrended, which means the linear trend estimated with best least squares fit is removed, because the power contained in the VLF component of the PSD otherwise masks all other components [Wiklund et al., 1997].

The power related to the LF and HF frequency bands can be expressed in absolute values, logarithmic values, as well as percentage of the total power. The LF/HF ratio and the peak frequency in each band are then used to quantify the sympatho-vagal balance of the ANS, and can also be used to detect events of agitation [Lam et al., 2003; Lam, 2003; Starfinger, 2003].

Figure 3.3 displays PSDs obtained from the AR method and they reveal a good potential to correlate the ANS balance with episodes of agitation. The analysis is performed during a short time window and the VLF component is consequently ignored. Recent work by Lam et al. [Lam et al., 2003] and Chase et al. [Chase et al., 2004c] have revealed a correlation between the LF/HF ratio and the event of agitation as simulated on normal individuals and assessed on ICU patients during clinical trials. The basic concept considered is that as agitation increases, so does HR, and the HF band power decreases. Thus, increased agitation was associated with decreased LF/HF ratio as well as decreased overall HRV power.

Previous studies associate anxiety with the decrease of the overall HRV power [Yeragani et al., 2004]. The overall power of HRV decreases during agitation and the LF/HF ratio increases. These two conditions are compatible if the power in the HF band decreases during agitation. This behaviour is illustrated in Figure 3.3. Some short records on ICU patients allow matching agitation and ANS balance given by the LF/HF ratio.

3.3 Non-linear HRV

The heart is regulated by a variety of complex mechanisms and it is therefore realistic to assume a non-linear component in the heart dynamics. However, many

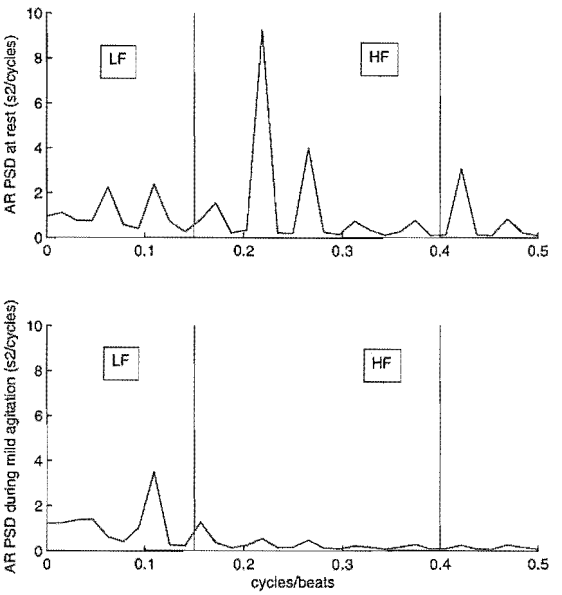

Figure 3.3 HRV analysis with PSD of a patient's tachogram obtained with AR parametric method.

non-linear methods are poorly interpreted and understood. Non-linear methods include the Largest Lyapunov Exponent (LLE), a measure of the non-linearity of a time series. This method is described and implemented by Yeragani et al. [Yeragani et al., 2004]. There is also the Poincaré plot [Niskanen et al., 2004; Rajendra Acharya et al., 2004], a relatively easy-to-compute non-linear graphical method. The Poincaré plot presents the evolution between consecutive RR time intervals, where the x-axis is the RR time interval at time n and the y-axis is the RR time interval at time $n + 1$. The geometry of the Poincaré plot reveals important clinical information. It produces a cloud of spread points, the shape of which mainly depends on the patient clinical condition.

Atrial fibrillation (AF) is a rhythm disturbance of the atria that results in irregular, chaotic, ventricular waveforms. Patients with atrial fibrillation produce a Poincaré plot that resembles a fan. The "fan" becomes wider as medicine is used to control the patient's condition [Paskeviciute et al., 2001]. This change in shape reflects an increase of the instantaneous variation between consecutive RR intervals, corresponding to the HF content of spectral HRV and the SDdRR metrics derived from temporal HRV analysis. Atrial flutter is a rhythm disturbance of the atria that results in regular tachycardic (suddenly rapid) ventricular waveforms. Atrial rates in atrial flutter are generally 240-400 bpm. Patients with

irregular atrial flutter produce a triangular Poincaré plot, while regular atrial flutter produces a disc.

Patients who present atrial fibrillation are candidates for restoration of sinus rhythm. Patients after restoration of sinus rhythm produce a Poincaré plot with a shape depending on the global level of HRV, as illustrated in Figure 3.4. High-HRV patients produce a Poincaré plot the shape of a comet; patients in normal cardiovascular condition produce an elliptic Poincaré plot sometimes referred to as a torpedo, while low-HRV patients produce a plot with a disc so small it looks like a single dot [Paskeviciute et al., 2001].

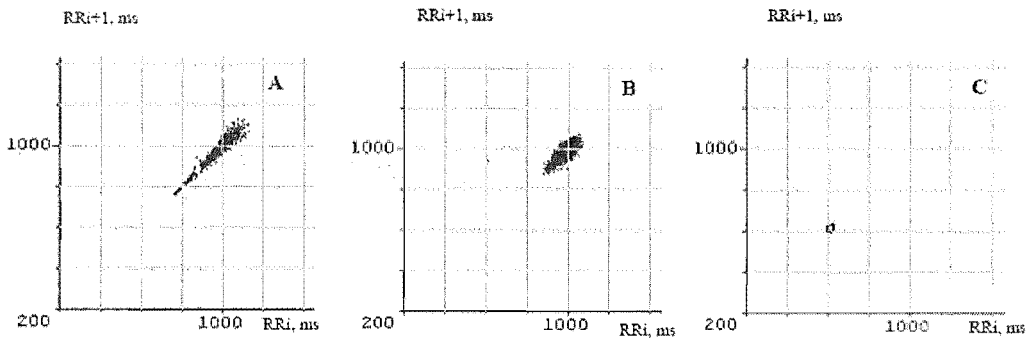

Figure 3.4 Different shapes of the Poincaré plot corresponding to high HRV (A), normal (B) and low HRV (C) patients [Paskeviciute et al., 2001].

All the patients examined in this research are critically ill, but they may not suffer these specific cardiovascular conditions. They very often produce an elliptic cloud of points, if only the relevant dense cloud is considered on the Poincaré plot. This data can be described by fitting an ellipse to the main cloud of points. This ellipse is fitted on the relevant part of the cloud of points, at 45° to the normal axis, called the line-of-identity. The short-term variability, or high frequency component, is described by the standard deviation of the points perpendicular to this line-of-identity, and is due to the respiratory sinus arrythmia [Niskanen et al., 2004]. The long-term variability, or low frequency component, is given by the standard deviation along the line-of-identity as illustrated in Figure 3.5 [Rajendra Acharya et al., 2004]. Further description of the Poincaré plot analysis is available in the literature [Niskanen et al., 2004; Paskeviciute et al., 2001; Rajendra Acharya et al., 2004].

Finally, the Poincaré plot offers an effective, graphical way to perform HRV analysis, unlike many mathematical approaches that require heavy computing and assumptions to fit in clinical environment. Its primary drawback is that

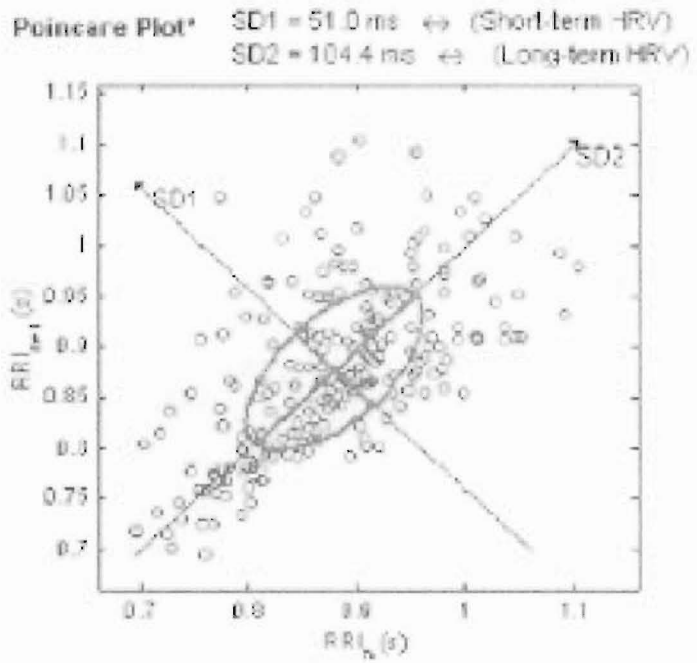

Figure 3.5 HRV graphical analysis from the Poincaré plot [Niskanen et al., 2004].

it requires human input to fit the appropriate contour on a set of data, which may not always be readily interpreted by computer alone. However, non-linear techniques in general are promising to study cardiovascular autonomic functions in addition to the temporal and spectral methods presented [Yeragani et al., 2004].

3.4 Limitation and review of HRV for measuring patient agitation

The metrics obtained by the different HRV methods are reviewed in this chapter. It is worth noting that HRV remains under extensive research and has not yet been validated in common clinical practice [Huikuri et al., 1999]. Although it is promising as a non-invasive measurement tool, there remain some contradictions among studies with regards to its clinical interpretation [Cammann and Michel, 2002].

Several studies support a correlation between the LF/HF ratio of the spectral HRV method with transient episodes of the heart, such as ischemic attacks (inability to provide enough oxygen to the heart muscle) or arrhythmia (abnormal

heart rhythms) [Bianchi et al., 1993; Pagani et al., 1986; Wiklund et al., 1997]. These are syndromes detectable on a beat-to-beat basis because they influence the fast fluctuations of the HR. Basically, it is logical to correlate heart dysfunctions with the autonomic nervous system that regulates cardiovascular functions, and the HRV method perfectly suits this environment.

However, in the context of agitation sensing, the HRV analysis is performed on a broader population, and the potential of HRV to produce an efficient marker of agitation in these conditions is investigated. Bartels et al. [Bartels et al., 2004] assess the effect of controlled breathing on HRV and BPV during exercise. ICU patients are under controlled or semi-controlled breathing and their physical stress and involuntary muscle contractions (sometimes termed "crispation") may involve the same fluctuations as exercise. Therefore, the findings of their research can present a clue to the potential detection of agitation with HRV. They report that the absence of changes in LF/HF ratio during exercise reveals the lack of sensitivity of HRV as an indicator of the modulation of the ANS during exercise. These findings are also supported by Chiu et al. [Chiu et al., 2003]. This research may notice the same lack of sensitivity with physical stress in the critically ill.

Cammann et al. [Cammann and Michel, 2002] have assessed more than 1000 normal subjects under mental stress. They report extreme inter-individual differences, which limit the potential to quantify a marker from HRV suitable for a whole population of patients, with different age and sex among other parameters. In addition, they suggest that rigid frequency band definitions used for LF and HF are unsuitable for correct spectral analysis of HRV because these rigid bands do not reflect physiological realities of cardiovascular regulations. More specifically, sympathetic and parasympathetic activities may overlap in the frequency domain. They conclude by underlining the strongly limited relevance of HRV as an independent marker, which may also be an issue in this research.

The physical stress induced by invasive neonatal procedures on infants has been assessed by Lindh et al using HRV [Lindh et al., 1997, 1999]. They reported detection of pain by increased HR and decreased HF component, corresponding to a lower vagal tone, and overall HRV. This result introduces the concept of assessing the total power of HRV as a marker for pain. Moreover, if LF decreases and HF remains constant, then LF/HF decreases. Their study does reveal a good qualitative detection method, but quantification of a marker from HRV remains

challenging, due to the inter-individual differences of HRV that can confound the achievement of consistent results.

The effect of mental stress on normal subjects has been studied by Seong et al [Seong et al., 2004]. Mental stress was induced by the coin stacking task. They report a sharp increase of the LF/HF ratio. This result introduces the eventuality that mental stress and pain compensate each other from the LF/HF ratio point of view leading, in combination, to little change. The review of HRV by Terathongkum et al. [Terathongkum and Pickler, 2004] also states that some medication can affect HRV significantly.

Rajendra Acharya et al. [Rajendra Acharya et al., 2004] have studied the differences of HRV between a sitting and a lying posture. This is very relevant for ICU patients who can be found both sitting or lying depending on the stage of therapy. The authors use temporal, spectral and non-linear methods to increase the consistency of their findings. Statistically significant markers were spectral LF/HF ratio, SD1 short-term standard deviation of the Poincaré plot, and the correlation dimension (CD), a measure of the fractal dimension. Fractal theory and its benefits in HRV analysis are beyond the focus of this research and details can be found in the literature [Rajendra Acharya et al., 2004]. Among the authors conclusions, when a subject is sitting, LF/HF is larger, the short-term high frequency trend given by SD1 and SDdRR is smaller. The overall findings of their research are described in [Rajendra Acharya et al., 2004]. Most importantly for this research, the posture of the patient influences the HRV variables. Therefore, the information obtained from HRV variables may be more accurate if the posture of the patient is taken into account.

This short review already outlines a lot of parameters that can modify HRV. The differentiation of agitation among other symptoms affecting HRV might be difficult. HRV is successfully employed on a narrow population under specific conditions, but it is more challenging to quantify a marker of agitation from HRV that is reliable over the broad population admitted in the ICU. If HRV metrics are included, the agitation sensing system may need more feedback on the patient posture, therapy, and clinical background accurately quantify agitation from HRV variables. HRV is investigated throughout this research, but the findings are considered carefully according to the advice of the literature on the subject.

3.5 Summary of different HRV methods

The pseudo-stationarity required by spectral analysis is obtained by removal of the baseline of the tachogram, so the resulting PSD frequency bands are not masked by the dominating VLF component. However, the baseline of the tachogram potentially contains the long-term forecast of the patient, particularly with regard to agitation. The first trials on healthy individuals in this study reveal a long-term heart rate increase when tested with stressful stimuli such as a Word Color Stroop Test [Lam et al., 2003; Deslandes et al., 2004] or cold pressor test [Lam et al., 2003; Annie Lambert and Schlaich, 2004] used to simulate agitation. Therefore, the slow trend of the tachogram is worth examining to increase the chance of detecting a pattern related to events of agitation. This motivates the choice of the temporal HRV method where the SDRR variable tracks the global trend of the tachogram. To increase the consistency of the HRV analysis, temporal and parametric spectral analysis are performed concurrently, and the LF and HF components derived from spectral HRV are compared with SDRR and SDdRR derived from the temporal HRV method. The Poincaré plot offers an alternative, and a good compromise may still be reached using a pattern recognition algorithm. A particular shape of plot may be produced during episodes of agitation and this assumption should be investigated in future work. However, at this stage, this research focuses on time and frequency HRV methods.

Figure 3.6 summarises the analytic HRV results for an ICU patient using both temporal and spectral methods. The HR is shown in the top panel, along with the subjective SAS score. The original tachogram is shown in the second panel. The third frame shows the LF/HF ratio derived from the AR spectral HRV method. The fourth frame illustrates the long-term variations of the tachogram as modelled by the SDRR HRV metric. Finally the bottom frame tracks the fast fluctuations with the SDdRR HRV marker.

A more flexible and stable analysis method is therefore introduced to overcome the several limitations of HRV as a dynamic index. The heart rate first-order time derivative is presented as an alternative. This approach utilises a moving average that estimates the baseline trend of the tachogram. This method provides information based on the slow moving part of the tachogram, as opposed to spectral HRV that provides information based on the beat-to-beat fast fluc-

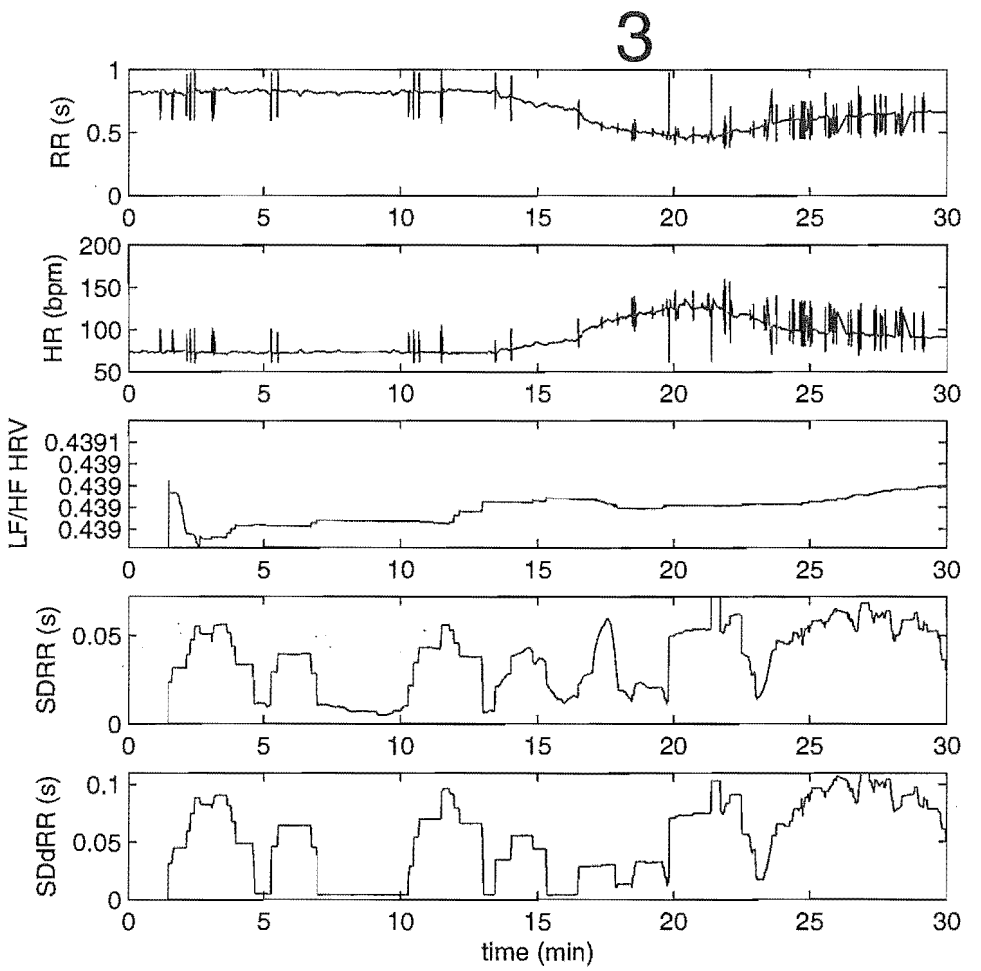

Figure 3.6 HR and HRV metrics of an ICU patient during a grade "3" agitation reported on the SAS scale by the clinician in charge. In this example, the different metrics are calculated over a 100-sample wide window.

tuations of the tachogram. The long-term baseline and fast trends of HR are illustrated in Figure 3.7. Hence, it focuses on the very slow moving, long-term variations ignored by the spectral HRV method, that can predict changes in patient agitation state more independently of cardiac conditions, posture or other factors affecting HRV.

3.6 Heart Rate Derivative

The heart rate first-order time Derivative (HRD) is introduced as a way to complement the information obtained from the HRV analysis of the ECG signal in the

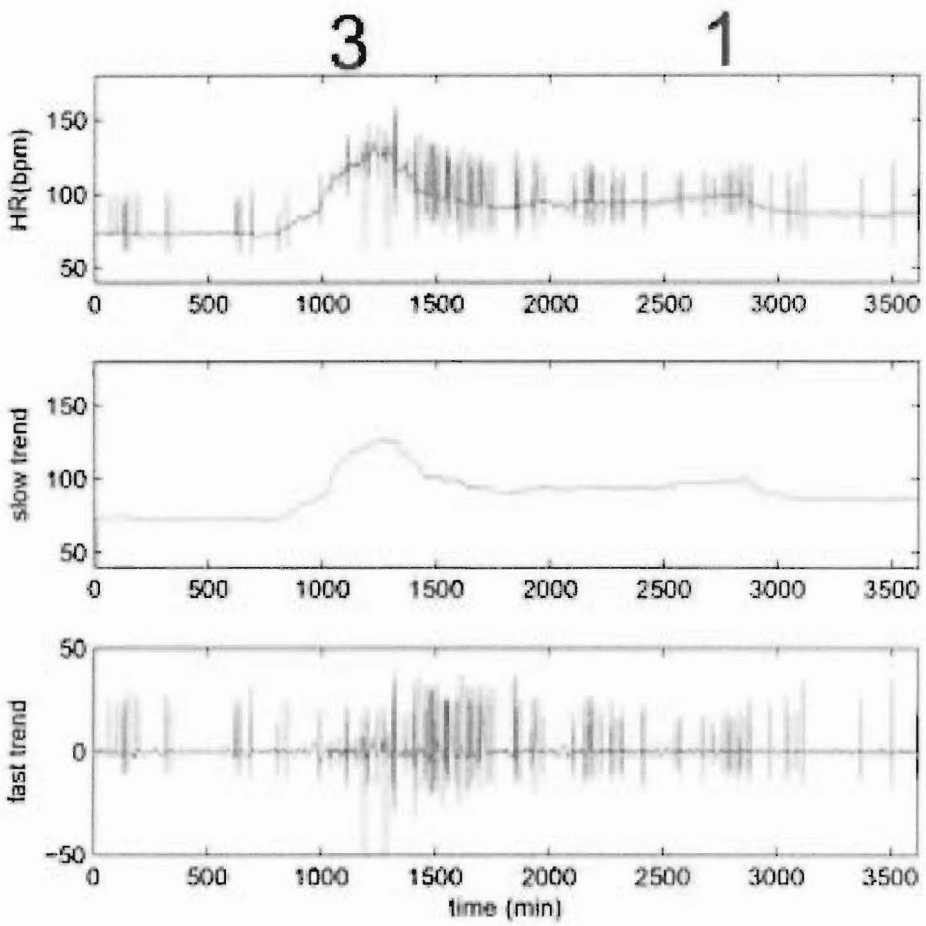

Figure 3.7 Slow and fast trends of HR. The HRD analysis focuses on the slow trend of the baseline, whereas the spectral HRV is performed on the fast trend. Temporal HRV is performed on the original tachogram.

context of critically ill patients. It also adds a near-future forecast of agitation based on the baseline of the tachogram ignored by spectral HRV methods.

The instantaneous heart rate derivative (in beats/min^2) is evaluated as the difference between two consecutive instantaneous HR values.

$$HRDi(n) = \frac{(HR(n) - HR(n-1)) \times 60}{RR(n)} = (HR(n) - HR(n-1)) \times HR(n) \tag{3.11}$$

It produces a noisy fluctuating signals that is then processed through a Moving Average (MA) window. The HRD instantaneous values are summed up along

a shift register, and then divided by the MA time length in samples to produce an average value that is smoother. This process yields the HRD metrics. Unlike the HR that is not smoothed directly, the HRD signal is first smoothed over a time window, the length of which has been empirically determined. This initial filtering eliminates the fast fluctuations shown in the third frame of Figure 3.7 already captured by the HRV methods introduced. Consequently, HRD focuses on the slow trend of the heart illustrated in the second frame of Figure 3.7.

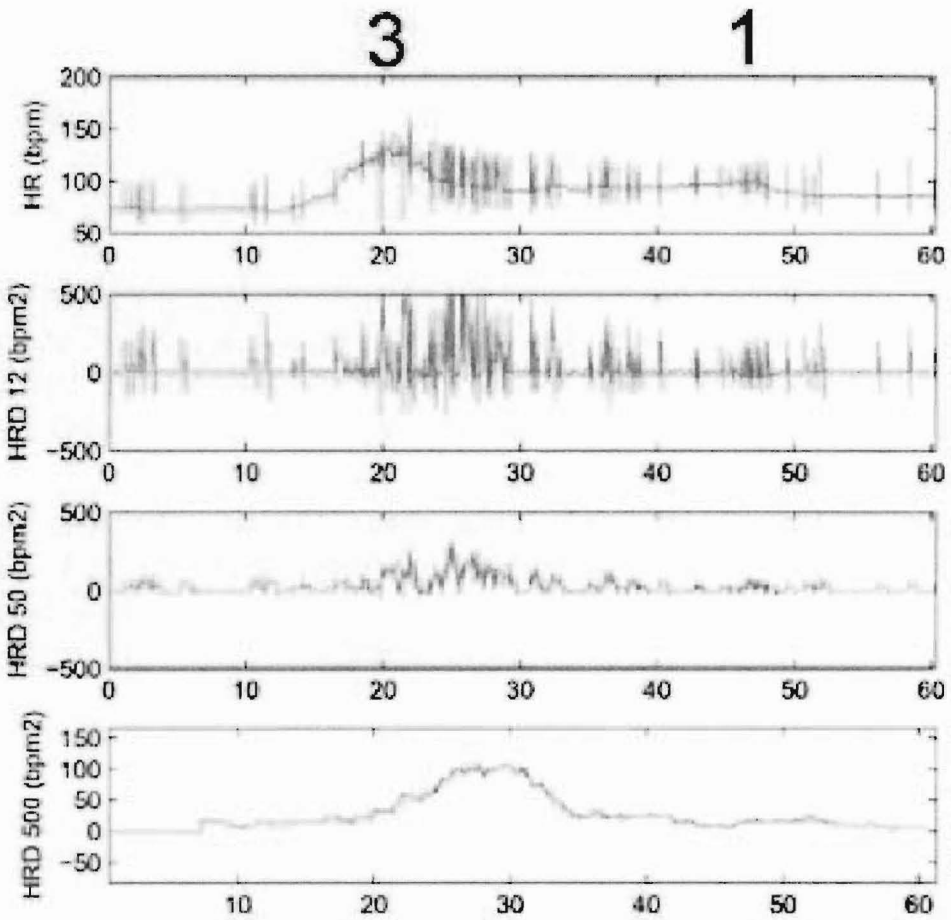

Figure 3.8 HRD example.

Experimental trials implement 10, 50 and 500-sample long MA filters that capture different trends of the heart. Specifically, the HRD metric examines periods of clinical significance that are much longer than those examined by HRV. An example of HRD analysis using MA filters of different lengths is shown in Figure 3.8 along with the associated subjective SAS scores from one clinician. The width of the MA temporal window is a critical parameter, as introduced in

Section 2.2.3. Figure 3.8 illustrates the tradeoff between smoothness and delay. The 10-sample-wide MA outputs a signal with nearly no delay, as the rise in HR is quickly followed by a response on the HRD signal. The 50-sample MA output is smoother, but still focus on a rather fast trend of the heart. However it is not delayed considerably. Finally, the 500-sample MA output is very smooth, and emphasise the long-tern trend of the heart that is ignored by the HRV methods, but it suffers too long a propagation delay to be clinically useful.

Alternatively, it is also possible to keep the instantaneous HRD value as the HRD metric, and only apply smoothing on the output agitation index. The optimal location of the MA filters will be discussed later in this thesis when combining the intermediate metrics into a fuzzy inference system. The goal is to minimise delay and noise to produce a smooth and time-relevant agitation index.

The HRD algorithm offers a simple and efficient way to track the slow heart rate dynamics potentially associated with agitation, as well as a more capable real-time algorithm than HRV methods. HRD is also less susceptible to noise and artifacts because it is the moving average of a series of consecutive values. An artifact is consequently smoothed out by the MA filter, and does not upset the processing for long periods, which is not the case for parametric HRV where artifacts and errors impact the results for very long periods. HRD is a very promising method to complement the findings of HRV in this research where the focus is on both the slow and fast trends of the heart.

3.7 Summary on heart dynamics and agitation

This chapter examines the possible metrics to track the heart dynamics. Although many clinicians and researchers use HRV to track cardiovascular dysfunctions, further research and investigation is required in the context of agitation sensing of ICU patients. Moreover, spectral HRV methods ignore the tachogram baseline, which potentially contains some information of clinical interest. Hence, the baseline may be used to produce a marker of agitation. Optimal signal processing of ECG focuses on several trends. Therefore, it requires the combination of HRV and HRD metrics to capture the different dynamics of the heart.

The short-term variability is tracked by the HF component of the tachogram

spectrum, as well as the SDdRR temporal variable. The ability of both method to model the fast evolution of the tachogram can therefore be assessed and compared during clinical trials to select the best method. The middle-term variability is given by the LF component of the tachogram. The global variations are given by the SDRR variable. These methods are investigated and compared in the context of ICU patient agitation during clinical trials. The slow trend ignored by HRV methods is retrieved by the the HRD method. The HRD focus on variable slow trends depending on the width of the time window. Different widths may be applied to calibrate the HRD technique in the context of ICU patients. The aim is to focus on long-term trend and a reasonably wide window should be used. As opposed to qualitative HRV analysis where the goal is to evaluate the balance of the ANS, the agitation sensor requires the quantification of markers to compute an objective agitation index. To obtain a linear response of the physiological markers to agitation, the variables are normalised, and potentially log-transform for the convenience of higher-level processing. The development of signal processing techniques is therefore more complex when the result is quantified than for qualitative analysis of the ANS.

Chapter 4

Arterial blood pressure

The blood pressure (BP) is defined as the pressure, or force per unit area, that the blood applies on the walls of the blood vessels. The arterial BP (ABP) refers to the BP on the walls of large arteries, such as the brachial artery of the arm where the sphygmomanometer (inflatable cuff attached to a manometer) is placed during medical examinations.

The ABP signal fluctuates during the cardiac cycle. The left ventricle ejects blood into the aorta (see Figure 2.2), which raises the aortic and global ABP to a maximum, called the systolic BP (SBP). Then the left ventricle relaxes and refills, and the ABP falls accordingly to the minimal ABP, called the diastolic BP (DBP).

To measure the ABP, the examiner inflates the cuff of the sphygmomanometer until the brachial artery is completely occluded. Then the pressure in the cuff is slowly released, while the examiner listens to the artery at the elbow with a stethoscope. A pounding sound is heard when blood flow slightly resumes, and the pressure at which this sound started is noted . The value obtained is the SBP. The cuff pressure is further released until the sound can no longer be heard, delivering the DBP.

Clinicians commonly measure the ABP in millimetres of Mercury (mmHg), because the mercury manometre has been the standard ABP measurement tool reference for a long time. Pressure is a force per unit area, and it is matched to a length of liquid, i.e. millimetres of mercury. For instance a pressure of 50mmHg means that the force exerted on the surface of the vessel being measured is sufficient to push a column of mercury to a level 50mm higher. BP may also be

measured in centimeters of water (cmH_2O). A pressure of $10cmH_2O$ is sufficient to raise a column of water 10cm higher. The conversion from mmHg and cmH_2O to International System pressure unit (Pascal, Pa) is defined.

$$1mmHg = 1Torr = 1.36cmH_2O = 133.322Pa \tag{4.1}$$

where 1mmHg equals $1.36cmH_2O$ because the density of mercury is equals to 13.6, which means the volumetric mass of mercury is 13.6 times greater than water, or $13600kg/m^3$. Normal range for SBP in adult humans is 90–135 mmHg (12–18 kPa) [Guyton, 1980; Guyton and Hall, 1996]. Normal range for DBP is 50–90 mmHg (7–12 kPa)[Guyton, 1980; Guyton and Hall, 1996].

Although mmHg is still the common pressure unit in medical applications and particularly ABP, high-fidelity ABP measurements is not performed by mercury manometers, because its inertia does not enable variations faster than 2 or 3s to be detected. Hence, electronic pressure transducers are currently preferred.

4.1 Effect of agitation symptoms on ABP related parameters

As previously discussed, the ECG reacts to feelings of pain and anxiety, which are some of the main symptoms of agitation in ICU patients. However, the significance of ABP and derived metrics is not so supported in the literature. Shinn et al. [Shinn et al., 2001] investigated whether depression and anxiety were related to the development of elevated blood pressure and hypertension, that is elevated blood pressure beyond the normal acceptable range. Their results do not verify their initial assumption that anxiety and depression potentially increase the chance of developing hypertension. However, Yeragani et al. [Yeragani et al., 2004] associate the development of hypertension with an increase of ABP variability. They also report anxiety being associated with an increase in ABP, in contrast to Shinn et al. [Shinn et al., 2001]. Because the impact of anxiety on ABP is unclear, it is worth investigation in the context of the ICU, where anxiety is only one potential symptom leading to agitation.

A response is triggered in the sympathetic part of the ANS (see Figure 3.1) by mental or physical stress [Guyton and Hall, 1996]. This response is called the sympathetic stress response, and it instinctively increases the ability of the human body to perform muscle activity in the following ways:

- Increased ABP
- Increased blood flow to muscles
- Decreased blood flow to organs concurrently
- Increased rates of cellular metabolism
- Increased blood glucose concentration
- Increased glycolysis (breakdown of glucose into energy) in the liver and muscles
- Increased muscle strength
- Increased mental activity
- Increased rate of blood coagulation

Such mental and physical stress is assumed to be developed by patients in the ICU environment and the ABP values and corresponding dynamics are consequently investigated as a potential agitation sensor input. The signal-processing required to extract instantaneous and dynamic values from the ABP signal is presented in this chapter.

4.2 Instantaneous ABP values

Figure 4.1 displays a typical ABP temporal signal. The vertical axis represents the output voltage of the pressure transducer, in volts (V). The horizontal axis represents the discrete time, in samples. This example in Figure 4.1 is sampled at 1kHz, so a sample represents 1ms.

Three values are obtained from the ABP signal, namely the systolic (SBP), mean (MBP) and diastolic (DBP) ABP values. In Section 2.2 the ECG signal

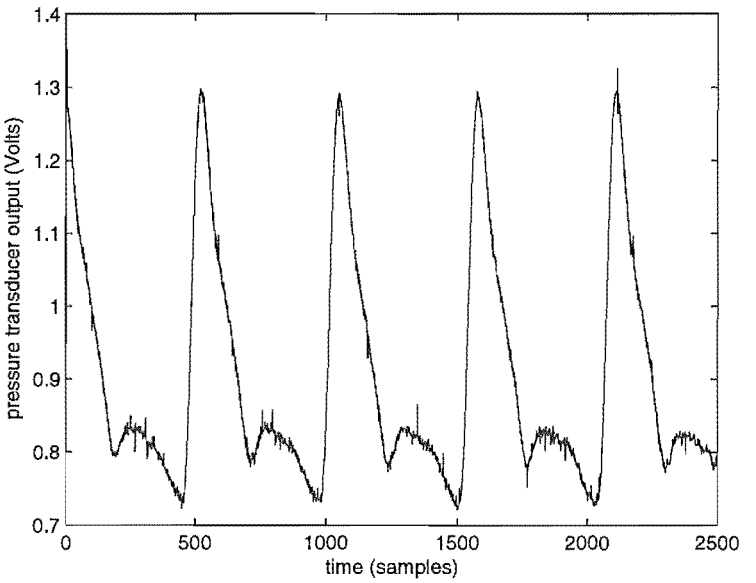

Figure 4.1 ABP signal waveform sampled at 1kHz.

is processed to extract time intervals between consecutive R peaks. The key factor in that previous case is the signal-to-noise ratio, and the vertical units may remain arbitrary. For ABP values, however, it is crucial to restore the vertical axis in pressure units, to determine the three ABP values of interest. The conversion from voltage to pressure unit, in mmHg, depends on the sensitivity of the pressure transducer. The monitoring device used in the Christchurch hospital ICU acquires the ABP signal of a patient using a transducer with a sensitivity of 100 mmHg/V. The first operation performed on the signal is a multiplication by factor 100 to convert the vertical axis to a pressure dimension.

The following signal-processing consists of a maximum and minimum ABP detection, followed by the computation of MBP. There is no need to compute the peak-to-peak time interval of the ABP signal, because it is strictly equal to the RR time interval computed in Section 2.2. However, there is a phase shift between ECG and BP maxima depending mainly on the location of BP measurement. Basically, the further away from the aorta, the longer the phase shift.

The maxima and minima are detected by a peak detection algorithm, similar to the technique used to detect R peaks in the ECG signal, detailed in Section 2.2.2. The detection of SBP and DBP is also based on adaptive thresholds updated with SBP and DBP.

The ABP signal contains high frequency (HF) noise, as illustrated by the high frequency fluctuations of the ABP signal in Figure 4.1. The removal of this noise can be performed by a 8ms-long moving average MA filter. The removal of HF noise is most valuable when artifacts occur near extrema where they can be confused with SBP or DBP values by the detection algorithm.

The adaptive threshold peak detection works as illustrated in Figure 4.2. The first threshold for SBP detection Tsbp1 and the threshold for DBP detection Tdbp1 are evaluated from the initialisation phase that detects the extreme values of the ABP signal during a 2s period. The thresholds are empirically defined:

$$Tsbp = DBP + 0.6 \times (SBP - DBP) \tag{4.2}$$

$$Tdbp = DBP + 0.25 \times (SBP - DBP) \tag{4.3}$$

where Tsbp is the SBP threshold level and Tdbp is the DBP threshold level.

Once the initialisation phase is completed, the peak detection algorithm starts at point A in Figure 4.2. As the signal exceeds the "Tsbp1" threshold the system expects a systolic peak to occur, and therefore it updates the maximum BP buffer every time the signal is greater than previously recorded potential SBP values, much like the peak detection algorithm introduced in Section 2.2. The maximum BP buffer is overwritten until the signal reaches SBP1, which correspond to the SBP value. The signal decreases until it returns below the Tsbp1 threshold value, and the new maximum BP value kept in the buffer is validated by the system as the SBP value. It is then stored in the SBP value array.

The MBP value is defined from the extreme ABP values:

$$MBP = DBP + \frac{1}{3}(SBP - DBP) \tag{4.4}$$

Note that Equation (4.4) is the medical definition [Guyton and Hall, 1996] based on the bisector method rather than the arithmetic mean. Consequently, the

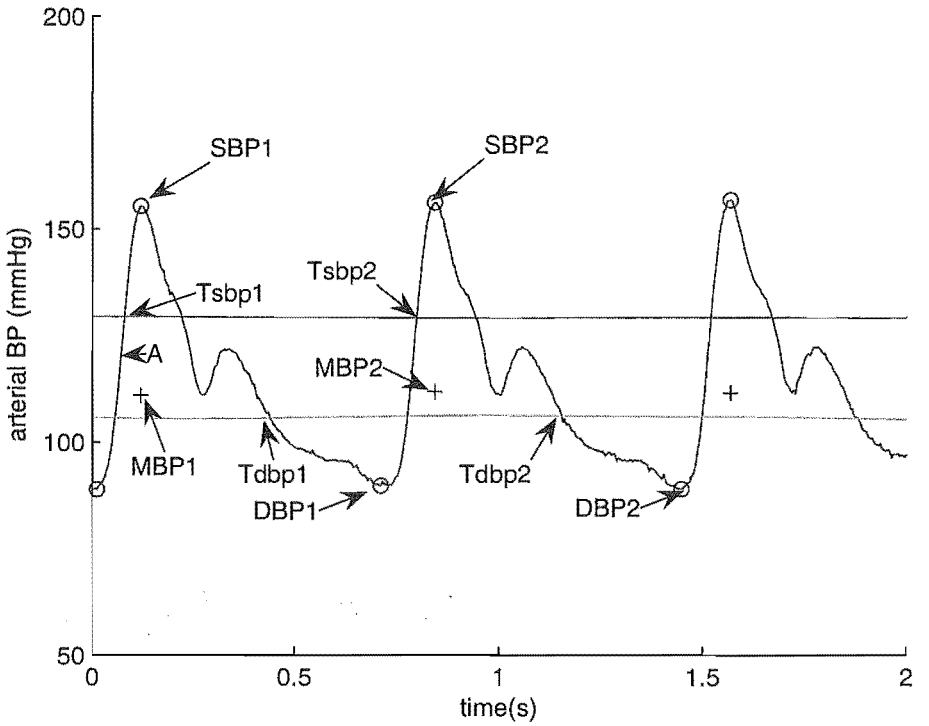

Figure 4.2 Detection of the systolic, diastolic and mean BP values with adaptive thresholds.

update of the SBP value SBP1 involves the update of the MBP value MBP1 and the DBP threshold to Tdbp1.

The ABP signal is located between the systolic and diastolic threshold values and nothing happens until the signal drops below the DBP threshold Tdbp1. The system expects a diastolic negative peak, and it updates the ABP local minimum if the value is smaller than any previously recorded ABP values since threshold crossing. The ABP signal start to rise until it exceeds the DBP threshold. The new local minimum BP value is then validated by the system as the DBP value. The update of the DBP value involves the update of the systolic threshold value from Tsbp1 to Tsbp2.

The signal then exceeds the new systolic threshold Tsbp2 and the system detects the new local maximum ABP value. Then the signal returns below the threshold Tsbp2 and the system validates the local maximum value as the SBP value SBP2 in Figure 4.2, which involves the update of the MBP value to MBP2 and the update of the DBP threshold to Tdbp2.

To succeed, this method requires the detection thresholds to be set at the right level, and updated at the right time. The cycle repeats as long as the system runs. This concept of adaptive threshold peak detection offers a consistent detection of the ABP values of interest, despite of the many ABP fluctuations encountered with agitated ICU patients. Overall, the detection of SBP, MBP and DBP contribute important clinical information on the patient present and future condition.

Clinically, a patient transient episode, such as ICU agitation, may correlate with an increased ABP, as explained in Section 4.1. The information provided by the ABP values may also be complemented by their dynamics. The variability of the ABP signal can be extracted using several methods, including ABP variability BPV and averaged first order derivative BPD.

4.3 Blood pressure variability

The activity of the autonomic nervous system (ANS, see Figure 3.1) is commonly analysed using HRV to establish the balance between the activity of the sympathetic and para-sympathetic parts of the autonomic nervous system [Huikuri et al., 1999; Mendez et al., 2004; Niskanen et al., 2004]. The same signal-processing techniques may be applied to all three ABP markers to verify or modify the diagnosis based on HRV [Bianchi et al., 1993; Pagani et al., 1986].

The temporal, spectral or non-linear variability analysis (refer to Chapter 3 for detailed description of each method) is applied to consecutive SBP values the same way it is applied to the tachogram to compute HRV, and it performs the blood pressure variability BPV analysis and its derived metrics.

Several research teams [Pagani et al., 1986; Kuusela et al., 2003; Pfeiffer and Netzer, 1997] perform variability analysis on consecutive SBP values. Hence, it is decided to similarly perform the BPV analysis on the SBP values. However, it can also be performed concurrently on the MBP and DBP to augment the results from the systolic BPV [Yeragani et al., 2004]. The information extracted from BPV analysis is then used to match the activity of the ANS with cardiovascular functions and the development of hypertension, which is associated with end organ damage and cardiovascular morbidity.

The different temporal and spectral techniques available to analyse the variability of the ABP signal are similar to the signal-processing methods applied to the tachogram, but the diagnosis made from the results is radically different. A summary of the different BPV methods is displayed in Figure 4.3. The top frame displays the consecutive SBP values. The second frame is the variability obtained by spectral estimation using an AR model of order 12. This order has been found to be optimal by Kuusela et al. [Kuusela et al., 2003]. The middle frame presents the result of BPV as given by the standard deviation of a series of consecutive SBP values (SDSBP), shown in the top frame, and gives the overall variation in the time interval [Niskanen et al., 2004]. The fourth frame displays the standard deviation of the difference between consecutive SBP values (SDdSBP). It describes the short-term variations within the time window considered. The final frame introduces the SBP values derivative (BPD).

The illustration in Figure 4.3 shows a rise in agitation from grade "0" to "2" on the SAS. The SBP rises and oscillates a lot more from 800s onwards. The AR BPV displayed in the second frame in Figure 4.3 is showing a waveform from which it is hard to quantify a marker, and the AR BPV markers is fluctuating a lot. These fluctuations are due to the lack of stationarity of the data, on which it is hard to apply an AR filter. The third and fourth frames are derived from the temporal BPV method based on standard deviation of the SBP values. The standard deviation is calculated over 12 samples, and the output signal is fluctuating a lot. However, these two signals smoothed by the right MA filter have the potential to derive a good dynamic metric to associate with the ABP values. The last frame represent the BPD method based on the first order time derivative. It shows fast fluctuations from 800s, and a MA filter may also be added to produce a dynamic metric at higher level signal-processing.

Clinical trials reveal a decrease in HF power of HRV spectrum during physical activity such as standing posture after rest, whereas the opposite occurs with BPV [Pagani et al., 1986; Yeragani et al., 2004]. The overall power of the BPV spectrum also increases with development of hypertension. The increase of BPV is associated with cardiovascular morbidity. On the other hand, cardiovascular mortality is associated with a decrease of the overall power of the HRV spectrum [Kuusela et al., 2003]. More generally, the LF/HF ratio derived from HRV that measures the sympatho-vagal balance of the ANS behaves inversely when computed from BPV. Hence, the balance of the ANS is assessed by the HF/LF

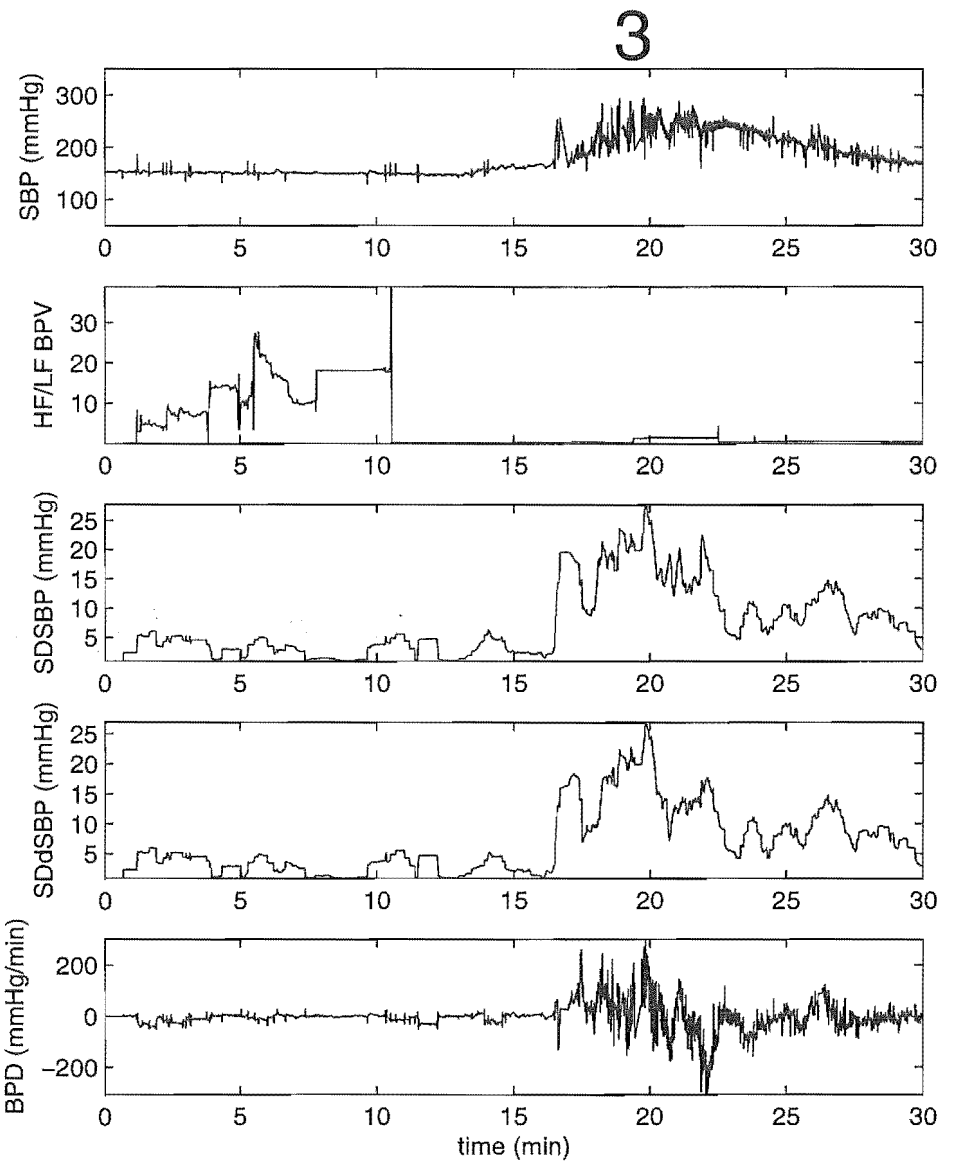

Figure 4.3 Variability of ABP obtained with different methods during an episode of SAS grade "3" agitation.

ratio.

Similar to using the HRV spectral method, the low frequency baseline of the SBP series is removed before the BPV analysis is performed using spectral methods. This baseline removal is achieved in this research by subtracting the best linear least square fit to the signal. The size of the time window is equal to the order of the AR model in the parametric method. Therefore, the AR

BPV method is also computed on a beat-to-beat basis. Although it is possible to match some information from the BPV with specific parts of the ANS and corresponding cardiovascular functions, it may not be the best method to track long-term fluctuations of the ABP for the same reasons as HRV outlined in Section 3.4. Therefore, the blood pressure derivative is introduced to focus on the slower trends of the ABP signal and complement BPV that emphasises on the faster fluctuations of ABP.

4.4 Blood pressure derivative

The blood pressure derivative (BPD) is the first-order time derivative of the SBP time series. Unlike the BPV that utilises a high-pass filter to detrend the values before processing, the BPD is smoothed after computing using a low-pass filter to reveal only the low frequency content of the BPD. Consequently, it focuses on a different frequency band, and complements the information obtained from BPV. In this research, the information revealed by both BPV and BPD are interesting from a clinical standpoint.

The BPD contains a broad frequency range as shown in the bottom frame of Figure 4.3 and a slower trend is revealed by use of a moving average MA filter, to smooth the desired output BPD signal. This approach is illustrated in Figure 4.4 for different length of MA filters. These slower trends are potentially illuminating in terms of tracking long-term trends in critical care.

The 12-sample and 100-sample MA do not smooth the BPD signal enough and still focus on the fast trend of ABP. The 500-sample MA is long enough to emphasise the slow trend ignored by the HRV methods, but the delay of propagation is significant. Therefore, 100 samples represent the maximal length of MA filter to apply on the BPD series for this application where delays must be limited. The averaged BPD series provides a great complementary information with the instantaneous SBP value and the different BPV markers to estimate the patient level of agitation.

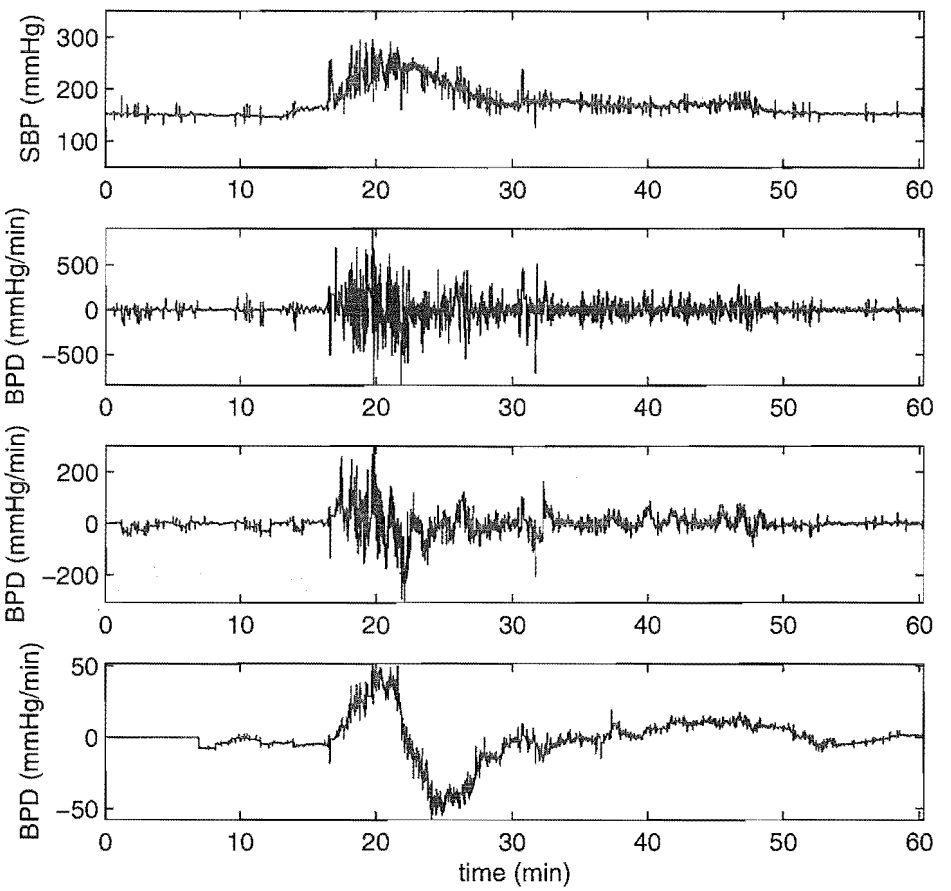

Figure 4.4 BPD signal smoothed by three different MA filters.

4.5 Summary of ABP processing

Much like the signal-processing applied on the ECG signal, the BPV variability methods focused on the beat-to-beat, short term fluctuations. It is very important to estimate the sympatho-vagal balance of the ANS, particularly in cardiac patients, but potentially also in critically ill patients examined in this research. The BPD metric provides a more global marker of long-term agitation. The averaged first order time derivative offers a simple noise-proof method to forecast the near future of patient agitation from the ABP signal.

The BPV and BPD methods are complementary to track episodes of agitation. Similarly to HRV, temporal BPV methods are preferred on a long non-stationary time series. Finally, the instantaneous ABP values detect hypertension and the combination of the three methods namely SBP, BPV and BPD offers a

potential input to quantify the patient's agitation level with an objective sensor.

Chapter 5

Respiration

The physiological goals of respiration are to provide oxygen to the tissues and to remove carbon dioxide [Guyton and Hall, 1996]. There are four main dynamics involved.

- *pulmonary ventilation*: The inflow and outflow of air between the atmosphere and the alveoli of the lungs allows intake of oxygen and diffusion of carbon dioxide.
- *diffusion*: Oxygen is diffused from the lung alveoli to the pulmonary capillaries. The carbon dioxide carried back from the cells to the pulmonary capillaries is diffused to the alveoli where the lower partial pressure of carbon dioxide, PA_{CO_2}, of the alveoli allows its diffusion. Thus, carbon dioxide diffuses in the opposite direction of oxygen at each point of the gas transport chain.
- *transport*: Oxygen is carried from the pulmonary blood to the tissue capillaries, principally by haemoglobin, for use by the cells. Most of the oxygen used by the cells is turned into carbon dioxide. The oxygen metabolism involves fluctuations in the pressure of oxygen (Pa_{O_2}) and Pa_{CO_2} along the circulatory system of the body. The carbon dioxide returns to the pulmonary capillaries for diffusion out of the body.
- *regulation*: Ventilation and other facets of respiration are regulated to avoid alteration of Pa_{O_2} Pa_{CO_2} during respiratory stress induced by exercise for example [Guyton and Hall, 1996]. At the arterial end of the pulmonary capillaries the typical Pa_{O_2} is 104 mmHg once oxygen has been diffused to the alveoli. The Pa_{O_2} of the venous blood leaving the tissue capillaries is

typically equal to 40mmHg. This range of blood oxygen pressure defines the normal physiological range and can be expressed as a ratio called the haemoglobin saturation in oxygen, given as a percentage. It is evaluated by the pulse oximetry, another signal linked to the respiration process.

The whole process of respiration consequently offers markers of the patient clinical condition and the variables derived from the respiration are investigated to track episodes of agitation.

5.1 Effect of agitation on respiration

Among the several physiological signals related to respiration and available from an ICU bed environment, the flow rate and the pulse oximetry (SpO_2) are investigated as potential markers of patient agitation. Both signals are assumed to be affected by the symptoms of agitation, and their derived metrics could consequently be utilised as an input to the agitation sensing system.

5.1.1 Flow rate and airway pressure during episodes of agitation

Many critically ill patients require breathing assistance during a part of their stay in the ICU and ventilators are used for this task. Relaxed and paralysed patients are mechanically ventilated. The ventilator can provide a measurement of the flow rate and airway pressure, which can be examined before and during episodes of agitation. Passive controlled mechanical ventilation is the most favorable mode for measurement of physiological signals. During mechanical ventilation , optimal settings for patient ventilation can be obtained by observation of airway pressure and gas flow [Lotti and Braschi, 1999]

When the ventilator runs in assisted mode, the patients can breathe spontaneously, and the machine only supports ventilation. If the patient fails to trigger the inspiration spontaneously, the ventilator provides minimal ventilation to the patient. The assisted mode is more flexible and it permits spontaneous breathing

at some points of the cycle [Carrasco, 2000]. It is therefore more consistent to track agitation based on the patient condition rather than the ventilator parameters. In ICU most of the patients spend most of their time in assisted ventilation mode [Lotti and Braschi, 1999].

Flow rate and airway pressure monitoring via the ventilator logically requires patients to be intubated. Intubation is not a limitation in the context of this research which takes place during the patient intubated period. Therefore the respiration flow rate is available along the entire study if required. This signal provides a way to derive the tidal volume (Vt) and breathing rate (BR), both of which potentially offer a marker of increased stress. Note that the breathing rate BR is more often referred to as respiratory rate, but in this thesis the "RR" abbreviation is assigned to the time interval between two ECG R peaks. It is assumed that BR can increase during periods of agitation [Lam et al., 2003]. Clinical trials from other research groups also observed significant correlation between BR and mental or physical stress [Masaoka and Homma, 1997]. The variations of Vt can also be investigated as a marker of increased stress [Molke Borgbjerg et al., 1996].

Potentially, BR and Vt can improve the accuracy and reduce the delay of agitation quantification, because respiration patterns often reveal the rising potential for agitation, according to the observation of clinicians at Christchurch hospital ICU. Therefore, it offers potential to be an input of the agitation sensor. The pulmonary pressure signal follows a different pattern, whether the patient is breathing passively or actively. This change from passive to active breathing is believed to be a marker of the increased of level of consciousness, during which episodes of agitation may be more likely. The shape of the pressure signal is also worth investigating to extract more information on the present and future agitation level of the patient.

5.1.2 Pulse oximetry and agitation

The maximum amount of oxygen carried by the haemoglobin of a normal person is 20mL per 100mL of blood when the haemoglobin is 100% saturated [Guyton and Hall, 1996]. This value depends strongly on the P_{O_2} based on the oxygen-haemoglobin dissociation curve. While a 100% oxygen saturation requires a P_{O_2} of 140 mmHg, the normal saturation for a typical arterial P_{O_2} of 95 mmHg is

97%, which corresponds to 19.4mL oxygen per 100mL blood. In normal venous blood where P_{O_2} is equal to 40 mmHg, the oxygen saturation of the haemoglobin is about 75%.

The arterial blood oxygen saturation is often referred to as SaO_2 and it is used to evaluate the condition of the respiratory system from the lungs to the tissue metabolism. This value is used in the ICU to adjust the settings of the mechanical ventilators, when the patient requires breathing assistance. The SaO_2 cannot be directly measured non-invasively. Instead, it is estimated using pulse oximetry, SpO_2. The SpO_2 value estimates the saturation of oxygen from the blood colour. The standard monitoring of pulse oximetry has probably reduced peri-operative morbidity and mortality, although large differences may occur between SpO_2 and SaO_2 in critically ill patients [Van de Louw et al., 2001].

Pulse oximetry has the potential to track events of agitation, mainly because the symptoms of agitation affect the oxygen saturation of the arterial blood. However, several other parameters can impact the acceptable range of SpO_2, and agitation is only one of them. Consequently, it is hard to differentiate the different causes of pulse oximetry fluctuations and it is therefore currently too difficult a signal to be used as an input for the agitation sensor.

5.2 Processing of respiratory flow rate

The flow rate, in litres per minutes (Lpm), measures the air flow in and out of the lungs. It produces a signal that is periodic with respiration. The positive flow represents the lungs being filled with fresh air, while the negative flow represents the lungs expiring air with a greater concentration of carbon dioxide. Hence, the signal crosses over 0 Lpm twice per breathing cycle.

Threshold crossing detection, such as the method utilized to detect R wave peaks in Section 2.2, provides a way to derive BR from this signal, by counting the threshold crossings over a period of time. The result is a threshold crossing frequency in cross/min. As the full breathing cycle crosses twice over zero, BR is equal to half the 0-crossing frequency.

The tidal volume (Vt) is the volume of air inhaled by the lungs during in-

spiration. Both BR and Vt can potentially indicate the regulation of respiration against an event of stress, such as agitation of ICU patients. As a means to regulate respiration, the tidal volume can increase, while BR remains the same. The tidal volume is obtained from integration of the flow rate, in Lpm, to give the tidal volume in litres (L).

BP and Vt are patient and condition specific variables, depending on patient size and fitness, as well as the medication used by the ICU therapy, among other parameters. Therefore, absolute BR and Vt are not very useful. However, the first-order time derivative of BR and Vt could emphasise the dynamic trends while eliminating the patient specific magnitudes of these variables.

5.3 Processing of pulmonary pressure

The pulmonary pressure is also a periodic signal related to the respiration cycle. It measures the pressure in the airways of a ventilated patient. The period of this signal is similar to the period of the flow rate to derive BR. However, the shape of the pressure signal is different depending on whether the patient is breathing actively or passively.

Basically, the ventilator ensures a minimum period of breathing to supply oxygen to the patient. However, a rise in the level of consciousness or agitation may lead to the patient starting to breath spontaneously, referred to as active breathing. Spontaneous breathing considerably changes the shape of the signal, and increases the potential for the patient to be agitated, as they increase their BR as a result of stress. This switches the ventilator from passive to assisted mode. Complex pattern recognition of the waveform or detection of the depression induced by spontaneous inspiration is required for passive and active breathing differentiation.

5.4 Summary of respiration

The respiration of ICU patients is characterised by BR, Vt and SpO_2. Because pulse oximetry is affected by too many parameters, such as therapy, morbidity,

and altitude, the differentiation of pulse oximetry fluctuations due to agitation among other causes remains challenging. However, this research focuses on ventilated patients whose agitated behaviour can be detected by an increased breathing rate. Hence, the air flow and pressure signal are promising to provide preemptive agitation detection and variables derived from these signals should be included as an input to improve the agitation sensing.

Chapter 6

Patient motion

In the context of ICU patients, motion usually results when patients are already agitated. Most subjective definitions of agitation [Crippen, 1990; Riker et al., 1999] have a significant component associated with excessive patient motion. Consequently, the detection of agitation based on motion can be late, and ideally agitation should be identified before the patient begins to move significantly [Lam et al., 2003]. However, if the system fails to detect a coming event of agitation from the trends of physiological variables, motion analysis allows detection and objective measurement of patient agitation at last.

In a number of biometric applications similar to agitation sensing it is important to identify the actions of the human body or certain parts of it. Motion sensing consists of the detection and quantification of the physical activity of a part or a whole body. There are three major fields of motion sensing [Wang and Singh, 2003]: motion analysis involving individual body parts; human body motion and behaviour analysis using single or multiple cameras; and higher level analysis of human dynamics using computer modelling. The motion analysis related to agitation sensing is composed of a single camera body motion analysis and specific body part analysis. The benefits and limitations of these different techniques are discussed in this chapter.

The video analysis is performed using several motion sensing methods. These video-processing techniques emphasise different aspects of motion detection, such as specific body parts, as well as overall body motion. Motion sensing applied to bioengineering applications in general makes use of a variety of video-processing techniques. These include the use of Kalman filters [Kuo et al., 2002; Piovoso and Laplante, 2003; Zingaretti and Zanoli, 1998; Zhu and Ji, 2004], polynomial

models [Chiang et al., 2003], frame-based thresholding [Tseng, 2004] and other techniques extensively described in the scientific literature. This research attempts to quantify motion using four different techniques. Previous work by Lam et al. [Lam et al., 2003] presents frame subtraction, phase correlation, and template correlation. Frame-based correlation is later introduced [Chase et al., 2004a] as a means to counter some of the limitations of previous methods.

6.1 Several approaches to motion sensing

Initial clinical trials using video recording use an analogue video camera, and require a digital conversion from video tapes to audio-video interleaved (avi) format video files. As the audio component is neither required nor permitted for ethical reasons, it is not recorded. The resulting video files are compressed for storage convenience. The video record is then processed off-line, which allows virtually any algorithm complexity. There are no real-time limitations at this stage and the video-processing algorithm can divide the main frame in several regions of interest (ROIs), increasing the computational burden. The division into ROIs allows the system to focus on different body parts, such as the head, torso, each limb, as well as a ROI for the outside area which detects interference from medical staff, as shown in Figure 6.1.

The decomposition of the body into ROIs enables a more accurate diagnosis according to which body part is moving. For instance, mild motion detected from an arm or leg may be considered as normal recovery. However, specific movements such as the grasping for tubes exiting the body are always taken as clear indications of agitation [Lam et al., 2003; Lam, 2003; Starfinger, 2003; Chase et al., 2004a]. Although these two motions may have the same magnitude of motion, they are diagnosed differently. Hence the use of ROIs enhance the motion sensing as a measure for monitoring patient agitation.

This first attempt to quantify motion from the patient video footage is based on a substraction of consecutive frames and is entitled block comparison [Lam et al., 2003]. The block comparison method begins with the conversion of the Red-Green-Blue (RGB) video signal of a video frame into a 2D matrix of pixel intensity values in grey scale. The gray scale conversion reduces the amount of

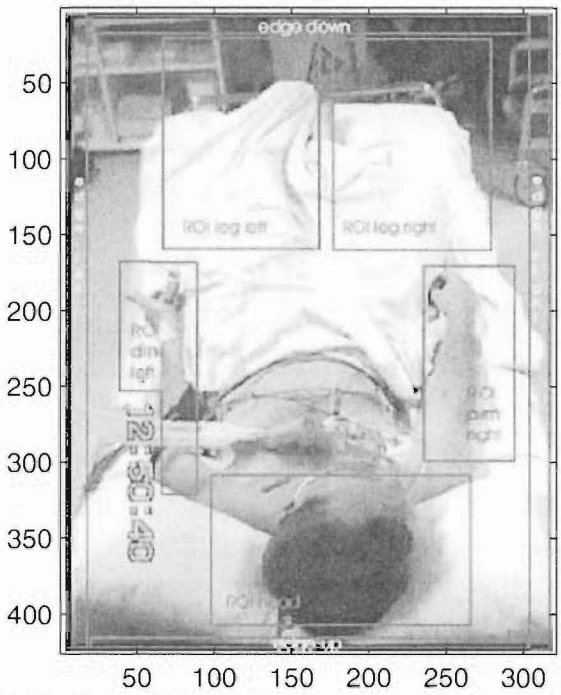

Figure 6.1 Subdivision of video frame into regions of interest [Lam et al., 2003].

information, and hence the corresponding processing time, by a factor of three. The conversion from RGB to gray scale is not a balanced sum of the three colors, as it yields poor contrast. Each color is a discrete value on 8 bits between 0 and 255. The conversion is defined.

$$Pixel_{Gray} = 0.5 \times Pixel_{Red} + 0.2 \times Pixel_{Green} + 0.3 \times Pixel_{Blue} \qquad (6.1)$$

where $Pixel_{Gray}$ is the discrete value of a pixel in gray scale. $Pixel_{Red}$, $Pixel_{Green}$ and $Pixel_{Blue}$ are the discrete values of the red, green and blue components of a color pixel in 24bit RGB video format.

The coefficients applied to each color strongly depend on the environment of application of the motion sensing technique. For instance, the hospital ICU where this research takes place, and particularly the patient's bed where the motion sensing is focused, is mainly white. Hence the right choice of coefficients is required to maintain good contrast. On the other hand, motion sensing performed

outdoors may require another set of coefficients to achieve good contrast. These coefficients are determined empirically within the environment of interest. After the gray scale conversion, each video frame 2D matrix is subtracted from the matrix obtained from the previous video frame to determine a level of motion. Although the division of the main frame into ROIs results in several matrices for a single frame, the same total number of pixels are processed and the processing time remains the same.

The matrix obtained from the difference of two consecutive frames is squared, eliminating the sign of the difference. The sign of the difference is not relevant in this algorithm because a positive or negative pixel difference translates the same amount of motion. Higher level analysis produces a motion analysis according to which ROI contains the motion. Different compositions of ROI motions are combined to create a diagnosis of agitation level. Clinicians interference is detected and also taken in consideration.

Finally, this method is computationally simple, and is capable of detecting a change in a specific region of the video frame. The magnitude of motion is defined empirically, proportional to the pixels difference. However, it is sensitive to light contrast, for instance when a curtain is pulled or one light switched. This situation produces an unwanted artifact and may be filtered by higher-level processing.

The second video-processing technique employed is phase correlation [Lam et al., 2003]. Phase correlation is based on the principle that a translation in the spatial domain (x,y) results in no magnitude change in its corresponding Fourier domain, but only a phase shift. This effect is referred to as the shift theorem for Fourier transforms [Larkin et al., 1997]. Using this property, if the phase of the Fourier transforms of two images that have undergone pure translation are subtracted, the inverse Fourier transform results in a delta function located in the direction of the translation magnitude. However, this technique requires a 2D Fourier transform and inverse Fourier transform, which considerably increases the computing time and effort.

The third technique attempted is template correlation [Lam et al., 2003; Zhu et al., 2004; ?]. This method applies a cross-correlation between a template video frame and a current video frame. It requires obtaining templates of body parts

when the patient is at rest and increasingly agitated, from different angles and poses. Therefore, the calibration required is time-consuming, and the success of this method strongly depends on the quality of the calibration which may not be guaranteed in the ICU environment.

These latest two detection methods are efficient and allow detecting the direction of the motion. However, they do not offer a good quantification tool, as they are more qualitative and oriented that the purely quantitative result desired [Lam et al., 2003]. A more efficient frame-based method is introduced and implemented to counter the limitations encountered with the two previous techniques.

6.2 Implementation of motion sensing

The current method implemented is a tradeoff between accuracy and computation requirements, that can be easily translated from off-line simulation to real-time motion sensing. It is frame-based and considers the human body as a whole, ie the whole patient is fitted in a single ROI, using small edge regions to detect interference motion by clinical staff or relatives

The subdivision of the video frame into ROIs is maintained, because it can significantly improve the accuracy of the motion sensing [Lam et al., 2003]. However, the complexity of the high-level processing is proportional to the number of ROIs. Therefore, the video frame is initially split into two ROIs, namely patient and nurse areas. This approach still allows detecting the interference of the staff on the patient and avoiding artifacts. However, it means that the motion of separate body parts cannot be differentiated with regards to agitation.

The novel method of video-processing used in this research is similar to the frame-based block subtraction introduced in Section 6.1. It does not require spectral analysis and the corresponding Fourier and inverse Fourier transforms that dramatically increase the computational cost. Instead, this method is based on time series and correlation coefficients between two matrices of pixel intensity values obtained from subsequent frames. The RGB to gray scale conversion is also maintained.

To initiate motion sensing the patient and nurse areas need to be defined.

A digital webcam is placed above the patient's bed so that the patient appears lying horizontally in the middle of the video frame. The nurse area is defined above and below the patient frame, so that it can detect the nurse coming from the sides of the patient. This architecture is acceptable since the nurses access the patient from the side most of the time, and there are few artifacts due to the nurse accessing the patients from above the head or below the feet. An example frame using simulated patient is shown in Figure 6.2, where the horizontal lines on the patient's side define the nurse-patient regions boundaries. The frames are acquired from the video footage and stored as bitmap (BMP) files.

Figure 6.2 Subdivision of video frame into 3 regions of interest.

From the video processing point of view, the limits between the upper nurse area and the patient area, as well as the limit between the patient area and the lower nurse area are represented by the line in the frame. The pixels are scanned and processed line by line, and then recorded in the nurse or patient matrix depending whether the processed line of pixels belongs to the patient or nurse area. The upper and lower nurse frames are combined into the overall nurse area and corresponding matrix, while the patient area produces the patient matrix. This approach creates two matrices per frames, from which a motion index is derived.

Motion sensing using block comparison does not account for variable lighting situations and camera settings [Chase et al., 2004a]. For instance, a curtain drawn around a patient's bed can result in significant changes in pixel intensity values independent from motion. The motion sensing technique presented here eliminates artifacts produced by the change in lighting. More specifically, consecutive frames are compared using the Pearson correlation coefficient, often simply referred to as the correlation coefficient [Petrie and Sabin, 2000]. The normalisation performed by the correlation coefficient technique is applied on the time series of pixel intensity values. This correlation coefficient approach eliminates the effect of contrast in surrounding light around the patient's bed, which is proportional to the video frame variance. Basically, if the variance of the matrix is normalised by the correlation coefficient technique, so is the light contrast of two consecutive frames. Hence, this approach examines relative changes rather than absolute.

If two consecutive frames are similar, as a consequence of video footage containing no motion, the pixel intensity values of both frames are similar at each point and the difference between these consecutive frames is null. However, if two consecutive frames are different, as a result of a footage with motion, many pixels will differ within two consecutive frames. This difference between consecutive frames is proportional to the number of pixels differing, also proportional to the amount of motion. The coefficient of correlation is defined [Petrie and Sabin, 2000].

$$r = \frac{cov(f_t, f_{t+1})}{\sqrt{var(f_t) \times var(f_{t+1})}} \tag{6.2}$$

where f_t and f_{t+1} are the video frames acquired at discrete time t and $t+1$. The abbreviation *cov* stands for covariance and *var* stands for variance. The variance of a video frame and the covariance between two consecutive video frames are defined:

$$var(f_t) = \frac{\sum_{x,y} \left(f_t(x,y) - \bar{f}_t\right)^2}{N} \tag{6.3}$$

$$cov(f_t, f_{t+1}) = \frac{\sum_{x,y}\Big(\big(f_t(x,y) - \bar{f}_t\big)\big(f_{t-1}(x,y) - \bar{f}_{t-1}\big)\Big)}{N} \tag{6.4}$$

where x and y are the coordinates of the pixels $f_t(x,y)$ and $f_{t+1}(x,y)$ within the video frames f_t and f_{t+1} acquired at discrete times t and $t+1$ respectively, $\bar{f}_t$ and $\bar{f}_{t+1}$ are the mean pixel intensity values of frame f_t and f_{t+1}, and N is the total number of pixels within one video frame.

$$R = r^2 = \frac{\big(cov(f_t, f_{t+1})\big)^2}{\big(var(f_t) \times var(f_{t+1})\big)} \tag{6.5}$$

The resulting normalised correlation coefficient varies between -1 and 1. If two series yield a correlation coefficient of -1, they are still perfectly correlated, but 180 degrees out of phase. If the correlation coefficient is equal to 0, the two series are totally independent and not correlated at all. Two series with similarities and differences produce a correlation coefficient between -1 and 1. The correlation coefficient offers a means to quantify the differences between two frames, and consequently a means to quantify motion from frame to frame.

In most cases, the coefficient of determination r^2 defined in Equation (6.5) is preferred to the correlation coefficient to compare two series, because its dimension directly represents the proportion of variability attributed to the relationship between the two series [Petrie and Sabin, 2000]. In this imaging context it represents the amount of similarity between the two frames, because the pixel intensity varies similarly around their mean value if the frames are similar.

In this research, the two series correspond to pixel intensity values. Motion is quantified into a motion index. If there is no motion at all, two consecutive frames are identical, so the series of pixel values produce a coefficient of determination equal to 1. If there is wide motion within the video frame, two consecutive frames are different and their covariance is low. Consequently, the coefficient of determination tends to 0. Finally, motion is quantified on a 0 to 1 scale, inversely related to the coefficient of determination. The ROI motion index (RMI) defined in Equation (6.6) is the motion index specific to a ROI. An instance of the motion sensing is described using random frames processed as a single ROI. If the method is applied to two identical frames, such as those shown in Figure 6.3,

the covariance equals the square root of the product of the variance of each frame. In this case it produces a correlation coefficient equal to 1, and a corresponding motion index equal to 0.

$$RMI = (1 - R) \tag{6.6}$$

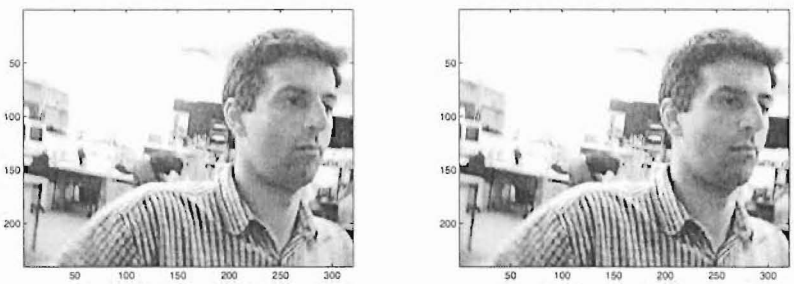

Figure 6.3 2 identical frames.

If the same method is applied to different frames obtained from a video record containing motion, the motion index varies accordingly. The method is tested on 2 different frames acquired from a video footage containing motion, as shown in Figure 6.4. The frame difference shown in Figure 6.5 illustrates the presence of pixels with a different value in the 2 frames. This results in the covariance of the two frames being smaller than the square root of the product of the variance of each frame in Equation (6.5), and the correlation coefficient is consequently smaller than 1. Hence the motion index is greater than 0, proportionally to the amount of pixels being different between the consecutive frames, as well as the amount of difference between them.

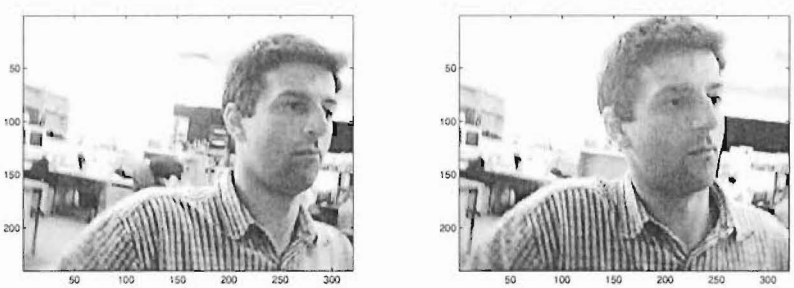

Figure 6.4 2 different frames. The correlation coefficient between these frames is $r = 0.26$ and the resulting motion index is equal to $MI = 0.93$

In the context of this research, the difference between pixels is assumed to be directly proportional to the magnitude of the motion. This assumption can be

optimistic because camera angle, skin tan, and parts of the body covered or not with bed sheets may fluctuate over time, producing a different motion index for the same magnitude of motion and grade of agitation. However, the outputs of the video processing of each ROI are processed by a Fuzzy Inference System (FIS) that deals with these fluctuations. In addition, these fluctuations are not as likely to be significant over the clinical time frames considered for the development and occurrence of patient agitation, which can develop quite rapidly.

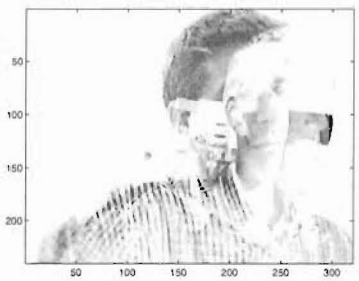

Figure 6.5 Difference between frames.

It is important to note that the frame rate of the video acquisition is a key parameter. For a given motion, the difference between two consecutive frames is greater if the acquisition rate is slower. The acquisition rate is of course a compromise between the hardware and software capabilities, but it also depends on the speed of motion to be detected. The conventional standard for real-time motion application is 30 to 40 frames per second [Piovoso and Laplante, 2003]. Applications such as eye position calculation with high velocity head turns, require sampling rates up to 200 frames per second [Zhu et al., 2004]. However, ICU patients do not perform extremely fast motions, and an acquisition rate of one frame per second is enough to perform the fundamental motion sensing, required without losing track of the patient motion even during extreme agitation [Chase et al., 2004a].

The second main parameter is the camera angle with the subject of interest. For ICU patients, a part of the video frame contains parts that rarely move or change, such as the sides of the bed and the floor in the background. Therefore, some pixels always remain the same. If the motion sensing and quantification is performed on a relatively small area of the video frame, an empirical coefficient may be added to produce a motion index that still ranges between 0 and 1, although the correlation coefficient variations are limited. In addition, if the angle between the camera and the patient is extreme, perspective may cause some

motions nearer the camera to appear much larger than equal motions further away. This last issue can be solved already using coordinate transform if the camera angle is known.

The motion sensing algorithm produces a motion index from the patient area as well as the nurse area. Consequently, motion sensing produces a patient-related motion index and a nurse-related motion index. Both are combined using a non-linear technique based on clinicians knowledge modelled in a fuzzy inference system (FIS). This combination seeks to account for motion in the patient ROI due to clinical staff by assuming such motion is associated with motion in the nursing ROI. This strategy aims at reducing artifacts produced by clinicians' interference.

Part II

Fuzzy inference systems for patient monitoring

Chapter 7

Structure of a Fuzzy Inference System

Fuzzy inference systems (FIS) are derived from the fuzzy set theory, also referred to as soft computing. Soft computing is a way to improve the relationship between humans and computers. If the capabilities of humans and computers could be combined, a remarkable system would emerge [Terano et al., 1987]. This philosophy already improves some engineering fields such as monitoring and diagnosing [Sokolowski, 2004]. For instance, the non-linear experience-based field of rock engineering, may be improved using fuzzy logic [Sonmez et al., 2003; Gokceoglu and Zorlu, 2004]. Fuzzy sets are also used to design fuzzy controllers, that may assist humans in piloting a plane [Melin and Castillo, 2003], or control the balance of a challenging system such as an inverted pendulum or beam-and-ball system [Godfrey et al., 1995]. Other applications require human knowledge and the capability to deal with non-linearity, such as electricity demand forecast [Abraham and Nath, 2001], traffic control [Lin and Kuo, 2001] factory production prediction [Chen, 2003] or economic forecast [Frantti and Mahonen, 2001].

Fuzzy set theory is also highly suitable for developing knowledge-based biomedical engineering applications. A FIS may be implemented in medical areas such as interpretation of medical findings [Kwok et al., 2003], syndrome differentiation in Eastern medicine [Phuong and Kreinovich, 2001], diagnosis of diseases in Western medicine [Reis et al., 2004] and real-time monitoring of patient data [Starfinger, 2003; Coughlin et al., 2004]. The ability of FIS to combine computation and crisp values with rule-based clinical experience is particularly well suited to clinical applications where analytical answers are unavailable.

This research is an application of real-time patient monitoring, and the insertion of several FIS at crucial points enhances the final diagnostic, because

expert knowledge can be modelled and inserted in the system. The general structure of a FIS is introduced first, and specific designs used in this thesis are then fully described. The self-learning structures include Adaptive Network-based FIS (ANFIS), hybrid FIS (HyFIS) and Adaptive Neural Networks, and are covered in literature. This chapter focuses on the structure of a FIS, as defined by Mamdani [Mamdani and Assilian, 1999].

Fuzzy logic, and the different structures it provides, are based on the human brain. Each processing element is an artificial neuron, and the final structure is an artificial neural network, similar to the human brain that is a biological neural network. The artificial neuron is inspired from the structure and behaviour of the biological neuron.

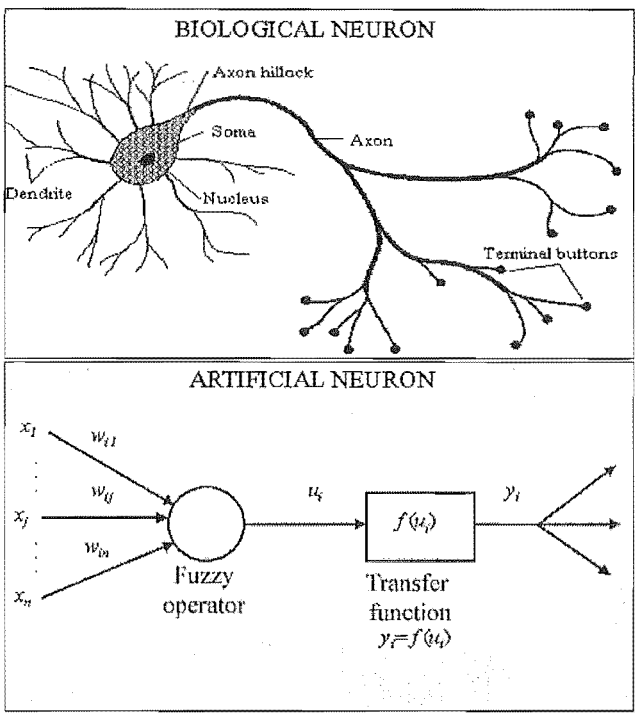

Figure 7.1 Schematics of biological and artificial neurons.

The analogy between the biological and artificial neuron, shown in Figure 7.1, is the foundation of the fuzzy theory and its applications. First, the inputs of the artificial neuron corresponds to the dendrites of the biological neuron. The strength and polarity of the weight applied to each input of the artificial neuron (w_{ij} in Figure 7.1) is equivalent to the physical and neurochemical characteristics of each synapse of the biological neuron. The synapse of a neuron is the connection between the axon of the previous neuron and the dendrite of this neu-

ron. Finally, the biological neuron produces a binary output signal, depending on whether the inputs exceed a particular threshold or not. The artificial neuron presents different non-linear transfer functions that make them more versatile to suit different applications, from quasi-linear (linear + saturation effect) to sigmoidal and trapezoidal functions. The shape of the transfer function is a key parameter to determine the global behaviour of a neural network.

The axon, output of the neuron nucleus, propagates the output to one or several neurons of the next layer of the network by the synapses. The schematic structure of an artificial neuron presented in Figure 7.1 depends on its location in the network. The transfer function, number of inputs and outputs mainly depends whether the neuron is located in the input layer, output layer, or a middle layer often called hidden layer.

Different structures are obtained from combining several artificial neurons into a network and can be classified into three main groups depending on their features: the FIS, the hybrid Adaptive Network-based FIS (HyFIS, ANFIS), and the adaptive neural networks (ANN). The FIS is a transparent design where the user determines every detail of the final structure of the network. It is very user-friendly since each part performs a clear task within the diagnostic process.

The ANN is more suitable and performs better in some circumstances because it presents self-learning capabilities. Because it does not need human interference to adapt to a set of data, the ANN is similar to a black box from the user point of view, with a given task of classification or diagnostic. The network is trained using algorithms and training sets of data to initialise, where the user does not interfere. HyFIS and ANFIS are a compromise between the transparent user-defined fixed network that is the FIS, and the self-learning capabilities of the ANN. Possible upgrades exist from a FIS to HyFIS, ANFIS or ANN and it offers some relevant advantages for future work that are discussed at the end of this thesis.

Ultimately, the neural networks are inserted into real-world contexts with crisp inputs and outputs. Therefore, the input and output layers of the network are the interface between crisp variables and the fuzzy reasoning, and the hidden layers perform the fuzzy reasoning. The conversion between crisp and fuzzy logic is called fuzzification. The fuzzy reasoning is then based on a set of rules,

modelled in the hidden layers, that are defined by the user in the case of FIS, and can be also derived from training sets of data by self-learning algorithms in more advanced NN. Finally the fuzzy output is converted back to a real-world crisp value by the defuzzification process.

7.1 Fuzzification

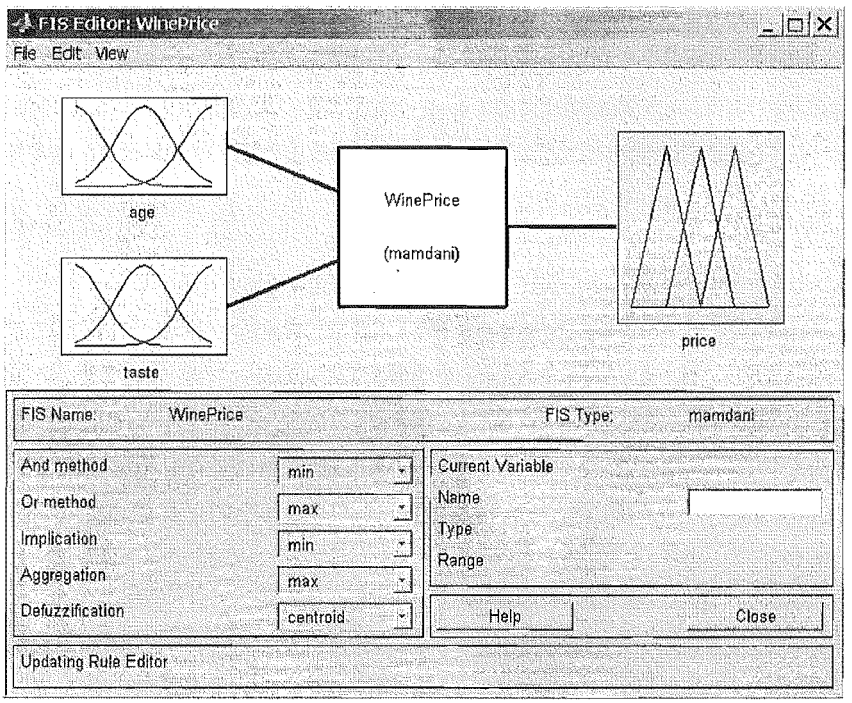

Figure 7.2 FIS "Wine Price" defined in Matlab fuzzy toolbox GUI. This window allows setting AND, OR, Implication, Aggregation and Defuzzification methods.

The first step to apply fuzzy logic on real world crisp variables is called fuzzification. It consists of converting a crisp variable into a set of fuzzy classes, so-called membership functions (MF), specified by a linguistic value. It is similar to the way a human brain performs classification. This process is best described with a simple example. The description of the FIS is illustrated in this Section by a simple FIS used to estimate the retail price of a wine bottle, in Euros, defined in the Matlab fuzzy toolbox and illustrated in Figure 7.2.

The two inputs to the system are the taste, as assessed by professional wine tasters on a 0–10 scale, and the age of the bottle, between 0 and 10 years. The output of the FIS is the recommended price of the bottle, up to 1000 Euros. The

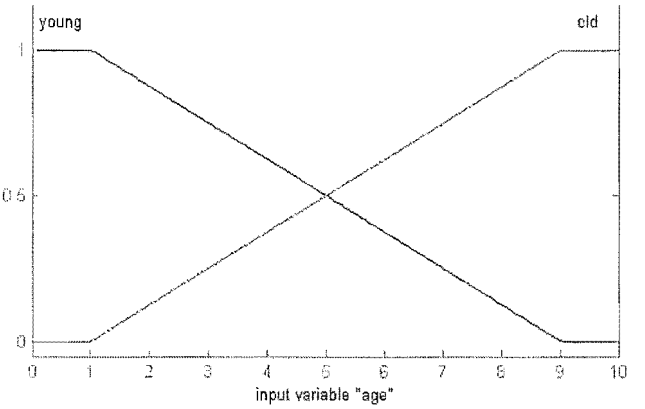

Figure 7.3 Fuzzy set "age" composed of 2 MFs "young" and "old".

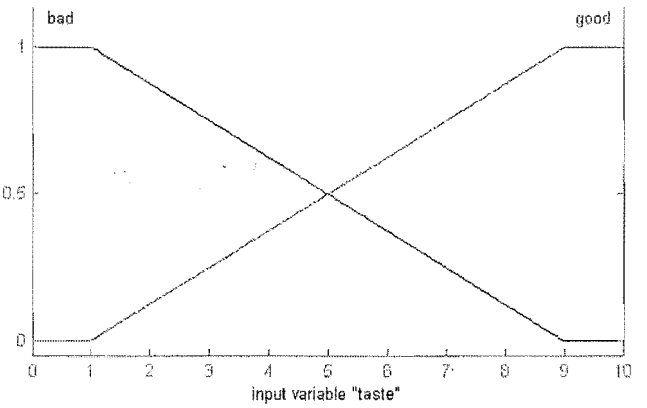

Figure 7.4 Fuzzy set "Taste" composed of 2 MFs "bad" and "good".

set of MFs utilised to fuzzify a crisp input is called a fuzzy set. The fuzzy set "taste" contains 2 MFs, respectively "bad" and "good", to fuzzify the 0–10 taste range. The fuzzy set "age" contains 2 MFs, respectively "young" and "old", to fuzzify the 0–10 years age of the bottle. The shape of the MF is trapezoidal in this example. The different MF available in the Matlab fuzzy toolbox are triangular, trapezoidal, bell-shaped, Gaussian, asymmetrical Gaussian, sigmoidal, s-shaped, z-shaped and pi-shaped MF. These MFs are illustrated for these two variables in Figures 7.3 and 7.4. It is important to note how crisp values in the range 0–10 are turned into fuzzy linguistic levels. The shape of MFs and the way they overlap contribute significantly to the overall transfer function of the FIS.

The fuzzification of a crisp input variable is easily described graphically in Figure 7.5. A vertical line is drawn through the input value on the horizontal axis. It crosses one or several MF curves at given points and the ordinate of each MF intersection is the degree of membership associated with that MF. The vertical axis is the degree of membership or degree of ambiguity, often referred

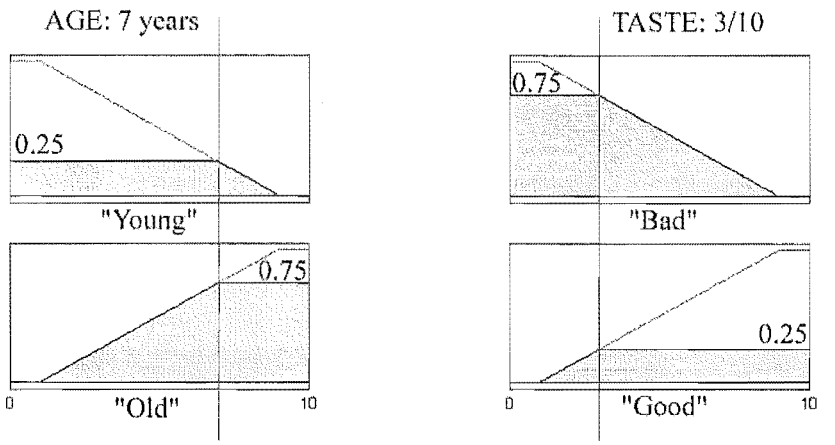

Figure 7.5 Fuzzification of a set of crisp input: age = 7 years, taste = grade 3/10.

to as μ [Terano et al., 1987].

In the example of the wine price estimation FIS, a bottle is 7-year-old and its taste graded 3/10. If this set of input variables is fuzzified by the input layer of the FIS, The vertical line corresponding to 7 years of age crosses the "young" MF curve at ordinate 0.25. This means the FIS fuzzifies a 7-year-old bottle as being "young" with a degree of membership $\mu_{young} = 0.25$. The same vertical line crosses the "old" MF curve at ordinate 0.7. The FIS fuzzifies a 7-year-old bottle of wine as being "old" with a degree of membership $\mu_{old} = 0.75$. Similarly, a bottle of wine with a taste grade of 3/10 crosses the "bad" MF curve with degree of membership $\mu_{bad} = 0.75$, and the "good" MF curve with degree of membership $\mu_{good} = 0.25$.

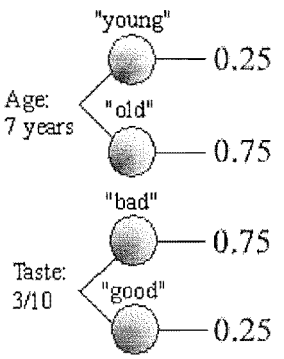

Figure 7.6 Input layer of the FIS neural network.

The fuzzification process can therefore classify a single input into several MFs with different degrees of membership. This corresponds to the way the brain is processing real-world variables. For instance, a person drinking wine

may say some wine is not very good, but not too bad either, which corresponds to classifying the wine in several linguistic values with corresponding degrees of confidence. The same process can be represented graphically by an input neuron layer as illustrated in Figure 7.6. Each MF is modelled as a neuron, and the fuzzification process is modelled as the input neuron layer. Each neuron transfer function corresponds to the MF curve it represents.

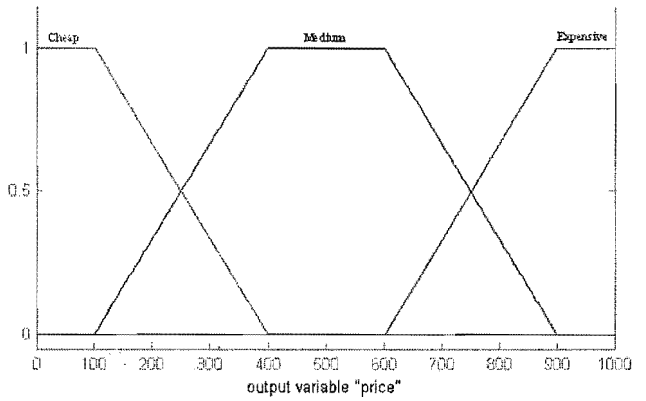

Figure 7.7 Fuzzy Set "Price" and its 3 MFs: "Cheap", "Medium" and "Expensive".

The output of the input layer is an array of degrees of confidence that propagates to the next layer of neurons. This next layer represents the set of rules on which the system is based. The rules link the input fuzzy sets to the output fuzzy sets. In the example of the wine bottle price estimation FIS, the output fuzzy set is the price of the bottle, in Euros. The fuzzy set "price" contains 3 MFs, with respective linguistic values "cheap", "medium" and "expensive", as illustrated in Figure 7.7.

7.2 Fuzzy rules

The behaviour of the FIS is defined by a set of rules, which performs the mapping between input fuzzy sets and output fuzzy sets. Each rule is modelled as a neuron, and it is connected to the appropriate MF of each input fuzzy set. So-called "If-Then" rules define the behaviour of the system by mapping antecedent inputs to consequent outputs

The output of a rule is a MF of the output fuzzy set, weighted with a degree of support. The degree of support of a rule μ_{rule1} is derived from the degrees of membership of each antecedent input. If a rule depends on a single input,

the rule degree of support is equal to the input degree of membership. If a rule is based on several inputs, the antecedent degrees of membership are combined with the "AND" method or the "OR" method.

The choice of the appropriate AND or OR operator is crucial because the propagation of several antecedent degrees of membership into the rule degree of support must reflect the true meaning of the rule. For instance, the same wine price estimator processes a bottle that is 10 years of age with a taste of 6/10. According to the fuzzy set "age" illustrated in Figure 7.3, a 10-year-old bottle belongs to the linguistic class "old" with degree of membership $\mu_{old} = 1$. The fuzzy set "taste" illustrated in Figure 7.4 fuzzifies the bottle with a taste of 6/10 into the linguistic class "good" with degree of membership $\mu_{good} = 0.625$. Then the philosophy of the FIS and corresponding heuristics is translated into a set of rules.

First, the price of the bottle can be based on rule A: IF age is old AND taste is good THEN price is expensive. In this case, the bottle is expensive only if it is old and good. The degree of support must take into account the smaller degree of membership to produce a consequent output. The family of fuzzy operators suitable for this operation is called T-norm (Triangular norm) operators and are defined to meet specific requirements. A T-norm operator is a binary mapping T(.,.) satisfying:

- Boundary: T(0, 0) = 0, T(a, 1) = T(1, a) = a
- Monotonicity: T(a, b) $\leq$ T(c, d) if a $\leq$ c and b $\leq$ d
- Commutativity: T(a, b) = T(b, a)
- Associativity: T(a, T(b, c)) = T(T(a, b), c)

Common T-norm operator include:

$$Minimum : MIN(\mu_{input1}, \mu_{input2}) = \mu_{input1} \wedge \mu_{input2} \tag{7.1}$$

$$Product : PROD(\mu_{input1}, \mu_{input2}) = \mu_{input1} \cdot \mu_{input2} \tag{7.2}$$

Second, the price of the bottle can be based on rule B: If age is old OR taste is good THEN price is expensive. In this case, the bottle is expensive if the wine is either old or good. Therefore, a young bottle that tastes good is expensive, and a old bottle that tastes bad is also expensive. This rule reflects a different philosophy to estimate the retail price of wine bottle. In this case, the stronger degree of membership is taken into account to produce the rule degree of support. The operators suitable in this case are the T-conorm (or S-norm) operators. A T-conorm operator is a binary mapping S(.,.) satisfying:

- Boundary: S(1, 1) = 1, S(a, 0) = S(0, a) = a
- Monotonicity: S(a, b) $\leq$ S(c, d) if a $\leq$ c and b $\leq$ d
- Commutativity: S(a, b) = S(b, a)
- Associativity: S(a, S(b, c)) = S(S(a, b), c)

Common T-conorm operators include:

$$Maximum : MAX(\mu_{input1}, \mu_{input2}) = \mu_{input1} \vee \mu_{input2} \tag{7.3}$$

$$BoundedSum : SUM(\mu_{input1}, \mu_{input2}) = (\mu_{input1} + \mu_{input2}) \wedge 1 \tag{7.4}$$

A set of rules is defined in the Matlab fuzzy toolbox rule editor to model the behaviour of the wine price estimate FIS, and shown in Figure 7.8. A bottle of wine is 7-year-old and its taste is given 3/10. The fuzzification process will produce the array of degrees of membership as given in Figure 7.6. The T-norm operator used to perform the AND method is "minimum". The subsequent degrees of support for the set of rules is processed with this particular input.

$$\mu_{rule1} = \mu_{YoungAge} \wedge \mu_{BadTaste} = 0.25$$

$$\mu_{rule2} = \mu_{OldAge} \wedge \mu_{GoodTaste} = 0.25$$

$$\mu_{rule3} = \mu_{YoungAge} \wedge \mu_{GoodTaste} = 0.25$$

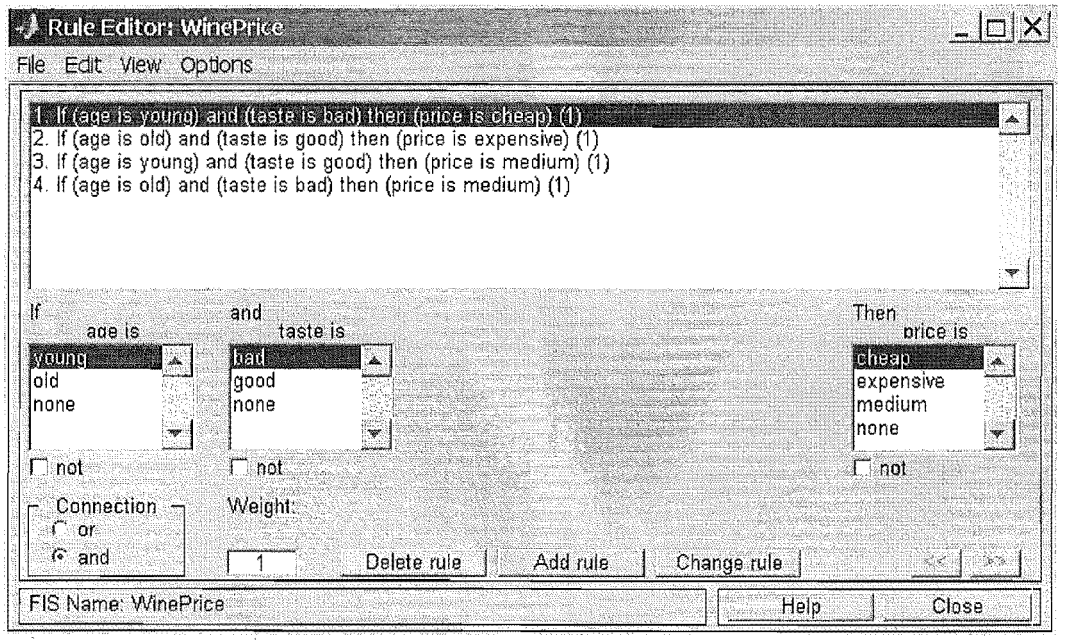

Figure 7.8 Set of fuzzy rules defined in Matlab fuzzy toolbox. Each rule can be assigned a weight, and its antecedent can be combined with either AND or OR method

$$\mu_{rule4} = \mu_{OldAge} \wedge \mu_{BadTaste} = 0.75$$

The same operation performed using the "product" operator produce another set of degrees of support.

$$\mu_{rule1} = \mu_{YoungAge} \cdot \mu_{BadTaste} = 0.1875$$

$$\mu_{rule2} = \mu_{OldAge} \cdot \mu_{GoodTaste} = 0.1875$$

$$\mu_{rule3} = \mu_{YoungAge} \cdot \mu_{GoodTaste} = 0.0625$$

$$\mu_{rule4} = \mu_{OldAge} \cdot \mu_{BadTaste} = 0.5625$$

The "Minimum" operator takes only the smallest degree of membership into account, whereas the "Product" operator takes every degree of membership into account to produce the degree of support of the rule.

The degree of support of a rule is taken into consideration to compute the output of this rule. The process of weighing a rule output according to the degree of support is called the implication. It uses the degree of support of the rule to shape the output MF. The consequent of a fuzzy rule assigns a MF to the output.

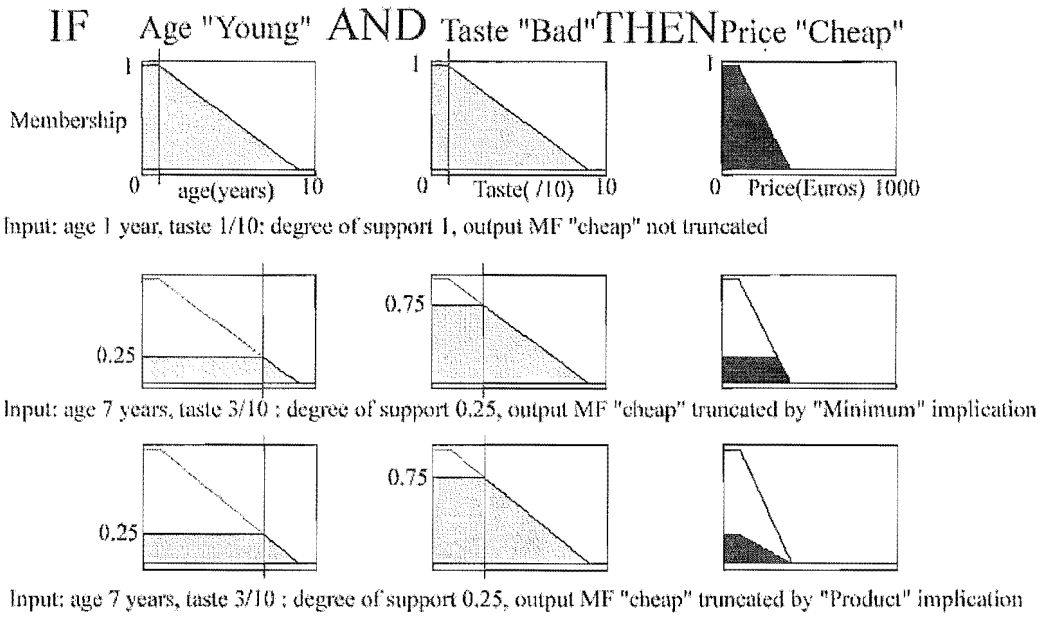

Figure 7.9 Implication of rule 1 with "minimum" AND method. The top frame illustrates no implication with degree of support = 1. The middle frame illustrates "minimum" implication. The bottom frame illustrates "product" implication.

This MF is chosen to indicate the quality of the consequent. In this example, it indicates whether the price is expensive, medium or cheap. If the antecedent is only partially true, (i.e. the degree of support is less than 1), then the output MF is truncated according to the implication operator, as illustrated in Figure 7.9. The implication is done by a T-norm operator, such as minimum or product, to perform the weighing of the output MF.

Each rule is implicated by its own degree of support and output a truncated output MF. The wine estimate FIS is based on a set of 4 rules, and each rule produces an output MF. The output of the FIS is obtained from the neuron of the last layer that performs the composition and defuzzification.

7.3 Composition and defuzzification

The crisp input variables have propagated through the fuzzifying input layer and the set of rules modelled in the second layer of neurons. This propagation produces a MF per rule, which depends on the consequent degree of support of that rule. The fuzzy output of the FIS is a MF composed of the individual

output MF of each rule of the hidden layer of neurons that models the set of rules. The rules with the greater degree of support have the bigger membership and they should weigh more than less supported rules to compute the final output. Consequently, the composition task is performed by a T-conorm operator such as "Bounded sum" or "Maximum".

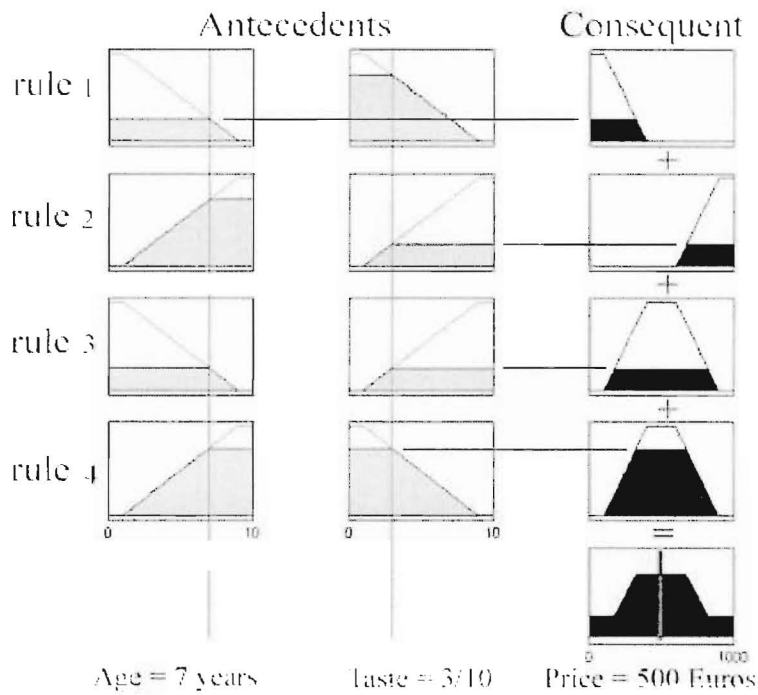

Figure 7.10 Fuzzy Inference diagram of the "Wine Price" FIS. Each row corresponds to a rule. The inference is performed with "Minimum" AND operator, "Minimum" Implication operator, "Maximum" Composition operator and "centroid" defuzzification method.

The composition, also called aggregation, produces one single output MF. However, the real-world applications in which FIS are inserted require a crisp output value. The process of extracting a crisp value from a fuzzy output MF is called defuzzification. Common defuzzification methods include "centroid", "bisector", "middle of maximum", "largest of maximum", and "smallest of maximum".

The "centroid" is the centre of mass of the output MF. The "bisector" is the centre of area. The middle, largest and smallest of maximum methods consider the maximum membership of the output MF. If the peak membership corresponds

to a flat part of the MF, there is a range of output values corresponding to the largest membership. Therefore, the "largest of maximum" method process the largest output value with maximum membership as the FIS output value. The "middle of maximum" and "smallest of maximum" methods respectively detect the middle and smallest output values with maximum membership as the FIS output value.

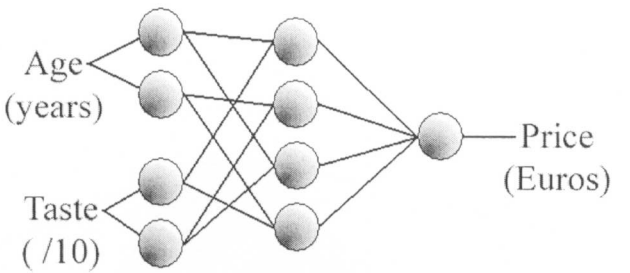

Figure 7.11 Neural network structure of the wine price estimate FIS. Each antecedent MF connects appropriately to the middle layer of neurons modelling fuzzy rules

The FIS designed to estimate the price of a wine bottle according to its age and taste is now completed, and it can process a crisp input such as the age of the bottle, and produce a crisp output such as the price of the bottle, as shown in Figure 7.10. The FIS can be represented as a neural network with three layers: the input fuzzification layer, the middle rule based layer and the composition/defuzzification output layer, as illustrated in Figure 7.11. The input layer requires a neuron per input MF, the middle layer contains a neuron per rule, and the output layer is made of a neuron per output variable. The overall transfer function of the FIS is graphically examined with a surface plot, such as the Wine price FIS transfer function displayed in Figure 7.12. The shape of the transfer surface represents the behaviour of the FIS related to two variables. The response of the FIS can be modified by the set of rules, as well as the shape and overlap of the MFs of each fuzzy set.

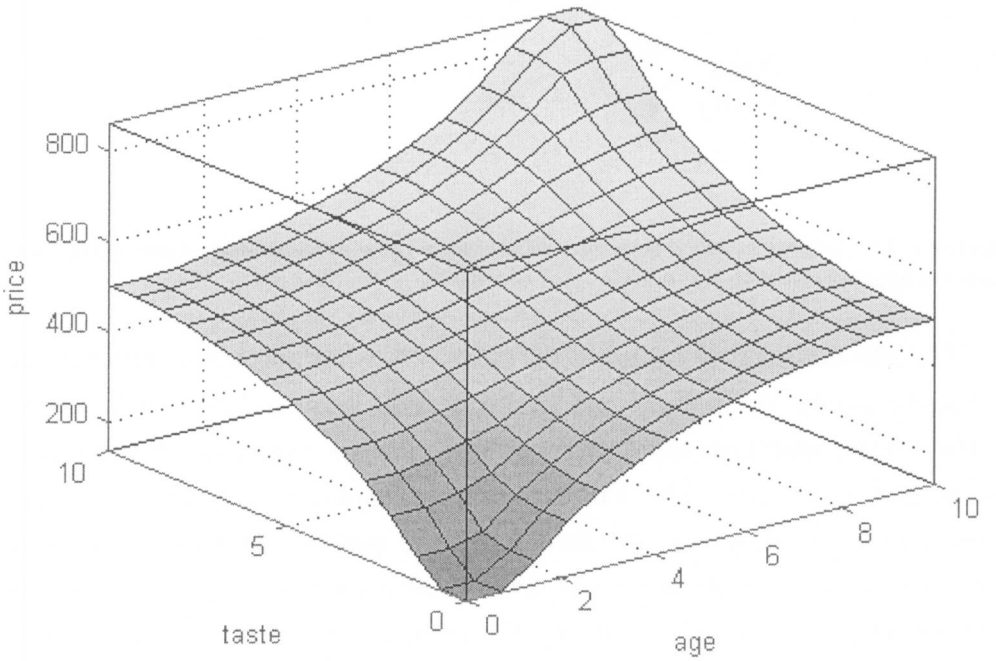

Figure 7.12 Transfer surface of the wine price estimate FIS

Chapter 8

Video FIS

The first FIS inserted in the agitation sensor computes a motion index from the several ROIs motion indices. The video frame is split into nurse and patient areas, and each motion is detected and quantified independently. For the last stage, which consists of computing an agitation index, it is useful to summarise the video-processing into one single motion index (MI).

8.1 Fuzzy sets of the video FIS

The inputs of the video FIS are the ROI-related motion indices. The video-processing algorithm of the agitation sensor divides the main video frame into two ROIs. Therefore the Video FIS defined in Figure 8.1 has two inputs, namely patient motion index and nurse motion index, both ranging from 0 to 1. The two input fuzzy sets shown in Figures 8.3 and ?? are composed of two trapezoidal MFs, with linguistic values "low" and "high" magnitude of motion, and the output fuzzy set is composed of three trapezoidal MFs, namely "small", "medium" and "large" MI.

Note that the output fuzzy set shown in Figure 8.4 cover the -20–120 range although the motion index ranges 0–100. This oversize range enables a better distribution of the output along the 0–100 range after defuzzification, which practically does not reach the end of the range.

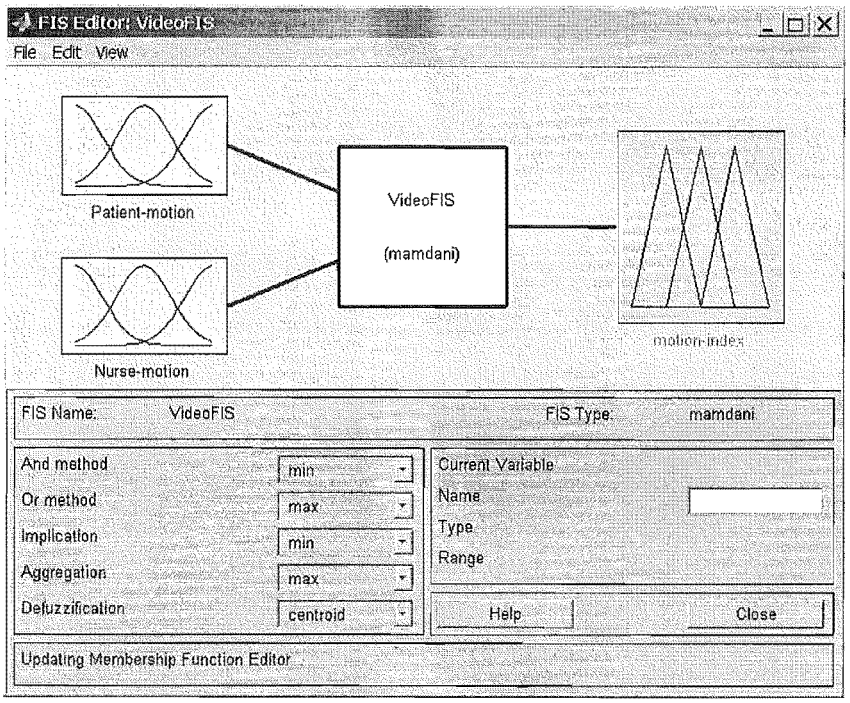

Figure 8.1 Video FIS defined in Matlab fuzzy toolbox

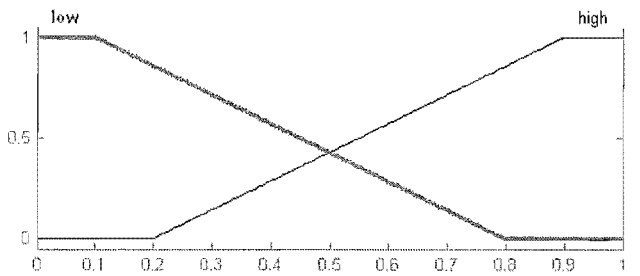

Figure 8.2 "Patient motion" input fuzzy set. patient motion index vs. degree of membership

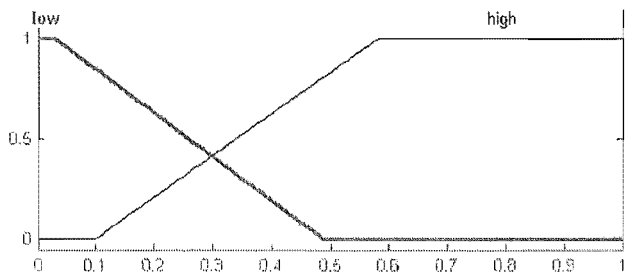

Figure 8.3 "Nurse motion" input fuzzy set. nurse motion index vs. degree of membership

8.2 Fuzzy rules of the video FIS

The video FIS behaviour is defined by 3 fuzzy rules. The antecedents are combined with a "Minimum" operator, and the consequent MF is truncated using a

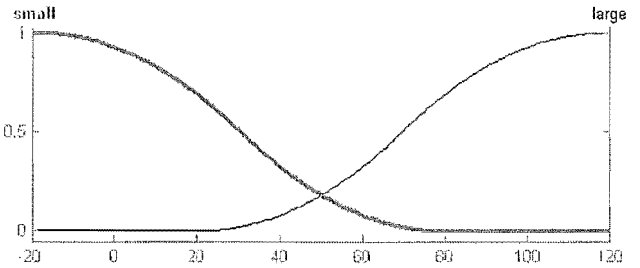

Figure 8.4 "Motion index" output fuzzy set. motion index vs. degree of membership

"Minimum" implication operator. The output MF of the fuzzy rules are aggregated with the "Maximum" operator. The implication and aggregation operators are selected in the main window of the Matlab fuzzy toolbox displayed in Figure 8.1. The three fuzzy rules are defined.

1. If patient motion is low THEN MI is small.
2. If patient motion is high AND nurse motion is low THEN MI is large
3. If nurse motion is high THEN MI is small (virtually off)

This set of rules tries to filter the artifacts created when a nurse enters the patient area. The motion due to the nurse can be interpreted as patient motion and agitation so the video-processing has to be designed properly. The nurses access the patient from the side of the bed, which form the nurse area, and provokes the nurse motion index to rise. Shortly after entering the video frame from the nurse area, a nurse usually overlaps the patient from the camera's point of view, and the patient motion index also rises. This scenario creates an artifact in the motion sensing, which subsequently creates a false positive response of the agitation index. So the patient motion is only fully taken into consideration when there is little or no motion in the nurse area. The more motion is detected in the nurse area, the more attenuated is the motion index. In extreme conditions of agitation where nursing staff actually restrain the patient from moving, the nurse motion is very high and the motion index is kept very low (virtually switched off) and the agitation level is then based primarily on the physiological input variables. The fuzzy transfer function for these rules is shown in Figure 8.5.

Note that the Video FIS was based on another philosophy and corresponding set of rules when first introduced [Chase et al., 2004a]. The MI was kept along

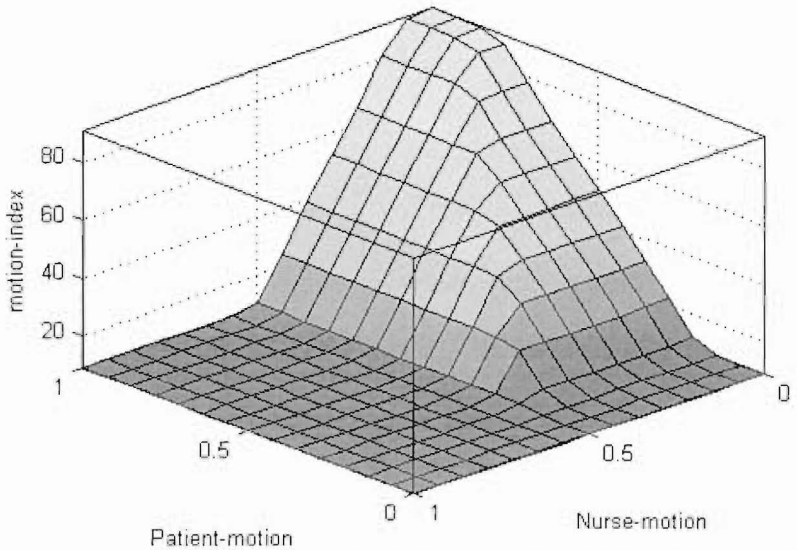

Figure 8.5 Video FIS transfer surface. The motion sensing is off when too much motion is detected within the nurse area

with the other input parameters during extreme nurse motion. However, this approach resulted in a lot of unwanted artifacts, and the set of rules had to be changed for consistency of the motion sensing of agitated patients. The modification of the Video FIS is modelled through rule 3 that virtually switches the motion sensing off when too much nurse motion is detected in the nurse area. Finally, the MI produced by the video FIS inputs the final FIS with the other markers HR, HRD, SBP and BPD.

Chapter 9

Agitation FIS

The agitation FIS combines the five intermediate variables HR, HRD, SBP, BPD and MI obtained from preceding signal-processing stages into the agitation index (AI). The structure of the agitation FIS is summarized in Figure 9.1.

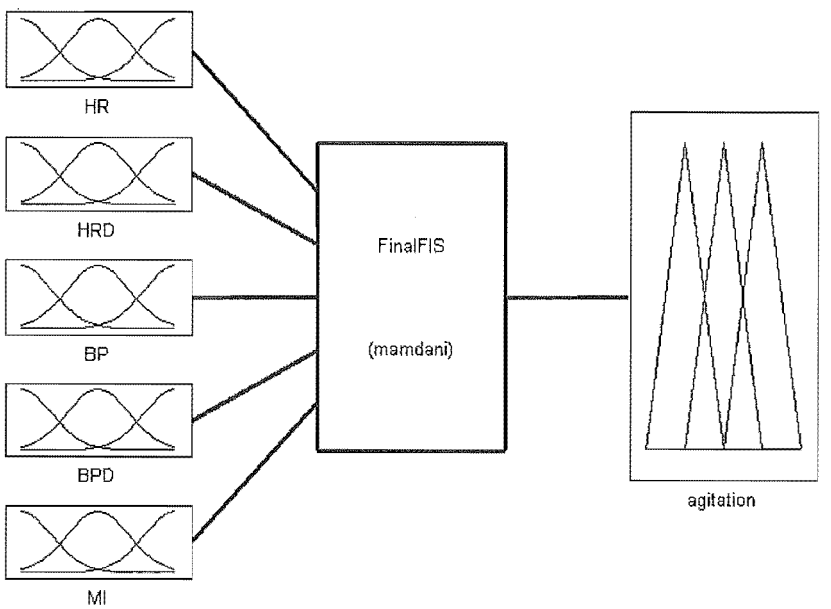

Figure 9.1 Diagram of agitation FIS. output is the agitation index in the range 0–100.

9.1 Fuzzy sets of the agitation FIS

This first instance of the agitation FIS is based on a reliable set of inputs. Basically, the HRV and BPV are often used on a qualitative manner , but it remains challenging to quantify a marker from these variability metrics. In this first instance of FIS, the HRD and BPD values are used. Therefore, the state and

dynamic of ECG is modelled by HR (bpm) and HRD (bpm^2). The "HR" fuzzy set is composed of linguistic classes "low" modelled by a "Z" MF, and "high" modelled by a "S" MF, as illustrated in Figure 9.2. The input of the HR fuzzy set ranges from 50 to 200 bpm. The "HRD" fuzzy set is made of the "low" MF with "Z" shape, and the "high" MF with "S" shape. The "HRD" input ranges from 0 to 500 bpm^2 according to observation of data, and the fuzzy set is displayed in Figure 9.3.

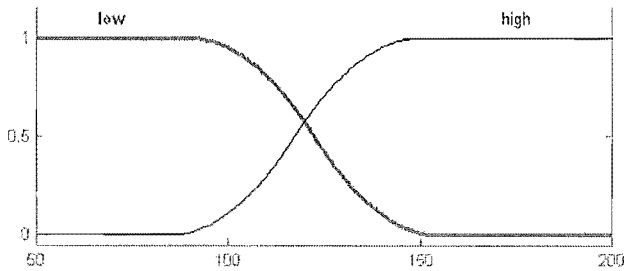

Figure 9.2 Final FIS input fuzzy set HR

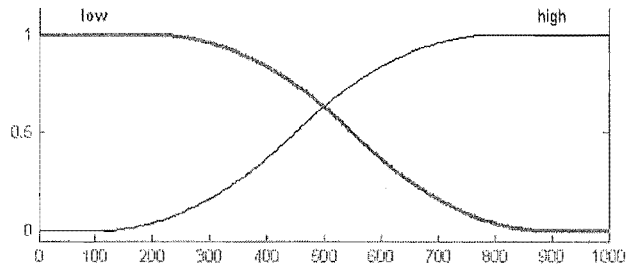

Figure 9.3 Final FIS input fuzzy set HRD

Similarly, the ABP state and dynamic is modelled by SBP (mmHg) and BPD (mmHg/min). The SBP fuzzy set shown in Figure 9.4 ranges from 50 to 250 mmHg. The "low" linguistic class is a "Z" shape MF, and the "high" class is a "S" shape MF. Saturation would result in assigning a degree of membership of 1 in the border class, which wouldn't impair the fuzzy reasoning of the agitation FIS. For example a SBP value of 250 mmHg is classified in the "high" MF with degree of membership of 1. A SBP value of 350 mmHg, which is physiologically possible to reach, will also be classified as "high" with degree of membership of 1. The saturation is not an issue in this particular case. The BPD fuzzy set shown in Figure 9.5 ranges from 0 to 500 mmHg/s. The "low" linguistic class is a "Z" shape MF, and the "high" class is a "S" shape MF. Finally MI is also incorporated to prevent missing an episode of agitation during of a lack of physiological reactions to mental or physical stress. The input of the motion fuzzy set ranges from 0 to 100. The "low" and "high" linguistic values are modelled by triangular MFs.

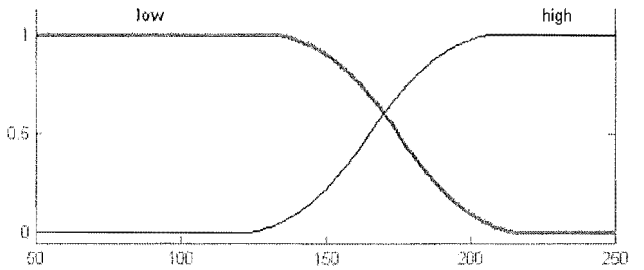

Figure 9.4 Final FIS input fuzzy set SBP

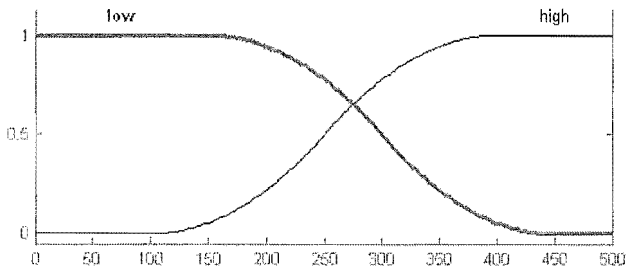

Figure 9.5 Final FIS input fuzzy set BPD

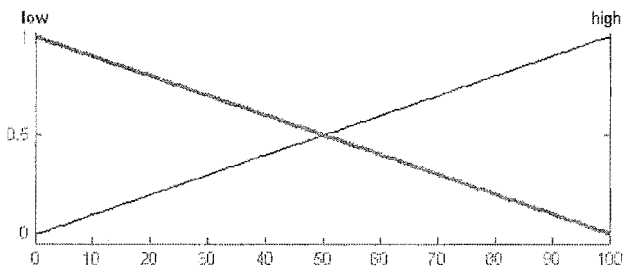

Figure 9.6 Final FIS input fuzzy set MI

The output fuzzy set "AI" is composed of three linguistic values. The "low" class is a "Z" MF, the "medium" class is a "pi" MF and the "high" class is a "S" MF, as shown in Figure 9.7. The output ranges from -20 to 120, and this permits to reach extreme AI values of 0 and 100, because fuzzy reasoning hardly reaches the extremes of the output range. The heuristic between the five inputs and AI is modelled by 6 fuzzy rules.

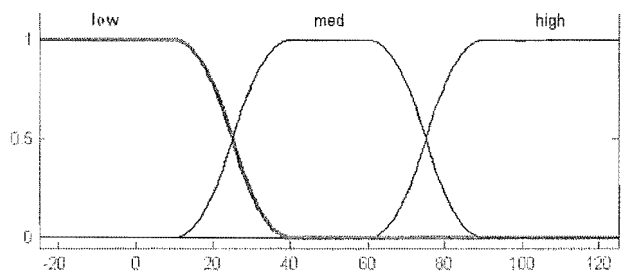

Figure 9.7 Final FIS output fuzzy set AI

9.2 Fuzzy rules of the agitation FIS

The final FIS is used to model the diagnostic process of agitation by clinicians. The clinicians' expert knowledge is modelled into 6 rules.

1. If MI is high then agitation is high.
2. If HR is high and MI is low then agitation is high.
3. If BP is high and MI is low then agitation is high.
4. If HR is low and HRD is low and BP is low and BPD is low and MI is low then agitation is low.
5. If HR is low and HRD is high and BP is low and BPD is low and MI is low then agitation is medium.
6. If HR is low and HRD is low and BP is low and BPD is high and MI is low then agitation is medium.

The degree of support of each rule is obtained from the combination of the antecedent degrees of membership using a "Minimum" operator. The degree of support is then applied on the rule output MF with a "Minimum" operator. The output MFs of the 6 rules compose the final output MF with a "Maximum" aggregation operator. The agitation index is obtained after "centroid" defuzzification.

This set of rules is defined from clinical advice and knowledge of critical care agitation, as well as direct observation and reports in the literature. Rule 1 is the worst case scenario where the sensor could not detect the growing potential for an agitation episode. The patient starts to move and the agitation index rises accordingly. This detection is of less clinical use as the patient is already moving. However, it does ensure consistency between the current subjective observation approach and the system. As a result, there is no advanced clinical warning available when the system reaction is triggered by rule 1.

The other five rules try to forecast agitation based on physiological variables introduced as agitation sensor inputs. Rule 2 specifies that an elevated HR is

a sign of a strong potential for agitation. Rule 3 is triggered by an elevated SBP, potentially hypertension, which is also a sign of potential agitation. Rule 4 is used to calibrate the system and shape the corresponding transfer surface. It stipulates that low inputs correspond to low AI. Although it seems trivial, this rule is required to obtain the desired transfer function of the agitation FIS, which is illustrated in Figure 9.8. Rules 5 and 6 try to detect early changes in HR and BP using their corresponding dynamics. If HR is low and HRD is high, then HR will soon be higher, and the agitation index reflect this evolution with a "medium" AI linguistic value. If BP is low and BPD is high, then BP will also be high soon, and AI is "medium". These last two rules smooth the transfer surfaces and provide preemptive detection of the evolution of patient agitation, which is a major goal for this system as it would enable preemptive sedative management action.

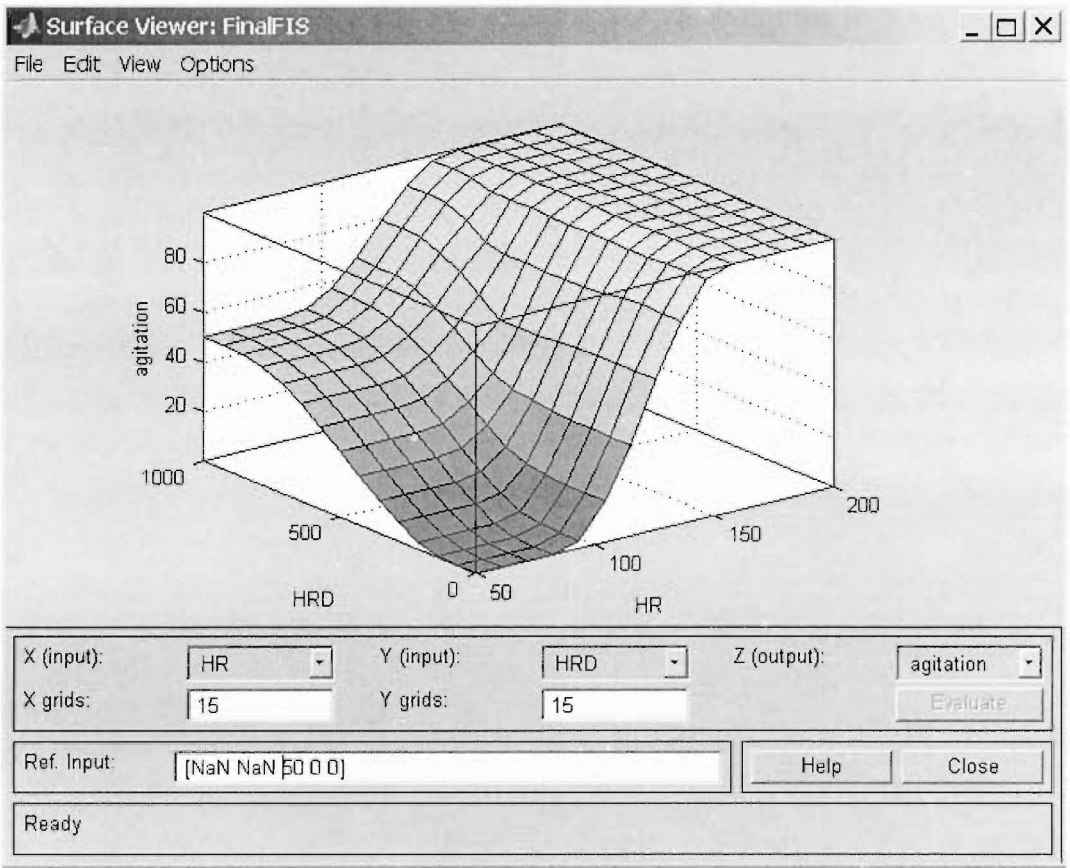

Figure 9.8 Agitation FIS surface plot with HR and HRD variable with BP = 50mmHg, BPD = 0mmHg/min, MI = 0 defined in the field "Ref. Input"

This FIS has 5 inputs and it is therefore impossible to represent the behaviour of the FIS with a single 3D plot. However, it is possible to focus on the effect of

two variables while the other inputs are given reference input values to display the transfer surface. The 5 inputs can be sorted into 10 different combinations (HR-HRD, HR-BP, HR-BPD, HR-MI, HRD-BP, HRD-BPD, HRD-MI, BP-BPD, BP-MI, BPD-MI). Therefore, the transfer function of the FIS needs 10 surface plots to be fully represented. One such surface plot is shown in Figure 9.8. The final FIS is inserted in the agitation sensor that now needs to be calibrated and fine-tuned through clinical trials.

Part III

Clinical validation

Chapter 10

Clinical trial methods

At this stage, the signal-processing algorithms and fuzzy inference systems are developed to monitor patient agitation, and need to be verified and further improved from clinical results. The aim is to produce an agitation index in the 0–100 range. This task requires calibration of the signal-processing, as well as development and tuning of the two FIS used to combine the information from the physiological and video input signals. This chapter describes the methods used from the first trial used to develop and calibrate each signal-processing algorithm, to the statistical analysis of the clinical trials using the real-time monitoring system.

10.1 Overall approach

The physiological and video signals contain unique useful information, which need to be combined into an overall index. The access to ICU patients should be restricted to the trial of a consistent and accurate system, and the initial development of the system is first performed on normal, healthy individuals. This stage requires a set of tests that simulates the physical and mental stresses related to patient agitation. This simulation reveals the potential effect of agitation on the individuals physiological signals. These results lead to the first prototype of the agitation sensor.

The next step consists of adapting the agitation sensor prototype to ICU patients. The first calibration performed on normal healthy individuals is based on different physiological conditions, as ICU patients are sedated and seriously ill.

Hence, the possibility that some physiological responses may differ or be blunted as compared to healthy individuals must be addressed. The motion sensing is calibrated only on ICU patients in their specific environment, accounting for nursing staff interference within the video frame. The second calibration is therefore initiated by a preliminary set of investigative clinical trials on ICU patients to assess any major differences to the initial development based on healthy individuals.

Finally, the fully developed system can be tested more rigorously. Limitations of the preliminary clinical trials require a second set of more rigorous trials on ICU patients to validate the real-time agitation sensor as an objective system on which nursing staff can rely. Therefore, the method for the second ICU clinical trial is slightly different and rigorously seeks statistical correlation and calibration with the SAS scale currently used in the ICU.

10.2 Normal subjects: method and trials

The first trial on normal subjects is used to validate the fundamental, initial assumptions concerning the physiological reactions to agitation. It is crucial to develop a consistent test to simulate the physical and mental stresses that are believed to trigger agitation in ICU patients. This test is then applied on normal healthy individuals and the response of HR, SBP, DBP, and BR is recorded.

The physical stress is stimulated using the Cold Pressor Test (CPT) [Lam, 2003; Annie Lambert and Schlaich, 2004]. The CPT requires the individual to put a forearm in iced water for 30 seconds, as illustrated by a fellow researcher in Figure 10.1. This test is applied on each arm of the individual, 5–10 minutes apart to allow the individual time to return to a calm state.

Mental stress is induced by the Word Colour Stroop Test (WCST) [Lam, 2003]. The WCST assesses the cognitive mechanisms that make decisions based on contradictory lexical and perceptual information [Deslandes et al., 2004]. Basically, the subjects are presented with the printed name of a colour, and then asked to name the printed colour of what they read. In addition, difficulty is added by a vocal stimulus speaking a third color for each frame. There is a choice of four colours: blue, red, green and yellow. The name and colour and vocal stimulus indicate a different colour, referred to as the colour-word inter-

Figure 10.1 The cold pressor test is used to stimulate physical stress and physiological responses on normal individuals [Lam, 2003].

ference, and it corresponds for instance to the word "blue" displayed in green, while vocal information indicates "red". The correct answer is "green". This test requires subjects to mark correct answers under time constraints, and induces mental stress in trying to keep up and be accurate. It is an approach that is well accepted in the psychology literature.

The aim of the test in the context of agitation sensing is slightly different to common implementations [Deslandes et al., 2004] aimed to assess the cognition of individuals, because the cognitive mechanisms of healthy individuals are not contested here. This test is rather used for its ability to put the patient in a state of mental stress that is assumed to trigger agitation-like physiological responses. Therefore, the number of correct answers does not matter for the research, and the physiological signals are instead the main focus of attention. However, the subjects are told that correct answers are important so that mental stress is induced.

The WCST employed in this first set of trials consists of 630 different words displayed for 2s each. A 2s period is short enough to provoke significant mental stress in the patient trying to pick the right answer on the answer sheet. To add some difficulty to the test, the order in which the colors are printed on the

answer sheet is different from one answer line to the next. The entire word color test lasts 21 minutes. The overall test used to simulate agitation on normal individuals consists of the following stages:

- 30 min of rest when the patient sits in a comfortable armchair listening to relaxing music in a room with the lights dimmed.
- The WCST follows for 21 min.
- The individual is given 15 to 30 min to calm down after the mental stress induced by the color word test.
- The CPT is performed on the first forearm of the individual.
- The individual is given 5-10 min to recover.
- The CPT is performed on the second forearm of the individual.
- The individual recovers, lying down and listening to music for 10 min.

$\Rightarrow$ Physiological signals are recorded throughout.

The test method and objectives are described on an information sheet that is given to the potential participant. If the individual agrees to participate to the normal healthy individual trial, a consent form must be signed. Consent for this research was given by the Canterbury Ethics Committee.

This test serves to verify the original assumptions concerning the physiological response to agitation, such as HR and BP variations. It proves the concept of objective agitation sensing by testing the underlying assumptions. However, the conditions in critical care are very different and accurate results require trials and calibration on ICU patients.

10.3 ICU patients: Initial trial methods

The first trials on normal subjects are used to validate the proof of concept of physiologically based objective agitation quantification. The ECG and ABP

signals are consequently selected. The airway pressure signal is not initially selected because the passive ventilation often used in the ICU limits its continuous use. On top of physiological signals, the video record of ICU patients is performed with an overhead mounted camera. As opposed to physiological signals assumed to forecast agitation, the motion derived from the video record reflects their current level of agitation. The video-processing was not applicable for the normal subject trials.

Once patients are enrolled in this research, the research team is allowed to go to the ICU and start the study. A signal acquisition software is compiled and installed on a laptop computer. The monitoring device used in the ICU outputs the ECG, ABP and SPO2 signals to the computer via a custom made 8-channel A/D USB card. In this first trial, 4 channels are assigned:

1. ECG waveform
2. ECG ground
3. ABP waveform
4. ABP ground

The use of separated ground channels corresponds to the inner wiring of the monitoring device and allows optimal noise removal. The signals are converted to digital format at a sampling frequency of 1kHz and the samples are conveyed through the USB port and recorded in binary files. Nursing staff feedback on the patient level of agitation is also recorded using the modified SAS described in Table 1.3, to compare and initially validate the agitation sensor. The signal-processing is performed off-line in the Matlab environment. A first Matlab algorithm produces RR, HR, HRD, SDRR, SDdRR, LF, LFnu, HF, HFnu and LF/HF ratio from the ECG signal, and SBP, MBP and DBP from the ABP signal, followed by BPD, SDSBP, SDdSBP, LF, LFnu, HF, HFnu and LF/HF ratio from the SBP values. These signals are described in detail in Part I.

The video is recorded by an analogue camera onto a tape. The camera is located above the patient's head so it can acquire a frame that contains the entire patient from head to feet for higher level processing. The analog tape is then converted into a digital video file in AVI format. The resolution of the video frame

is 320*240 pixels. The video-processing algorithm converts the video file into an array of video frames at a rate of one frame per second. The motion sensing is then performed on this array of video frames using the technique introduced in Section 6.2.

The first pre-processing stage produces the intermediate metrics HR, SBP and MI, including applicable signal variability. These different methods of tracking the dynamics of HR (see Chapter 3) and ABP (see Section 4.3) are evaluated to aid in the selection of the final set of inputs for the agitation sensor. The relevant metrics are then combined into a single agitation index by the agitation FIS created on the Matlab/Simulink platform. The agitation FIS is designed and tuned to match, and possibly forecast, the trend given by the clinicians through their subjective assessment feedback recorded by the signal acquisition software.

Validation of the system requires extensive clinician feedback to make best use of the data. However, nursing staff do not necessarily have the time to provide enough feedback to allow validating the agitation sensor developed as part of this trial. In essence, an objective sensor cannot be compared to a single clinician's assessment, because the decision of a single clinician is subjective and therefore possibly biased. Consequently, a second set of clinical trials is designed and carried out to overcome these limitations and potentially statistically validate the agitation sensor.

10.4 ICU patients: Capstone trial methods

The fundamental goal of the second trial is to statistically and objectively validate the agitation sensor. This task is only possible if the system agitation index is compared to an objective reference. It is therefore decided to compare the system with the median assessment of 5 different clinicians to decrease the impact of subjective human assessments on patient agitation and increase the statistical significance of the results. This trial is carried out using specially selected data sets that uniformly cover the different levels of agitation as defined by the modified SAS in Table 1.3.

First, the real-time agitation sensor gathers data, produces an agitation index and records clinician feedback over several patient-days. The application GUI and

front end of the agitation sensor visible to clinical staff is shown in Figure 10.2. The records of the patients enrolled in the second ICU trial are used to produce forty 5-minute clips of video and physiological data. The forty different clips are selected to cover the four different levels of agitation of the modified SAS score. Periods of agitations are detected within the data using the real-time clinician feedback, as well as motion sensing. This approach saves time when scanning the entire data for periods of agitation within long periods when the patient is calm and still.

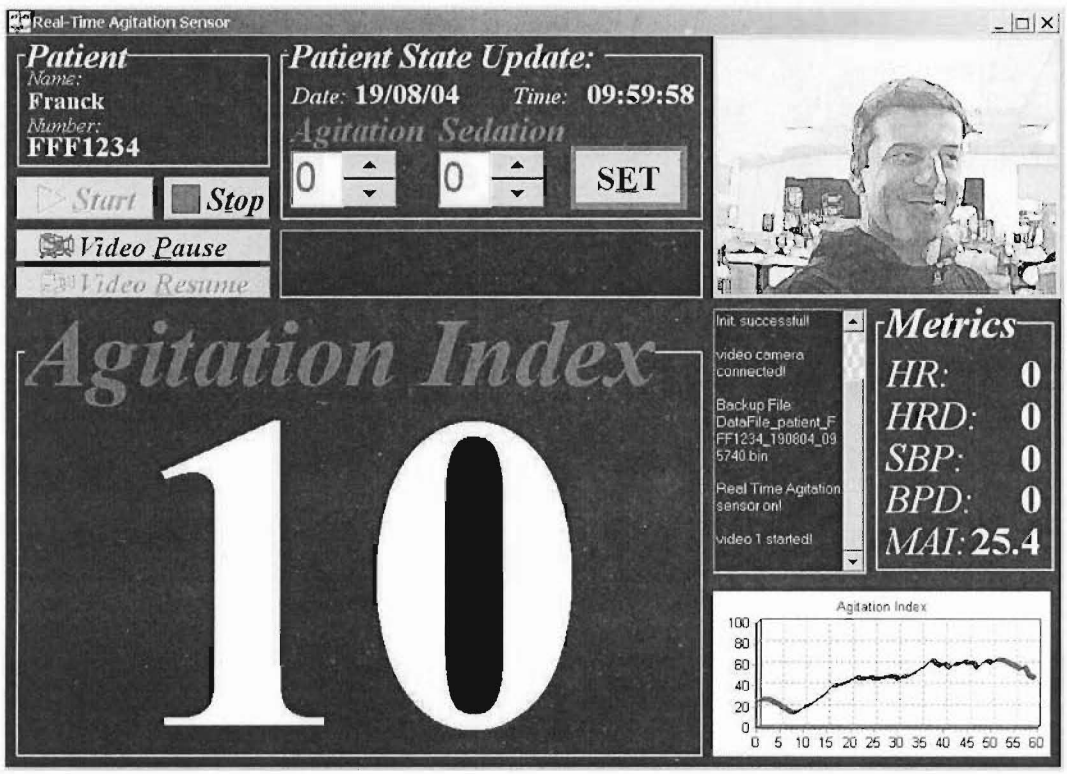

Figure 10.2 Real-time agitation sensor GUI, demo version.

Five different clinicians review each clip off-line using custom software to display HR and SBP variables with the video clip. For statistical relevance, it has been determined that each clip required a minimum of five reviews, which means a total of 40 different nurses, each assessing five clips, are required to ensure statistical relevance. The nurses assess the level of agitation of the patient and update it using the GUI buttons of the software to classify between the 4 discrete levels of agitations 0-3, as defined by the modified SAS defined in Table 1.3 .

This approach aims to produce a distribution of the system output among the modified SAS levels. Ideally, 50min of data corresponding to each level of agitation of the modified SAS are enrolled to produce a balanced distribution. This balance is a-priori checked by senior ICU doctors to ensure a valid trial. Note that due to the subjective methods of assessment currently used there is no perfect guarantee of exact balance, as no objective measure of patient agitation currently exists. The distribution of the system output along the modified SAS is then used for statistical analysis and potential validation of the agitation sensor.

Chapter 11

Normal subject clinical trial results

The simulation of patient agitation conditions is carried out on 10 normal individuals, who reveal different insights on the way physiological signals can be used to quantify agitation. The findings of two individuals are illustrated in detail in this chapter to illustrate these results and how the original structure of the agitation sensor is first determined.

11.1 Effect on ECG and derived metrics

The resting heart rate varies significantly between subjects, so the first 30 min of the test are provided for the normal individual to rest and define a reference value of resting heart rate. After this time, the effect of WCST and CPT can be observed on the heart rate signal relative to this baseline. The tests involve a response in the HR to mental and physical stress. Individual 1 in Figure 11.1 shows a sudden 40% HR increase shortly after the start of the mental stress induced by the WCST. HR slowly decreases as the individual copes better with the mental stress, but it remains higher than the reference HR at rest. At the end of the WCST test, HR slowly comes back to the reference value within a few minutes. The response of HR to physical stress is not as significant compared to the effect of the WCST. The CPT only produces a 17% HR rise at best, occuring just after the second CPT test. Although the contrast of the CPT is not as obvious as WCST, HR also responds to the physical stress induced by CPT.

Individual 2 reacts differently to the trial. Figure 11.2 reveals a 37% HR increase due to the mental stress related to the WCST, indicating a significant

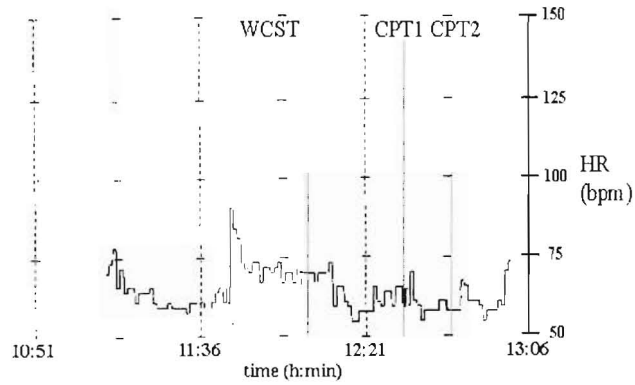

Figure 11.1 HR response to the trial of Individual 1.

effect on the HR of the second individual. The same pattern is also observed subsequently, as HR slowly decreases, but never reaches the reference value at rest. At the end of the WCST, HR slowly decreases and reaches the reference value after 5 min of recovery. The CPT is performed after 10 min of recovery. Unlike Individual 1, the HR of Individual 2 also reacts significantly to the CPT-induced physical stress, with a 27% HR increase at the beginning of the first CPT test, and 47% HR increase shortly after the beginning of the second CPT test.

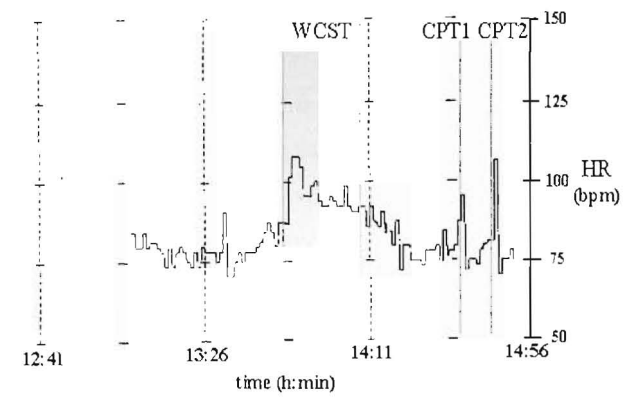

Figure 11.2 HR response to the trial of Individual 2.

Similar results were seen for HRV, as shown for Individual 1 in Figure 11.3. There is a significant physiological response to WCST and CPT. However, note that VLF is used to compute HRV in this case, and it is measured for a short period (< 60mins). Therefore, its value at any given time may be biased, as discussed in Chapter 3.

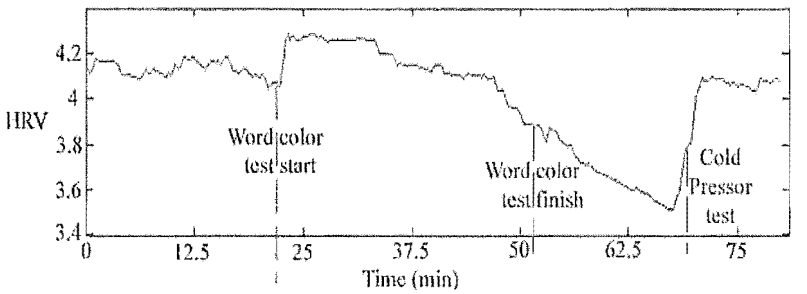

Figure 11.3 HRV response to the trial of Individual 1 [Lam, 2003].

Finally, all eight other individuals had similar reactions to Individual 1 and Individual 2 [Chase et al., 2004c]. In each case, the relative response to WCST and CPT varied, but was significant for these controlled trials. This first trial on normal subjects validates the fundamental theoretical assumptions that HR and its derived metrics react to mental and physical stress. Therefore, HR and derived metrics offer the potential to track periods of agitation in the context of ICU patients under mental and physical stress.

11.2 Effect on ABP and derived metrics

The ABP signal is first used to derive SBP, MBP and DBP as described in Chapter 4. Similar to HR, these values are subjective and the 30 min period of rest allows defining reference values at rest. The effect of WCST and CPT is then considered relatively to these reference values. Individual 1 in Figure 11.4 shows a ABP reaction to the WCST. The three variables SBP, MBP and DBP increase at the start of the test by 17%, 12% and 50% respectively. The rise of the SBP, MBP and DBP series is not as steep as the rise of HR, and the maximum pressures are observed halfway through the test, after which they decrease, but remain greater than the reference pressures at rest. These references are reached after 20 min of recovery. The CPT is started after 30min of recovery from WCST.

The BP values of Individual 1 show little reaction to the CPT test. SBP, MBP and DBP rise 14%, 17% and 30% respectively. Individual 2 also shows a reaction to the test through the ABP values in Figure 11.5. The WCST test involves a rise of SBP, MBP and DBP by 18%, 25% and 33% respectively. The

CPT also provokes a reaction of the ABP values. SBP, MBP and DBP rise by 18%, 25% and 27% respectively.

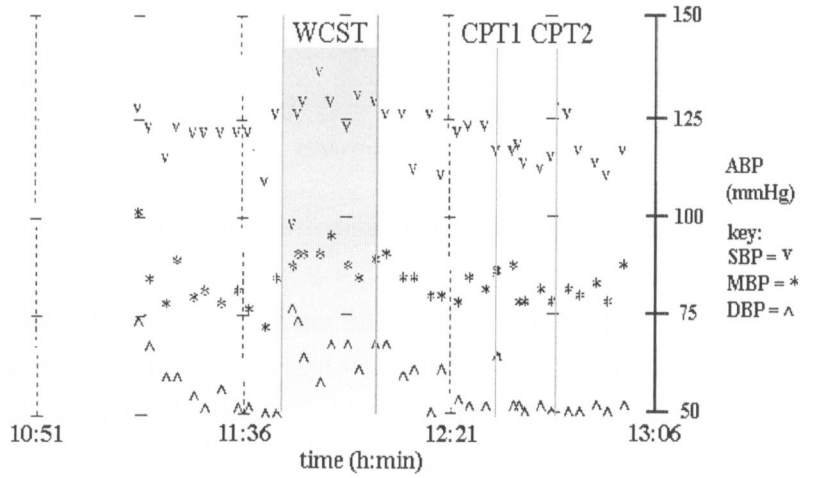

Figure 11.4 ABP response to the controlled trial of Individual 1.

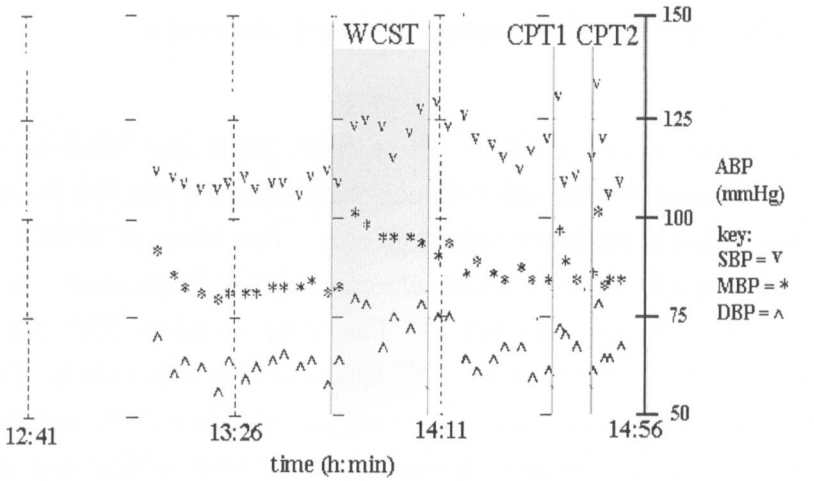

Figure 11.5 ABP response to the controlled trial of Individual 2.

Note that the BPV metric is not computed during this trial, because the ABP values are only recorded every three minutes, which does not give enough

data points with a suitable resolution. Continuous recording of ABP is only possible with an arterial line, which is an invasive method not approved for trials on healthy volunteers. However, it is available for many critically ill patients and will therefore be investigated in the trials on ICU subjects.

The ABP signal and its derived metrics provide a potential means of detecting periods of agitation, and this trial validates the theoretical assumptions regarding the effect of mental and physical stress on ABP. At this stage, any of the three blood pressure values SBP, MBP or DBP may be used to track agitation, as they all react to stress. Note that the longer recovery times may indicate ABP values could be useful to measure long-term recovery from agitation episodes.

11.3 Effect on respiration and derived metrics

The third physiological signal assessed on normal individuals is BR introduced in Chapter 5. The volunteers rest 30min and reach their reference BR values. Mental and physical stress is then applied and the reaction assessed. Individual 1 in Figure 11.6 breathes faster once the WCST begins, and BR rises by 167%. This strong reaction to mental stress offers a significant means of detecting mental stress in a patient. The CPT test follows 30min of recovery and the reaction of BR is again significant, rising by 70% and 80% after the two CPT tests.

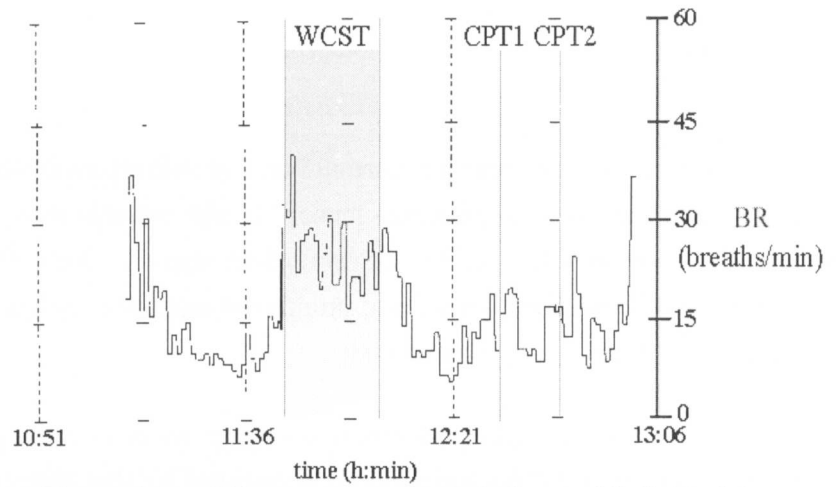

Figure 11.6 BR response to the trial of normal Individual 1.

Individual 2 in Figure 11.7 also reacts to mental and physical stress by an

increase in BR. The WCST test provokes a 275% rise of BR and the CPT induces a rise of 60% and 70% respectively during the two tests. The rise of BR is larger after the second CPT test in most cases, and this difference could reveal a lack of recovery between the two CPT tests. It can also be due to an increased sensitivity to pain after the first CPT or a lag in the reduction of physical stress effect after a CPT.

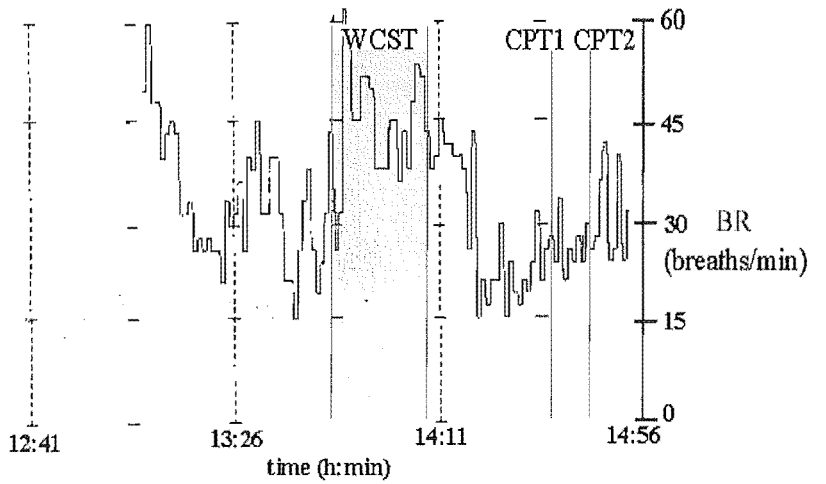

Figure 11.7 BR response to the trial of normal Individual 2.

The analysis of BR during the trials on normal individuals also reveals great potential to track periods of agitation. It can therefore be included as an input to the agitation sensor when ICU patients are breathing spontaneously.

11.4 Summary

The results obtained from the trials on normal healthy volunteers is very useful in developing the structure of the agitation sensor. It also reveals some important guidelines in the interpretation of the physiological signals. Note that motion could not be examined in these cases and simulated agitation videos were used in previous work by Lam et al. [Lam, 2003].

The effect of mental and physical stress is highly variable between individuals, as clearly seen for the two individuals illustrated in this chapter. Hence, several physiological variables should be combined to reinforce the final assessment of agitation. Therefore, the metrics derived from the ECG and ABP signals

should be combined into the agitation sensor. Although motion and BPV are not assessed on normal healthy individuals, it is added to the trial protocol for ICU patients.

Finally, BR is also sensitive to mental and physical stress but the use of mechanical ventilator requires special attention to process BR in the ICU, according to the mode in which the ventilator is used. The signal-processing needed to differentiate in which mode the ventilator is running is not currently available, and the agitation sensor initially computes the agitation index in the ICU from ECG, ABP, their derived metrics, and the video signals. The signal-processing algorithms need to be specifically calibrated on ICU patients in their environment, and this task is the aim of the first clinical trial on ICU patients. This first set of ICU trials will also deny any false assumptions, and reveal the significant differences in response between the healthy individuals and tests used to develop the agitation sensor in this chapter, and the targeted ICU population.

Chapter 12

ICU patients: Initial trial

The first clinical trials on normal healthy volunteers has determined the initial choice of the input signals ECG, ABP and motion. The motion index needs to be calibrated on ICU patients. In addition, the processing of the ECG and ABP signals needs to be further developed, because several metrics can be derived from ECG and ABP to model the different dynamic components of these signals. After strategic choice of algorithms, the processing applied on ECG and ABP signals also requires calibration on ICU patients, whose physiological reactions are assumed to be somewhat different from healthy subjects. Physiological differences between ICU patients are also expected, so normalisation may be necessary on certain variables to provide consistency.

The initial set of trials is performed on 12 ICU patients. Two relevant episodes of agitation recorded during these trials, and their effect on the physiological markers, are described in detail in this chapter to illustrate the effect and accuracy of the signal-processing techniques utilised in the context of ICU agitation. Each signal is processed and calibrated separately in this trial to evaluate the range of physiological fluctuations of ICU patients.

The ECG and ABP signals are processed with the spectral AR method, described in detail in Section 3.2, to obtain the dynamic trends of these signals in the original work by Starfinger et al. [Starfinger et al., 2003; Starfinger, 2003], Lam et al. [Lam et al., 2003; Lam, 2003] and Chase et al. [Chase et al., 2003, 2004c]. This research investigates the temporal HRV and BPV methods and introduces the novel HRD and BPD method to complement and verify the information given by the spectral HRV and BPV methods, using a more real-time capable algorithm.

More specifically, spectral HRV analysis of orders 12 and 20 combined with a forgetting factor $\omega = 0.995$ produce the optimal AR filters according to the research of Kuusela et al. [Kuusela et al., 2003]. Bianchi et al. [Bianchi et al., 1993] compute spectral HRV with AR filters of order 50 with $\omega = 0.98$ and order 100 with $\omega = 1$. Therefore, each set of data in this research is computed over 12, 20, 50, 100-sample-wide windows, based on the findings of these previous works, followed by implementation of order $p = 500$ for investigation. Note that the same sampling frequency must be used to compare results with other researches.

Several forgetting factors $\omega = 0.8, 0.9, 0.995, 1$ are combined with the different AR filter orders. The forgetting factor plays an important role to keep the AR filter stable. If the forgetting factor is close to 1, the error vector is considered equally along its entire length. However, if a technical artifact occurs, it will impair the AR filter for p iterations and possibly make the filter drift away. Moreover, if the forgetting factor is too small, the error vector of the AR filter is damped too quickly and the AR coefficients are updated taking only a few samples into account, which does not consequently provide an accurate estimation of the PSD. Therefore, a good tradeoff must be reached for the order and forgetting factor combination.

There is a limited range of orders on which forgetting factor can be used to be relevant. Because the forgetting factor weighs the error vector exponentially, the use of forgetting factors much smaller than 1 on large order filters is not meaningful, because the corresponding weight of the oldest sample is irrelevant. The weight of the oldest error value corresponding to different combinations of orders and forgetting factors are determined in Table 12.1. Recall that the weight of all the p samples considered by an AR filter of order p and forgetting factor $\omega = 1$ is equal to 1.

If the parameters of Bianchi et al. [Bianchi et al., 1993] are considered then a weight greater than 10^{-5} is relevant. Hence, some combinations of AR orders and forgetting factors are not consistent because the older samples are not taken into account to update the AR coefficients. For instance, AR order $p = 500$ combined with forgetting factor $\omega = 0.8$ produces a weight for the p^{th} previous sample equal to 3.5×10^{-49}, which is so small the AR coefficients are updated without taking all the samples into consideration. The result of this simple calculation yields guidelines for relevant signal-processing analysis.

Table 12.1 AR weights

forgetting factor ω	AR order p	weight of p^{th} error value
0.8	12	0.069
0.8	20	0.012
0.8	50	1.4×10^{-5}
0.8	100	2.0×10^{-10}
0.8	500	3.5×10^{-49}
0.9	12	0.28
0.9	20	0.12
0.9	50	5.2×10^{-3}
0.9	100	2.7×10^{-5}
0.9	500	1.3×10^{-23}
0.995	12	0.94
0.995	20	0.90
0.995	50	0.78
0.995	100	0.61
0.995	500	8.2×10^{-2}

AR filters of order 12, 20 and 50 are analysed with forgetting factors $\omega = 0.8$, 0.9, 0.995 and 1. The AR filter of order 100 is analysed with forgetting factors $\omega = 0.9$, 0.995 and 1. Finally, the AR filter of order 500 is analysed with forgetting factors $\omega = 0.995$ and 1. The combinations of orders and forgetting factors recommended by Kuusela et al. [Kuusela et al., 2003] and Bianchi et al. [Bianchi et al., 1993] are first computed, and then compared to other combinations. This investigation of spectral HRV and BPV along with temporal metrics on ICU patients ECG and ABP signals is also described in this chapter.

Note: that in the sections describing the processing of ECG and ABP signals, all figures referenced are printed at the end of the section they are first referenced in for clarity due to their size and number.

12.1 Effect of the trial on ECG derived metrics

As introduced in Chapter 3, several variables derived from the ECG signal can potentially track periods of agitation. These variables include temporal, spectral and non-linear markers. During this first clinical trial on ICU patients, the physiological reactions of agitated patients are observed on temporal variables HR,

HRD, SDRR, SDdRR, and frequency variables LF, LFnu, HF, HFnu and LF/HF ratio, to select a pertinent combination of input variables derived from the ECG signal.

12.1.1 Analysis of ECG, Patient 1

The first ECG off-line analysis of Patient 1 is performed on a 12-sample time window. Thus, the time domain HRV variables are computed over 12 samples, and the AR estimates the tachogram PSD using a Kalman filter of order 12 and forgetting factor $\omega = 0.995$. The HRD metric is the average of 12 consecutive instantaneous first-order time derivative values. The "3" and "1" indices correspond to real-time agitation feedback of the nursing staff using the SAS scale. This first illustration shown in Figure 12.1 reveals a clear reaction of ECG to events of agitation as the HR signal rises and fluctuates. The fluctuations of the tachogram contain both low and high frequency components. Several metrics are defined in Chapter 3 to track both long term, low frequency variations as well as fast high frequency fluctuations of the tachogram.

Note that it is hard at this stage to reach a conclusion on the ability of the system to forecast agitation. During the study of Patient 1, the feedback of the nurse given on top of Figure 12.1 is reported over a minute after the physiological signals detect some change in the patient state. However, after verification on the video record, this delay is due to the priority of the nurse to help the patient before updating the agitation level on the computer. Therefore, no conclusion of the ability to forecast agitation is done in this chapter.

HR is clearly a good marker of agitation for Patient 1 because of its significant increase that is easily detectable by the final FIS. However, other symptoms not related to agitation can provoke an increase of HR, such as adrenaline infusion therapy used to revive the patient. Therefore, HR alone cannot produce a pertinent diagnostic of agitation.

Temporal HRV variables correlate with both episodes of agitation, but they lack the smoothness required for efficient high-level processing without technical artifacts, as shown in Figure 12.1. A wider time window may produce better results in the time domain analysis. Spectral HRV metrics HF and LF computed

over the same time window fail to correlate with the trends of SDRR and SDdRR shown in Figure 12.1. Note that the SDdRR metric is also referred to as SDSD in the literature. However, this method is also applied to the ABP signal, which would result in two variables called SDSD, Therefore the markers are called SDdRR and SDdSBP respectively in this thesis. The lack of correlation between the spectral markers and the episodes of agitation may correspond to a lack of stationarity of the tachogram, or an inappropriate combination of order and forgetting factor, even though it corresponds to the recommendation of Kuusela et al. [Kuusela et al., 2003]. Therefore, the spectral HRV analysis is performed with the same order combined with different forgetting factors, before higher AR orders are investigated.

The spectral analysis is performed by an AR filter of order 12 combined with a forgetting factor of 0.8, 0.9 and 1, and it fails to produce a pertinent marker of agitation. Similarly, the forgetting factors of 0.9 and 1 do not improve the correlation of the HRV variables with the event of agitation. Temporal HRV variables SDRR and SDdRR as well as HRD correlate with the episodes of agitation reported by the nurse when computed on a 20-sample-wide window, as illustrated in Figure 12.2. It seems to fluctuate more, but an hour of data is displayed, which slightly affect the ability to appreciate the smoothness of the marker. However, the marker derived from an analysis of order 20 offers a reliable marker when observed in real-time.

The variables derived from spectral analysis of order 20 fail to correlate with the episodes of agitation, and they do not provide a marker for agitation in this case. To assess the efficiency of the spectral HRV analysis of order 20, different forgetting factors are also employed. The attempt using forgetting factors $\omega = 0.8$, 0.9 and 1 all fail to improve the results. Therefore, the recommendations of Kuusela et al [Kuusela et al., 2003] failed to provide consistent results in the context of agitation quantification. This result could be due to the broader population studied in this research, as well as the lack of stationarity and different precision of calculation. In addition, as discussed in Section 3.4, HRV may not be well suited for this application. Further investigation is needed to answer this issue.

The ECG temporal analysis is performed on a 50-sample window and shown in Figure 12.3, which corresponds to the recommendations of Bianchi et al.

[Bianchi et al., 1993]. The temporal variables SDRR, SDdRR and HRD are smoother, but the propagation delay becomes significant. For instance, the sharp rise in SDRR corresponds to the episode of grade-3 agitation, but occurs slightly after the potentially delayed feedback from clinicians. Therefore, the optimal order employed for temporal HRV analysis is 20 in this case. No temporal analysis is performed over longer windows to avoid longer delays.

The spectral analysis is performed using a forgetting factor of 0.8, corresponding to the parameters used by Bianchi et al. [Bianchi et al., 1993]. The overall HRV power increases shortly before the episode of grade-3 agitation. However, both the LF and HF components fail to follow the agitation trend, and drift away. The same drifting of the AR filter is observed when using a forgetting factor 0.9, 0.995 and 1. The AR PSD estimation is also performed with a filter of order 100 and forgetting factor 1, which corresponds to the second set of parameters used in Bianchi et al. [Bianchi et al., 1993]. The resulting spectral HRV markers are displayed in Figure 12.4. The overall HRV as well as LFnu and LF/HF are increasing with the first episode of agitation, but also fail to follow the agitation trend afterwards, and drift away. Other forgetting factors are applied, and the same observations are made from the results of AR spectral analysis with order 100 combined with forgetting factors $\omega = 0.9$ and 0.995.

Finally, the spectral analysis is based on AR PSD estimation of order 500, with forgetting factor 1. The results are shown in Figure 12.5. This AR model configuration produces pertinent markers of agitation. First, both LF and HF are correlated with the episodes of agitation, which indicates a rise of the overall HRV power as agitation increases. Although their scale is very small, this issue can be compensated for using logarithmic or normalised units. LFnu correlates successfully with both grade "3" and grade "1" episodes of agitation, and the trend is proportional to the grade of agitation, which may permit the quantification of a marker of agitation. The LF/HF ratio also correlate very well with both epochs of agitation, and show very good potential to be used as an HRV marker of agitation. The AR filter of order 500 is also combined with a forgetting factor $\omega = 0.995$, which doesn't significantly modify the results. The same correlated trends are observed on LF, LFnu, HF and LF/HF. This introduces the idea that both overall HRV power, which is the sum of power contained in both LF and HF frequency bands, as well as LF/HF ratio may increase during agitation.

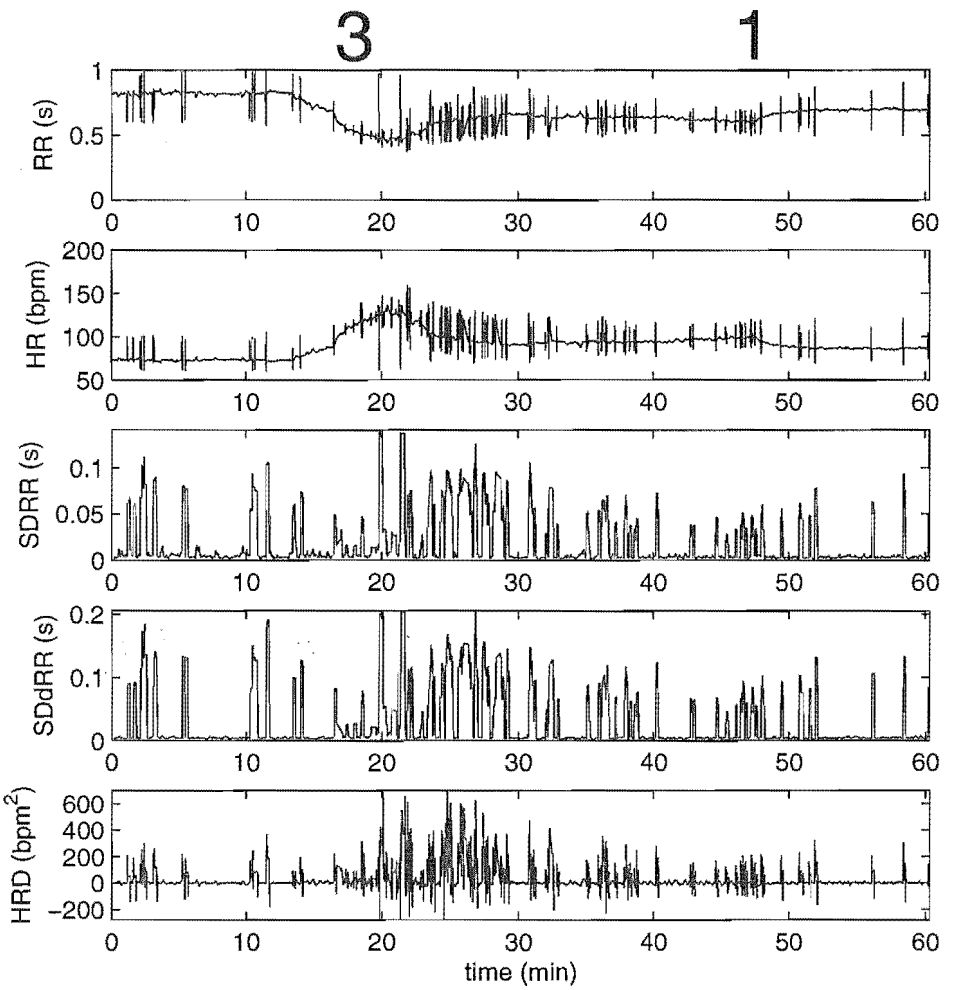

Figure 12.1 ECG analysis of Patient 1 with temporal variables HR, SDRR, SDdRR and HRD during agitation. SDRR, SDdRR and HRD are calculated over a 12-sample window. Agitation is assessed on the modified SAS, and reported on top of the Figure.

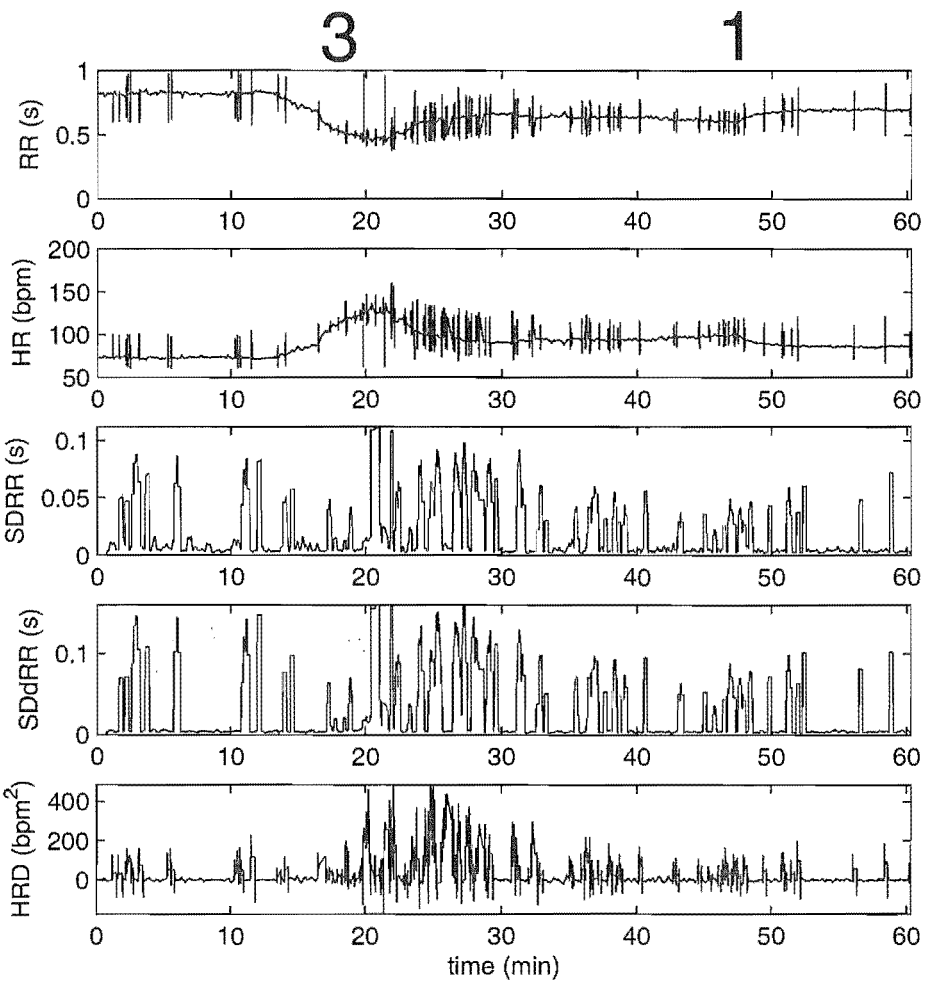

Figure 12.2 ECG analysis of Patient 1 during grade 3 and grade 1 agitation on the modified SAS. Processing of temporal variables HRD, SDRR, SDdRR over a 20-sample window

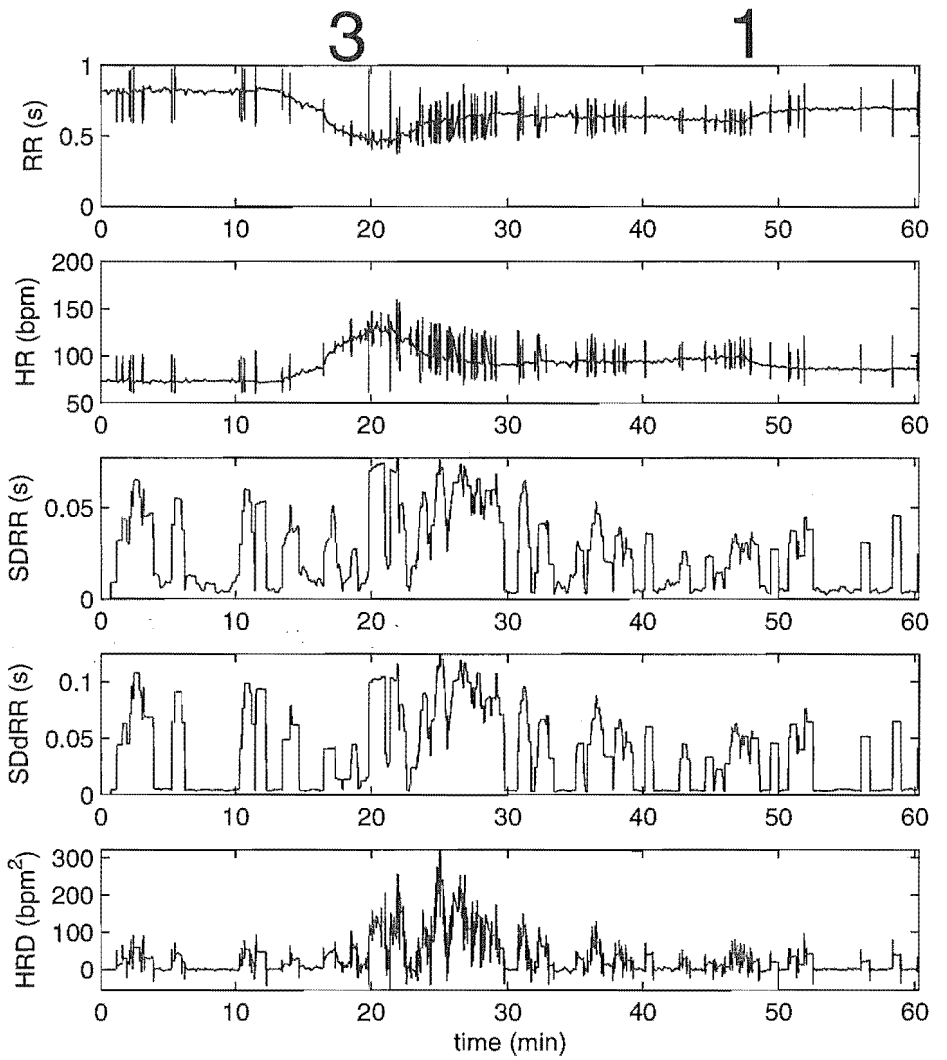

Figure 12.3 ECG analysis of Patient 1 during grade 3 and grade 1 agitation on the modified SAS. Processing of temporal variables HRD, SDRR, SDdRR over a 50-sample window

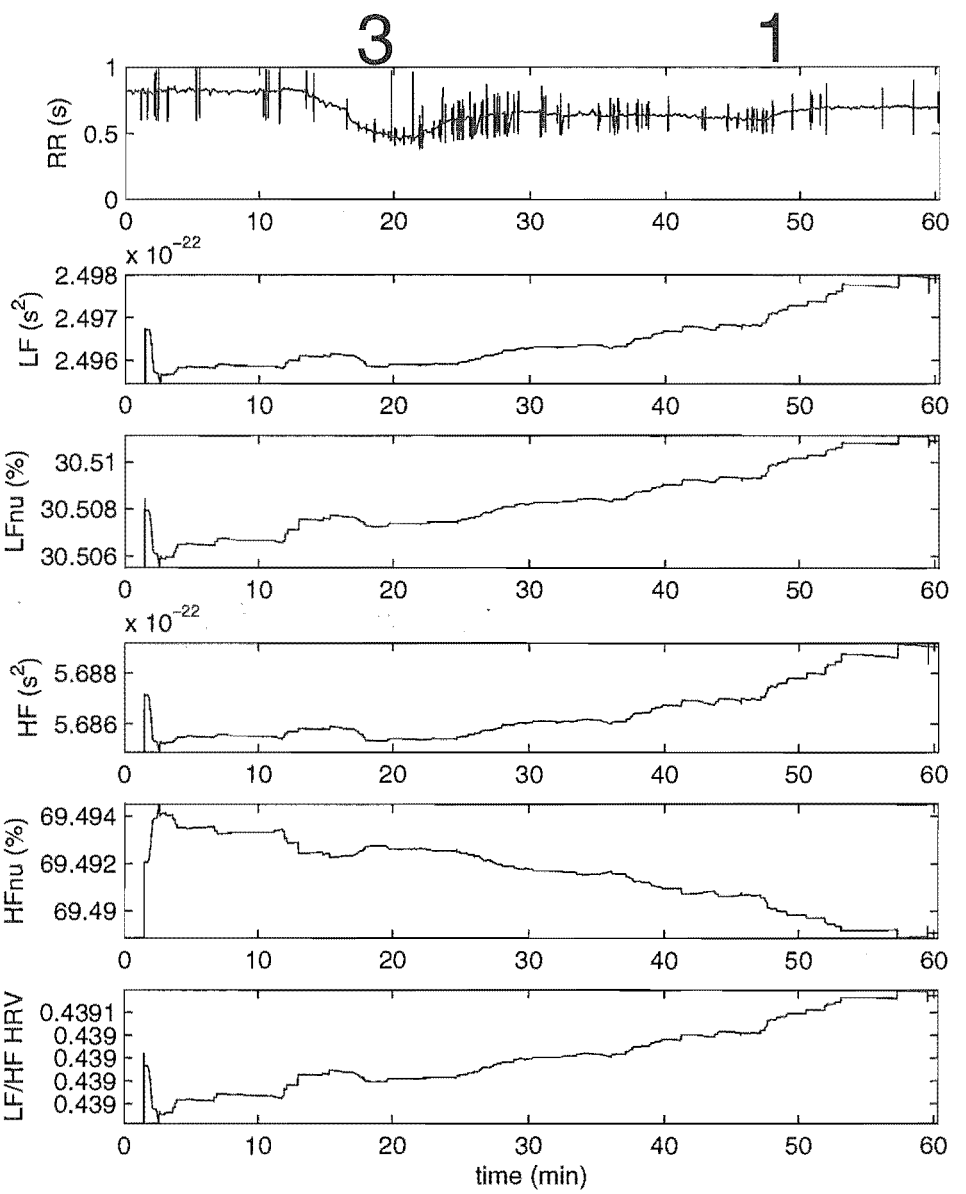

Figure 12.4 ECG analysis of Patient 1 with spectral variables LF, LFnu, HF, HFnu and LF/HF during agitation. The PSD is estimated by an AR filter of order p=100 and forgetting factor ω=1.

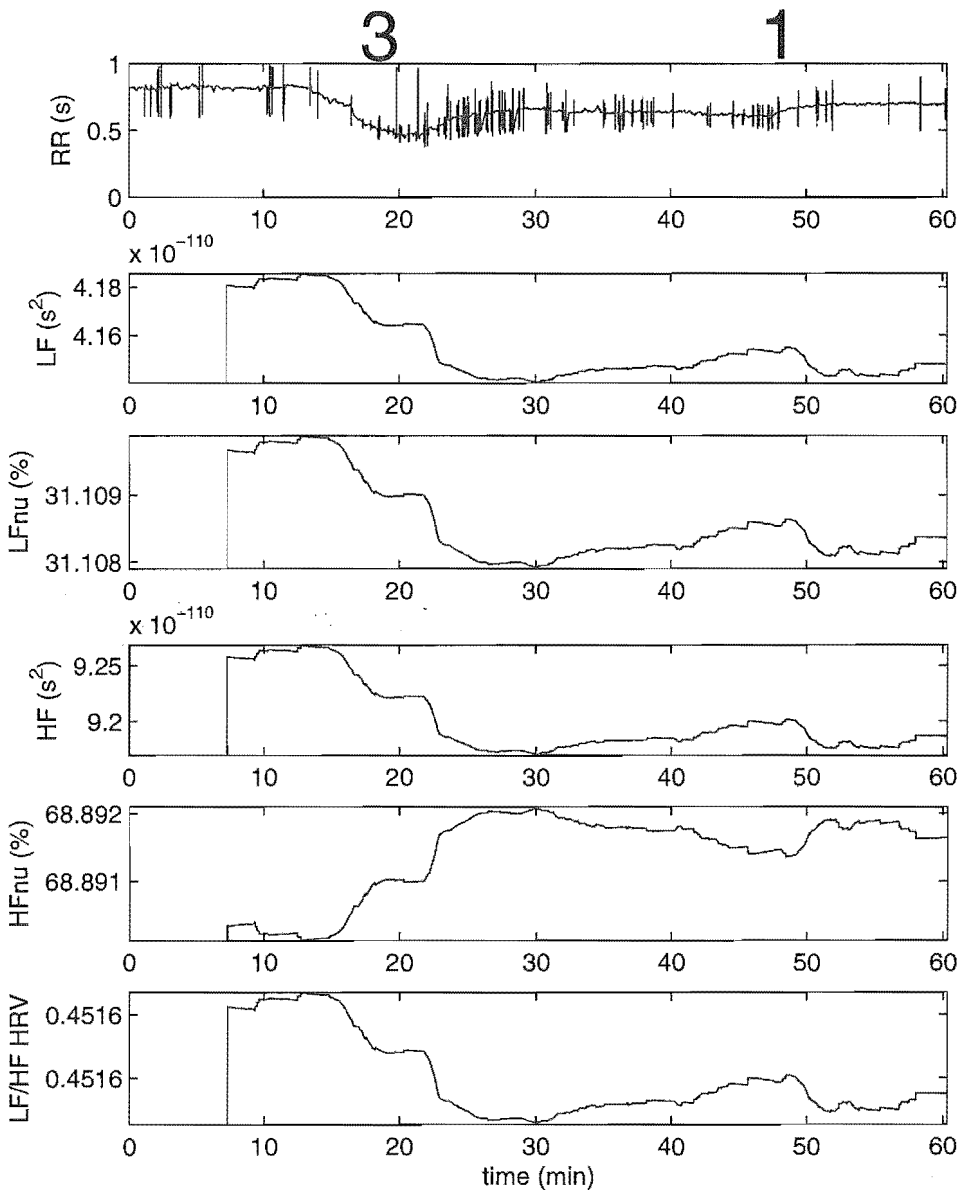

Figure 12.5 ECG analysis of Patient 1 with spectral variables LF, LFnu, HF, HFnu and LF/HF during agitation. The PSD is estimated by an AR filter of order p=500 and forgetting factor ω=1.

12.1.2 Summary of ECG, Patient 1

The overall results for Patient 1 can be summarised for each variable:

- HR: The HR of Patient 1 reacts with episodes of agitation, providing a pertinent physiological marker.
- HRD: The derivative is a simple and effective marker of the dynamics of the heart, and it clearly correlates with both episodes of agitation reported by clinicians. A smooth HRD metric is shown with order 50 in Figure 12.3.
- SDRR: This overall temporal marker is a good indication of the variability of the heart, which in the case of Patient 1 also correlates with agitation. The best tradeoff between smoothness and delay is observed for order 50, shown in Figure 12.3.
- SDdRR: It also correlates well with the agitation reported for Patient 1. The optimal order is also 50, as illustrated in Figure 12.3.
- LF: The low frequency component of the PSD computed over a 500-sample window with forgetting factor 1 correlates with agitation, as shown in Figure 12.5. It tends to drift away with smaller orders
- HF: The high frequency component of the PSD also correlates with the episodes of agitation when computed over the 500-sample window illustrated in Figure 12.5.
- LF/HF: The HRV ratio shows good correlation with episodes of agitation when computed over a 500-sample window, as displayed in Figure 12.5. It is otherwise unstable and drifts away.

Patient 1 offers good agitation markers from the ECG signal. The findings from the ECG signal are compared and validated with other markers derived from the ABP and video signal. In this case, the ECG alone offers a good means of detecting agitation, but no conclusions can be reached from the result of a single patient.

12.1.3 Analysis of ECG, Patient 2

The data for Patient 2 contains three episodes of agitation, and frequent feedback of the clinician is available to estimate the accuracy of the markers obtained from the signal-processing methods. The ECG is first processed using temporal analysis on a 12-sample window and the resulting markers are shown in Figure 12.6. Unlike Patient 1, the ECG does not produce any marker that correlates significantly with the episodes of agitation reported by the clinicians. This result could reveal the inconsistency of ECG-derived markers to correlate with agitation, or could be the result of cardiac drug therapy or patient condition. No matter the cause, it indicates the necessity to use multiple signals given inter-patient variability. Several peaks can be observed in Figure 12.6 on the SDRR, SDdRR and HRD series from minute 45 to 60, even though no episode is reported by the clinician at this time, and further verification on the corresponding video record does not reveal agitation either. This is a typical physiological artifact, where a peak is not due to agitation. In this case, a specific cardiac condition is detected by a rise in the three temporal markers. This is a major issue to improve the reliability of the overall agitation sensor, as discussed later.

The spectral analysis is performed by an AR filter of order 12 with forgetting factor $\omega = 0.995$ following the guidelines from Kuusela et al. [Kuusela et al., 2003]. The correlation between the spectral markers and the episodes of agitation is ambiguous because the total HRV power along with the LF/HF ratio decrease after the three episodes of agitation, but it does not fluctuate between the different episodes. The correlation in this case is partial, and the markers obtained are not accurate with the feedback of the clinician. However, this feedback is subjective to the particular clinician in charge of this patient. Another clinician may diagnose a continuous state of agitation throughout the entire period, and in this case the markers could be pertinent. Further investigation is carried out with forgetting factors $\omega = 0.8$, 0.9 and 1. The same trend is observed with different forgetting factors. The spectral markers HRV total power, which combines LF and HF, as well as LFnu and the LF/HF ratio all decrease after the two episodes of agitation. Hence, it bears repeating that HRV spectral method may not be best suited for this clinical application. At least, the order 12 is not suitable, and higher orders are implemented.

The temporal analysis is performed over a 20-sample window and there is

still no correlation between the temporal markers and the episodes of agitation reported by the clinician. The spectral decomposition is performed by an AR filter of order 20 and forgetting factor $\omega = 0.995$. The resulting markers quickly become unstable and drift away according to the trends of LF and HF components. The instability of the AR filter of order 20 is verified with forgetting factors $\omega = 0.8$, 0.9 and 1. This result reinforces the assumption that HRV spectral markers are not fully consistent with agitation.

The temporal analysis performed over a 50-sample window is displayed in Figure 12.7. No correlation is clearly observed between any of the temporal markers and the episodes of agitation reported by the nurse. Several peaks are observed in the SDRR series during the episodes of agitation. No higher order temporal analysis is performed because a 50-sample window already introduces a significant propagation delay, similar to the observation done on the ECG processing of Patient 1 shown in Figure 12.3.

The spectral decomposition is performed with an AR filter of order 50 with forgetting factor $\omega = 0.8$. The LF and HF components both correlate with the episodes of agitation. However, HF drifts away after the last grade "1" episode of agitation. These parameters are similar to the ones used in Bianchi et al. [Bianchi et al., 1993]. The findings are also considered carefully due to the very small magnitude of variations. The very small order of the variations of LF and HF spectral markers for this patient is verified with forgetting factors $\omega = 0.9$, 0.995 and 1. The implementation with $\omega = 0.9$ is illustrated in Figure 12.8.

A log-transform is applied on the instance with forgetting factor 0.9 to emphasize the very small variations, as shown in Figure 12.9. The spectral analysis is performed by AR filter of order 100 with forgetting factor $\omega = 1$. The spectral marker LF, LFnu, HF and the LF/HF ratios show a decreasing trend that correlate with the decreasing level of agitation, as shown in Figure 12.10. This result corresponds to the findings with order 50. However, the order 100 AR filter does not drift afterwards, and remains stable, ready to detect other episodes of agitation. The processing of the same AR filter with forgetting factor $\omega = 0.9$ and 0.995 does not change the results. This confirm the findings of Kuusela et al [Kuusela et al., 2003] that the order of the method is the primary parameter, and the forgetting factor does not affect the outcome as much. The spectral markers issued from order 500 correlate with the level of agitation reported by the clin-

ician, but the order of variations is very small for this patient. Log-transform may also offer a range of variation that is easier to quantify and process at higher level in this case.

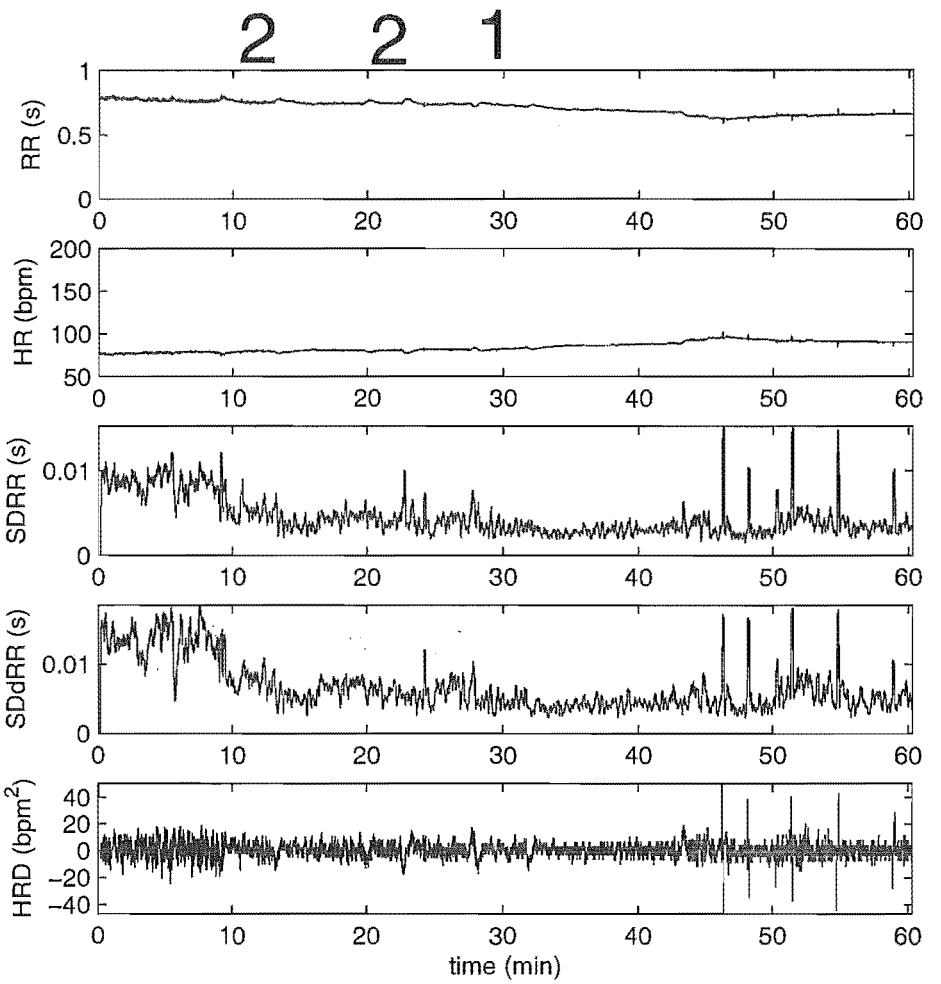

Figure 12.6 ECG analysis of ICU Patient 2 with temporal variables HR, SDRR, SDdRR and HRD during agitation. SDRR, SDdRR and HRD are calculated over a 12-sample window. Agitation is assessed on the modified SAS, and reported on top of the Figure.

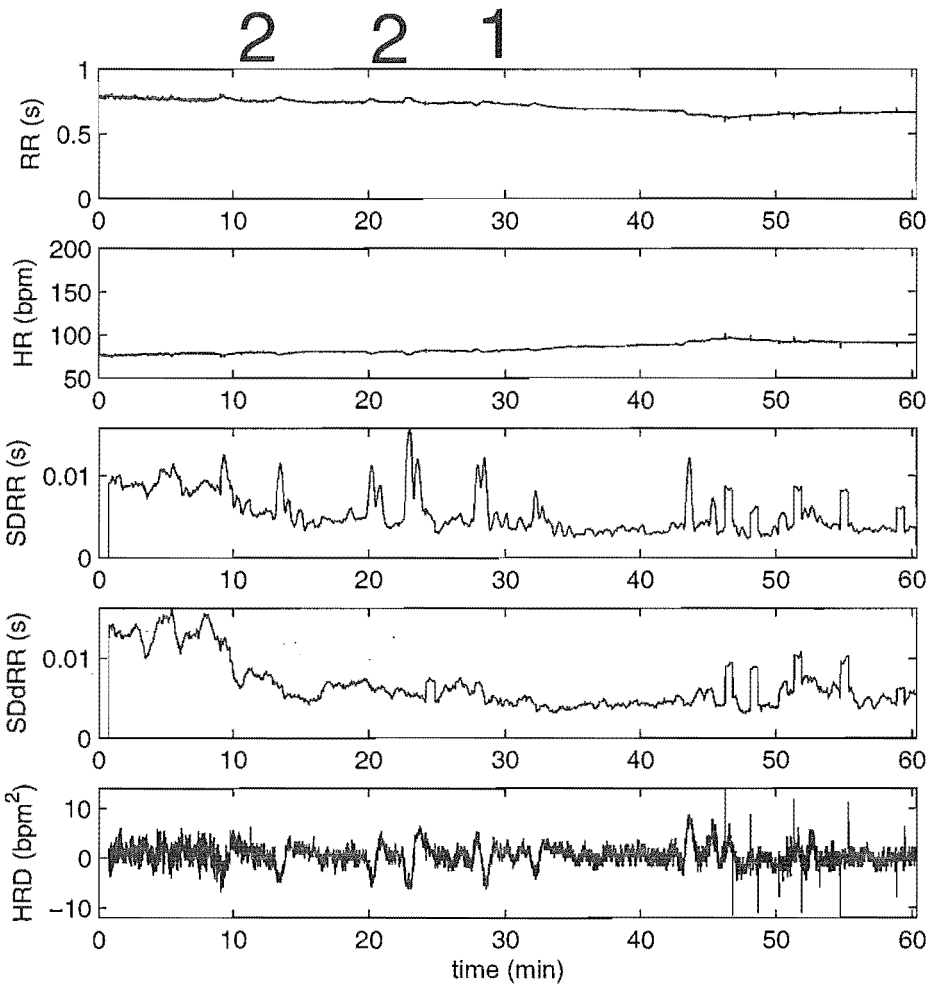

Figure 12.7 ECG analysis of ICU Patient 2 with temporal variables HR, SDRR, SDdRR and HRD during agitation. SDRR, SDdRR and HRD are calculated over a 50-sample window. Agitation is assessed on the modified SAS, and reported on top of the Figure.

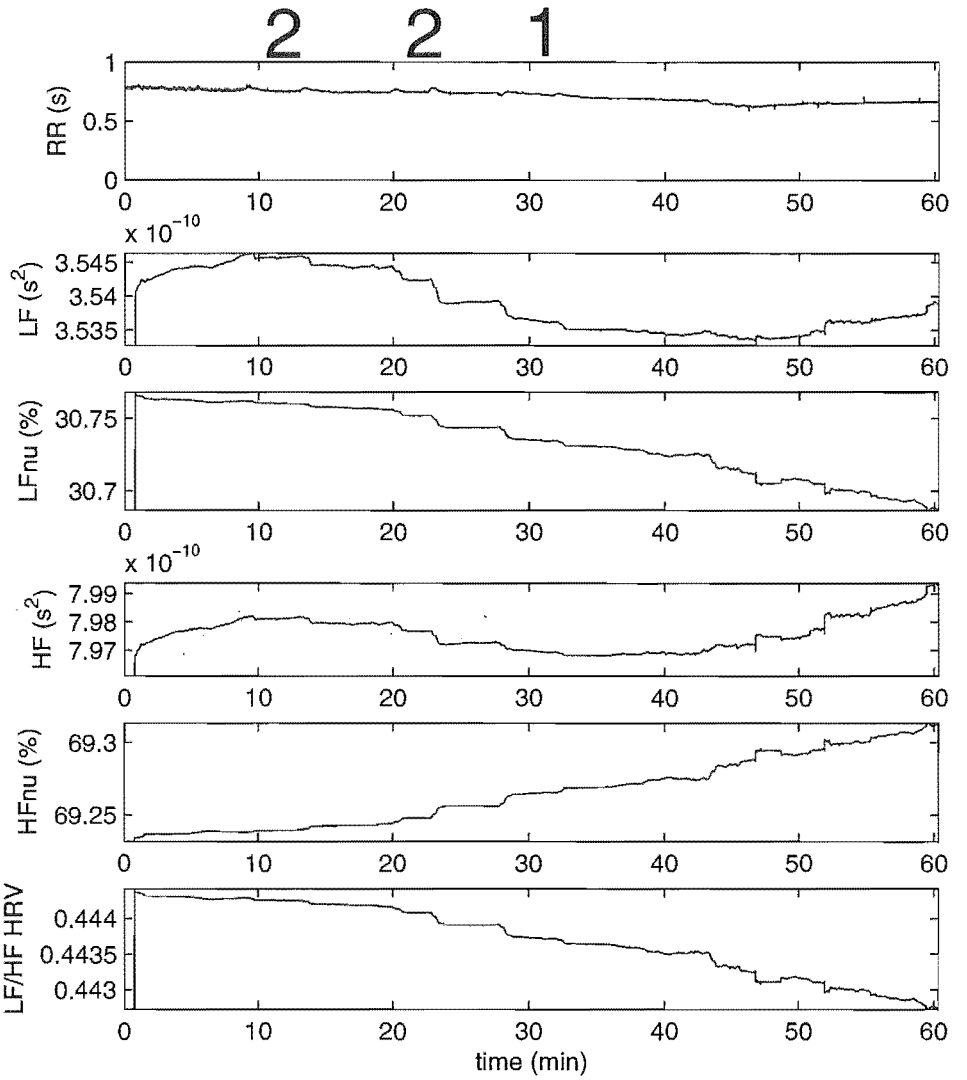

Figure 12.8 ECG analysis of ICU Patient 2 with spectral variables LF, LFnu, HF, HFnu and LF/HF during agitation. The PSD is estimated by an AR filter of order p=50 and forgetting factor ω=0.9.

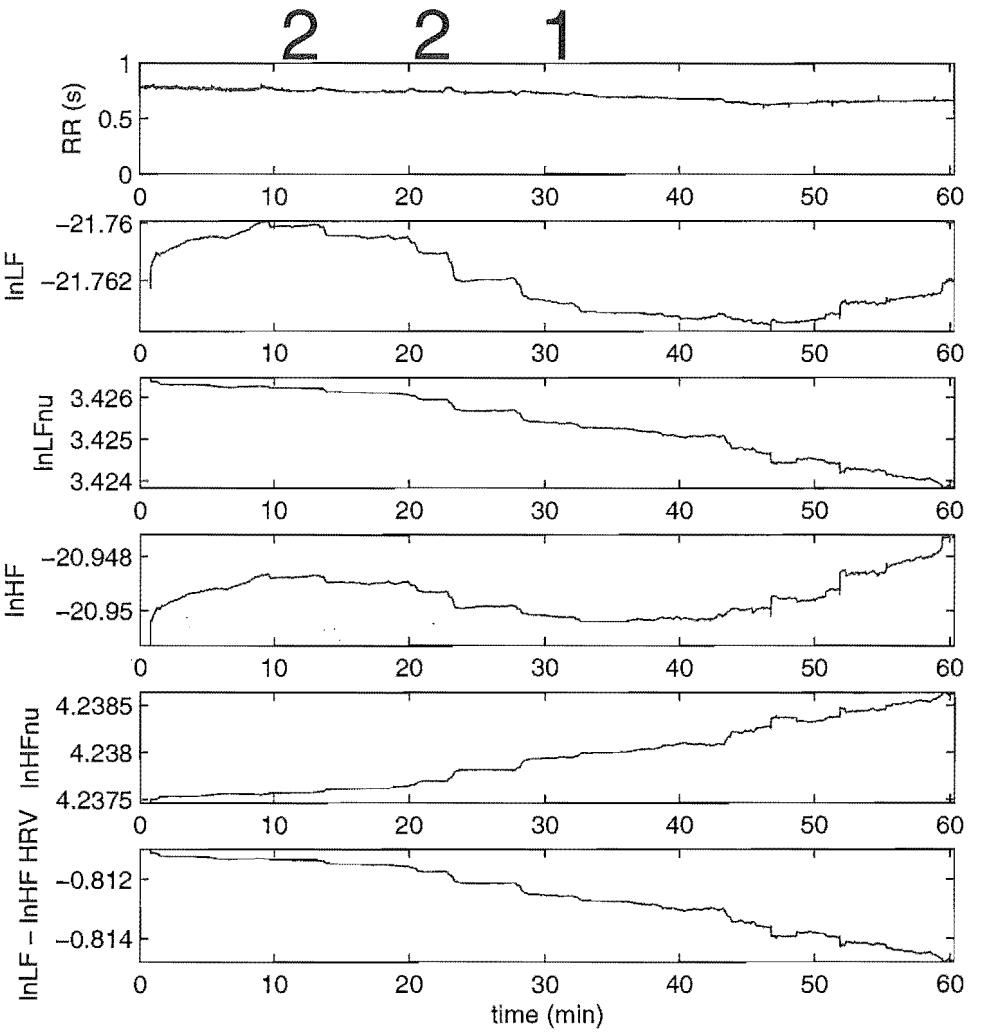

Figure 12.9 ECG analysis of ICU Patient 2 with spectral log-transformed variables lnLF, lnLFnu, lnHF, lnHFnu and lnLF - lnHF during agitation. The PSD is estimated by an AR filter of order p=50 and forgetting factor ω=0.995.

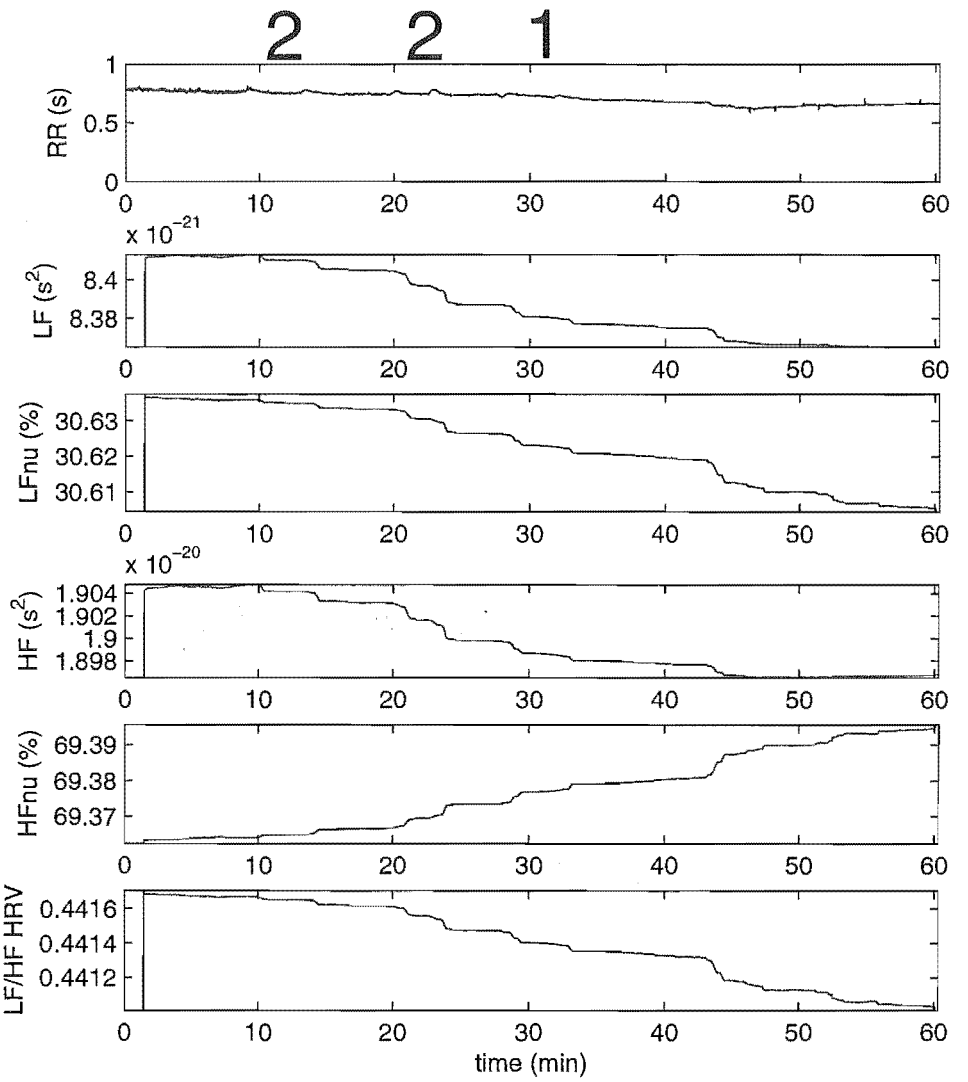

Figure 12.10 ECG analysis of ICU Patient 2 with spectral variables LF, LFnu, HF, HFnu and LF/HF during agitation. The PSD is estimated by an AR filter of order p=100 and forgetting factor ω=1.

12.1.4 Summary of ECG, Patient 2

The overall results for Patient 2 can be summarised for each variable:

- HR: Unlike Patient 1, the HR of Patient 2 does not offer clear indication of agitation, as the HR signal does not correlate with the reported episodes of agitation
- HRD: The HRD variable also fails to indicate agitation, and the signal suffers physiological artifacts, shown for instance in Figure 12.6.
- SDRR: The SDRR marker of Patient 2 oscillates more during periods of agitation, but suffers physiological artifacts and does not provide a simple way to quantify agitation.
- SDdRR: The SDdRR marker also fails to provide an efficient marker of the three episodes of agitation reported for Patient 2.
- LF: The low frequency component of the PSD computed with AR filter of order 50 offers a consistent tracking of agitation, as shown in Figure 12.8.
- HF: The high frequency component of the PSD does not correlate with episodes of agitation in the case of Patient 2.
- LF/HF: The HRV ratio fails to produce relevant indication of agitation with any combination of order and forgetting factor.

Patient 2 emphasises the need to incorporate markers derived from several physiological signals to derive the agitation index. The ECG signal for Patient 2 does not contain consistent information to detect and forecast agitation.

12.1.5 Analysis of ECG over 12 patients

Similarly, mixed results were seen for all 12 ICU patients. The temporal and spectral HRV markers derived from the ECG are not consistent with reported agitation for all the patients. Some episodes of agitation are not detected by

the ECG markers. Moreover, other symptoms can affect the ECG markers, producing unwanted physiological artifacts that impair the overall agitation index. This result confirms the assumptions and expectations from Section 3.4. Spectral HRV may not be suitable for the application of continuous agitation quantification on a broad population of critically ill patients. Possible reasons include lack of stationarity, beat-to-beat analysis of the ANS from which it is hard to differentiate agitation from other symptoms such as atrial fibrillation or other heart dysrhythmias that affect HRV. Further research on the relation between ECG markers and agitation of ICU patients is required to produce a pertinent marker out of the ECG signal.

12.1.6 Summary of ECG over 12 patients

The overall findings for the 12 ICU patients are summarised for each variable:

- HR: The HR tends to rise with episodes of agitation. However, episodes of agitation have been reported where there is little or no effect on HR. Moreover, other symptoms as well as therapies also provoke a rise in HR, and subsequent physiological artifacts.
- HRD: The HRD is strongly related to HR, and suffer the same limitations. Some episodes of agitation are missed by the HRD markers, while other symptoms produce physiological artifacts on the HRD signal.
- SDRR: The SDRR suffers physiological artifacts and does not consistently provide a simple way to quantify agitation. Although promising results were obtained on Patient 1, as shown in Figure 12.3, as well as the majority of other patients, the SDRR marker proved to be inconsistent during some episodes of agitation.
- SDdRR: The SDdRR marker also fails to provide an efficient marker during some episodes of agitation among the 12 ICU patients.
- LF: The LF component is not always a pertinent marker, much like other ECG derived markers. Also, the range of fluctuations witnessed during episodes of agitation sometimes requires a log-transform to be processed at higher level, as shown in Figure 12.9.

- HF: The HF is also inconsistent over the 12 different patients. It shows a correlating trend during some episodes of agitation, but quantification of agitation remains challenging from the HF marker.

- LF/HF: This commonly used marker of the ANS balance suffers from the AR filter instability. Many research groups implementing the LF/HF ratio as a marker of the ANS balance do so in a qualitative manner. However, the quantification attempted in this research on a broad population of ICU patients is more challenging.

The variable findings over the 12 patients definitely emphasize the need for other physiological signals to consistently derive the agitation index.

12.2 Effect of the trial on ABP derived metrics

12.2.1 Analysis of ABP, Patient 1

The analysis of Patient 1 reveals good correlation between ECG derived markers and episodes of agitation. However, Patient 2 episodes of agitation were not detected by the ECG-derived markers. Hence, ABP analysis is also performed to provide more physiological markers and improve the agitation sensor. The SBP values of the ABP signal are processed similarly to the tachogram. The temporal analysis provides SDSBP, SDdSBP, and BPD, as shown in Figure 12.11 for Patient 1. The spectral decomposition provides the LF, LFnu, HF, HFnu markers. Global balance of the ANS is this time represented by the HF/LF ratio, as opposed to the LF/HF ratio.

Keep in mind that this inverse relation (HF/LF vs. LF/HF) is related to the diagnostic generally performed on HRV and BPV [Kuusela et al., 2003]. Overall increase of HRV is clinically healthy, whereas a decrease in variability is related to increase morbidity and mortality. On the other hand, a decrease of BPV is healthy, and overall increase of BPV is related to increased morbidity. Basically, a healthy cardiovascular system would rather increase the variations of HR to decrease the variation in ABP as much as possible. Hence the inverse ratio is

established from spectral components to estimate the balance of the ANS and potentially track agitation.

The LFnu marker of order 12 and forgetting factor 0.995 reacts to the episodes of agitation with a rising trend, and a large peak that correlates with the acute episode of grade "3" agitation. The other markers fail to correlate with the episodes of agitation. Different forgetting factors $\omega = 0.8$, 0.9 and 1 are implemented to potentially improve the quality of the spectral markers, but no significant improvements are observed.

The same analysis is repeated over a 20-sample long window. The temporal markers BPD, SDSBP, SDdSBP and BPD are shown in Figure 12.12. The correlation with the episodes of agitation is also observed in this case and the resulting markers are smoother in shape, hence easier to process at higher level.

The spectral decomposition performed by AR estimation of order 20 and forgetting factor 0.995 is shown in Figure 12.13. The LFnu marker offers a pertinent marker of agitation in this case. The contrast between the agitation grades "1" and "3" is neat. The other spectral markers do not correlate with agitation in this case. Other forgetting factors are also implemented, and they do not change the data. This result confirms the statement of Kuusela at al. [Kuusela et al., 2003] that the order is the crucial parameter of the AR filter.

The temporal analysis of the ABP signal is performed over a 50-sample wide sliding window, and the corresponding markers are observed in Figure 12.14. Unlike the ECG-derived markers that are dramatically delayed when computed over a 50-sample wide window, The ABP-derived markers do not suffer from a long lag, and are still consistent markers of agitation symptoms. However, wider windows are not suitable and the 50-sample-wide window is found to be the best compromise between smoothness and propagation delay. Temporal analysis is consequently not performed over longer windows.

The spectral markers obtained for Patient 1 with order 50 and $\omega = 0.8$ do not correlate with the episodes of agitation in this case. Therefore, none of them is considered as a persistent marker of agitation. The use of different forgetting factors does not improve the trend of the spectral markers.

Finally, the spectral decomposition is performed by AR estimation of order

100 and 500, with starting forgetting factor $\omega = 1$, similar to Bianchi et al. [Bianchi et al., 1993]. The spectral markers in both cases do not offer good correlation, and a sharp peak is observed shortly after initialisation, which is probably a sign of instability of the filter. This instability issue usually occurs when the filter is initialised on a non-stationary set of data. Several other forgetting factors fail to improve the quality of the spectral markers.

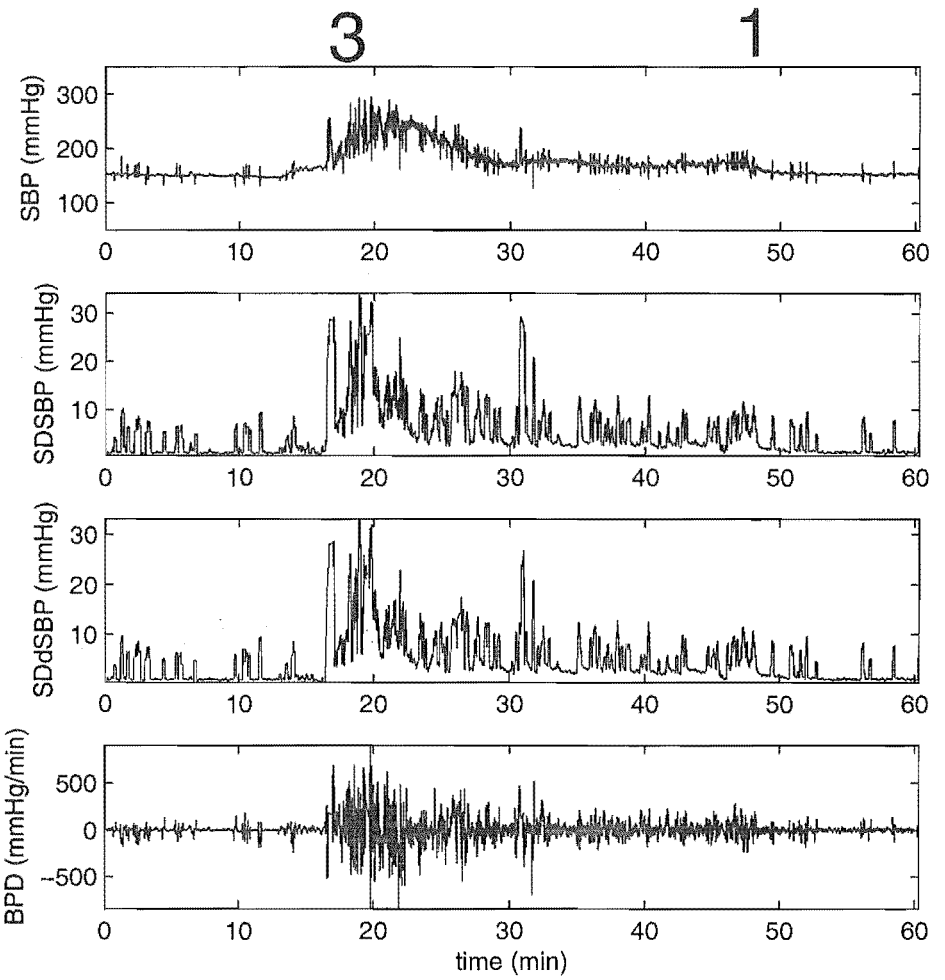

Figure 12.11 ABP analysis of ICU Patient 1 with temporal variables SBP, SDSYS, SDdSYS and BPD during agitation. SDSYS, SDdSYS and BPD are calculated over a 12 sample window. Agitation is assessed on the modified SAS, and reported on top of the Figure.

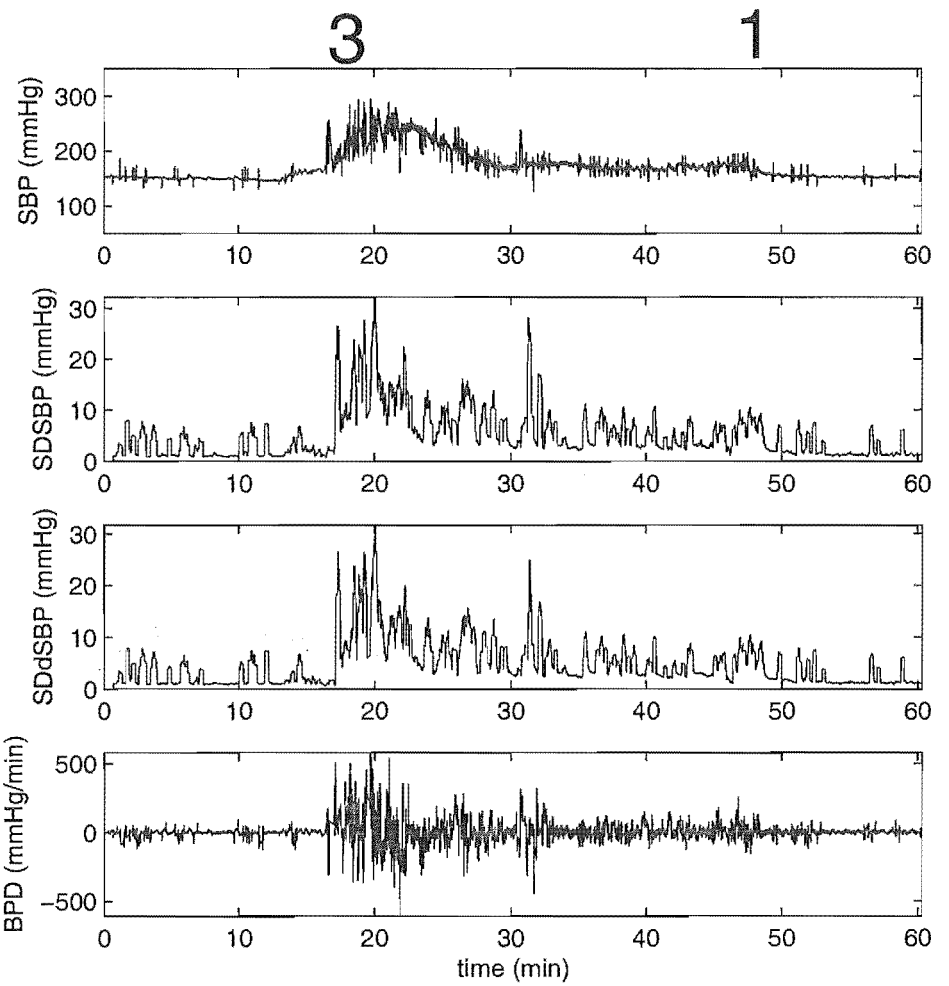

Figure 12.12 ABP analysis of ICU Patient 1 with temporal variables SBP, SDSYS, SDdSYS and BPD during agitation. SDSYS, SDdSYS and BPD are calculated over a 20 sample window. Agitation is assessed on the modified SAS, and reported on top of the Figure.

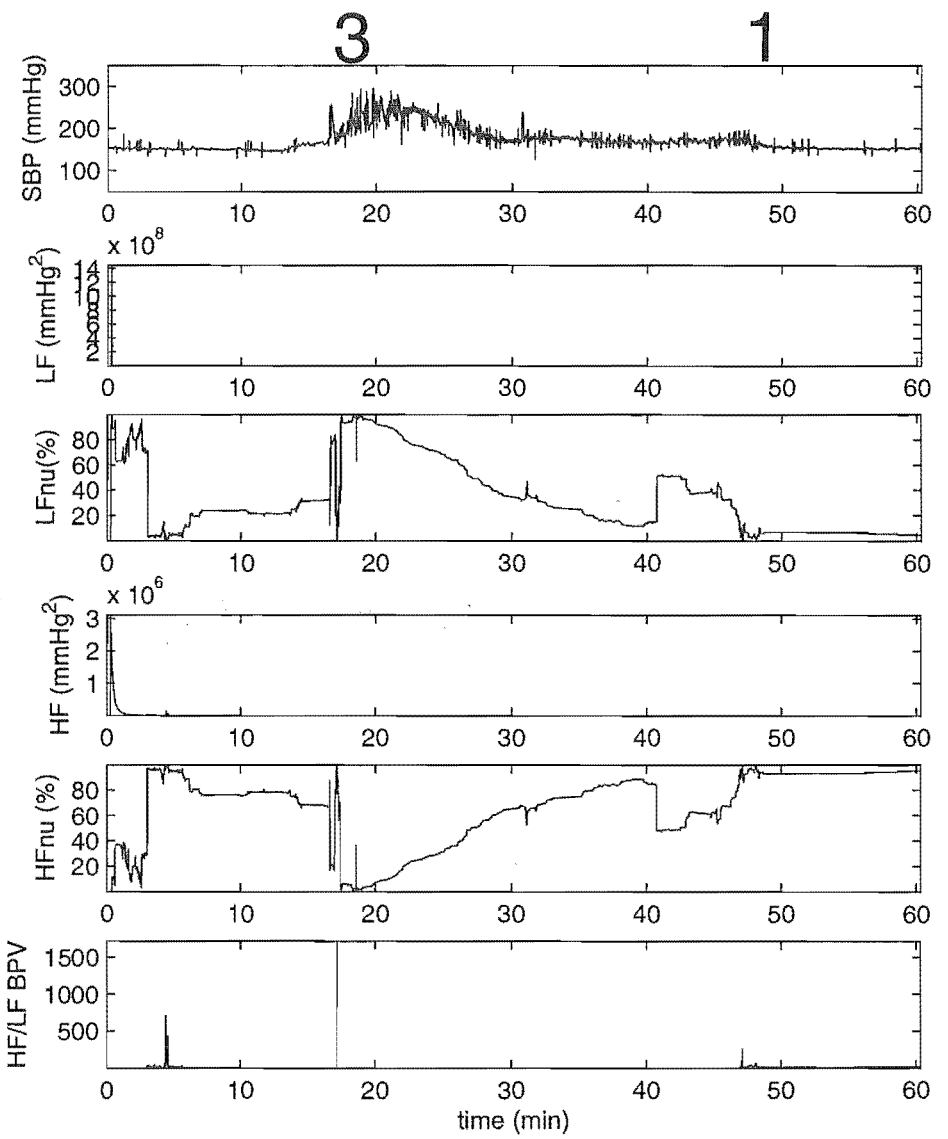

Figure 12.13 ABP analysis of ICU Patient 1 with spectral variables LF, LFnu, HF, HFnu and LF/HF during agitation. The PSD is estimated by an AR filter of order p=20 and forgetting factor ω=0.995.

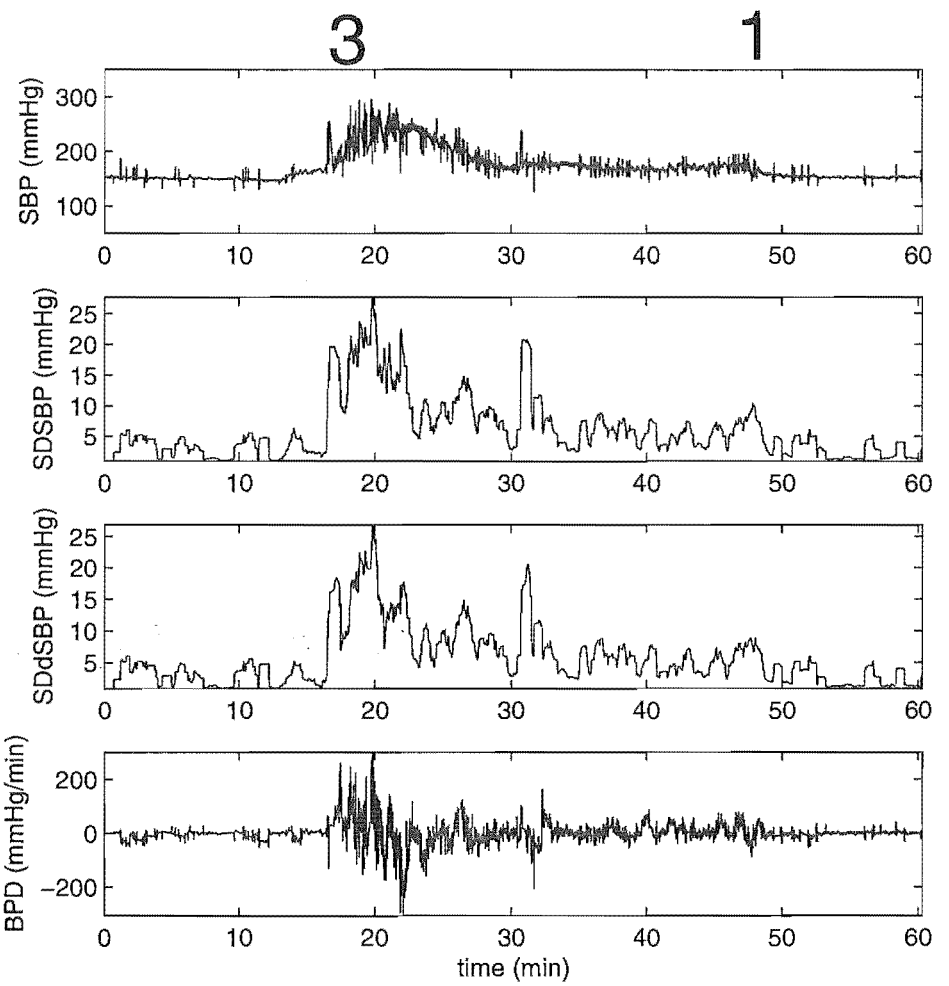

Figure 12.14 ABP analysis of ICU Patient 1 with temporal variables SBP, SDSYS, SDdSYS and BPD during agitation. SDSYS, SDdSYS and BPD are calculated over a 50 sample window. Agitation is assessed on the modified SAS, and reported on top of the Figure.

12.2.2 Summary of ABP, Patient 1

The results of ABP analysis for Patient 1 with various methods is summarised for each marker:

- SBP: The SBP marker correlates well with the two episodes of agitation as shown in Figure 12.11.
- BPD: The derivative is a pertinent marker of agitation when computed over 50 samples, as shown in Figure 12.14. It oscillates too much and lacks smoothness when computed on shorter windows, and is too delayed on longer windows.
- SDSBP: The global temporal marker SDSBP provides a consistent marker of agitation in the case of Patient 1, processed over 50 samples and displayed in Figure 12.14.
- SDdSBP: Similarly to SDSBP, a smooth pertinent marker is obtained when the data is processed over 50 samples. The optimal SDdSBP marker is displayed in Figure 12.14.
- LF: The implementation of AR filters on the SBP series is also challenging and unstable. However the normalised LFnu marker correlates with the episodes of agitation reported for Patient 1 when processed over 20 samples, as shown in Figure 12.13. Note that it corresponds to different optimal parameters than the AR filters implemented on the tachogram.
- HF: The high frequency component of the SBP series does not correlate with episodes of agitation with combinations of parameters implemented in this research.
- HF/LF: The common frequency BPV marker fails to correlate with the episodes of agitation reported for Patient 1.

These findings are compared with data from other patients for consistency.

12.2.3 Analysis of ABP, Patient 2

The temporal and spectral analysis is performed with different combinations or orders and forgetting factors on the ABP signal of Patient 2. The temporal analysis is performed on 12, 20 and 50-sample long windows. The episodes of agitation are possibly detected by the sharp peaks of the SDSBP, SDdSBP and BPD markers shown in Figure 12.15. Detecting agitation from the ABP markers in Patient 2 is crucial since all the ECG markers failed to produce a pertinent marker of agitation. The ABP markers are smoother when computed over 20 and 50-sample wide windows. The 50-sample-wide implementation of the temporal analysis is shown in Figure 12.16. Similar to the results from the analysis of the ABP signal of Patient 1, 50-sample-wide temporal analysis offers the best tradeoff between smoothness and propagation delay.

The spectral decomposition is performed using the relevant combinations defined in Table 12.1. The most pertinent marker in this implementation is the normalised low frequency component LFnu that oscillates during the three episodes of agitation reported by clinicians. The spectral decomposition of order 500 with forgetting factor 1 is shown in Figure 12.17 as an example. Other forgetting factors do not improve the markers obtained from the spectral decomposition.

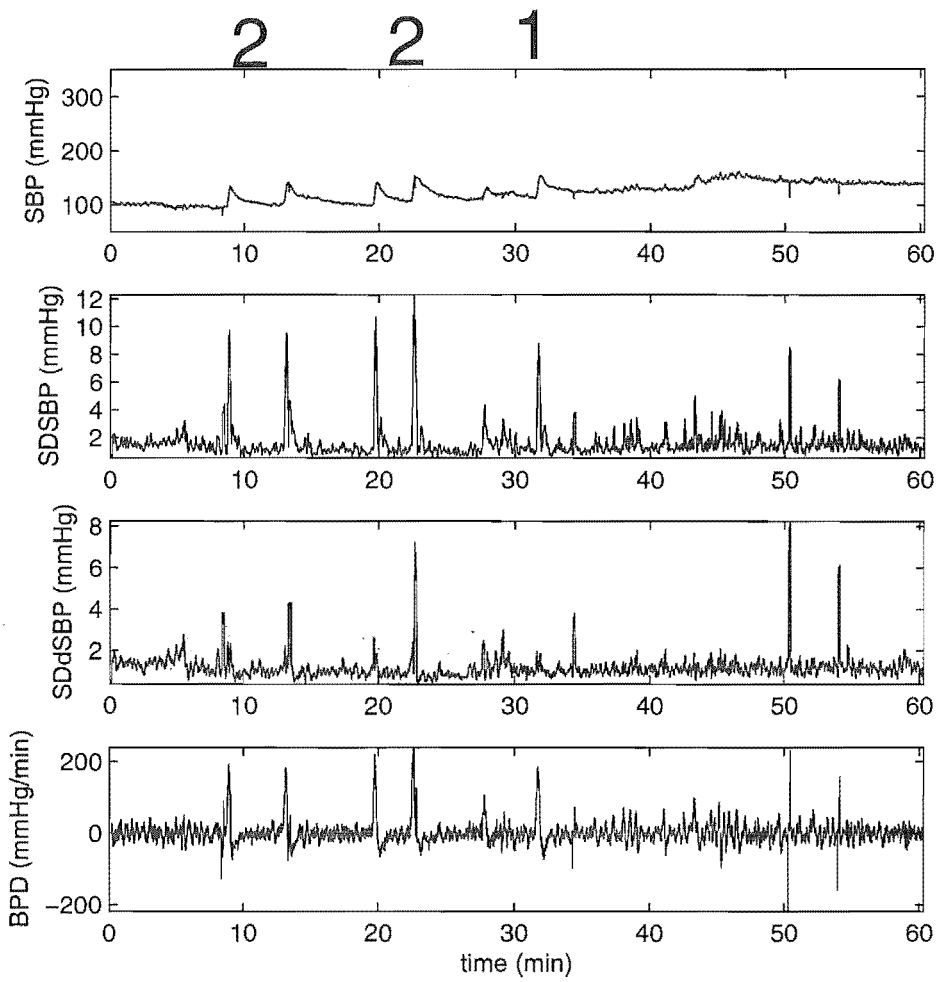

Figure 12.15 ABP analysis of ICU Patient 2 with temporal variables SBP, SDSBP, SDdSBP and BPD during agitation. SDSBP, SDdSBP and BPD are calculated over a 12 sample window. Agitation is assessed on the modified SAS, and reported on top of the Figure.

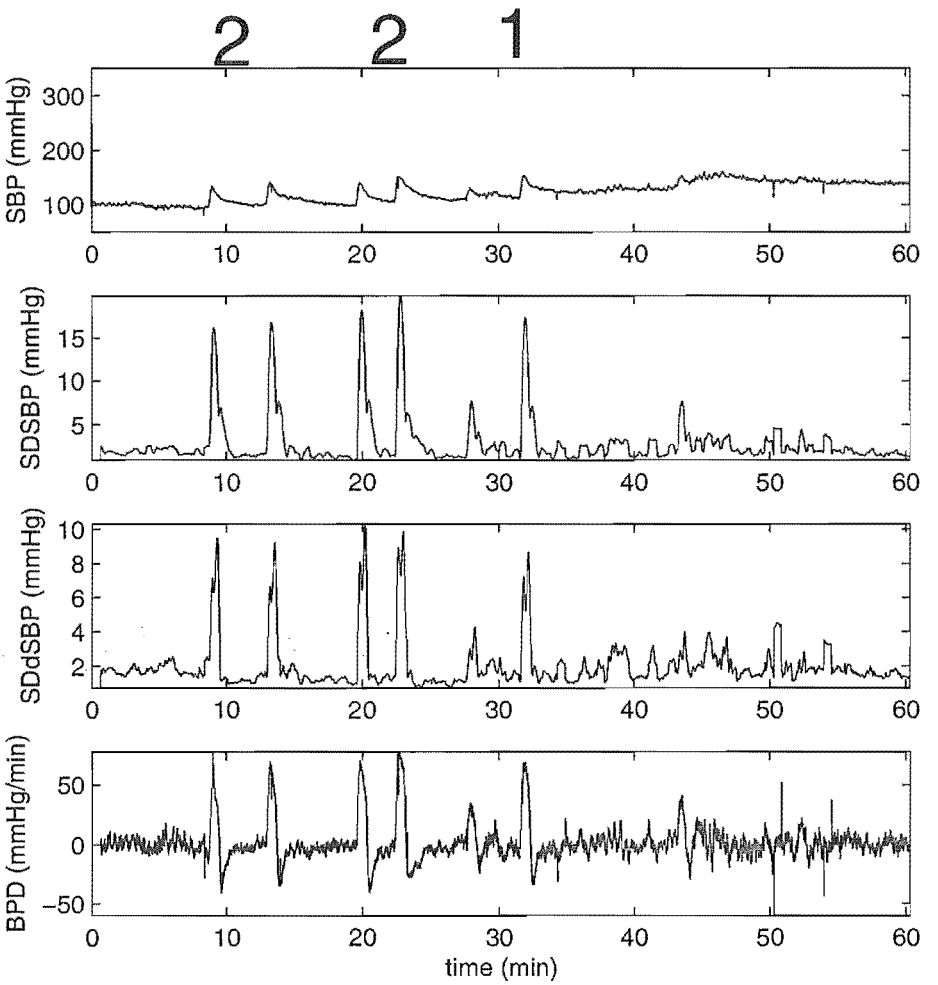

Figure 12.16 ABP analysis of ICU Patient 2 with temporal variables SBP, SDSBP, SDdSBP and BPD during agitation. SDSBP, SDdSBP and BPD are calculated over a 50 sample window. Agitation is assessed on the modified SAS, and reported on top of the Figure.

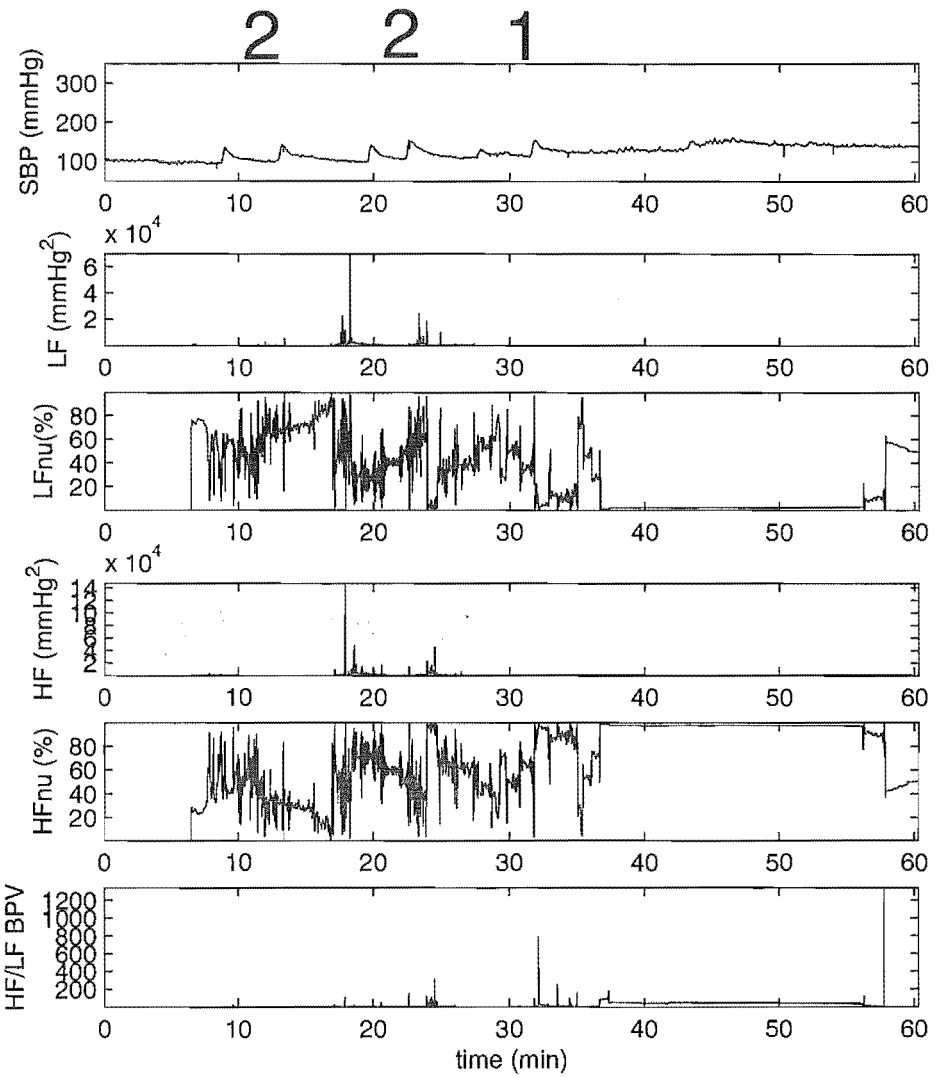

Figure 12.17 ABP analysis of ICU Patient 2 with spectral variables LF, LFnu, HF, HFnu and LF/HF during agitation. The PSD is estimated by an AR filter of order p=500 and forgetting factor ω=1.

12.2.4 Summary of ABP, Patient 2

The results of ABP analysis for Patient 2 with various methods is summarised for each marker:

- SBP: The SBP variable shows fast oscillations during the episodes of agitation reported for Patient 2. This can be used to detect coming agitation. However, the long term rise of SBP does not correlate with agitation.
- BPD: BPD contains large peaks during agitation, but physiological artifacts occur outside episodes of agitation. Artifacts are reduced while agitation-related peaks are emphasized over a 50-sample window, as illustrated in the fourth frame of Figure 12.16.
- SDSBP: The SDSBP variable smoothed over a 50 sample long MA filter offers a reliable means to quantify agitation, while artifacts are filtered, as shown in the second frame of Figure 12.16.
- SDdSBP: The SDdSYS variable is also reacting during the episodes of agitation reported for Patient 2, and quantification of agitation is also possible from this marker displayed in the third frame of Figure 12.16.
- LF: The normalised low frequency component computed over 500 samples is dominant over the high frequency during the three episodes of agitation, as shown in the third frame of Figure 12.17. This does not correspond to the data of Patient 1 where the optimal order is 20.
- HF: The high frequency component of BPV does not offer a reliable marker to detect and quantify agitation for the data of Patient 2.
- HF/LF: The HF/LF ratio fails to correlate with agitation in the case of Patient 2.

The spectral components do not seem appropriate in the case of Patient 2. However, temporal markers offer an better means to quantify agitation from the magnitude and number of peaks within the markers, by means of averaging for instance.

12.2.5 Analysis of ABP over 12 patients

The ECG proved a lack of consistency in detecting agitation, and so have the ABP derived markers when all 12 patients are considered. However, the combination of both markers can improve the detection of episodes of agitation based on physiological markers. Growing knowledge from further research and observation may improve the reliability of markers derived from temporal and spectral BPV, and particularly which order to use.

Meanwhile, BPD averaged over 50 samples can be used as a marker of the dynamics of ABP potentially related to agitation. For all patients BPD was generally consistently able to identify agitation episodes that affected ABP. This metric is also easily calculated for real-time application and does not require stationary data. Finally BPD and temporal BPV focus on different trends of the ABP, which as discussed in Chapter 3 may be complimentary with the information obtained by the spectral BPV method.

However, more physiological markers are clearly required to reduce the number of physiological artifacts. This can be achieved by developing and including agitation-specific markers derived from respiration, and consequently developing the high-level heuristics based on the new set of markers. If all the physiological markers available still fail to detect agitation, the agitation index is based on motion sensing.

12.2.6 Summary of ABP over 12 patients

The results of ABP analysis over the 12 patients is summarised for each marker:

- SBP: The effect of agitation on the SBP signal is varied, and is seen to continuously rise, oscillate, or simply fail to respond. The SBP appears to be an inappropriate marker of agitation.
- BPD: BPD is consistent when agitation affects the trend of the SBP signal. It otherwise fails when SBP is not affected by agitation.
- SDSBP: The SDSBP variable offers a reliable means to quantify agitation

when there is an increase of the overall BPV power. Further research is required to associate the BPV overall power with episodes of agitation.

- SDdSBP: The SDdSBP variable has the potential to quantify agitation when fast oscillation of the SBP series are provoked by agitation. Analysis of the 12 patients revealed that it is not consistent, and some episodes of agitation are missed by the SDdSYS marker.

- LF: The low frequency component, and alternatively its normalised version (LFnu) offer variable results. The optimal AR order is different from a patient to the next, and this is a challenge for use as an agitation sensor for a variety of different patients. This issue introduces the possibility of adding patient-specific input parameters to the sensor to improve the output.

- HF: The high frequency component of BPV does not offer a reliable marker for the detection and quantification of agitation.

- HF/LF: The BPV ratio is not reliable over the population studied in this research.

No markers from ABP can be used exclusively to quantify agitation. The episodes of agitation reported over the 12 patients reveal different patterns in the different markers.

12.3 Motion Sensing Trials

Motion sensing provides complementary information that is useful to avoid missing events of agitation. At best, the agitation sensor detects a pattern within the physiological signals that predicts agitation. Consequently, the agitation index rises and the sedation can be updated accordingly to provide optimal care of the patient.

The worst case scenario lacks well-known patterns within the physiological markers and the agitation sensor cannot predict or detect, and ultimately aid in the prevention of agitation. Therefore, agitation occurs. This result very often involves motion of the patient, which should be monitored to detect an episode

of agitation as it occurs. At this stage the agitation cannot be prevented but it can be blunted by immediate action.

Motion sensing therefore also adds consistency to the system. Basically, if the system cannot lead the clinicians by early detection of emerging agitation, it should at least agree that agitation occurs when motion is widely detected. Particularly, harmful motion is a major input to subjective definitions and assessment of agitation. The task of motion detection is performed using the video-processing technique described in Chapter 6.

12.3.1 Analysis of motion, Patient 1

The motion index, MI, computed using the frame-to-frame correlation technique is shown in the top frame of Figure 12.18 for Patient 1. The moving average over 10 consecutive values is referred to as MI10 and is shown in the bottom frame of Figure 12.18. MI10 contains a peak of value 0.64, which is reasonably high, and therefore correlates with the clinician in charge, whose feedback indicates severe grade "3" agitation.

Note that the motion index is rising before the feedback of the clinicians. This result is not consistent with motion sensing being considered as a late detection technique. However, the video record shows clinicians taking care of the patient, and restraining motion, before the feedback is given. Therefore, the episode of agitation is starting before the clinicians have a chance to access the computer to give their feedback. The motion sensing of Patient 1 is showing good contrast and correlation with the episode of agitation, and it can be used to quantify agitation when no reaction has been detected on physiological markers.

12.3.2 Analysis of motion, Patient 2

The motion detected from Patient 2 shown in Figure 12.19 reveals a weakness of this initial form of motion sensing. In fact, the first episode of agitation is not detectable from the preceding calm period, due to a lack of contrast. The second episode of agitation is better detected with more contrast. The clinician feedback

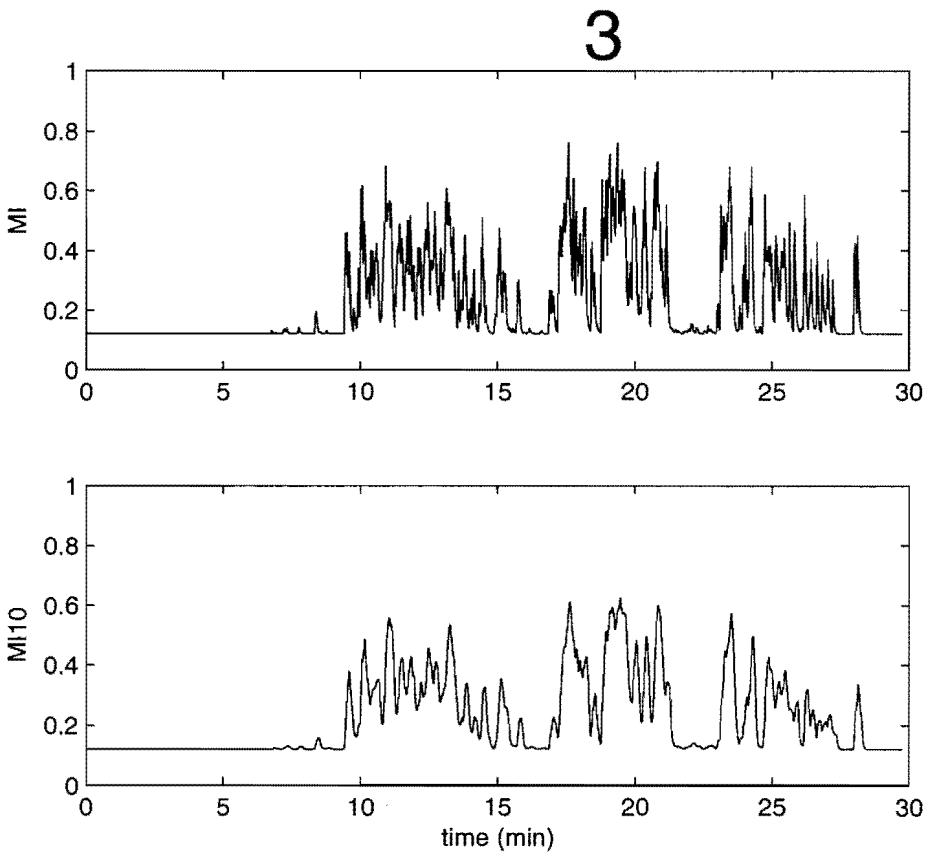

Figure 12.18 Motion sensing of Patient 1 in top frame, moving average over 10 samples in bottom frame.

is done at the very beginning of the period of motion detected, so it matches well.

12.3.3 Summary of motion sensing

Motion sensing is used in this research to avoid completely missing an episode of agitation when physiological markers do not produce well-known agitation-related patterns. Similar results as noted for Patients 1 and 2 are seen for all 12 patients. Overall, motion correlates well with recorded agitation.

There is a lot of room for improvement through increasing the number and precision of ROIs, as well as corresponding high-level processing of specific body parts motion. In its current form, the motion sensing produces a lot of technical artifacts due to interference of clinicians and relatives with the patient. Physi-

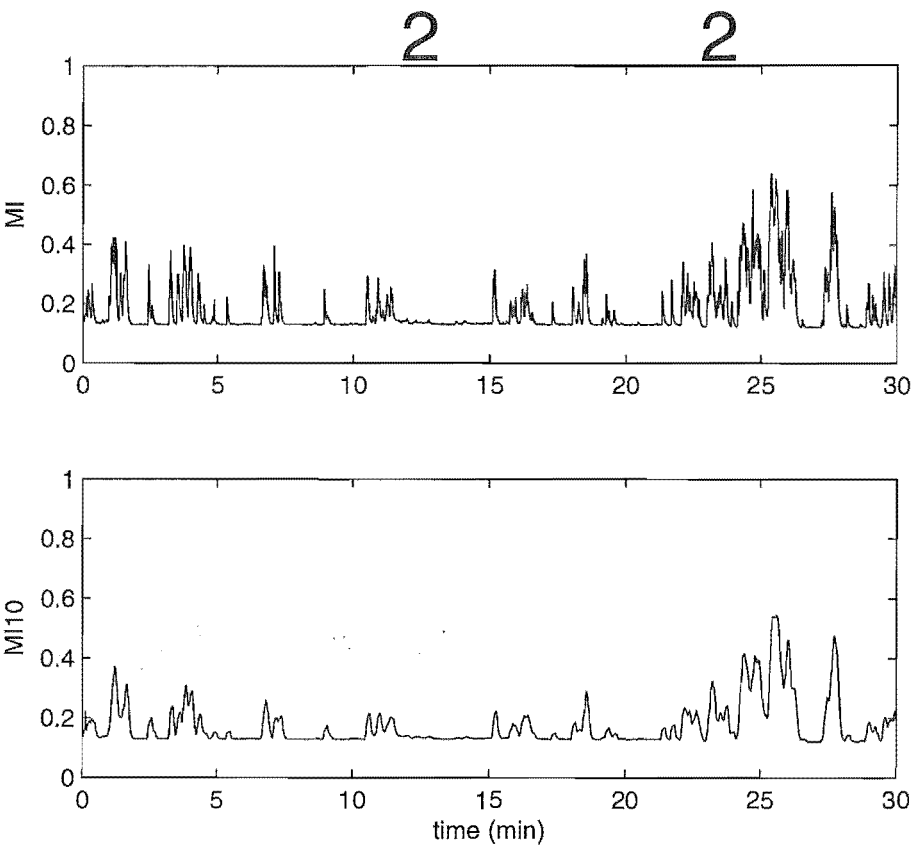

Figure 12.19 Motion sensing of ICU Patient 2 in top frame, moving average over 10 samples in bottom frame.

ological artifacts are also observed because mild motion of the patient limbs is detected and processed as agitation, whereas it is negligible from a clinical aspect. Guidelines to improve motion sensing are given in Chapter 16.

12.4 Summary of the 12 ICU trials

It is necessary to analyse several patients to obtain enough patterns of agitation. This process is useful to avoid misinterpretation of the results of the signal-processing of HR and ABP derived metrics. If the results of ABP processing are combined with the results of ECG processing, a more reliable and accurate diagnostic tool is developed, because ICU therapies may modify the physiological reactions of the patients to mental and physical stress, and the combination of

different signals and their derived metrics improve the potential to detect an upcoming episode of agitation, and reduce artifacts. Therefore the essence of this agitation sensor is to combine concurrent and complementary information from several physiological sources to produce a more accurate diagnostic.

Overall, spectral HRV and BPV originally introduced are not as consistent as temporal HRV and BPV as well as HRD and BPD in a real-time environment. The direct HR and SBP variables correlated well. The combination of ABP and ECG markers detect most episodes of agitation, but produce a lot of physiological artifacts from other symptoms than agitation. More markers, such as respiration-related variables may be added in the future to reduce artifacts. The results of these first trials are discussed to analyse the structure of the agitation sensor being developed.

The structure of the agitation sensor designed for the capstone trial and presented in Figure 12.20 is based on 5 inputs: HR, HRD, SBP, BPD and MI. The agitation FIS that combines these five inputs is described in Chapter 9. The HRV and BPV are not included in this first real-time implementation of the agitation sensor. Spectral HRV and BPV have proved to be very efficient markers for the assessment of patients in specific conditions, such as atrial fibrillation [Paskeviciute et al., 2001] or arrhythmia [Tsipouras and Fotiadis, 2004]. Globally, it is complex to quantify a metric from the HRV or BPV markers when it is computed on a broad population. ICU patients follow different therapies through ventilation and medication among other parameters, that invariably affect their ANS and subsequent responses of HRV and BPV metrics.

At this stage, the semi-automated sedation management project is divided into two separate research fields: sedation modelling and agitation sensing. There is a strategic choice to be made, whether the agitation sensor receives parameters concerning the patient therapy, or the agitation sensor uses metrics that assess a more global trend of a physiological signal such as HRD, BPD and potentially BRD in the near future. Although HRV and BPV are state-of-the-art physiological metrics, more research is needed in the context of ICU patients to quantify and incorporate HRV and BPV markers to the agitation sensor. More details about the future work is given in Chapter 16.

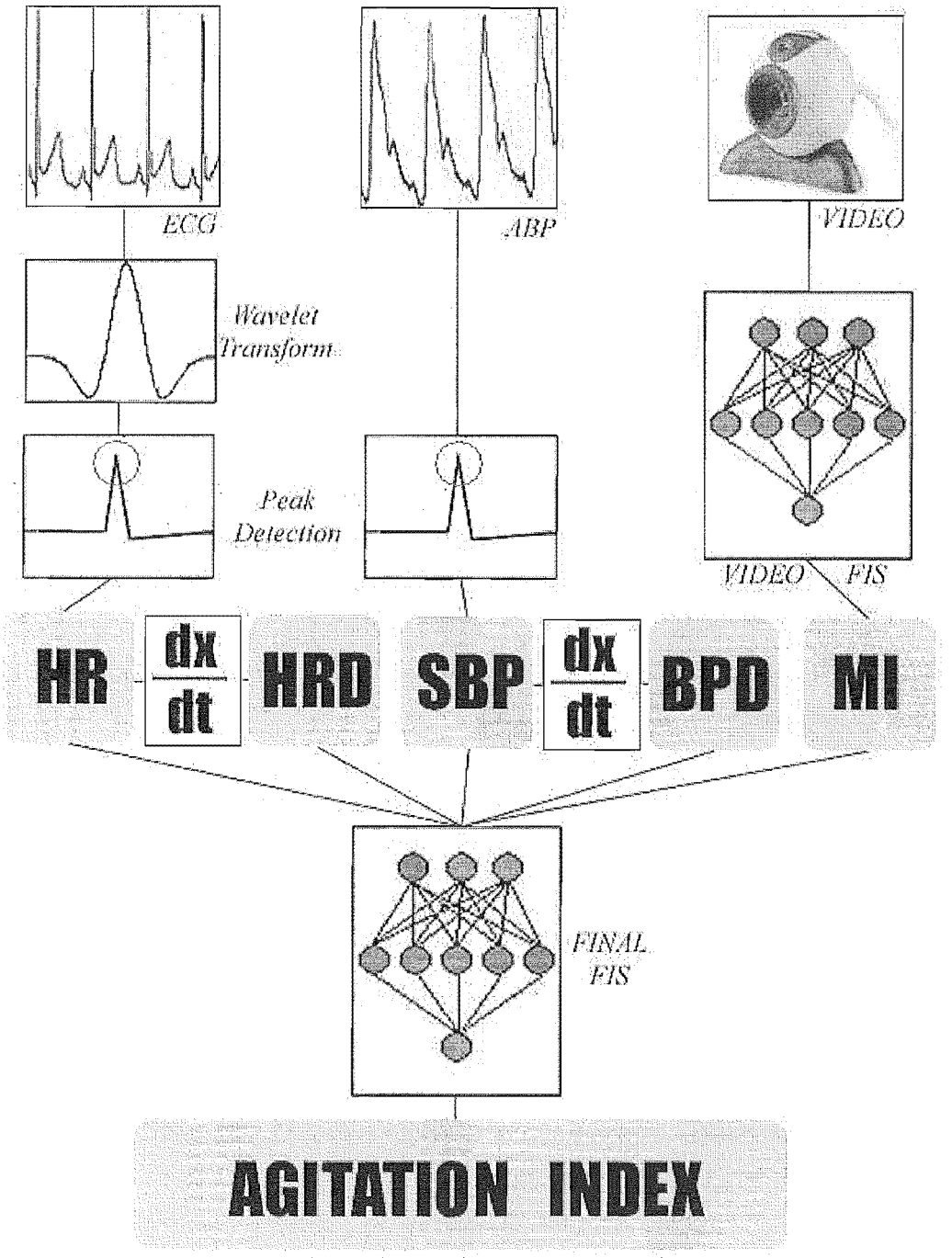

Figure 12.20 Signal-processing diagram of real-time software used for ICU capstone trial of this agitation assessment research.

Chapter 13

ICU patients: Capstone trial

The structure of the prototype agitation sensor is determined from the results of the initial clinical trials, and is shown in Figure 12.20. At this stage, this first prototype of the real-time agitation sensor needs to be more rigorously verified on ICU patients, and compared with the modified SAS used by the clinicians to assess agitation. This approach will further validate and calibrate the physiologically based agitation quantification system.

13.1 Goals

The capstone clinical trial of this research is designed to validate the agitation sensor using common statistical methods to estimate the potential correlation between the objective agitation index from the system and the subjective agitation index from the clinicians' assessment. This method of comparison introduces a paradigm, because the objective measurement system cannot be directly compared to the subjective assessment method. Therefore, the capstone clinical trial is designed specifically to counter the issue of subjectivity.

This set of trials is implemented off-line to decrease the subjectivity of the medical staff by taking the median averaging several clinicians' assessments into account. The trial is also designed to expose a given clinician to multiple episodes in a timely fashion so that significant data density can be obtained for validation, which did not occur in prior trials due to time constraints on staff. This approach also eliminates the issues of delayed report of agitation by busy clinical staff.

13.2 Method

Basically, the subjectivity of the modified SAS is decreased by having several clinicians assessing the same data, as well as by using data from different patients. At this stage, the optimal number of patients required for the validation trial is not known because only the inter-rater, not the intra-rater, subjectivity of the SAS has been quantified. Also, the current practical limitations only allow the study of approximately one patient per week.

This final trial is performed on data obtained from four different patients, each studied for over a week. This data represents 42 patient-days. Although more patients would potentially increase the statistical significance of the trial, this trial first focuses on trying to select segments of data equally distributed over the different levels of agitation. Forty 5-minute clips are selected to equally cover the different levels of agitation. This data corresponds to 200 minutes, and therefore the forty clips should theoretically contain 50 minutes of each grade of agitation of the SAS scale in the range 0–3.

Although it is practically impossible to a-priori guess what the clinicians assessments of a clip is going to be, the clips used are reviewed by senior clinical staff for balance prior to use. The real-time assessment given by the clinician in charge of the patient during the real-time study is not directly compared with the system output, but these ratings are utilised to a-priori locate relevant periods of data containing agitation. Hence, the real-time assessments were used to locate relevant episodes.

During the trials, the video clips and the corresponding HR and SBP series are independently assessed off-line by five different clinicians, and the median assessment of the five different clinicians is computed. This technique decreases the inter-rater subjectivity of the assessment. The subjectivity is further decreased by enrolling forty different clinicians in charge of assessing five clips. Hence, each clinician reviews only five of the forty clips, as selected randomly. Therefore, the overall trial is spread over forty different assessors to further minimise the impact of subjectivity. This off-line, multi-assessment trial provides a better reference for the agitation sensor validation. The random clip allocation for the forty nurses is given in Table 13.1

Table 13.1 Random allocation of five clips per nurse

Nurse No	First clip	Second clip	Third clip	Fourth clip	Fifth clip
1	15	30	26	28	1
2	27	38	25	32	1
3	32	26	8	22	10
4	22	3	24	17	8
5	3	4	13	38	39
6	23	40	28	10	33
7	37	6	28	13	26
8	19	37	10	29	14
9	20	19	29	10	27
10	35	17	18	38	33
11	28	12	35	39	13
12	40	18	1	13	28
13	20	21	22	23	24
14	6	5	26	30	2
15	2	36	31	9	39
16	22	31	25	40	3
17	39	9	37	27	19
18	3	19	32	12	11
19	29	24	30	25	40
20	7	9	33	3	22
21	8	29	12	5	21
22	35	25	38	5	33
23	25	34	8	26	5
24	19	6	4	24	23
25	11	10	2	16	35
26	23	17	9	21	29
27	35	30	40	31	20
28	36	2	38	12	27
29	24	4	20	36	31
30	27	8	14	30	13
31	14	1	6	11	36
32	15	12	5	36	14
33	21	16	34	33	18
34	6	7	15	11	20
35	4	31	7	9	16
36	21	15	4	18	11
37	37	23	34	2	32
38	14	32	37	39	18
39	17	16	34	1	7
40	7	15	34	16	17

The off-line assessment software user interface is shown in Figure 13.1. It records the off-line agitation assessment every second, and the clinicians are expected to update the level of agitation while watching the clip, every time they believe it has changed. This approach gives two values every second: the current clinician assessment and the system assessment. The clinicians assess agitation on the SAS 0–3 discrete scale and the agitation sensor estimates agitation on a 0–100 discrete scale. This off-line assessment is carried out in the staff room of Christchurch Hospital during break periods and is carried out over all shifts.

Figure 13.1 User interface of the off-line agitation assessment software. Note that the patient figure is blurred for ethical reasons.

This clinical trial produces the distribution of the system output with reference to the four different grades of agitation in the SAS. Statistical analysis is then performed on the system output distribution to assess the correlation between the system scale and the SAS scale. This correlation is used to estimate the calibration and reliability of the system. In essence, the statistical analysis emphasises the areas where major improvements are required. It can also identify the level of inter-rater variation and global subjectivity between the 40 clinical staff who took part in the trial.

13.3 Practical limitations

This trial is the first attempt to assess the agitation sensor capabilities in real-time using statistical methods and observation. The methodology of this trial has several practical limitations that may impact the results. These limitations include:

- The need to further train clinical staff to use the agitation sensor, such as adapting the camera angle to the patient bed after moving it. This lack of training can reduce the quality of the sensor output.
- The limited number of patients to possibly include in the study within a given time, due to the relatively small population of Christchurch and its 10-bed ICU.
- The lack of knowledge on the SAS subjectivity to estimate the number of patients and nurses to include for a trial to be statistically relevant.
- The early stage of this research and corresponding artifacts and inaccurate quantification of the agitation sensor.
- The complexity to differentiate whether the clinician or the system is wrong in its assessment, due to the subjective agitation assessment by the clinicians .
- The pre-selection of forty clips equally distributed along the four possible grades of agitation of the modified SAS either requires as much interaction with the clinical staff as the assessment, or is subjective to a single assesser but may not be equally distributed a-posteriori.

All these practical limitations can potentially limit the significance of this capstone trial. However, the trial introduces the basic methodology to assess the agitation sensor at any time of its development. More importantly, it presents a method of acquiring high density clinical feedback of assessment for a given patient, which would not be practical during real-time ICU operation.

13.4 Data gathering results

The agitation sensor is tested in real-time on 42 patient-days from four different ICU patients. This data gathering enabled evaluation of the capabilities of the overall system to complement the evaluation of individual signals performed during the first set of clinical ICU trials. Common sense and observation are initially used to analyse the results, before statistical methods are applied on the distribution of the system output. The results of this trial help to define the current state of the system and the guidelines for the future work.

13.4.1 Patient monitoring

During patient monitoring by the agitation sensor, many episodes of agitation are detected and quantified by the system. Empirically, the agitation sensor is expected to produce a higher agitation index during an episode of SAS grade "3" agitation than an episode of SAS grade "1" or "2" agitation. The agitation sensor is also expected to produce a very low agitation index during calm periods. This response is partially achieved, and examples of accurate detection as well as artifacts and inaccurate quantification are illustrated in this section. First, episodes of grade "3" agitation on the SAS scale are successfully quantified with a large agitation index, and one example is shown in the bottom frame of Figure 13.2. Note that the real-time nursing staff assessment shown in the second to last panel reports a grade "3" agitation.

From a calm state, the agitation index, shown in the bottom frame of Figure 13.2, rises progressively according to the information obtained from the physiological markers, until it reaches a maximum index of 100. Meanwhile, the clinician in charge of the patient reports a maximum intensity grade "3" agitation on the SAS scale, as shown in the second to last frame of Figure 13.2. This corresponds to an relatively accurate quantification of the agitation sensor. Similarly, accurate quantification of episodes of grade "1" and "2" agitation on the SAS scale is performed by the system, as illustrated for an episode of grade "2" agitation in Figure 13.3.

In this instance of grade "2" agitation quantification, the system could pos-

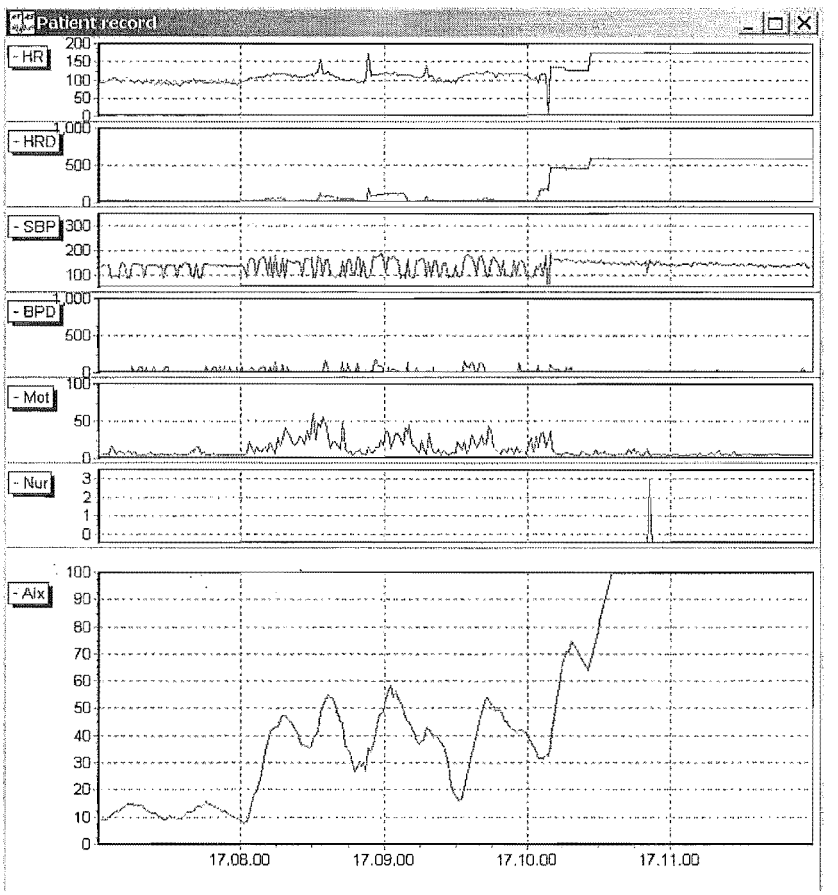

Figure 13.2 Successful detection of grade "3" agitation by agitation sensing system.

sibly produce a slightly higher agitation index, to make efficient use of the full 0–100 range. A grade "2" agitation is the second highest grade on the SAS scale, and should rather correspond to an agitation index located somewhere in the higher half of the scale to make optimal use of the range. However, the assessment of the patient agitation by a single clinician is subjective and another clinician may assess the same episode with a SAS grade "1". Therefore, it is hard to make any conclusions on the accuracy of the system from the comparison with a single clinician. Hence, several clips are assessed by five different clinicians in this trial, under controlled circumstances, to reduce the subjectivity of the human assessment, which is the essence of these clinical trials and this overall research.

Between episodes of agitation, patients are typically calm. Most of the time,

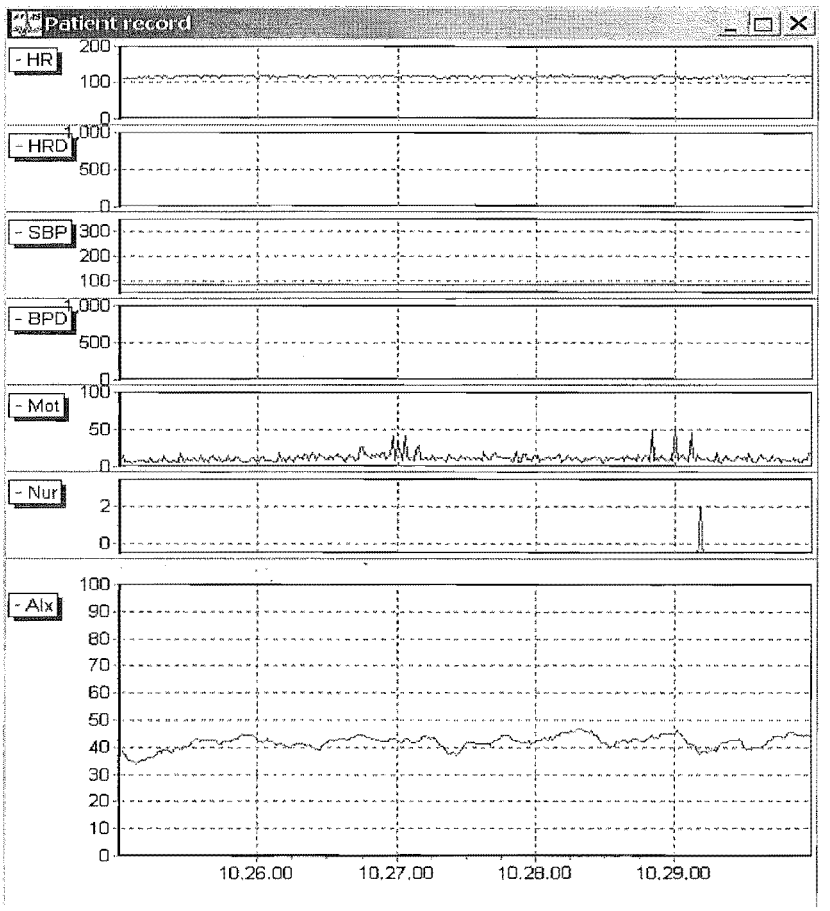

Figure 13.3 Successful detection of grade "2" agitation by agitation sensing system, with slight under-calibration problem.

the agitation sensor consequently produces a very low agitation index that corresponds to a calm state. This result is illustrated in Figure 13.4. The first five frames display the agitation markers, none of which indicates potential for agitation according to the current physiological knowledge on agitation. The sixth frame indicates the clinician's feedback of a grade "0" agitation level on the SAS score, which means the clinician in charge thinks the patient is calm. Finally, the seventh frame shows the output index of the agitation sensor, which is also very low. Therefore, the system successfully reports the patient to be calm. This result is repeated for most assessors on all the grade "0" episodes.

However, the reliability of the agitation index can be impaired by several

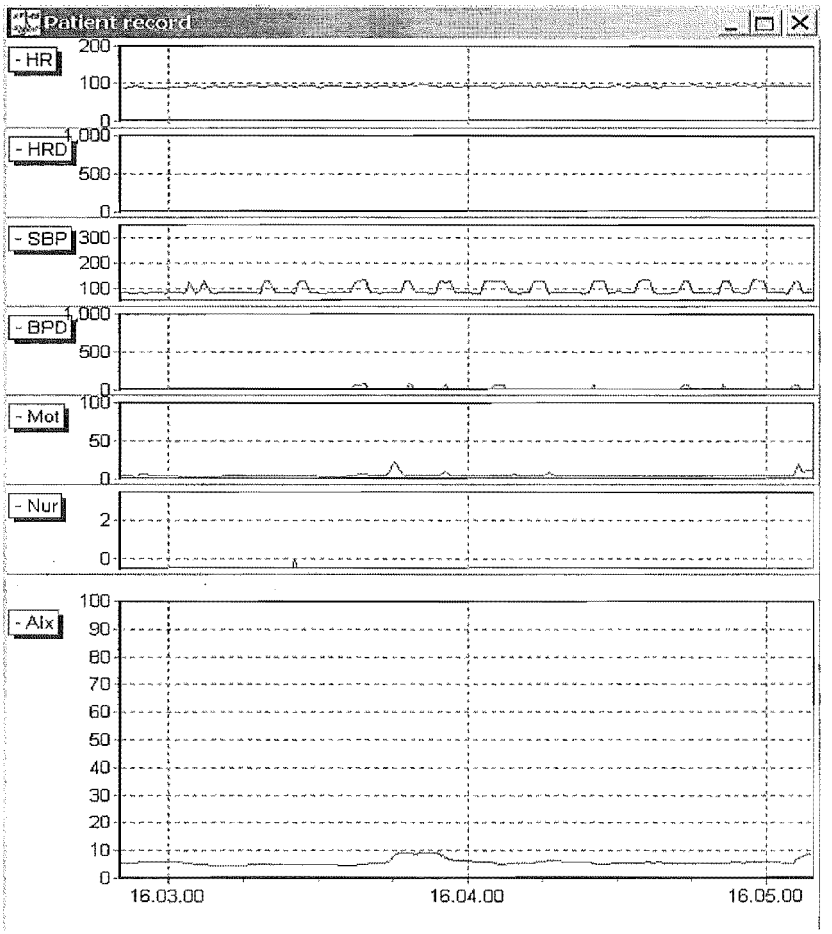

Figure 13.4 The agitation index remains low and free of artifacts during a calm period.

issues. A major issue is the occurrence of physiological artifacts. They occur when one of the physiological markers rises for a cause not related to agitation. For example, the infusion of adrenaline is common practice in the ICU to revive the patient. This therapy causes a sharp rise of heart rate and related HRD marker, while the patient remains calm and not agitated. This result is typically illustrated in Figure 13.5, where the agitation index reaches the maximum value of 100, whereas the patient remains calm and still, as reported by the nursing staff. This grading is due to the susceptibility of the physiological markers to symptoms other than agitation.

More specifically, excessive physiological markers, as seen in Figure 13.5, are

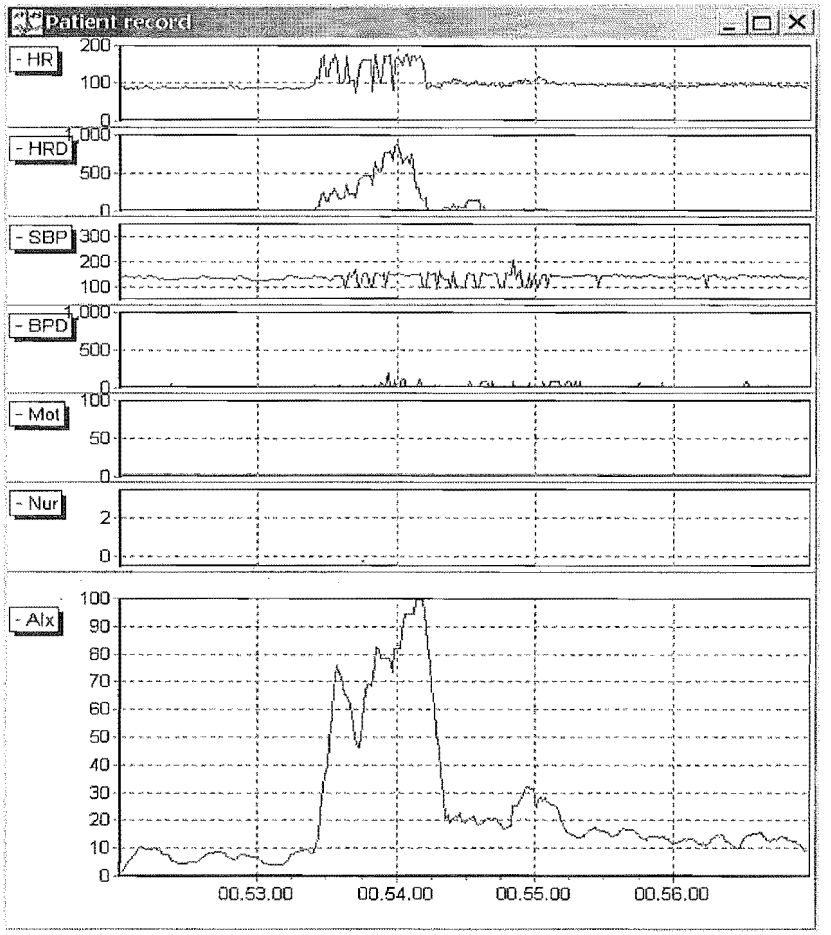

Figure 13.5 Physiological artifact produced by motion sensing of external interference overlapping the patient area.

not sufficient to define agitation, particularly if agitation is mainly defined by its treatment by sedative administration. In this case, sedatives would not treat the cause of this assessment by the sensor, i.e. HR rise. It would therefore not be considered as agitation.

The video FIS described in Chapter 8 is designed to filter technical artifacts due to the intrusion of people in the patient video frame. However, the system occasionally fails to differentiate staff interference motion and patient motion, leading to a technical artifact as illustrated in Figure 13.6. The motion sensing technique described in Chapter 6 is based on the initial knowledge of agitation at the start of this research. Both clinicians and engineers witnessed several

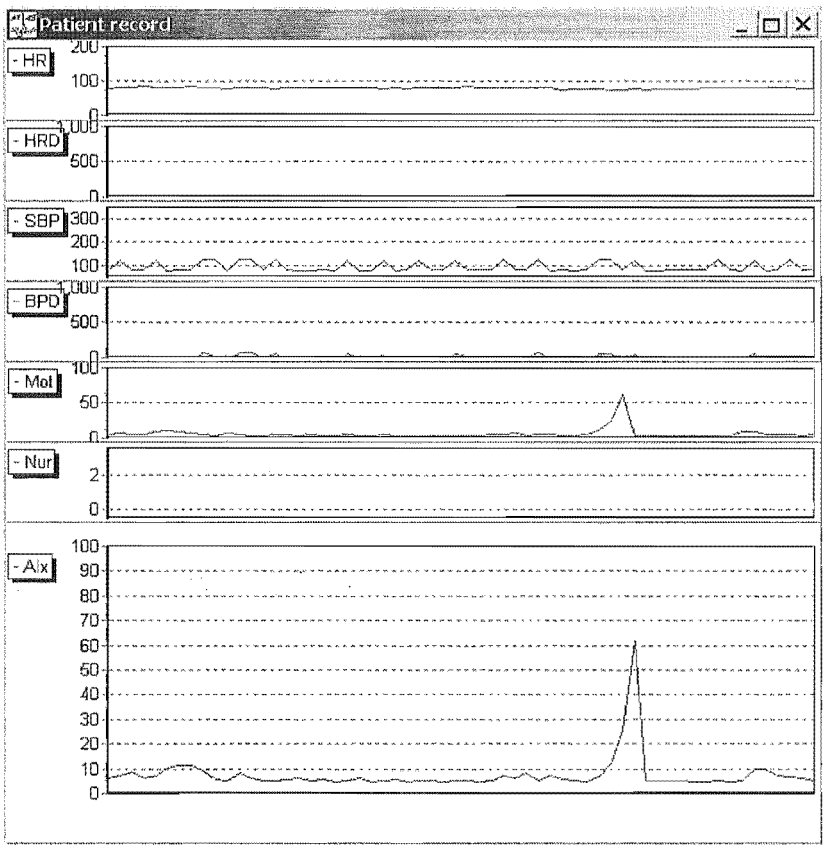

Figure 13.6 Technical artifact due to nursing staff intrusion in the patient ROI, propagated to the agitation index.

episodes of grade "3" agitation with very wide motion of the patient thrashing from side to side and eventually striking at the staff. This resulted in a perhaps simplistic motion analysis approach that the magnitude of body motion is roughly proportional to the level of agitation.

Because no specific motion or body part is differentiated at this stage, mild motions are simply recognised as mild agitation. Recent observation of patients during the ICU trials reveals mild motion of patients trying to grab the ETT or naso-gastric tube. This motion corresponds to a potentially dangerous level of agitation. The current implementation of the motion sensing technique quantifies mild motion as mild agitation, and specific motion differentiation is therefore crucial to improve this aspect of the agitation sensor. The result of this simplistic method of motion sensing is the quantification of a grade "3" episode of dangerous

agitation with a low agitation index , as illustrated in Figure 13.7

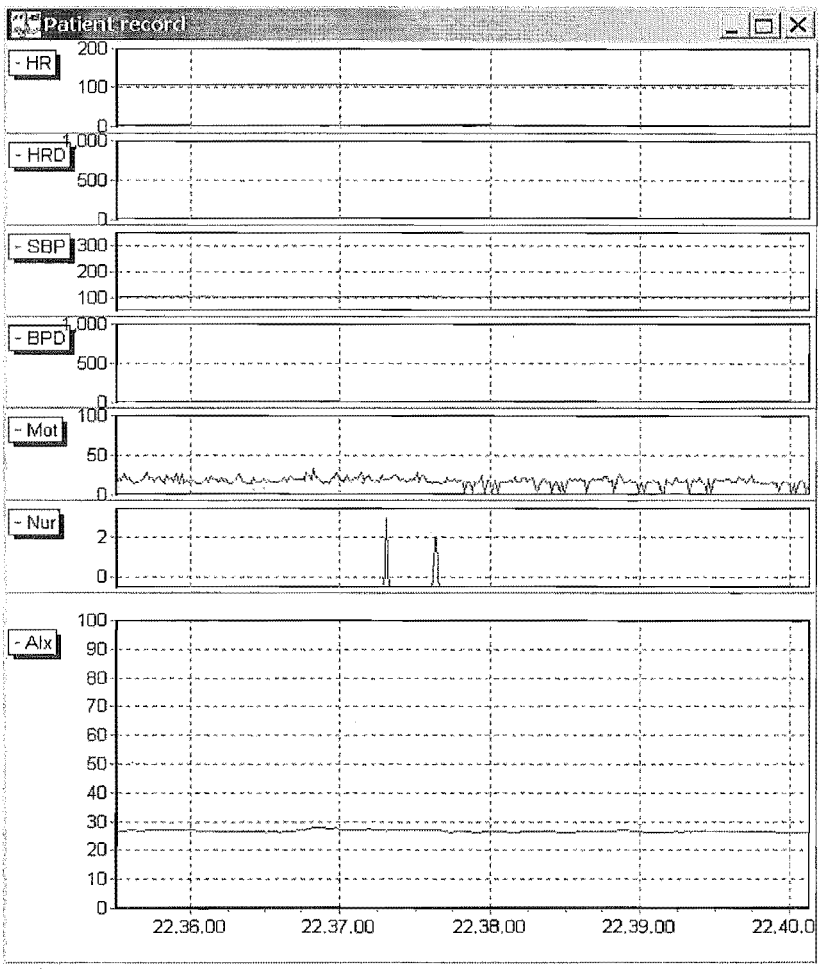

Figure 13.7 Episode of grade "3" agitation on SAS scale, underrated with a relatively small agitation index by the sensor.

13.4.2 Clips selection

The clips are selected from the real-time clinician feedback after the data gathering and initial analysis presented. Therefore, this approach allows the selection of data free of artifacts. However, the cause of most technical and physiological artifacts is known and the improvements required to filter them is under way. Therefore, this off-line analysis is used to focus on the calibration of the

artifact-free segments of data.

The series of clips is obtained from the real-time feedback of clinicians to locate relevant segments of data. The subjective assessment of the clinician in charge of the patient at the time of the study allows the economical detection of episodes of agitation within long calm periods, without the need to scan the entire 80 days of data. For example, the data related to the clip 20 is shown in Figure 13.8.

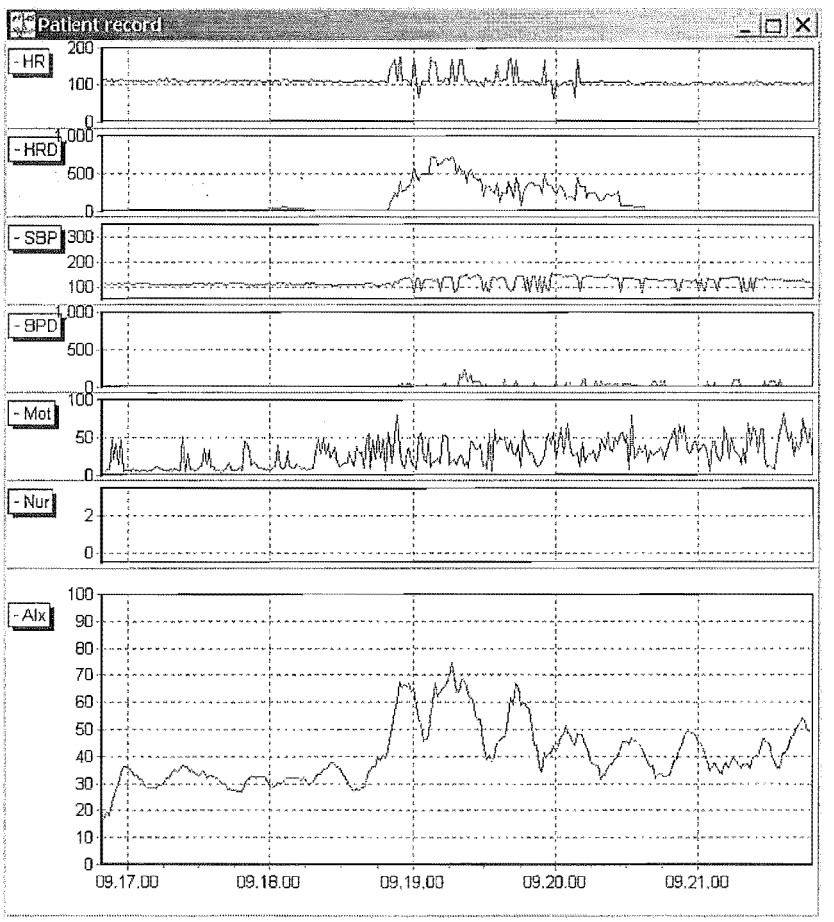

Figure 13.8 Data selected for clip 20. The HR and SBP series are shown off-line along with the video clip to five different clinicians to decrease the subjectivity of the SAS score.

The forty clips are previewed by a clinical ICU expert to check whether they approximately represent equally each of the four grades of agitation of the SAS scale. However, there is no way to a-priori know what the assessment of the forty

clips by the forty different clinicians is going to be during the trial. Therefore, there is no guarantee the selected segments of data equally represent each grade of agitation of the modified SAS.

The distribution of the agitation index for each grade of the modified SAS is obtained at the end of the trials using the features of the off-line assessment software, shown in Figure 13.9. The features include the comparison of the five assessments of the same clip by five clinicians to observe the inter-rater subjectivity of the modified SAS scale. It also allows the comparison of the five assessment of five clips by the same nurse to evaluate the intra-rater subjectivity on which little is currently known. Finally, it provides a platform to compare a single off-line assessment on the SAS scale with the objective agitation index. The software also computes the median agitation grade from the five different clinicians to produce the distribution of the agitation indices for each grade of the SAS.

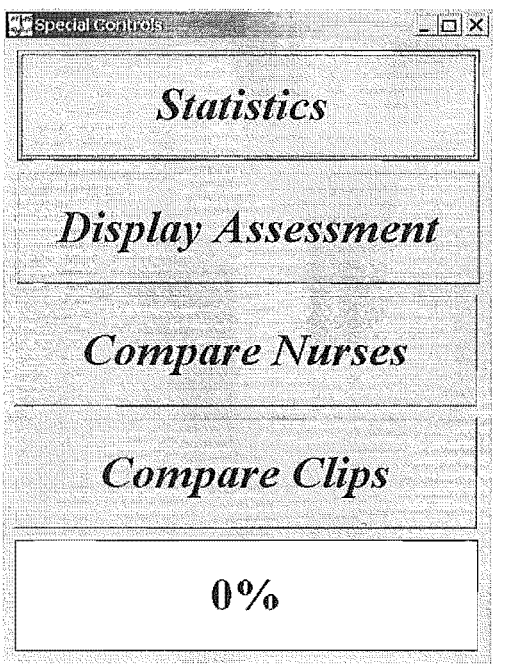

Figure 13.9 Additional features of the off-line assessment software to evaluate nurse inter-rater and intra-rater subjectivity, and to perform agitation sensor statistical analysis.

Chapter 14

Capstone trial statistical analysis

The comparison of the agitation sensor output with the median of the clinicians assessment on the SAS scale produces a distribution for each of the four SAS agitation grades. This statistical representation of the agitation sensor is used to verify the assumptions arising from the clinical observation and off-line trials of ICU patients presented in Chapter 13.

14.1 Methods

A SAS grade is matched with the agitation sensor objective index every second of each clip. This pair of values is used to create a distribution of agitation sensor outputs associated with each agitation grade of the SAS. The calibration of the agitation sensor is then assessed using the median value and the box plot of each SAS grade distribution.

14.1.1 Median

The median value of a distribution is calculated for each SAS grade after the agitation sensor output values are sorted in increasing order, and the frequency of each discrete value in the 0–100 range is determined, as illustrated in Table 14.1. The frequency, or number of appearance, of each value, in the second column in Table 14.1, is converted into the probability of appearance, after division by the total number of values in the distribution. This value is given in the third column. The probabilities are then summed to obtain the cumulative probability

in the fourth column. The median value is located when the sum reaches or exceeds 0.5. In the instance of Table 14.1, the cumulative probability reaches 0.5 after summing the probabilities up to, and including those for agitation index "29". Therefore, the median value is 29.

Table 14.1 An example of the distribution of the system output values that match a grade "2" agitation on the SAS according to several clinical experts. The overall distribution of this example contains 300 values

System agitation index	Frequency (#)	Probability	Cumulative Proba.
0	3	0.01	0.01
1	6	0.02	0.03
2	9	0.03	0.06
3	15	0.05	0.11
⋮	⋮	⋮	⋮
28	27	0.09	0.45
29	30	0.1	0.55
30	12	0.04	0.59
⋮	⋮	⋮	⋮
97	12	0.04	0.94
98	9	0.03	0.97
99	0	0	0.97
100	9	0.03	1

In this research, the median values of the distributions are expected to be in increasing order with the agitation score assessed on the SAS, which would indicate a correlation of increasing agitation sensor outputs with increasing SAS grades. The greater the difference between distribution medians, the greater the contrast between grades of agitation. This relationship is defined below:

$$median(Grade0) < median(Grade1) < median(Grade2) < median(Grade3)$$

14.1.2 Box plots

A box plot (or box-and-whisker plot) can be useful for handling many data values. They allow visual exploration of the data and its distribution in a concise fashion to draw informal conclusions when two or more variables are present. It

shows only certain statistics rather than all of the data. Five-number summary is another name for the visual representations of the box-and-whisker plot. The five-number summary consists of the median, the quartiles, and the smallest and greatest values in the distribution. Immediate visuals of a box-and-whisker plot are the center, the spread, and the overall range of a distribution.

The first step in constructing a box-and-whisker plot is to first find the median M, the lower quartile boundary Q1 and the upper quartile boundary Q3 of a given set of data. The set of data can be divided into the upper and lower sets by the median value M. Using the same technique, the median of the lower set is defined as Q1, and the median of the upper set is Q3. The series is divided in four quartiles: the first quartile ranges from the smallest point to Q1, the second quartile from Q1 to M, the third quartile from M to Q3 and the fourth quartile from Q3 to the greatest point.

At this stage, the interquartile range (IQR) is defined as the difference between the upper quartile and the lower quartile Q3 - Q1. The IQR is a very useful measurement, because it is less influenced by extreme values, and it limits the range to the middle 50% of the values. Empirically, the pertinent set of data ranges from the Q1-1.5IQR to Q3+1.5IQR, encompassing 75% of the data, and the points outside this range are considered outliers. A series represented by means of box-and-whiskers plots can isolate outliers that should not be considered for the series statistical analysis as they often corresponds to artifacts or under-ratings of the system under study.

Graphically, a rectangle "box" is drawn between Q1 and Q3, with a vertical delimiter set within the box at M. The "whiskers" are drawn from the first point greater than Q1 - 1.5×IQR to Q1 and from Q3 to the last point smaller than Q3 + 1.5×IQR, containing 75% of the total data. The remaining outliers are them marked with a "+" sign. These definitions are illustrated with a brief example using a random series of values defined below.

$$Y = [\ 2\ 4\ 7\ 8\ 8\ 8\ 8\ 9\ 9\ 9\ 9\ 9\ 10\ 10\ 10\ 10\ 10\ 10\ 10\ 11\ 11\ 11\ 11\ 13\ 14\ 17\ 18\ ]$$

The series contains 27 values sorted in increasing order, so the median of the

series is the 14^th value, M = 10. The series is now split into two halves of 13 samples, and the median values of the lower and upper halves Q1 and Q3 are respectively the 7^th and 21^st values, Q1 = 8 and Q3 = 11. At this stage the Inter Quartile Range that contain 50% of the data is defined, IQR = Q3 - Q1 = 3. The lower and upper boundaries LB and UB of the pertinent set of data is defined.

$$LB = Q1 - 1.5 \times IQR = 3.5$$

$$UB = Q3 + 1.5 \times IQR = 15.5$$

The box is drawn between Q1 and Q3 with a vertical delimiter set at M. The whiskers are then drawn from the values contained within the upper and lower boundaries. This graphical representation is illustrated in Figure 14.1

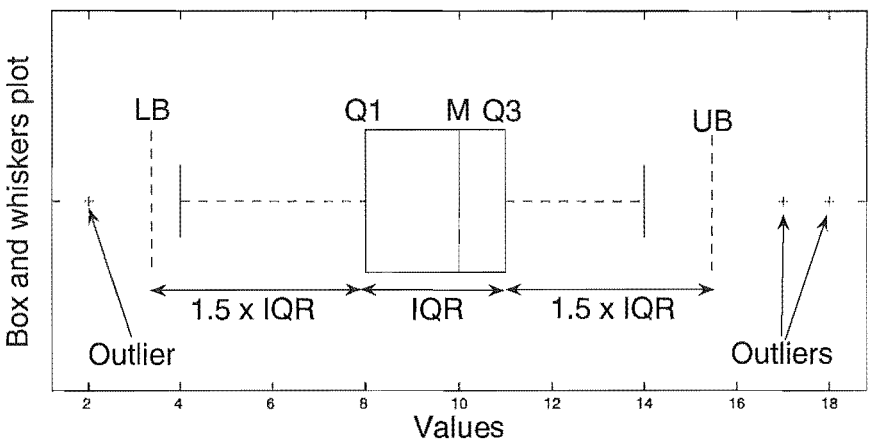

Figure 14.1 Illustration of the box-and-whiskers plot of a series.

14.2 Trial results

The statistical analysis is first performed on the original set of data. Then, the data points are weighted with a Bayesian method to emphasise the more reliable points in the distribution. The results of the analysis before and after the Bayesian weighting process are presented in this section.

14.2.1 Original data

The data consists of forty clips assessed five times each, while the system records the SAS grade assigned by the clinician every second. Each set of five assessments of the same clip is then used to produce the median assessment of each clip. This approach creates forty median assessments of 5 minutes updated every second and matched with the system agitation index, making 12000 pairs of data points. The distribution of the agitation sensor output is computed from this data for each grade of the SAS.

For a balance trial, each of the four agitation grades of the SAS should a-priori contain around 3000 points. Practically, the grade "0" distribution contains 6922 points, the grade "1" distribution contains 4325 points, the grade "2" distribution contains 753 points, and the grade "3" distribution does not contain any point after the median is determined.

This result is a sign of very large inter-rater subjectivity affecting the a-priori median and distribution. The clip data reviewed by a single expert originally equally represented each of the four grades of agitation on the SAS, but the median assessment of five clinicians yields this unequal distribution.

Meanwhile, the distribution of the agitation sensor output values for each of the four SAS grades of agitation can be converted into the probability of appearance. In spite of the dominance of the SAS grades "0" and "1", it remains pertinent to look at the unweighed probability of appearance of each of the four grades, as shown in Figure 14.2. The median agitation index of each grade is also evaluated and indicated by a dashed vertical line in Figure 14.2.

This set of median agitation indices rises in increasing order, 17 for grade "0", 28 for grade "1" and 37 for grade "2", which suggests a positive correlation between the SAS and the agitation sensor. However, the precision of the median values is impaired by the unbalanced representation of the four different grades. Hence, this set of median values cannot lead to any reliable conclusion on the agitation sensor. The probability plot indicates values above 65 and up to 100 that are classified as grades "0" "1" and "2", which further emphasises a problem of underrating some episodes of SAS grade "3" agitation with a lower grade.

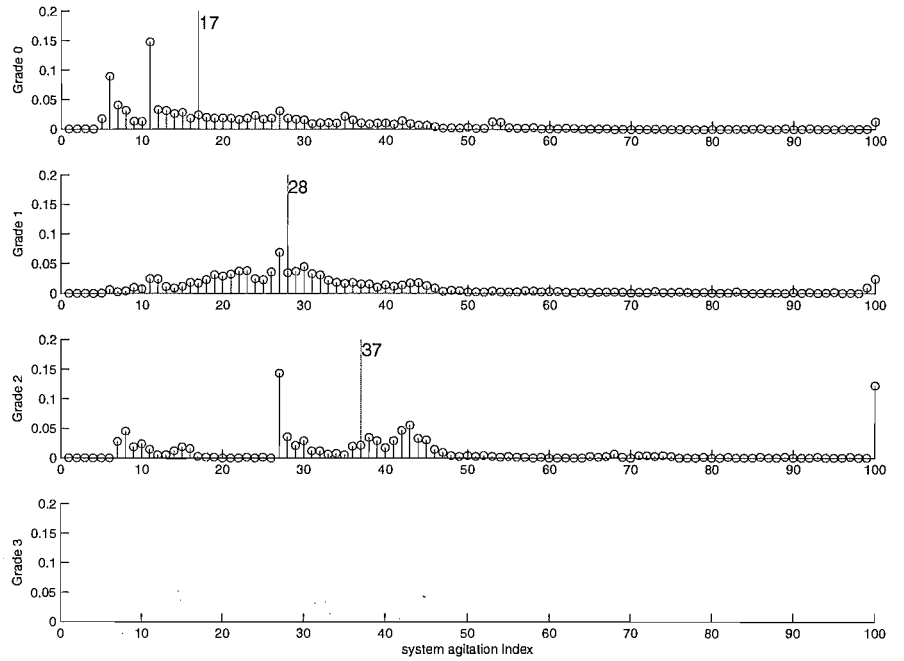

Figure 14.2 Probability of appearance of each 0–100 index for each SAS grade, with median value indicated by dashed line.

The box-and-whiskers plot in Figure 14.3 is produced to provide a summary of the distribution of each SAS grade. The first graphical observation of the plots shows a lack of contrast between the four grades of agitation of the SAS with a strong overlap of the boxes and inefficient use of the full 0–100 scale. The box plot of the SAS grade "0" significantly overlaps the box of the SAS grade "1" and diminishes the contrast of the agitation sensor. This result is due to episodes of mild agitation being underrated with a SAS grade "0".

There are two main reasons for such a misjudgment to occur. The video camera currently used does not provide a very detailed resolution of the facial features of the patient. For example, the grimacing and biting of ETT, that translates for many nurses discomfort and agitation cannot be clearly seen by the clinician during the off-line trial. As a result, a mildly agitated patient can be misjudged as a calm patient, when compared to the expected real-time assessment in this formal trial. This issue remains open for improvements in a future trial.

The biased judgement of some episodes of agitation is also due to the fact that the trial is carried out off-line. At the time of the assessment, the quality

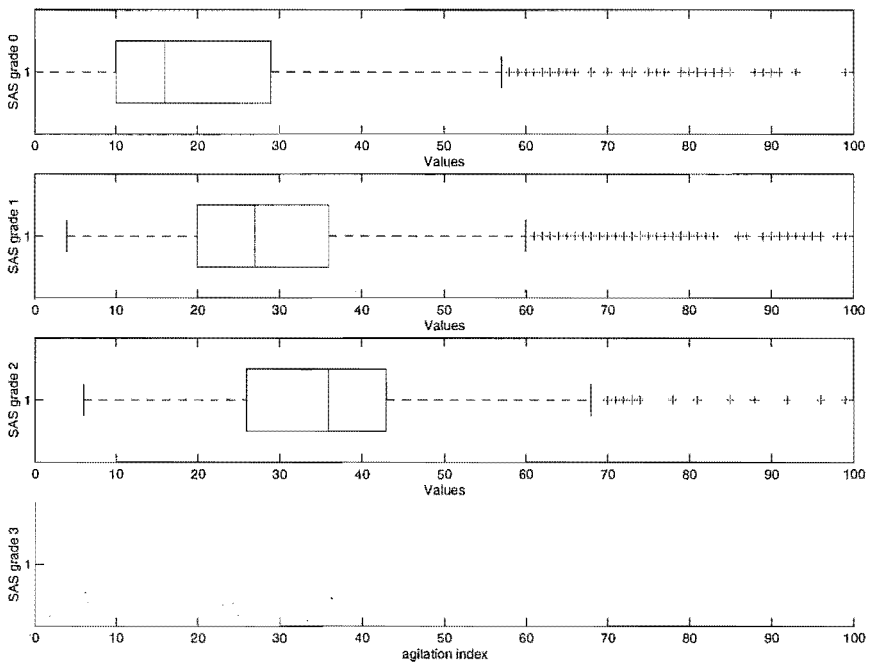

Figure 14.3 Box plots of each SAS grade, with median value lower and upper quartile defining the box and outliers shown by crosses. Both the boxes and whiskers strongly overlaps due to a lack of contrast. Overall, the correlation with the SAS scale is positive, but the contrast and use of the 0–100 range are poor.

of patient care does not depend on the accuracy of the nurse judgment anymore. The off-line aspect therefore relieves the time pressure associated with real-time agitation assessment, on which the comfort and safety of the patient depend. There is certainly evidence that working under time pressure results in different decision making processes than when not under time pressure [Gaba et al., 1994]. Moreover, many argue that high time pressure leads to poorer decision making [Mackenzie et al., 1994], which can explain the inter-rater variability of the assessment in real-time. The consequences of the time pressure is a spontaneous non-reflective assessment in real-time before an agitated patient, different from reflective thinking more likely to occur off-line. Therefore, the nurses are assumed to be using non-reflective modes of thinking in real-time situations, but may be more likely to use reflective modes in off-line set-up [Montgomery, 2001].

The box plot of the SAS grade "1" also overlaps with the box of the SAS grade "2". This result is due to the inter-rater subjectivity of the SAS scale used in the trial. The same magnitude of motion can be ignored by a first nurse, while it can be a sign of mild or moderate agitation for a second nurse. This subjective

aspect can explain the large variability and overlap between the SAS grades "0" and "1", as well as between grade "1" and "2". To the nursing staff's credit, the definition of the different SAS grades of agitation does not explicitly or implicitly facilitate the differentiation between grades, a flaw of these subjective indices as a whole.

The SAS grade "2" whiskers of the box plot covers most of the agitation index range, which is due to several reasons. The higher end of the whiskers translates the misjudgment of SAS grade "3" agitation, which would confirm the effect of reflective thinking in absence of real-time scenario time pressure, as well as the findings from the probability plot. The lower end of the box plot corresponds to the lower end of the agitation index range, and may emphasise a limitation of the agitation sensor. More particularly, the motion sensing underrates mild motion related to ETT grasping, which explains why a SAS grade "2" episode of agitation as defined by nursing staff is underrated by the sensor with a low agitation index. Finally, the absence of grade "3" agitation confirms the aspects of subjectivity and time pressure that limits this off-line trial methodology based on the median assessment of five nurses on the SAS scale.

14.2.2 Bayesian analysis

The subjectivity of the trials is investigated in more detail using a Bayesian method. Using a multinomial model for the nurses' assessments and a Dirichlet (distribution model) prior for the multinomial probabilities, the posterior distribution for these probabilities remains a Dirichlet, from which the probabilities can be estimated by the mean of the distribution [Bernardo and Smith, 1994]. Basically, this Bayesian method is used to estimate the probability that the median of the five assessments at a given time is a reliable reference of agitation to validate the system. Hence, each median can be weighted by its reliability to reduce the impact of inter-rater subjectivity.

Suppose the median value occurs k times in the five assessments (i.e. k can be 1,2,3,4 or 5). According to the Bayesian method, the probability that the median is a reliable reference agitation grade for this trial methodology is approximately $(k+1)/9$. In general, with 5 values, the probability that the median is the "true" agitation index is approximately between 2/9 and 6/9 (i.e. between 0.22 and

0.67). The probability of reliability is determined for every second of data, and reported for specific time values in Tables 14.2 and 14.3 located at the end of this chapter due to its size.

The average probability over the 12000 data points is equal to $p = 0.48$. This relatively low probability emphasises the high level of variability between assessors, which is also confirmed in several studies [Weinert et al., 2001]. More specifically, any probability below 0.5 indicates that the results are effectively random and therefore not representative of a systematic, consistent assessment. Hence at $p = 0.48$ the median of any given assessment is more random than systematic, as can be seen visually in Tables 14.2 and 14.3, for the five assessment at any given point in time.

Each point of data is weighted proportionally to the probability of the median to be reliable, i.e. $(k+1)$, so the more reliable points are emphasised in the final representation. The average probability of the weighted set of data is increased to 0.51 when the more reliable data points are emphasised, which is slightly better and over the 0.5 threshold. The probability of appearance after the weighting process is shown in Figure 14.4, which can be compared to Figure 14.2 with the unweighed distribution.

The box-and-whiskers plot is also computed for this weighted set of data as a means to consider the reliable data more importantly. There are slight improvements after the Bayesian weighting process. The median values are further apart, 16 for grade "0", 27 for grade "1" and 39 for grade "2", which gives a better contrast between the SAS grades. However, some problems persist, such as the inefficient use of the full 0–100 scale and the lack of SAS grade "3" episodes.

The Bayesian method could be used in a larger more intensive trial of the same form to provide a more reliable set of data and differentiate the issues of the SAS and the issues of the agitation sensor. Note that it would not provide a solution to the impact of off-line versus real-time assessment, particularly for SAS grade "3" agitation misclassification. More research is required to design a robust set of trials to get the best analysis.

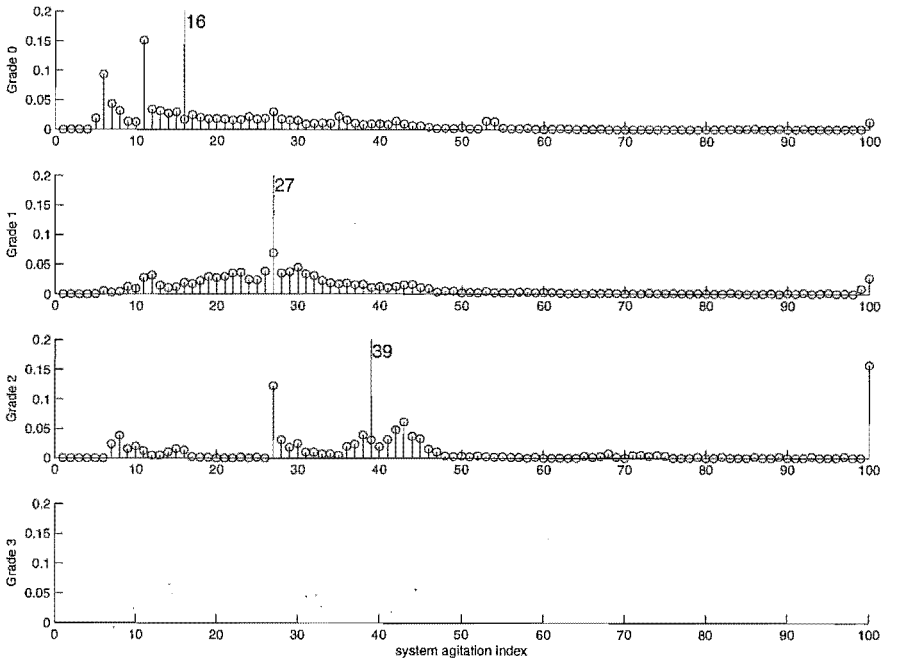

Figure 14.4 Probability of appearance of each 0–100 index for each SAS grade, with median value indicated by dashed line.

14.3 Overall discussion

The trials implemented in this research are at least partly limited by their methodology which limits making decisive final conclusions about the agitation sensor developed. Hence, the agitation sensor, promising during observation in real-time, cannot be completely validated with these clinical trials as a reference. However, these trials were a very good means to evaluate consistently the extent of SAS subjectivity. The different aspects revealed during the data gathering and off-line assessment are discussed to conclude on the present state of the agitation sensor and to develop guidelines for the future work.

The clinical trials were originally organised to compare the response of the agitation sensor with the median assessment of five clinicians. The independent assessment of five different clinicians for the same patient at the same time requires the trial to be carried out off-line. The correlation between the real-time assessment of clinicians and the agitation sensor is consistent over several episodes of different grades of agitation, such as the illustrations in Figures 13.2 – 13.4, and discussed in Chapter 13.

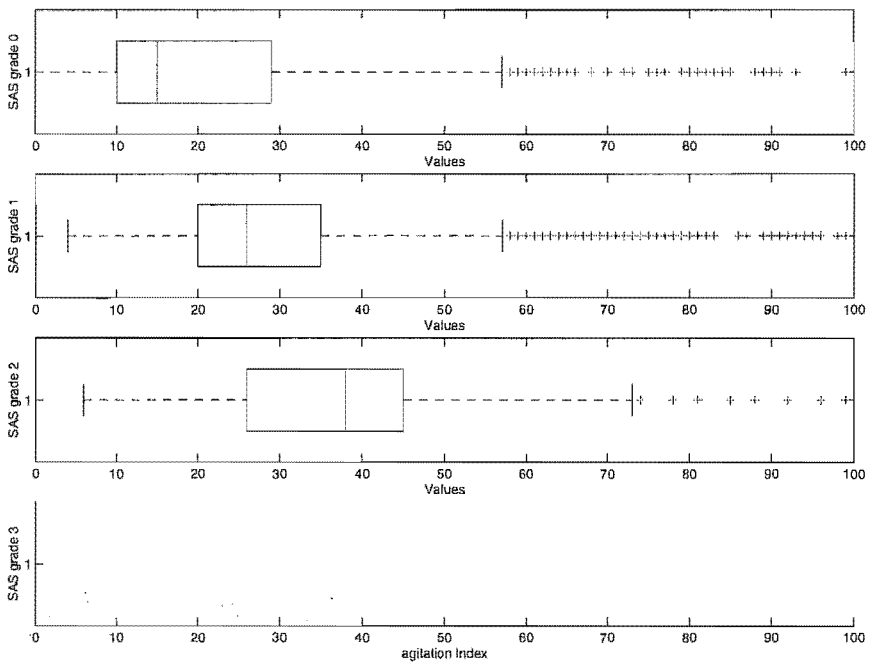

Figure 14.5 Box plots of each SAS grade, with median value lower and upper quartile defining the box and outliers shown by crosses.

Therefore, the potential for correlation between the agitation sensor and the off-line assessment is very promising. The agitation sensor is at the early stage of its development, and the areas that need improvements, such as motion sensing focused around the face and ETT, are clearly identified. However, the limitations of the agitation sensor only explain a smaller part of the differences between the statistical results and the a-priori expectations.

The inter-rater and intra-rater subjectivity of the SAS scale remains an important issue of this trial, which needs to be more accurately assessed to determine the optimal conditions of a significant trial. These trials did not permit full validation of the current correlation of the agitation sensor, but it has been very useful to clearly detect the practical limitations to overcome. This off-line assessment emphasises the very large overall variability of the SAS agitation scale, despite very good κ inter-rater agreement found by Riker et al. [Riker et al., 1999] in structured trials with specifically trained staff.

Although the clinicians are given clear instructions on how to assess the clips and are very experienced with this scale, there remain differences between

individual methods of assessment. During the clips off-line assessment, the same segment of data is assessed with different SAS agitation grades, all the way from "0" to "3" in the illustration of clip 10 in Figure 14.6. A small variability of one SAS grade between the five clinicians is generally not critical and the subsequent median assessment is reliable, but a large variability of several grades among clinicians, as seen in Figure 14.6, significantly reduces the reliability of the trial methodology.

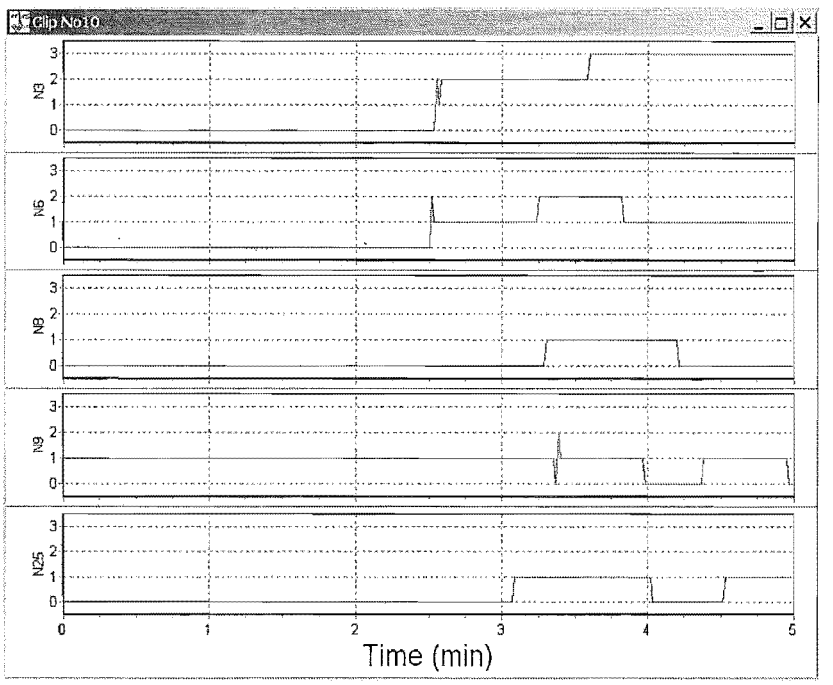

Figure 14.6 The off-line assessment of clip 10 reveals extreme inter-rater variability at minute 4 when the five assessment of agitation on the SAS are respectively (3,1,1,0,1), covering all the possible range of agitation grades.

Moreover, the frequency at which the agitation index is updated by the clinicians adds to the subjectivity of the SAS scale. More specifically, there is no recommendation on how often the clinicians should update the SAS agitation grade. Consequently, different clinicians update their agitation assessments at different times. This different use of the SAS scale depends primarily on the experience of the clinicians. For example, a clinician has witnessed a patient calming down for one minute between two episodes of agitation in the past. After this experience, the clinician may not update the agitation score for several minutes, to ensure that the patient is definitely back to a calm state. A second

clinician with a different experience may consider a patient calm 15 seconds after an episode of agitation. These variations are illustrated in Figure 14.7.

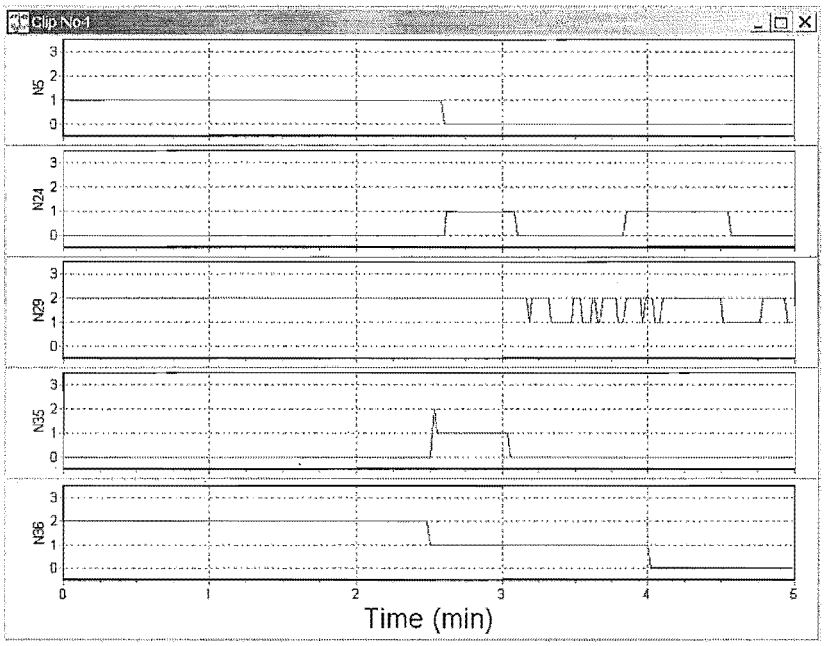

Figure 14.7 The off-line assessment of clip 4 showing variations in the frequency at which the grade is updated by the nurses. note the difference from minute 3 to 4 during which Nurse 29 illustrated in the third frame update the agitation grade 12 times, while Nurse 7 illustrated in the first frame does not change the agitation grade

To add extra subjectivity, and in spite of the instructions given to the clinicians during this trial, they variably give either the maximum or the average agitation index over the period of time considered. Note that the maximum agitation grade was requested and is desired in this trial. The different experiences of the clinicians strongly affects their assessment of agitation. This agitation update period varies from a few seconds to a few minutes. It results in a first clinician giving a single agitation score, either maximum or average grade, over the whole five minutes of the clip, while a second clinician will update the agitation score every 5 seconds. This different assessment approach adds extra subjectivity and further impairs the final statistical representation.

Consequently, the median assessment originally obtained from the five clinicians is reliable with an average probability of 0.48. Hence, the median of five assessments is not very reliable to validate an objective index. The weighting

method of the data using the Bayesian theory improves reliability, but it needs more data to significantly enhance the distribution, and cannot provide the reference required over the different SAS grades at this stage. The issue of the large inter-rater subjectivity has to be dealt with using more data from more assessors. The concurrent assessment of the same clips by seven nurses might consistently increase the reliability of the reference agitation grade based on the median assessment. Realistically, a larger number of 10–30 nurses per clip could deliver results, but may be impractical, especially in a smaller ICU such as Christchurch.

The method used to obtain the statistical representation is also arguable. A major problem is to match the preemptive response of the agitation sensor with the correct SAS grade. In the example in Figure 13.2, the agitation sensor responds to the physiological markers by raising the agitation index nearly three minutes before it is reported by the clinician in charge of the patient. If the clinician updates the SAS agitation score on the SAS too often, this preemptive rise of the agitation index is matched with a grade "0" on the SAS scale, because agitation is not yet likely to be detected by the clinician at this time. This result impairs the final statistical representation. Hence, the clinicians were asked to first observe the patient video clip and corresponding HR and SBP values for 50% of the clip duration, which corresponds to 2.5 minutes, so the pre-emptive response of the agitation sensor would be correctly matched, for example a grade "3" on the SAS in Figure 13.2.

This approach presents the drawback of matching the same SAS grade to the first half of the clip, which is not optimal in the event of short periods of agitation, such as the illustration in Figure 14.9. However, if the SAS agitation grade is updated too often, it will emphasise the long calm periods between episodes of agitation, and the final statistical representation of the grade "0" will contain even more points, further accentuating the trial imbalance.

Finally, in spite of the limitations of the off-line trials, the agitation sensor was also tested in real-time during data gathering, and several features of the agitation sensor were improved as a result. In fact, the correlation with recorded nursing assessment was very good in this period as discussed in Chapter 13.

However, the rigorous statistical validation has not been achieved and a new trial has to be designed with the right methodology to provide a reference on

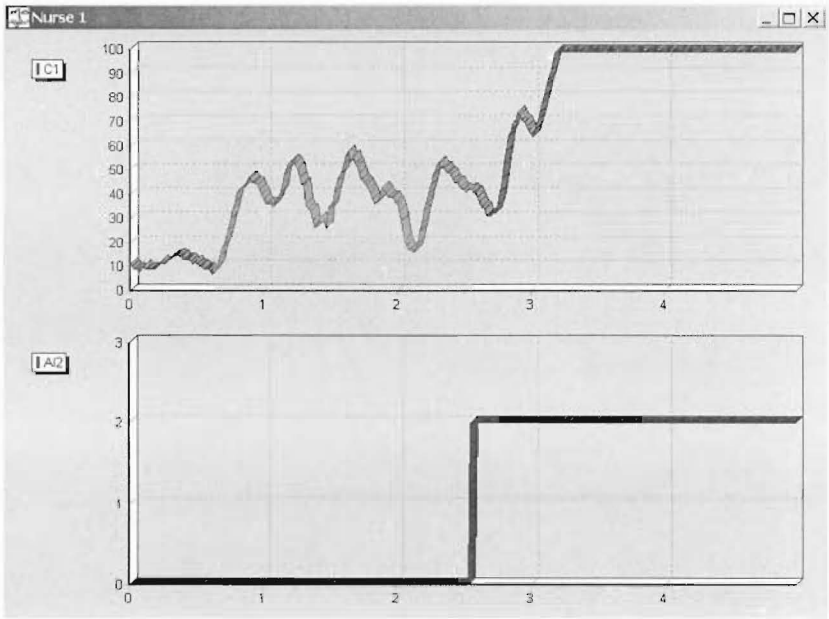

Figure 14.8 The assessment of Clip No 1 by Nurse No 1 illustrates a preemptive response of the agitation sensor mismatched with a grade "0" during the period shaded. This is a limitation of the trial ,methodology, because this is the expected behaviour of the sensor and should be a positive outcome instead of a mismatch.

which the agitation sensor can be compared and appropriately calibrated.

14.4 Methodology of potential future clinical trials

The implementations of the different sets of off-line and real-time trials during these research have permitted to focus on different aspects of the research. Particularly, the agitation sensor has been shifted from a Matlab off-line workspace to a real-time clinical environment. However, the trials have also emphasised the subjectivity of the SAS scale that needs attention for the overall research to succeed.

The global subjectivity of the SAS needs to be further studied to define a more significant and useful set of trials. The capstone trial in its current form is not appropriate because it does not sufficiently reproduce the real-time conditions in which the clinicians assess agitation. This difference includes the lack of video

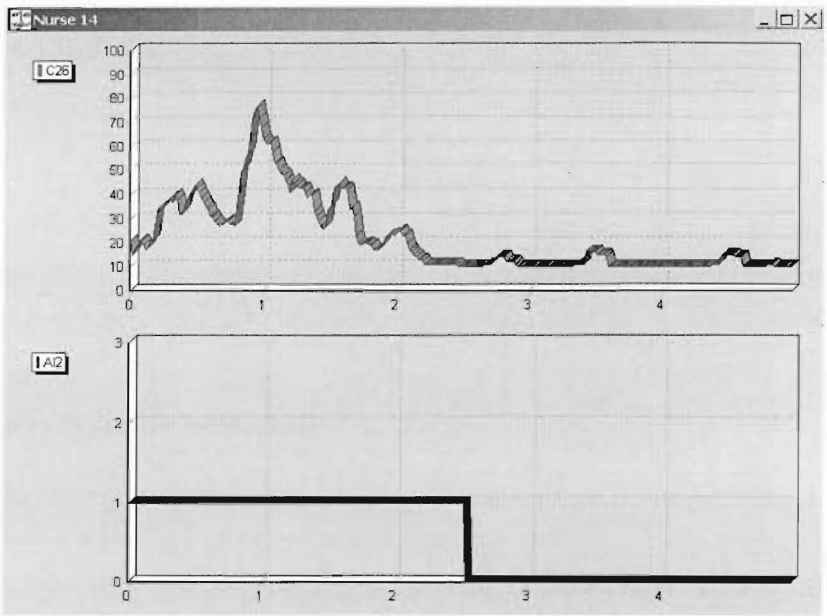

Figure 14.9 The assessment of Clip 26 by Nurse No 14 illustrates a short episode of agitation matched with the average agitation grade over the first half of the clip

resolution and the relief from the time pressure, which can consequently lead the nurses to underrate some episodes of agitation. If the clinical trial is performed in real-time, several clinicians are expected to assess the agitation simultaneously and independently, which is hard to obtain in real-time, because clinicians would not be available.

Alternatively, if a future trial is carried out off-line, it should try to better reproduce the conditions of real-time assessment to reduce the effect of the time pressure relief. The improvements of the off-line methodology include knowledge of the patient clinical background and a more detailed video record of the facial area to focus for instance on the grimacing, biting, and coughing that are symptoms related to agitation currently hard to observe with the video configuration. This approach involves the upgrade to a more accurate video camera, as well as the update of the high-level processing that is required to reach the desired image-processing capabilities. Each clip should also be assessed by more nurses to increase the quality and average probability of the set of data weighted with the Bayesian method. Moreover, the acquisition and selection of more clips is required to increase the effectiveness of the Bayesian weighting process.

The presentation of this research to the scientific community has sparked the interest of many other research groups, whose collaboration could considerably accelerate the pace of this research by using several agitation sensors to record agitation clips from the ICU of other hospitals.

Table 14.2 Bayesian probability of the median assessment reported for four different times of the first set of 20 clips. The series contain the five nurses' assessments, the median, and the probability that this median is reliable as a reference value

Clip No	2min30s	3min20s	4min10s	5min
1	(0,0,0,1,0) M=0, p=0.56	(2,2,1,2,2) M=2, p=0.56	(2,1,1,2,2) M=2, p=0.44	(2,0,1,2,1) M=1, p=0.33
2	(1,3,0,2,0) M=1, p=0.22	(2,3,1,2,2) M=2, p=0.44	(2,3,1,2,2) M=2, p=0.44	(2,3,1,2,2) M=2, p=0.44
3	(0,1,0,1,0) M=0, p=0.44	(1,1,1,1,1) M=1, p=0.67	(1,2,1,1,1) M=1, p=0.56	(1,2,1,1,1) M=1, p=0.56
4	(1,0,2,0,2) M=1, p=0.22	(0,0,1,0,1) M=0, p=0.44	(0,1,2,0,0) M=0, p=0.44	(0,0,1,0,0) M=0, p=0.56
5	(1,0,1,1,1) M=1, p=0.56	(1,0,1,1,1) M=1, p=0.56	(1,0,0,1,0) M=0, p=0.44	(1,0,1,1,0) M=1, p=0.44
6	(1,1,0,1,0) M=1, p=0.44	(1,1,1,0,1) M=1, p=0.56	(1,1,1,0,1) M=1, p=0.56	(0,1,1,1,1) M=1, p=0.56
7	(0,0,0,0,1) M=0, p=0.56	(0,0,0,0,0) M=0, p=0.67	(0,0,1,1,0) M=0, p=0.44	(0,0,0,0,0) M=0, p=0.67
8	(0,0,0,0,0) M=0, p=0.67	(1,1,0,1,1) M=1, p=0.56	(1,1,0,1,1) M=1, p=0.56	(3,1,0,1,1) M=1, p=0.44
9	(2,1,0,0,0) M=0, p=0.44	(3,1,1,2,2) M=2, p=0.33	(1,2,1,2,1) M=1, p=0.44	(1,2,1,1,1) M=1, p=0.56
10	(0,0,0,1,0) M=0, p=0.56	(2,2,1,1,1) M=1, p=0.44	(0,1,0,1,0) M=0, p=0.44	(0,1,0,0,1) M=0, p=0.44
11	(0,0,1,0,0) M=0, p=0.56	(0,0,1,0,1) M=0, p=0.44	(0,0,0,0,0) M=0, p=0.67	(0,0,0,0,0) M=0, p=0.67
12	(0,0,0,0,1) M=0, p=0.56	(0,0,0,0,0) M=0, p=0.67	(0,0,0,0,0) M=0, p=0.67	(0,0,0,0,0) M=0, p=0.67
13	(1,0,0,2,0) M=0, p=0.44	(0,0,2,1,0) M=0, p=0.44	(1,0,1,2,0) M=1, p=0.33	(1,0,1,1,0) M=1, p=0.44
14	(0,3,1,1,1) M=1, p=0.44	(0,2,1,1,0) M=1, p=0.33	(0,2,1,0,1) M=1, p=0.33	(1,2,2,1,1) M=1, p=0.44
15	(0,1,0,0,3) M=0, p=0.44	(0,1,1,0,1) M=1, p=0.44	(0,1,1,0,1) M=1, p=0.44	(0,0,0,0,0) M=0, p=0.67
16	(0,0,0,0,1) M=0, p=0.56	(0,1,2,2,1) M=1, p=0.33	(0,1,1,1,1) M=1, p=0.56	(0,2,1,1,1) M=1, p=0.44
17	(0,0,0,0,1) M=0, p=0.56	(0,0,0,0,0) M=0, p=0.67	(0,0,0,1,0) M=0, p=0.56	(0,0,0,1,0) M=0, p=0.56
18	(0,0,0,0,1) M=0, p=0.56	(0,1,3,1,0) M=1, p=0.33	(0,1,2,1,1) M=1, p=0.44	(0,1,2,1,1) M=1, p=0.44
19	(0,1,1,1,0) M=1, p=0.44	(2,1,1,1,1) M=1, p=0.56	(0,0,0,0,0) M=0, p=0.67	(1,0,0,0,0) M=0, p=0.56
20	(1,0,2,2,1) M=1, p=0.33	(1,1,1,2,1) M=1, p=0.56	(0,1,1,1,0) M=1, p=0.44	(0,1,1,1,0) M=1, p=0.44

Table 14.3 Bayesian probability of the median assessment reported for four different times of the second set of 20 clips. The series contain the five nurses' assessments, the median, and the probability that this median is reliable as a reference value

Clip No	2min30s	3min20s	4min10s	5min
21	(0,0,0,0,0) M=0, p=0.67	(0,0,0,0,0) M=0, p=0.67	(0,0,0,1,0) M=0, p=0.56	(0,0,0,1,0) M=0, p=0.56
22	(0,0,0,0,0) M=0, p=0.67	(1,1,1,1,0) M=1, p=0.56	(2,1,1,1,0) M=1, p=0.44	(3,0,1,1,0) M=1, p=0.33
23	(0,0,1,0,0) M=0, p=0.56	(0,0,0,0,0) M=0, p=0.67	(1,0,0,1,3) M=1, p=0.33	(1,0,0,1,0) M=0, p=0.44
24	(0,0,0,1,1) M=0, p=0.44	(1,0,0,2,2) M=1, p=0.22	(0,0,0,0,1) M=0, p=0.56	(0,0,0,1,1) M=0, p=0.44
25	(0,0,0,1,0) M=0, p=0.56	(1,0,1,0,0) M=0, p=0.44	(0,0,0,0,0) M=0, p=0.67	(1,0,0,0,0) M=0, p=0.56
26	(0,0,0,1,0) M=0, p=0.56	(0,1,0,0,0) M=0, p=0.56	(0,1,0,0,1) M=0, p=0.44	(0,1,0,0,1) M=0, p=0.44
27	(0,1,1,0,0) M=0, p=0.44	(0,0,0,0,0) M=0, p=0.67	(0,0,0,0,0) M=0, p=0.67	(0,1,0,0,1) M=0, p=0.44
28	(0,0,1,0,0) M=0, p=0.56	(0,1,0,0,0) M=0, p=0.56	(0,0,0,0,0) M=0, p=0.67	(0,0,0,0,0) M=0, p=0.67
29	(0,1,0,0,0) M=0, p=0.56	(0,0,0,0,0) M=0, p=0.67	(0,0,0,0,0) M=0, p=0.67	(0,0,0,0,1) M=0, p=0.56
30	(0,1,0,2,1) M=1, p=0.33	(0,0,0,0,0) M=0, p=0.67	(0,0,0,0,0) M=0, p=0.67	(0,0,0,0,0) M=0, p=0.67
31	(3,0,2,2,0) M=2, p=0.33	(0,0,0,0,0) M=0, p=0.67	(1,0,0,0,0) M=0, p=0.56	(1,2,0,0,0) M=0, p=0.44
32	(0,0,1,0,1) M=0, p=0.44	(0,1,0,0,0) M=0, p=0.56	(1,2,0,0,0) M=0, p=0.44	(1,2,0,0,1) M=1, p=0.33
33	(0,0,0,1,0) M=0, p=0.56	(0,0,0,0,0) M=0, p=0.67	(0,0,0,0,0) M=0, p=0.67	(0,0,0,0,0) M=0, p=0.67
34	(0,0,0,0,1) M=0, p=0.56	(1,2,0,2,1) M=1, p=0.33	(1,2,2,2,1) M=2, p=0.44	(1,2,2,2,1) M=2, p=0.44
35	(1,0,1,0,1) M=1, p=0.44	(0,1,0,0,2) M=0, p=0.44	(0,1,0,1,1) M=1, p=0.44	(0,1,0,0,1) M=0, p=0.44
36	(3,0,2,1,1) M=1, p=0.33	(1,1,2,1,0) M=1, p=0.44	(1,2,2,1,0) M=1, p=0.33	(1,2,3,1,1) M=1, p=0.44
37	(1,0,1,0,1) M=1, p=0.44	(0,1,1,0,1) M=1, p=0.44	(0,0,1,1,1) M=1, p=0.44	(0,1,1,1,1) M=1, p=0.56
38	(0,1,0,1,2) M=1, p=0.33	(1,1,0,1,2) M=1, p=0.44	(1,0,0,0,1) M=0, p=0.44	(1,0,0,0,1) M=0, p=0.44
39	(1,0,2,2,3) M=2, p=0.33	(2,0,1,3,3) M=2, p=0.22	(1,0,1,2,1) M=1, p=0.44	(1,0,2,1,2) M=1, p=0.33
40	(0,0,0,1,2) M=0, p=0.44	(2,1,1,1,2) M=1, p=0.44	(2,1,1,1,1) M=1, p=0.56	(1,1,1,1,2) M=1, p=0.56

Part IV

Conclusions and future work

Chapter 15

Conclusions

The study of patients during periods of agitation has revealed specific patterns based on the combination of physiological markers. This research is based on the processing of selected physiological and video signals, as well as observation of other interesting signals to be potentially included in the future. Although considerable work remains to ultimately achieve a clinically reliable agitation sensor, this research has solved many issues and provided some insight for future work. This chapter concludes on the validity of the signal-processing techniques implemented in the real-time agitation sensor. The physiological knowledge of agitation acquired from observation of ICU patients during the clinical trials is also discussed. Finally, the overall structure of the agitation sensor is validated.

15.1 Current markers of agitation

Real-time capable signal-processing techniques have been investigated, taking into account a variety of symptoms observed on ICU patients. This allows the differentiation of several methods available to process the ABP, ECG and video signals, which are the initial signals investigated of this research.

15.1.1 Physiological markers

This thesis provides a review and investigation of the different HRV and BPV methods, and it also introduces the HRD and BPD methods, as well as the temporal HRV and BPV methods to complement the spectral methods in the specific

context of this research. The derivative and temporal variability methods offer a simpler approach to model the ECG and ABP dynamics when too many parameters affect the ICU patients to permit fully-automated real-time implementation of spectral HRV and BPV.

Clinical trials have confirmed that temporal HRV and BPV, as well as HRD and BPD methods offer a better potential to track agitation, whereas spectral HRV and BPV may not be the most suitable method for this research. Spectral methods are unstable and not suitable in the context of continuous real-time monitoring of a broad population such as ICU patients. As a matter of fact, long-term fully automated real-time implementations of spectral HRV method on a broad population of ICU patients are unknown to the author.

However, the current signal-processing algorithms produce many physiological artifacts that impair the quality of the agitation sensor and need to be better filtered by both low-level and high-level processing. The combination of HRD and temporal HRV improves the filtering of artifact by the high level algorithms [Agogué et al., 2005], but there is a strong need for more agitation specific markers to further limit the occurrence of these physiological artifacts. Throughout this research, patients are observed during their stay in the ICU. For instance, patients are often found to react to anxiety by breathing faster. This is detectable by processing of the airway pressure and air flow signals, readily available from the ventilator.

Precisely, both the level of consciousness and potential for agitation rise when the patients breathing rate becomes faster than the default setting of the ventilator, which means patients takes over the ventilator to breathe spontaneously. These signals were originally left aside because they only provide meaningful information during a very limited period of time. Finally, the potential offered by the breathing rate, tidal volume and other markers derived from respiration for early detection of agitation means they should be the next addition to the set of physiological markers.

15.1.2 Motion index

The motion sensing is very useful to complement the physiologically based detection of agitation. Motion is a very important parameter for clinicians to assess agitation, so the motion sensing feature should be kept in the agitation sensor. The first instance implemented in this research successfully detects agitation during clinical trials, but it produces many artifacts and occasionally misjudges some episodes of agitation.

Technical artifacts are produced when a clinician or relative enters the patient ROI of the video frame, even though the video FIS is designed to limit their occurrence. Physiological artifacts are produced when mild limb motion of calm patients is misinterpreted for agitation. Both artifacts need to be filtered to increase the quality of the resulting agitation index. The accuracy of the motion sensing needs to be improved so that mild motion related to ETT biting and pulling can be differentiated from limb motion and produce an appropriate high grade of agitation, instead of being confused with mild limb motion and assigned with a low grade of agitation.

15.2 Structure of agitation sensor

The structure of the agitation sensor is composed of two distinct levels: the low-level signal-processing and the high-level clinical heuristics. Other bioengineering applications are successfully based on this structure, such as the tuberculosis and lung disease detection [Phuong and Kreinovich, 2001], or the neonatal resuscitation prediction expert system [Reis et al., 2004]. This structure provides a great platform to update the signal-processing techniques independently from the fuzzy set of rules that model clinical knowledge of agitation.

The FIS is a simple implementation of the artificial intelligence theory and it does not provide a self-learning feature. However, clinicians appreciate the transparency of the set of rules that corresponds exactly to their advice and knowledge, unlike more advanced neural networks that appear like "black boxes" from the clinicians' point of view. This aspect is a positive outcome of this research and future implementation of the agitation sensor, as well as other bioengineering

application, may be based on the same design.

This research has developed a novel approach to quantify agitation of ICU patients. The concept of physiologically based fuzzy quantification and the structure used for this task are a positive achievement, but there are important issues to deal with for the ultimate development of a clinically reliable agitation sensor. The recommendations and guidelines to achieve this ultimate goal are given in the next chapter. Most attention is focused so far to develop the real-time agitation sensing platform, and it is also crucial to focus on the development the trial methodology that can be used as a reliable reference.

Chapter 16

Future work

The practical implementations of signal and video-processing techniques on ICU patients presented in this thesis have proved successful in some aspects, but failed to achieve consistent results in numerous aspects. However, through success and failure, knowledge and understanding of patient agitation in critical care has grown considerably. This results provide guidelines for future research that will contribute to the design of a reliable agitation sensor.

Significant improvements are required to diminish the occurrence of low-level technical and high-level physiological artifacts, and to ensure accurate judgment of agitation during most of the time. The growing knowledge of agitation will also allow the upgrade of the higher level heuristics, on which the core of the system is based.

16.1 Physiological input signals and technical artifacts

Physiological signal pre-processing is crucial to enable real-time continuous monitoring in ICU conditions. When patients become agitated, they create fluctuations in the data recorded from the electrodes and arterial lines. This pre-processing step is the foundation of the system. If it introduces too many technical artifacts, such as baseline jump or premature heart beats in the case of ECG, the agitation index is significantly biased and clinically ineffective. Hence, the low-level processing must be performed by very reliable algorithms. Some of the signal-processing methods implemented continuously in real-time in this research have proved to be very reliable, while other techniques only offer a first approach

with large room for improvement.

16.1.1 Recommendations for ECG processing

Several methods described in Section 2.2 have been investigated throughout this research. The wavelet approach offers the most reliable detection of R peaks within the QRS complex of the ECG period. However, this approach also has limitations. The ECG is currently processed by a single wavelet, acting like a band-pass filter. The frequency content of the wavelet utilised is fixed by its scale. However, the frequency content of the R wave and the QRS complex is changing with the heart rate. If the heart beats faster (slower), then the ECG periods are shorter (longer) and the frequency content of the R wave is higher (lower). Whereas the wavelet scale chosen for the R peaks detection suits most heart rate, it offers a smaller signal-to-noise ratio at lower heart rate, and other waves of the ECG period produce technical artifacts.

Therefore, several solutions exist to strengthen the R peak detection algorithm. First, if lower frequencies are not detected by the scale chosen in the first attempt, a larger scale wavelet containing a lower frequency band can be utilised However, the same problem may occur, but at higher frequencies. Alternatively, the combination of several scales can be implemented [Bahoura et al., 1997], and the larger wavelet coefficient selected for higher level processing. The band-pass filtering performed by two wavelets of consecutive scales should be enough to cover the wide range of HR seen in critical care and the corresponding spectrum of the R peaks.

The ECG can also be computed with a different wavelet family, such as the Daubechies and Coiflet wavelet families implemented by Sternickel et al. [Sternickel, 2002]. Although these wavelets have a shape more similar to the QRS complex than the basic Haar wavelet implemented in this research, different heart rates still require the use of different scales. The use of several wavelets of different scales can also be replaced by morphological filtering. This technique has the potential to suit the QRS detection task better, given the changes it can undergo over an individual or variety of critical care patients.

Morphological operators have been widely used in the signal and image-

processing fields because of their robust and adaptive performance in extracting the shape information, in addition to their simple and quick computation [Sun et al., 2002]. Basically, the morphological filtering consists of erosion (shrink) and dilation (expand) operators that are perfect to dynamically adapt to the dynamics of the ECG whose R peak also shrinks and expands with fluctuating heart rates. Hence, this approach is a promising method that is worth investigation in the context of ECG pre-processing.

16.1.2 Recommendations for ABP processing

The ABP does not require as much attention as the ECG. It is recorded from an arterial line that contains a pressure transducer. Hence, it involves far fewer motion-induced artifacts than ECG recorded from contact electrodes. The ABP does not require baseline correction, and the electric signal produced by the pressure transducer of the arterial line is relatively clean of noise and ready to process. The adaptive threshold detection introduced in Section 4.2 has proved to be efficient in the ICU patient monitoring conditions. Although there is always room for improvement, the time and energy of new research should not be spent on the development of a new ABP signal processing algorithm, since the method implemented in this research has been successful in all of the conditions encountered during this research.

16.2 Agitation markers and physiological artifacts

The real-time agitation sensor developed in the clinical trials corresponds to a fairly simple architecture, and enabled this research to reach real-time capability. However, the structure of the software can be considerably improved, starting with the set of input markers of the agitation FIS.

16.2.1 Combination of HRD and HRV

The ICU clinical trials underline the complementary nature of HR, HRD, and time and frequency HRV metrics, as they focus on different trends of the tachogram.

Although frequency HRV requires pseudo-stationarity and time to initialise and stabilise, the information from both time and frequency HRV analysis can be compared to strengthen the agitation assessment based on ECG derived metrics. The temporal HRV analysis is far more reliable in the context of the ICU agitation sensing, and could be preferred because stationarity is not required. This aspect is more realistic with ICU patients data that are not stationary. In addition, they are less computationally intense.

The decision making core of the system modelled by the final FIS should therefore include one of the temporal HRV metrics to ameliorate the quality of the final diagnostic. Because HRD is a reliable tracker of the slow fluctuations of the tachogram, SDRR and SDdRR should be included to track the fast and overall trends of the tachogram respectively, that also reveal clinical information on the patient. This approach would enable detection of atrial fibrillation in addition to, and different from, patient agitation. However, the correlation between HRV metrics and ICU patient agitation is not always clear, as discussed, and further research is necessary to differentiate the effects of agitation on HRV from other symptoms to provide a reliable agitation marker.

16.2.2 Combination of BPD and BPV

Much like the ECG signal, ABP contains slow and fast fluctuations and both reveal complementary clinical information. The combination of BPD and BPV can provide great improvement in the diagnostic of patient condition, but the correlation between BPV and agitation has not been consistent in this research and further research is required to differentiate the effect of agitation on BPV among other symptoms. Similar to HRV it would be recommended that SDSBP and SDdSBP be used for BPV metrics as a first investigation.

16.2.3 Addition of respiration markers

No marker related to respiration is included in the first prototype of the agitation sensor. The respiration potentially contains the ability to provide a great marker to forecast agitation because the change of the level of consciousness is

often first detected by the ventilator as the patient takes over the ventilator to breathe spontaneously. The BR variable, derived from the flow signal of the ventilator, is inconsistent and subjective to the patient and the therapy implemented. Therefore, it cannot be consistent to detect changes in patient condition or rising potential for agitation. However, the relative variations of BR are correlated with anxiety and discomfort that leads to agitation.

The rise of BR with mental stress was first demonstrated by the trials on normal subjects, and later verified during clinical trials. BR was not recorded and processed in the final trial, but it was empirically observed in a bid to understand the symptoms and markers of agitation. Therefore, BRD, the first-order time derivative of the RR variable, has the potential to detect anxiety and discomfort reflected on the patient breathing, and corresponding potential for agitation.

The airway pressure signal also has the potential to detect changes in consciousness and rising potential of agitation in a patient. The shape of the airway pressure signal changes as the patient interferes with the ventilator period. Moreover, the tidal volume may also be affected by agitation. These metrics require research to develop more complex signal processing. The airway pressure signal has the potential to reveal significant information on patient state, ventilation compliance and the patient agitation that may result. As a result the agitation sensor accuracy can be improved.

16.2.4 Summary of physiological signals and variability

This research differentiated the best signal processing techniques, taking into account the variety of symptoms observed in the ICU patients. The basic structure of the agitation sensor includes global markers that do not focus on detailed features of each signal such as the spectral components derived by HRV and BPV, investigated on ICU patients in this research. So far, this global approach allows a broad population of patients to be monitored by the same sensor without having to take into account the symptoms and therapies of each individual subject. Hence, the variability of each signal is initially modelled by the first-order derivative method. However, a basic knowledge of the clinical background of each patients could considerably improve the quality of the agitation sensor. Therefore, the advantages of a patient-specific structure should be addressed in the

future.

Improved versions of the agitation sensor could also include temporal HRV and BPV metrics to provide extra clinical features. For instance, atrial fibrillation detection can be readily included in the monitoring software. Other clinical features could also include the development of new illnesses such a sepsis that manifest loss of overall HRV power [Barnaby et al., 2002]. For this purpose, the main recommendation is the use of time domain HRV variables, such as standard deviation, to determine the short-term variability. This recommendation is based on the clinical trials that reveal the complexity of trying to implement AR filters continuously in real-time on non-stationary, long sets of data. Further research on HRV and BPV implemented on a population of ICU patients is required to possibly differentiate agitation from other symptoms.

Globally, the main recommendation to improve the low level of the system is the addition of a respiration marker in the agitation sensing set of inputs. This recommendation is based on improved knowledge of agitation and results from initial normal and ICU subjects clinical trials. It is potentially the first marker of increasing anxiety and discomfort. Therefore, a marker of respiration should be included in the set of physiological markers of the agitation sensor.

16.3 Motion sensing

Motion sensing is crucial for accurate agitation detection. It is a fundamental part of what clinicians define as agitation. However, the current motion sensing technique suffers many artifacts and is not enough specific to differentiate agitation grades. While wide patient motion is considered critical, mild facial motion such as ETT biting, and pulling is also a strong symptom of severe agitation. Lam et al. [Lam et al., 2003; Lam, 2003] introduced the concept of multiple ROIs for body segments and facial area in their initial work. While limb motion and corresponding body segments ROIs can very often be ignored in the context of this research, the concept of a facial ROI should be considered to avoid the misjudgment and under-rating of dangerous agitation episodes by the system. The improvement of the motion sensing technique requires both low-level and high-level video-processing algorithms to be modified.

16.3.1 Low-level video-processing modifications

The motion detection of specific body parts requires the patient area to be subdivided into several ROIs. The detection of body parts by different ROIs would permit high-level differentiation of mild leg movement that can very often be ignored in the context of the ICU, as opposed to facial motion that corresponds to discomfort and anxiety often leading to episodes of agitation [Lam et al., 2003].

Currently, both mild limb motion and head motion produce the same magnitude of motion as measured by frame-to-frame pixel intensity difference, producing the same response of the motion sensor. This method produces both technical and physiological artifacts. Moreover, episodes of dangerous agitation are misclassified as mild agitation and lead to a false assessment.

First, the overlap of a person over the patient area still produces technical artifacts, despite the video FIS that aims at detecting interference of an outside person. Second, patient limb movement is typical of patient recovery, and it is not always a sign of agitation. Finally, a patient can reach for the ETT tube without wide motion, and still be dangerously agitated. Therefore the patient ROI covering the whole body is not suitable to correctly classify episodes of agitation and avoid physiological artifacts from motion not related to agitation.

The detection of specific body parts within a video frame is under intense research, and several methods are available e.g. [Antoszczyszyn et al., 2000; Figueroa et al., 2003; Paschalakis and Bober, 2004; Zhu et al., 2004; Zhu and Ji, 2004]. The strategy chosen to detect body parts within an image strongly depends on the application. Body parts can be detected by fitting a wire frame, a stick figure or a grid over the whole body, or parts of it such as face or hands [Wang and Singh, 2003]. This summarises the relevant feature by a grid of points that can then be tracked in the consecutive frames of a video record. In this application, the body part of interest is the face area. Although the division of the body into individual parts can increase the accuracy of the subsequent diagnosis, it is not significant for the agitation sensing which remains the main purpose of the software. Moreover, the posture differs from a patient to the next, and the legs are covered by bed sheets, arms can be randomly in or outside the bed sheets, and this complicates the individual limb detection. Mild limb movement can be ignored in the context of agitation detection, so the patient ROI should focus

on the face of the patient as well as the close surrounding region containing the ETT and naso-gastric tubes. An instance of the possible subdivision of the video frame into ROIs is shown in Figure 16.1.

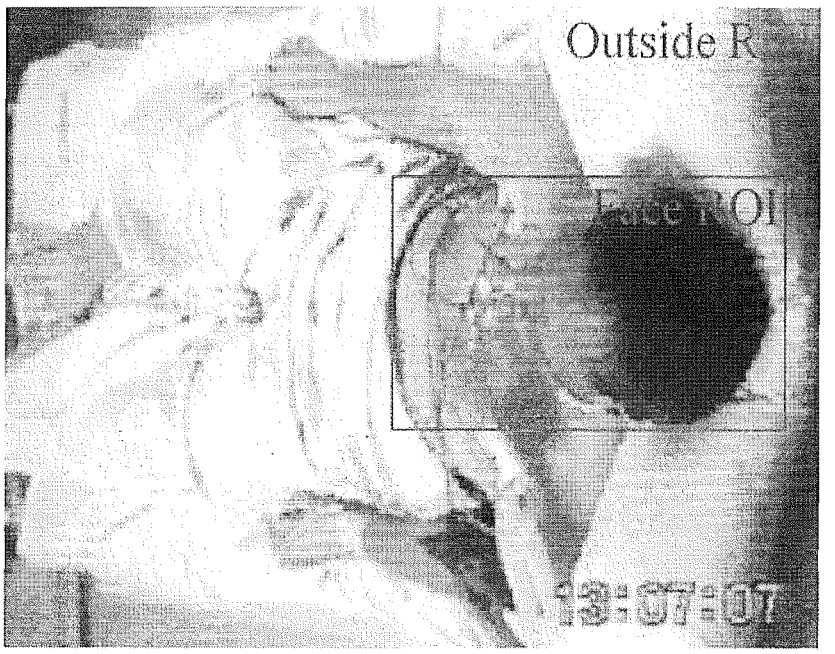

Figure 16.1 Subdivision of main video frame into facial ROI and outside ROI.

The face ROI first needs to be detected within the initial frame. Coughlin et al. [Coughlin et al., 2004] use eye tracking to locate the face and detailed features. However this is not suitable in the context of the ICU where most patients keep their eyes shut. The skin colour is easily detectable on a white background such as hospital bed, and the skin-filtering method developed by Paschalakis et al [Paschalakis and Bober, 2004] is relevant to detect the face of the patient within the patient area. This method is limited by the need to keep the RGB format of the video frame, which represent three times more information to process. However, once the face area ROI is defined the frame can be converted into gray scale for motion sensing. The face area can then be tracked in consecutive video frame to produce a face motion vector. The motion is estimated from the frame-to-frame correlation within consecutive face ROIs that detects face specific grimacing and biting, as well as from the face motion vector that quantifies the overall magnitude of motion.

The video-processing speed can be increased by only searching a limited area

around the previous position of the face ROI, assuming there is only a limited range of motion susceptible to occur. Alternatively the position of the face ROI can be estimated by the previous motion vectors processed by a filter such as Kalman estimator [Piovoso and Laplante, 2003].

The face can also be defined and tracked in consecutive video frame using the template matching technique [Lam et al., 2003; Zhu et al., 2004; Torres-Huitzil and Arias-Estrada, 2004]. The motion sensor algorithm is initialised by a first frame where the face ROI is defined by the user. Then the algorithm tries to find the best match within each video frame to track the face ROI. The video-processing can also be increased using motion vector estimation by a Kalman filter. Face inspection is a reliable marker of pain and anxiety. Extensive research aims at improving the detection of face features such as lips [Chiang et al., 2003] and eyes [Zhu and Ji, 2004]. The initialisation phase records a template of the face when the patient is relaxed, after which it becomes possible to detect stress through crispation and deformation of eyes, lips, and face muscles. This could be the second step to improve the motion sensing technique, but current detection methods require heavy computing that could limit the real-time implementation.

Note that the large motion of significant high-grade agitation would still be observed with this approach as such motion always "leads with the head" as the patient tries to sit up or thrashes from side to side, and it would corresponds to a large face motion vector. Focusing on the face area would also eliminate the need to discriminate as much clinical staff motion and technical artifact could be reduced. Basically, if the face is not detected, then the motion sensing should be paused, because there is obstruction of the patient by another person within the video field.

16.3.2 High-level video-processing modifications

The accuracy of the motion sensing can be improved by focusing the patient ROI on the facial area, but high-level processing also needs to be upgraded to make full use of the new video frame configuration. This high-level improvement consists of upgrading the frame-to-frame correlation method, because the patient motion corresponds to ROIs correlation and face motion vector. This improved version of motion sensing requires the design of a video FIS with more input

variables, namely face ROI correlation, face motion vector and outside motion. This consequently increases the complexity of the if-then rules on which the system is based.

Frame-to-frame correlation performed on the face ROI is believed to considerably reduce physiological and technical artifacts introduced by limbs motion, clinicians and relatives, thus improving the accuracy of agitation-specific motion sensing. However, template matching techniques are best implemented on a series of overlapping frames, and it may require a faster frame rate. Consequently, a faster camera is required, possibly streaming video frames through a Firewire or USB2 bus instead of the current USB1 web camera.

This new frame configuration may better detect ETT grasping and grimacing through the overall face motion vector, specific face features, and hands entering the face ROI. In fact, very detailed motion sensing can be performed if face features such as eyes and lips are detected within the face ROI. This approach permits the use of the faces pain scale to assess pain [Bieri et al., 1990] from the face features and grimacing of the patient. Although the detection of facial features requires very complex image-processing, but it could enable differentiating grasping from grimacing, which correspond to different levels of agitation.

16.4 FIS structure

The clinicians' knowledge of agitation is modelled in the FIS based on the artificial intelligence theory. FIS are the simplest instance available using artificial neural networks and can be upgraded to a more powerful structure including self-learning capabilities, such as hybrid FIS, ANFIS or ANN.

16.4.1 Improved clinical knowledge of agitation

The study of more patients going through periods of agitation reveals different patterns based on the combination of different input variables. The almost complete lack of physiological knowledge on ICU agitation complicates the detection of specific patterns of input variables. Further study of agitated ICU patients

may reveal specific input variable patterns that correspond to the rise in potential for agitation, which would make the final diagnostic capability much more reliable. The fuzzy rules are based on 5 input variables in this first instance of the agitation sensor. The addition of input variables such as BRD as well as the detection of agitation-specific patterns will require the tuning of the fuzzy rules based on the knowledge of clinicians as well as new findings from observation.

16.4.2 Structure improvements

The key feature of state-of-the-art neural networks is the self-learning ability, that is the ability to gain experience with new samples. The self-learning capability can be obtained for instance through back propagation of the error between the expected and true output value, but it requires network initial training using a training set of data and a testing set of data for the calibration and validation respectively.

The training and testing sets of data contain target values that are compared to the system output and the difference consists of the error, which is back-propagated to update the NN parameters and keep the error as low as possible using a least square method. These sets of data are constructed from expert knowledge and in the context of agitation sensing, it requires approval and acceptance of the 0-100 agitation scale introduced in this project by the clinicians community. This task requires hard work of testing in the hospital course as well as the training of staff with that new scale.

The overall project consists of sedation management and the agitation index will potentially remain invisible from the nursing staff point of view once a closed-loop sedation system is completed. The ultimate goal is to provide sedation infusion advice to assist the nursing staff, without requiring the nurse assessment of agitation. Therefore, it is preferable to keep a simple and transparent structure of the artificial intelligent core. Such a system could obviate training of the nursing staff with the agitation scale generated by the agitation sensor. However, an agitation score also provides additional clinical information that could assist decision support tool for diagnosis and management of intervention, and the use of an agitation score should be maintained. The agitation system requires tuning of the fuzzy rules and fuzzy sets as determined by recent findings on agitation and

results of calibration statistical analysis. Thus, the current overall FIS structure should remain unchanged, without self-learning structure in this application.

16.5 Agitation-sedation closed loop trial

The overall aim of this research programme is to develop a semi-automated sedation infusion protocol. The agitation sensor is required by the model to objectively estimate the optimal sedation infusion and provide that information to the nursing staff. The ultimate validation of the concept of objective agitation sensing of ICU patients requires a closed loop trial between the agitation sensor and the sedation controller. The sedation controller can be implemented directly in the infusion device, and the agitation sensor can be connected as an input of the model for clinical trial. In a first attempt, the sedation infusion estimation will be checked by a group of expert, and then manually entered in the sedation infusion device. After the findings of this research, further research is necessary on both the agitation and sedation part of the project, before such a trial can take place.

16.6 Agitation sensing in a different context

The same approach of combining physiological signal-processing and clinical heuristics with fuzzy systems can be used for a wide variety of patient monitoring and diagnostic systems [Phuong and Kreinovich, 2001; Reis et al., 2004]. Examples include monitoring the time course of disease or ARDS [Yuta et al., 2004], optimising and modifying ventilation therapy, preventive monitoring to identify or warn of stroke, or cardiac events, such as atrial fibrillation or other dysrhythmias, and the monitoring of major psychological disturbances manifesting stress. These applications can also be based on the same FIS core used to model expert knowledge with clinicians and engineers collaboration, with the same overall methodology and structure as this thesis.

References

Aboy, M., McNames, J., Marquez, O. W., Hornero, R., Thong, T., and Goldstein, B. (2004). Power spectral density estimation and tracking of nonstationary pressure signals based on kalman filtering. In Dumont, G., editor, *26th Annual International Conference of the IEEE EMBS*, pages 156–159, San Fransisco.

Abraham, A. and Nath, B. (2001). A neuro-fuzzy approach for modelling electricity demand in victoria. *Applied Soft Computing*, 1(2):127–138.

Agogué, F. A., Chase, J. G., and Shaw, G. M. (2005). HRD method to overcome limitation of spectral HRV in agitation quantification of ICU patients. *In review.*

Annie Lambert, E. and Schlaich, M. P. (2004). Reduced sympathoneural responses to the cold pressor test in individuals with essential hypertension and in those genetically predisposed to hypertension: No support for the "pressor reactor" hypothesis of hypertension development. *American Journal of Hypertension*, 17(10):863–868.

Antoszczyszyn, P. M., Hannah, J. M., and Grant, P. M. (2000). Facial motion analysis for content-based video coding. *Real-Time Imaging*, 6(1):3–16.

Bahoura, M., Hassani, M., and Hubin, M. (1997). DSP implementation of wavelet transform for real time ECG wave forms detection and heart rate analysis. *Computer Methods and Programs in Biomedicine*, 52(1):35–44.

Barnaby, D., Ferrick, K., Kaplan, D. T., Shah, S., Bijur, P., and Gallagher, E. J. (2002). Heart rate variability in emergency department patients with sepsis. *Acad Emerg Med*, 9(7):661–70. Journal Article.

Bartels, M. N., Jelic, S., Ngai, P., Gates, G., Newandee, D., Reisman, S. S., Basner, R. C., and De Meersman, R. E. (2004). The effect of ventilation on

spectral analysis of heart rate and blood pressure variability during exercise. *Respiratory Physiology and Neurobiology*, 144(1):91–98.

Baynard, T., Pitetti, K. H., Guerra, M., and Fernhall, B. (2004). Heart rate variability at rest and during exercise in persons with down syndrome. *Archives of Physical Medicine and Rehabilitation*, 85(8):1285–1290.

Bernardo, J. and Smith, A. (1994). *Bayesian theory*. John Wiley and sons, Chichester.

Bianchi, A. M., Mainardi, L., Petrucci, E., Signorini, M. G., Mainardi, M., and Cerutti, S. (1993). Time-variant power spectrum analysis for the detection of transient episodes in HRV signal. *IEEE Trans Biomed Eng*, 40(2):136–44.

Bieri, D., Reeve, R. A., Champion, G. D., Addicoat, L., and Ziegler, J. B. (1990). The faces pain scale for the self-assessment of the severity of pain experienced by children: development, initial validation, and preliminary investigation for ratio scale properties. *Pain*, 41(2):139–50.

Cammann, H. and Michel, J. (2002). How to avoid misinterpretation of heart rate variability power spectra? *Computer Methods and Programs in Biomedicine*, 68(1):15–23.

Carrasco, G. (2000). Instruments for monitoring intensive care unit sedation. *Crit Care*, 4(4):217–25.

Chase, J. G., Agogué, F. A., Starfinger, C., Lam, Z., Shaw, G. M., Rudge, A. D., and Sirisena, H. (2004a). Quantifying agitation in sedated ICU patients using digital imaging. *Computer Methods and Programs in Biomedicine*, 76(2):131–141.

Chase, J. G., Lam, Z., Starfinger, C., Shaw, G. M., Agogué, F. A., and Sirisena, H. (2003). Quantifying agitation in sedated intensive care patients. *NZ Medical Journal*, 116:444.

Chase, J. G., Rudge, A. D., Shaw, G. M., Wake, G. C., Lee, D. S., Hudson, I. L., and Johnston, L. (2004b). Modeling and control of the agitation-sedation cycle for critical care patients. *Medical Engineering and Physics*, 26(6):459–471.

Chase, J. G., Starfinger, C., Lam, Z., Agogué, F. A., and Shaw, G. M. (2004c). Quantifying agitation in sedated ICU patients using heart rate and blood pressure. *Physiological measurement*, 25:1–15.

Chen, T. (2003). A fuzzy back propagation network for output time prediction in a wafer fab. *Applied Soft Computing*, 2(3):211–222.

Chiang, C., Tai, W., Yang, M., Huang, Y., and Huang, C. (2003). A novel method for detecting lips, eyes and faces in real time. *Real-Time Imaging*, 9(4):277–287.

Chiu, H., Wang, T., Huang, L., Tso, H., and Kao, T. (2003). The influence of mean heart rate on measures of heart rate variability as markers of autonomic function: a model study. *Medical Engineering & Physics*, 25(6):475–481.

Couderc, J. P., Chevalier, P., Fayn, J., Rubel, P., and Touboul, P. (2000). Identification of post-myocardial infarction patients prone to ventricular tachycardia using time-frequency analysis of qrs and st segments. *Europace*, 2(2):141–153.

Coughlin, M., Cutmore, T., and Hine, T. (2004). Automated eye tracking system calibration using artificial neural networks. *Computer Methods and Programs in Biomedicine*, 76(3):207–220.

Crippen, D. W. (1990). The role of sedation in the ICU patient with pain and agitation. *Crit Care Clin*, 6(2):369.

De Jong, M. J., Moser, D. K., An, K., and Chung, M. L. (2004). Anxiety is not manifested by elevated heart rate and blood pressure in acutely ill cardiac patients. *European Journal of Cardiovascular Nursing*, In Press, Corrected Proof.

Deslandes, A. C., Veiga, H., Cagy, M., Piedade, R., Pompeu, F., and Ribeiro, P. (2004). Effects of caffeine on visual evoked potential (P300) and neuromotor performance. *Arq Neuropsiquiatr*, 62(2B):385–90.

Figueroa, P. J., Leite, N. J., and Barros, R. M. L. (2003). A flexible software for tracking of markers used in human motion analysis. *Computer Methods and Programs in Biomedicine*, 72(2):155–165.

Fleiss, J. L. (1973). *Statistical methods for rates and proportions.* John Wiley and Sons.

Frantti, T. and Mahonen, P. (2001). Fuzzy logic-based forecasting model. *Engineering Applications of Artificial Intelligence*, 14(2).

Fraser, G. L. and Riker, R. R. (2001). Monitoring sedation, agitation, analgesia, and delirium in critically ill adult patients. *Crit Care Clin*, 17(4):967–87.

Fung, Y. (1997). *Biomechanics: Circulation*. Springer-Verlag.

Gaba, D., Howard, S., and Jump, B. (1994). Production pressure in the work environment. *Anesthesiology*, 81:488–500.

Godfrey, N., Li, H., Ji, Y., and Marcy, W. (1995). Real time fuzzy logic controller for balancing a beam-and-ball system. In Li, H. and Gupta, M. M., editors, *Fuzzy Logic and Intelligent Systems*, volume 1 of *International Series in Intelligent Systems*, pages 157–185. Kluwer Academic Publishers.

Gokceoglu, C. and Zorlu, K. (2004). A fuzzy model to predict the uniaxial compressive strength and the modulus of elasticity of a problematic rock. *Engineering Applications of Artificial Intelligence*, 17(1):61–72.

Gold, D., Litonjua, A., Schwartz, J., Lovett, E., Larson, A., Nearing, B., Allen, G., Verrier, M., Cherry, R., and Verrier, R. (2000). Ambient pollution and heart rate variability. *Circulation*, 101(11):1267–73.

Guyton, A. C. (1980). The body's approach to arterial pressure regulation. In Saunders, W. B., editor, *Arterial Pressure and Hypertension*, Circulatory physiology 3, pages 1–9.

Guyton, A. C. and Hall, J. E. (1996). *Textbook of medical physiology*. Saunders, Philadelphia.

Haskell, R. M., Frankel, H. L., and Rotondo, M. F. (1997). Agitation. *AACN Clin Issues*, 8(3):335–50.

Huikuri, H. V., Makikallio, T., Airaksinen, K. E. J., Mitrani, R., Castellanos, A., and Myerburg, R. J. (1999). Measurement of heart rate variability: a clinical tool or a research toy? *Journal of the American College of Cardiology*, 34(7):1878–1883.

Inagaki, H., Kuwahara, M., and Tsubone, H. (2004). Effects of psychological stress on autonomic control of heart in rats. *Exp Anim*, 53(4):373–8.

Jaarsma, A. S., Knoester, H., van Rooyen, F., and Bos, A. P. (2001). Biphasic positive airway pressure ventilation (pev+) in children. *Crit Care*, 5(3):174–7.

Kress, J. P., Pohlman, A. S., O'Connor, M. F., and Hall, J. B. (2000). Daily interruption of sedative infusions in critically ill patients undergoing mechanical ventilation. *N Engl J Med*, 342(20):1471–7.

Kuo, C., Chao, C., and Hsieh, C. (2002). A new motion estimation algorithm for video coding using adaptive kalman filter. *Real-Time Imaging*, 8(5):387–398.

Kuusela, T. A., Kaila, T. J., and Kahonen, M. (2003). Fine structure of the low-frequency spectra of heart rate and blood pressure. *BMC Physiol*, 3(1):11.

Kwok, H. F., Linkens, D. A., Mahfouf, M., and Mills, G. H. (2003). Rule-base derivation for intensive care ventilator control using ANFIS. *Artif Intell Med*, 29(3):185–201.

Lam, Z. (2003). *Agitation measurement and signal processing of physiological variables for sedated subjects.* Masters thesis, dept of mechanical eng., University of Canterbury.

Lam, Z., Starfinger, C., Chase, J. G., Shaw, G. M., and Agogue, F. A. (2003). Movement quantification for use in agitation quantification in ICU patients. In *World congress on medical physics and biomedical engineering*, Sydney, Australia.

Larkin, K. G., Oldfield, M. A., and Klemm, H. (1997). Fast fourier method for the accurate rotation of sampled images. *Optics Communications*, 139(1-3):99–106.

Lin, J. and Kuo, K. Y. (2001). Application of fuzzy set theory on the change intervals at a signalized intersection. *Applied Soft Computing*, 1(2):161–177.

Lindh, V., Wiklund, U., and Hakansson, S. (1999). Heel lancing in term newborn infants: an evaluation of pain by frequency domain analysis of heart rate variability. *Pain*, 80(1-2):143–148.

Lindh, V., Wiklund, U., Sandman, P., and Hakansson, S. (1997). Assessment of acute pain in preterm infants by evaluation of facial expression and frequency domain analysis of heart rate variability. *Early Human Development*, 48(1-2):131–142.

Ljung, L., Morf, M., and Falconer, D. D. (1978). Fast calculation of gain matrices for recursive estimation schemes. *Int. J. Control*, 27(1):1–19.

Logan, H. L., Sheffield, D., Lutgendorf, S., and Lang, E. (2002). Predictors of pain during invasive medical procedures. *The Journal of Pain*, 3(3):211–217.

Lotti, G. A. and Braschi, A. (1999). Measurements of respiratory mechanics during mechanical ventilation. Technical report, Servizio di anestesia e rianimazione 1, IRCCS Policlinico S. Matteo.

Mackenzie, C., Craig, G., Parr, M., and Horst, R. (1994). Video analysis of two emergency tracheal intubations identifies flawed decision-making. *Anesthesiology*, 81:763–771.

Mallat, S. (1999). *A wavelet tour of signal processing.* Academic Press, second edition.

Mamdani, E. and Assilian, S. (1999). Experiment in linguistic synthesis with a fuzzy logic controller. *International Journal of Human Computer Studies*, 51(2):135–147.

Marple, S. (1987). *Digital spectral analysis with applications.* Prentice hall edition.

Masaoka, Y. and Homma, I. (1997). Anxiety and respiratory patterns: their relationship during mental stress and physical load. *International Journal of Psychophysiology*, 27(2):153–159.

Melin, P. and Castillo, O. (2003). Adaptive intelligent control of aircraft systems with a hybrid approach combining neural networks, fuzzy logic and fractal theory. *Applied Soft Computing*, 3(4):353–362.

Mendez, M. O., Bianchi, A. M., and Cerutti, S. (2004). Non-stationary analysis of heart rate variability during the obstructive sleep apnea. In Dumont, G., editor, *26th Annual International Conference of the IEEE EMBS*, pages 286–289, San Fransisco.

Molke Borgbjerg, F., Nielsen, K., and Franks, J. (1996). Experimental pain stimulates respiration and attenuates morphine-induced respiratory depression: a controlled study in human volunteers. *Pain*, 64(1):123–128.

Montgomery, H. (2001). Reflective versus nonreflective thinking: Motivated cognition in naturalistic decision making. In Salas, E. and Klein, G., editors, *Linking expertise and naturalistic decision making.*, pages 159–170.

Nasraway Jr, S. A., C., W. E., Kelleher, R. M., Yasuda, C. M., and Donnelly, A. M. (2002). How reliable is the bispectral index in critically ill patients? a prospective, comparative, single-blinded observer study. *Crit Care Med*, 30(7):1483–7.

Niskanen, J., Tarvainen, M. P., Ranta-aho, P. O., and Karjalainen, P. A. (2004). Software for advanced HRV analysis. *Computer Methods and Programs in Biomedicine*,. 76(1):73–81.

Pagani, M., Lombardi, F., Guzzetti, S., Rimoldi, O., Furlan, R., Pizzinelli, P., Sandrone, G., Malfatto, G., Dell'Orto, S., and Piccaluga, E. (1986). Power spectral analysis of heart rate and arterial pressure variabilities as a marker of sympatho-vagal interaction in man and conscious dog. *Circ Res*, 59(2):178–93.

Paschalakis, S. and Bober, M. (2004). Real-time face detection and tracking for mobile videoconferencing. *Real-Time Imaging*, 10(2):81–94.

Paskeviciute, R., Zemaityte, D., and Varoneckas, G. (2001). Heart rate variability in diagnostics of atrial fibrillation or atrial flutter. Technical report, Institute of psychology and rehabilitation Kaunas University of Medicine.

Petrie, A. and Sabin, C. (2000). *Medical statistics at a Glance*. Blackwell Science.

Pfeiffer, G. and Netzer, J. (1997). Spectral analysis of heart rate and blood pressure in guillain-barre patients with respiratory failure. *J Neurol Sci*, 150(1):39–48.

Phuong, N. H. and Kreinovich, V. (2001). Fuzzy logic and its applications in medicine. *Int J Med Inf*, 62(2-3):165–73.

Piovoso, M. and Laplante, P. A. (2003). Kalman filter recipes for real-time image processing. *Real-Time Imaging*, 9(6):433–439.

Rajendra Acharya, U., Kannathal, N., Lee, M. H., and Leong, M. Y. (2004). Study of heart rate variability signals at sitting and lying postures. *Journal of Bodywork and Movement Therapies*, In Press, Corrected Proof.

Ramsay, M. A., Savege, T. M., Simpson, B. R., and Goodwin, R. (1974). Controlled sedation with alphaxalone-alphadolone. *Br Med J*, 2(920):656–9.

Reis, M. A., Ortega, N. R., and Silveira, P. S. (2004). Fuzzy expert system in the prediction of neonatal resuscitation. *Braz J Med Biol Res*, 37(5):755–64.

Riker, R. R., Picard, J. T., and Fraser, G. L. (1999). Prospective evaluation of the sedation-agitation scale for adult critically ill patients. *Crit Care Med*, 27(7):1325–9.

Rudge, A. D., Chase, J. G., Shaw, G. M., Lee, D. S., Wake, G. C., Hudson, I. L., and Johnston, L. (2004). Impact of control on agitation-sedation dynamics. *Control Engineering Practice*, In Press, Corrected Proof.

Seong, H. M., Lee, J. S., Shin, T. M., Kim, W. S., and Yoon, Y. R. (2004). The analysis of mental stress using time-frequency distribution of heart rate variability signal. In Dumont, G., editor, *26th Annual International Conference of the IEEE EMBS*, pages 283–285.

Sessler, C. N., Gosnell, M. S., Grap, M. J., Brophy, G. M., O'Neal, P. V., Keane, K. A., Tesoro, E. P., and Elswick, R. K. (2002). The richmond agitation-sedation scale: validity and reliability in adult intensive care unit patients. *Am J Respir Crit Care Med*, 166(10):1338–44.

Shaw, G. M., Chase, J. G., Lee, D. S., Hooper, E. A., Rudge, A. D., and Agogue, F. A. (2004). Emerging methods for sedation and agitation management in critical illness. In *ANZICS ASM*, Wellington.

Shaw, G. M., Chase, J. G., Rudge, A. D., Starfinger, C., Lam, Z., Lee, D. S., Wake, G. C., Greenfield, K., and Dove, R. (2003). Rethinking sedation and agitation management in critical illness. *Critical care and resuscitation*, 5:198–206.

Shinn, E. H., Poston, W. S. C., Kimball, K. T., St. Jeor, S. T., and Foreyt, J. P. (2001). Blood pressure and symptoms of depression and anxiety: a prospective study. *American Journal of Hypertension*, 14(7):660–664.

Simon, D. (2003). Kalman filtering for fuzzy discrete time dynamic systems. *Applied Soft Computing*, 3(3):191–207.

Sokolowski, A. (2004). On some aspects of fuzzy logic application in machine monitoring and diagnostics. *Engineering Applications of Artificial Intelligence*, 17(4):429–437.

Sonmez, H., Gokceoglu, C., and Ulusay, R. (2003). An application of fuzzy sets to the geological strength index (GSI) system used in rock engineering. *Engineering Applications of Artificial Intelligence*, 16(3):251–269.

Starfinger, C. (2003). *Measurement of agitation in sedated ICU patients using biomedical signal processing.* Dipomarbeit thesis, dipl. inform. med., Universitat Heidelberg.

Starfinger, C., Lam, Z., Chase, J. G., Shaw, G. M., and Agogue, F. A. (2003). Measurement of agitation in sedated ICU patients using adaptive signal processing and fuzzy mathematics. In *World congress on medical physics and biomedical engineering*, Sydney, Australia.

Sternickel, K. (2002). Automatic pattern recognition in ECG time series. *Computer Methods and Programs in Biomedicine*, 68(2):109–115.

Sun, Y., Chan, K. L., and Krishnan, S. M. (2002). ECG signal conditioning by morphological filtering. *Computers in Biology and Medicine*, 32(6):465–479.

Terano, T., Asai, K., and Sugeno, M. (1987). *Fuzzy systems theory and its applications.*

Terathongkum, S. and Pickler, R. H. (2004). Relationships among heart rate variability, hypertension, and relaxation techniques. *Journal of Vascular Nursing*, 22(3):78–82.

Thong, T., Yung, I. O., Zajdel, D. P., Ellingson, R. M., McNames, J., Aboy, M., and Oken, B. S. (2004). Heart rate variability analysis of effect of nicotine using lomb-welch periodograms. In Dumont, G., editor, *26th Annual International Conference of the IEEE EMBS*, pages 294–297, San Fransisco.

Torres-Huitzil, C. and Arias-Estrada, M. (2004). Real-time image processing with a compact FPGA-based systolic architecture. *Real-Time Imaging*, 10(3):177–187.

Tseng, S. (2004). Motion estimation using a frame-based adaptive thresholding approach. *Real-Time Imaging*, 10(1):1–7.

Tsipouras, M. G. and Fotiadis, D. I. (2004). Automatic arrhythmia detection based on time and time-frequency analysis of heart rate variability. *Computer Methods and Programs in Biomedicine*, 74(2):95–108.

Van de Louw, A., Cracco, C., Cerf, C., Harf, A., Duvaldestin, P., Lemaire, F., and Brochard, L. (2001). Accuracy of pulse oximetry in the intensive care unit. *Intensive Care Med*, 27(10):1606–13.

Wang, J. J. and Singh, S. (2003). Video analysis of human dynamics–a survey. *Real-Time Imaging*, 9(5):321–346.

Weinert, C., Chlan, L., and Gross, C. (2001). Sedating critically ill patients: factors affecting nurses' delivery of sedative therapy. *Critical Care*, 10(3):156–167.

Wiklund, U., Akay, M., and Niklasson, U. (1997). Short-term analysis of heart rate variability by adapted wavelet transforms. *IEEE Eng Med Biol Mag*, 16(5):113–8, 138.

Yeragani, V. K., Mallavarapu, M., Radhakrishna, R. K., Tancer, M., and Uhde, T. (2004). Linear and nonlinear measures of blood pressure variability: increased chaos of blood pressure time series in patients with panic disorder. *Depress Anxiety*, 19(2):85–95.

Yuta, T., Chase, J. G., Shaw, G. M., and Hann, C. E. (2004). Dynamic models of ARDS lung mechanics for optimal patient ventilation. In *26th International Conf of IEEE Engineering in Med and Biology Society (EMBS 2004)*, pages 861–864, San Fransisco.

Zhu, D., Moore, S. T., and Raphan, T. (2004). Robust and real-time torsional eye position calculation using a template-matching technique. *Computer Methods and Programs in Biomedicine*, 74(3):201–209.

Zhu, Z. and Ji, Q. (2004). Robust real-time eye detection and tracking under variable lighting conditions and various face orientations. *Computer Vision and Image Understanding*, In Press, Corrected Proof.

Zingaretti, P. and Zanoli, S. M. (1998). Robust real-time detection of an underwater pipeline. *Engineering Applications of Artificial Intelligence*, 11(2):257–268.